



University of Cambridge

Department of Applied Mathematics
and Theoretical Physics

ASPECTS OF INFLATION AND THE VERY EARLY UNIVERSE

Raquel H. Ribeiro

This thesis is submitted to the University of Cambridge
for the degree of Doctor of Philosophy



Girton College
Cambridge, United Kingdom

PhD Dissertation, May 2012

Raquel H. Ribeiro

Department of Applied Mathematics and Theoretical Physics

&

Girton College

University of Cambridge, United Kingdom

*This thesis is dedicated to my grandparents,
and to Martinho Henriques and Corália Ribeiro Norton,
who I lost during my PhD.*

You taught me much of what I know about life, and I owe you too much.

Abstract

There is no exaggeration in the statement that we are living truly exciting times in Cosmology. Until recently our knowledge of the primordial curvature perturbation was relatively modest. Ever since *COBE* delivered its map of data we know the scalar spectrum of primordial perturbations is approximately flat, with the power being only slightly stronger at larger scales. Most inflationary models predict an approximately scale-invariant spectrum, which therefore cannot be used as a distinctive signature. To distinguish between different inflationary microphysics we need to study higher point statistics of the primordial perturbation, which can encode non-gaussian data. The first of these can be accessible through the bispectrum, or three-point function. A non-vanishing measurement of the bispectrum would be a key diagnostic tool for telling models apart and rule out entire classes of models.

In the first part of this thesis we study the bispectrum in all single-field models with a well-defined quantum field theory during a quasi-de Sitter inflationary phase. Any single-field models without ghost-like instabilities fall into this description: from canonical, to Dirac–Born–Infeld inflation and galileon inflation theories. We investigate the scale and shape-dependences of the bispectrum to *next-order* in the slow-roll approximation. We illustrate our results by applying them to different models and argue these corrections must be taken into account to keep the theoretical error below the observational precision set by the *Planck* satellite. We then explore the ability of using bispectrum shapes to distinguish between infla-

tionary models more efficiently. We further extend the study of the bispectrum of single-field models beyond the slow-roll approximation, demanding the spectral index to be close to, but not exactly, unity.

In the second part of this thesis we explore the process by which the universe is repopulated with matter particles at the end of a Dirac–Born–Infeld inflation phase. We place some mild bounds on the reheating temperature of these models. We argue that the constraints arising from the preheating analysis are complementary to those derived from the primordial perturbation.

Declaration

This dissertation is the result of my own work and includes nothing which is the outcome of work done in collaboration except where specifically indicated in the text. Nevertheless, following the tendency of modern research in Theoretical Physics, most of the material discussed in this dissertation is the result of research in a collaboration network. In particular, chapters 2 and 3, and part of 4, are based on work done in collaboration with Clare Burrage and David Seery, published in Ref. [1], and chapter 4 also contains material discussed in Ref. [2] in collaboration with David Seery. Chapter 5 is strongly based on Ref. [3], which is the result of my own work, whereas chapter 6 is the result of work done in collaboration with Nazim Bouatta, Anne-Christine Davis and David Seery and published as Ref. [4]. I have made major contributions to the above, both in terms of results and writing.

I hereby declare that my thesis entitled

Aspects of Inflation and the Very Early Universe

is not substantially the same as any that I have submitted for a degree or diploma or other qualification at any other University. I further state that no part of my thesis has already been or is being concurrently submitted for any such degree, diploma or any other qualification.

I further declare that this copy is identical in every respect to the soft-bound volume examined for the Degree, except that any alterations required by the Examiners have been made.

Contents

Abstract	iii
Declaration	v
1 Introduction	1
1.1 FLRW cosmology	4
1.2 Big Bang Model	8
1.3 Inflationland	11
1.3.1 A simple inflation model	13
1.3.2 Beyond the simplest inflation models	16
1.3.3 Seeding perturbations	19
1.4 Λ CDM: the concordance model	21
1.5 <i>Planck</i> : the ultimate ‘thermometer’	23
1.6 Summary of the outline of the thesis	24
2 Non-Gaussianity in Inflationland	29
2.1 Understanding non-gaussianities	30
2.1.1 Historical developments	32
2.1.2 Non-gaussianities in slow-roll inflation	36

2.2	Single-field inflation: an overview	39
2.2.1	Fluctuations	39
2.2.2	Two-point correlations	44
2.3	Three-point correlations	51
2.3.1	Third-order action	51
2.3.2	Schwinger–Keldysh’s <i>in-in</i> formalism	55
2.3.3	Boundary terms removed	59
2.4	Beyond $P(X, \phi)$ and towards Horndeski theories	60
3	Microphysics in Non-Gaussianity	63
3.1	The bispectrum beyond lowest-order	64
3.1.1	Sources of next-order corrections	65
3.1.2	Reference time, factorisation scale	66
3.1.3	Horndeski operators	68
3.2	Three-point correlations	69
3.2.1	The bispectra	71
3.2.2	Formulae for f_{NL}	77
3.3	Canonical single-field inflation	81
3.4	Non-canonical single-field inflation	82
3.4.1	Asymptotically power-law models	83
3.5	Tensor modes	92
3.6	Main results	94
4	Decoding the Bispectrum of Single-Field Inflation	99
4.1	Scale-dependence	100
4.2	Shape-dependence	104
4.2.1	Inner product and cosine	104
4.2.2	Bispectrum shapes from slow-variation parameters	110

4.3	Resolving the “drumlin” bispectrum shape	123
4.3.1	Harmonic decomposition	123
4.3.2	Distinguishing microphysics	129
4.4	Summary of results	136
5	Inflationary Signatures of Single-Field Models Beyond Slow-Roll	139
5.1	Background evolution beyond exact scale-invariance	142
5.1.1	The scalar power spectrum	146
5.1.2	Obtaining next-order corrections to the wavefunctions, ζ_k	147
5.2	Non-gaussianity in the bispectrum	152
5.2.1	Bispectrum of Horndeski theories	152
5.2.2	Features of the bispectrum of Horndeski theories	160
5.3	Summary of results	169
6	Preheating at the End of Inflation	173
6.1	Preheating: development of a theory	174
6.2	DBI dynamics	177
6.2.1	Coupling to matter fields	183
6.3	Non-perturbative preheating in DBI inflation	185
6.3.1	Brief review of parametric resonance	185
6.3.2	Inflaton production	187
6.3.3	Matter particle production	189
6.3.4	Preheating with a symmetry breaking term	190
6.3.5	Efficiency of narrow-resonance preheating	193
6.4	Perturbative reheating in DBI inflation	194
6.4.1	Estimates of reheating temperatures	196
6.5	Summary of results	197

7 Discussion	199
7.1 Questions addressed in this thesis	199
7.2 Summary of the main results	201
7.3 Outlook	203
A The slow-variation approximation	211
A.1 Propagator corrections	211
A.2 Integrals involving the exponential integral function, $Ei(z)$	213
A.3 Useful integrals	216
B Steps beyond exact scale-invariance	217
B.1 Dynamics in y —why?	217
B.2 The spectral index beyond exact scale-invariance	218
B.3 Next-order corrections—useful formulae	220
B.4 Useful integrals	222
B.4.1 Integrals involving the exponential integral function, $Ei(\xi)$	223
B.4.2 Other integrals	225
B.5 Listing variables	226
C Details of the preheating stage	227
C.1 Canonically normalised theory	227
C.2 Floquet exponents from Hill’s equation	229
C.2.1 $\theta_0, \theta_2, \theta_4 \neq 0$	229
C.2.2 $\theta_0, \theta_2, \theta_6 \neq 0$	230

List of Figures

1.1	CMB 2-year data showing the temperature anisotropies in the microwave sky (image courtesy of the <i>COBE</i> official website).	2
1.2	7-year <i>WMAP</i> data of the microwave sky (image courtesy of NASA/ <i>WMAP</i> science team).	2
1.3	Experimental data taken in 1998 for different values of redshift favours cosmological models where vacuum energy (dark energy) contributes to the total energy density in the universe. The plot is taken from an article written by Saul Perlmutter which appeared in <i>Physics Today</i> [5].	3
1.4	Simple (small-field) inflation potential and the dynamics of inflation.	14
1.5	As inflation proceeds, the inflaton undergoes quantum fluctuations which are the seeds for density perturbations.	20
1.6	The launch of the <i>Planck</i> satellite and the <i>Herschel</i> telescope by Ariane 5 (image courtesy of ESA-CNES-Arianespace, Optique Vidéo du CSG, P. Baudon).	23
2.1	Detailed map of the microwave sky as seen by <i>WMAP</i> . This is a snapshot of the universe when it was only 380,000 years old.	30
2.2	Integration contour for the Feynman path integral.	56
2.3	Tree-level Feynman diagrams associated with the three-point correlator.	57

3.1	Sources of next-order corrections in slow-roll in the tree-level Feynman diagram.	66
4.1	An arbitrary bispectrum built as a linear combination of fundamental harmonic shapes.	126
6.1	Plot of the numerical (red) and approximate (blue) solution of Eq. (6.11), and the cosine function (green).	183
7.1	Cartogram of significant developments in early universe theoretical cosmology roughly over the last 100 years.	204

List of Tables

1.1	The content of the universe given by direct measurements and induced parameter values obtained from <i>WMAP</i> & BAO data [6, 7]. t_0 denotes the age of the universe.	22
2.1	$n_s - 1$ at lowest and next-order in the slow-roll approximation. The first row applies for arbitrary positive, smooth z , as explained below Eq. (2.16). We assume this is the case throughout this thesis.	51
3.1	Coefficients of the leading-order bispectrum, where $K^2 \equiv k_1 k_2 + k_1 k_3 + k_2 k_3$. . .	72
3.2	Coefficients of the subleading corrections to the bispectrum, where $K^2 \equiv k_1 k_2 + k_1 k_3 + k_2 k_3$	74
3.3	Coefficients appearing in the function \mathcal{J} for each operators. Note that the γ_i contain complex numbers. The imaginary part is cancelled on addition of the + and - Feynman diagrams, and only the real part of these coefficients contribute. In an intermediate step for the three-point function of $\zeta(\partial\zeta)^2$, the cancellation of power-law divergences in τ (required by Weinberg's theorem [8]) depends on a real contribution generated from the product of two imaginary terms. . . .	75
3.4	Equilateral limit of f_{NL} at leading and next-order in the slow-roll approximation. The numerical constant ω satisfies $\omega = \frac{1}{2} \ln \frac{3}{2} = \coth^{-1} 5$	79

3.5	f_{NL} in the squeezed limit at leading and next-order in the slow-roll approximation.	80
4.1	Functions $f_m(k_i)$ determining the momentum dependence of the running of f_{NL} in Eq. (4.3).	102
4.2	Overlap cosines between common templates, depicted in Table 4.3.	108
4.3	The bispectrum templates used in CMB analysis in the Fergusson & Shellard [9], and Babich et al. [10] parametrisations. We see that the first parametrisation enhances the symmetry of the shape in $\{\alpha, \beta\}$ space.	109
4.4	Cosines between the leading-order shapes and the common templates.	110
4.5	Bispectrum shapes at leading-order in slow-roll for the operators in the action (3.3), using the Babich et al. [10], and Fergusson-Shellard [9] parametrisations.	111
4.6	Cosines between the S_H -shape (4.20) and common templates.	114
4.7	The S_H -shape in the Fergusson & Shellard parametrisation.	114
4.8	Highly orthogonally designed shape constructed by Creminelli et al. [11].	115
4.9	Lowest-order bispectrum shapes enhanced by c_s^{-2} in $P(X, \phi)$ models.	116
4.10	Overlap cosines for the bispectrum shape proportional to each slow-variation parameter. Sign information has been discarded.	117
4.11	Bispectrum shapes enhanced by c_s^{-2} at next-order in a $P(X, \phi)$ model.	118
4.12	The “orthogonal” shape O has zero overlap with both the shapes S_1 and S_2 .	120
4.13	Overlap cosines between the orthogonal shape O and common templates.	121
4.14	The bispectrum shapes S_H , O and the one found by Creminelli et al. [11].	122
4.15	Bispectrum basis shapes \mathcal{R}'_n in 2d and 3d plots up to $n = 9$.	125
4.16	Expansion of common templates in terms of the \mathcal{R}'_n basis.	127
4.17	Expansion of the S_H -shape (defined at leading-order in slow-roll), the O -shape (defined at next-order in slow-roll) [1] and the Creminelli et al. shape [11] in terms of the \mathcal{R}'_n basis.	128

4.18	Approximations to the S_H -shape and similar bispectra, up to the first ten harmonics in the \mathcal{R}_n expansion. The coefficients α_n are listed in table 4.17.	129
4.19	Cosines between \mathcal{R}'_n -approximations to the orthogonal shapes depicted in table 4.18 and the corresponding exact shape.	130
5.1	Coefficients of the functions appearing in the B^a bispectrum. For simplicity of notation, we define the quantities \tilde{k} , Ω_1 and Ω_2 in table B.1 of Appendix B.5. . .	154
5.2	Coefficients of the functions \tilde{J}_γ appearing in the B^a bispectrum, where Ω_{1*} and Ω_{3*} are defined in table B.1 of Appendix B.5. The functions \tilde{J}_γ are defined in Eq. (5.24) and discussed in detail in Appendix B.4.	155
5.3	Coefficients of the functions appearing in the B^b bispectrum for the first three operators, where $\vartheta_i = \frac{1}{k_t}(k_t - 2k_i)$, and Ξ and $f(k_1, k_2, k_3)$ are defined in table B.1 of Appendix B.5.	156
5.4	Coefficients of the functions appearing in the B^b bispectrum for the first three operators, where Ξ and $f(k_1, k_2, k_3)$ are defined in table B.1 of Appendix B.5. . .	157
5.5	Coefficients of the functions appearing in the B^b bispectrum for the last two operators, where $\vartheta_i = \frac{1}{k_t}(k_t - 2k_i)$, and Ξ is defined in table B.1 of Appendix B.5.	158
5.6	Coefficients of \tilde{J}_γ appearing in the B^b bispectrum. The functions \tilde{J}_γ are discussed in detail in Appendix B.4.	159
B.1	Collection of the abbreviated variables used in the tables included in chapter 5.	226

*Sometimes I think we're alone in the universe,
and sometimes I think we're not.
In either case the idea is quite staggering.*

Sir Arthur C. Clarke



Introduction

The universe is an incredibly fascinating subject of study. Ever since we gained the ability of logical thinking we have been staring at the sky bewildered by the enormous amount of space out there. It is in the cosmos that we find the oldest and longest journey of all times: that of the primordial perturbation.

The first major discovery in cosmology over the last century was due to Edwin Hubble who observed that galaxies were moving apart from each other: the further away they were the larger the speed of separation from us. We learned the universe was not static, but expanding. After this discovery much of the work in cosmology was theoretical. In the last few decades, however, this has changed since a remarkable collection of high-precision satellites was assembled. In the last two decades, our knowledge of the universe has grown tremendously as we have become acquainted with its extraordinary history. There are essentially two important events that allowed this to happen.

First, the launch of the *COBE* (COsmic Background Explorer) satellite¹ in 1989 established the beginning of measurements of the Cosmic Microwave Background Radiation [12], which we refer to as the CMBR from now on. The CMB was first discovered accidentally by Penzias

¹ <http://lambda.gsfc.nasa.gov/product/cobe/>, April 2012.

& Wilson in 1965, who collected the Nobel Prize in 1978. This breakthrough triggered many questions about the CMBR properties.

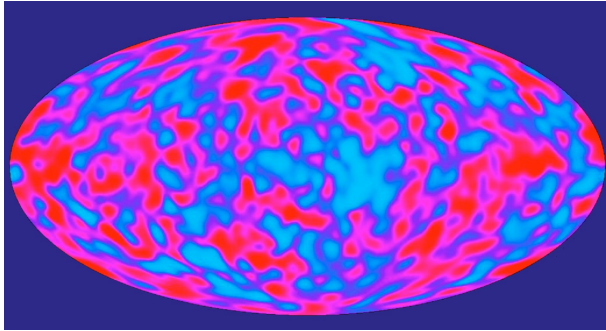


Figure 1.1: CMB 2-year data showing the temperature anisotropies in the microwave sky (image courtesy of the *COBE* official website).

Measurements of the CMBR are purely statistical, and so is our knowledge of the universe in its infancy. *COBE* performed the very first measurements of the anisotropies of the CMBR, as small as 1 part in 1,000, in a background radiation of roughly 2.7K. With *COBE* we learned that the CMBR has an almost perfect black-body spectrum.

It was with the follow-up mission of *WMAP* (Wilkinson Microwave Anisotropy Probe)², launched in 2001, that the details of the statistics of the CMBR became known. By comparing figures 1.1 and 1.2 we appreciate the amazing improvement of precision in temperature measurements. The details of the colour map in the second figure are undeniable evidence of the extraordinary advances in observational cosmology.

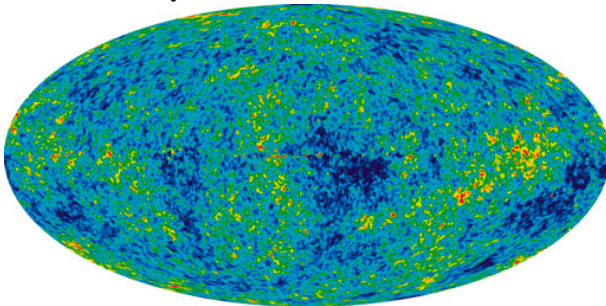


Figure 1.2: 7-year *WMAP* data of the microwave sky (image courtesy of NASA/*WMAP* science team).

These statistics are much more than just numbers. They encode detailed information about the early universe. They are remnants of an early, hot, violent epoch imprinted in the microwave radiation—they reflect the microphysics of the early universe.

With the launch of *WMAP* we entered the high-precision era of cosmology, and the story of fluctuations went from being purely theoretical to become observationally quantitative. This

²<http://map.gsfc.nasa.gov/>, April 2012.

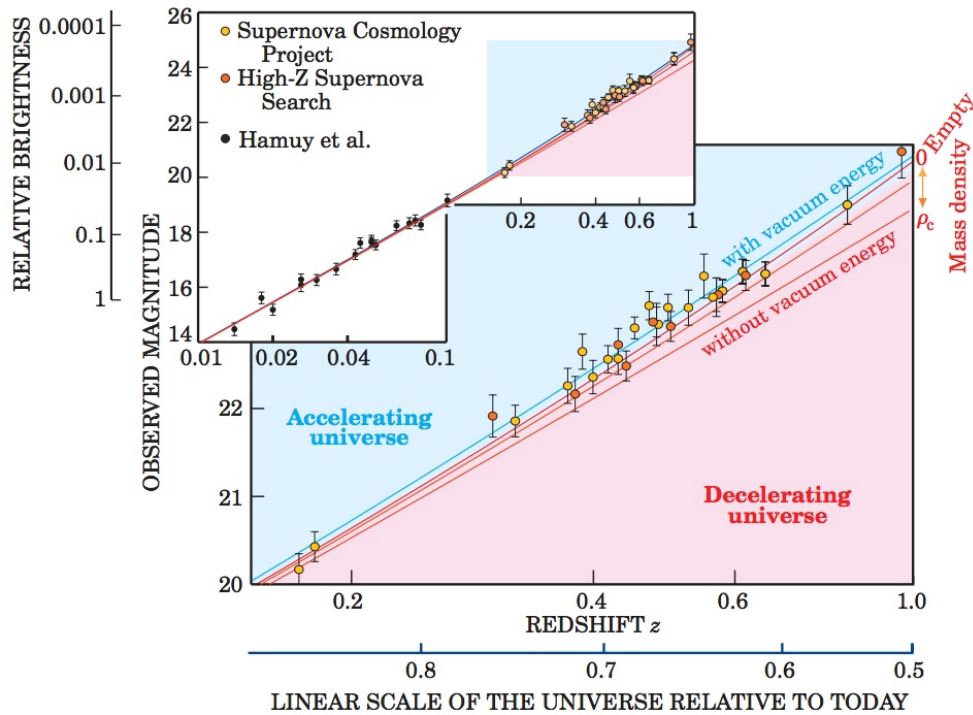


Figure 1.3: Experimental data taken in 1998 for different values of redshift favours cosmological models where vacuum energy (dark energy) contributes to the total energy density in the universe. The plot is taken from an article written by Saul Perlmutter which appeared in *Physics Today* [5].

understanding builds up the *early universe cosmology*.

Second, observations starting in 1998 from supernovae type IA showed that the universe today is undergoing an accelerated expansion [13, 14, 15]. As standard candles, these supernovae are important tools to measure cosmological distances, which made this discovery possible. This was a rather unexpected result. We would naturally expect that all the matter in the universe would cause the expansion to slow down. To explain this strange behaviour we have put forward the existence of a mysterious force that, against gravity, drives cosmological structures apart, faster and faster. To understand this “dark energy” component in the Cosmos is one of the main goals of the *late universe cosmology*.

It is no accident that both these events have earned the recognition of the Nobel Committee. Both branches of cosmology have brought together a global effort to understand our universe’s history, from the early times to today. In this thesis we will focus on the universe at

early times.

The CMBR is the oldest memory of the 13.7 billion year-old universe we live in. It is indeed the only fossilized record of microphysics in the early universe which shows evidence of a young, vibrant universe. The CMBR is the first light in the universe and its fantastic journey started at the surface of last scattering, when the universe was about 380,000 years old. We measure the anisotropies in the CMBR as fluctuations in temperature, against an almost uniform temperature field. The statistics in the temperature field can in turn be used to trace back what mechanism generated them. To understand the origin of these fluctuations in the temperature field, we need to discuss *inflation*.

1.1 FLRW cosmology

Cosmology is based on the simple observation that the universe at large scales is roughly homogeneous and isotropic. This is known as the *Cosmological Principle*. To describe it we assume a Friedmann–Lemaître–Robertson–Walker space-time, given by the line element

$$ds^2 = g_{\mu\nu} dx^\mu dx^\nu = -dt^2 + a^2(t) \left(\frac{dr^2}{1 - kr^2} + r^2 d\Omega_{\mathcal{S}^2}^2 \right), \quad (1.1)$$

where t is the cosmological time, a is the scale factor, k measures the spatial curvature, and $d\Omega_{\mathcal{S}^2}^2$ denotes the line element of a 2–sphere. The spatial sections of the 4-dimensional metric (1.1) are homogeneous and isotropic. This asserts that wherever we look in the sky, at large scales, we observe more or less the same temperature field distributions. Different values of curvature k correspond to different geometries: $k = 0$ corresponds to flat space, $k = -1$ corresponds to a 3–dimensional hyperboloid, and $k = 1$ corresponds to a 3–sphere. In Cartesian coordinates, for $k = 0$, the line element above reduces to

$$ds^2 = -dt^2 + a^2(t) d\mathbf{x}^2. \quad (1.2)$$

Conventions.—In this thesis we use Greek letters $\{\mu, \nu, \dots\}$ to denote space-time indices, whereas Roman letters $\{a, b, \dots\}$ are used for spatial indices. Equations are written in natural units, $c = 1 = \hbar$, and the reduced Planck mass, $M_p \equiv (8\pi G)^{-1/2}$, is set to unity. The space-time metric is written as $g^{\mu\nu}$ and the signature is mostly plus $(-, +, +, +)$. ∇ denotes the space-time covariant derivative, and ∂ represents a spatial derivative. Dots denote differentiation with respect to cosmological time, whilst primes denote differentiation with respect to conformal time (except when explicitly said otherwise).

It is usually assumed that the content of the universe can be represented by a perfect fluid. The energy-momentum tensor for a perfect fluid with energy density ρ and pressure density p is given by

$$T^{\mu\nu} = (\rho + p)U^\mu U^\nu + p g^{\mu\nu} , \quad (1.3)$$

where U^μ is the 4-velocity of the fluid. If such fluid is at rest in a geometry given by Eq. (1.1), and obeys the equation of state $p = w\rho$, then from the covariant conservation of the energy-momentum tensor, we can find that

$$\frac{d\rho}{dt} + 3H(1+w)\rho = 0 , \quad (1.4)$$

where $H \equiv \dot{a}/a$ is the Hubble parameter which quantifies the rate of growth of the scale factor.

The solution to the continuity equation (1.4) is

$$\rho \sim a^{-3(1+w)} . \quad (1.5)$$

For pressure-free matter, as the universe expands the energy density is diluted $\rho \sim a^{-3}$, whereas for radiation $\rho \sim a^{-4}$. An interesting behaviour occurs for $w = -1$, which corresponds to a fluid with negative pressure. In this case, the energy density is constant as the universe changes size. Nothing we know on Earth behaves this way. We will come back to this odd feature shortly.

The dynamics of the scale factor is controlled by Friedmann's equation

$$H^2 = \frac{\rho}{3} - \frac{k}{a^2} , \quad (1.6)$$

which depends on the total energy density and on the curvature of the spatial slices. Eqs. (1.4) and (1.6) are the fundamental equations for the dynamics of the scale factor, and imply Raychaudhuri's equation

$$\frac{\ddot{a}}{a} = -\frac{\rho}{6}(1 + 3w) . \quad (1.7)$$

For a universe mostly made of baryonic matter it is clear that the expansion has a *negative* acceleration. However, the present accelerated expansion means that the energy density of the universe is dominated by atypical matter, so that $w < -1/3$. This determines the equation of state of a fluid which generates repulsive gravity.

Energy density parameter.—To consider several possible contributions to the energy density in the universe, it is common to define the density parameter

$$\Omega_i \equiv \frac{\rho_i}{\rho_C} , \quad (1.8)$$

where ρ_C is the critical energy density for which the universe is flat. From Eq. (1.6) we find that $\rho_C = 3H^2$. We can write the total density parameter as a sum over the contributions from the individual fluids which build up the total energy density in the universe:

$$\Omega \equiv \sum_i \Omega_i . \quad (1.9)$$

In terms of this parameter, the Friedmann equation takes the form

$$H^2 = H_0^2 \left(\sum_i \Omega_i a^{-3(1+w_i)} + \Omega_k a^{-2} \right) , \quad (1.10)$$

where we are using the usual subscript '0' to denote evaluation at the present time, when by

convention $a(t_0) \equiv a_0 = 1$. Above we defined $\Omega_k = -k/H_0^2$ to be the density parameter of the curvature. Evaluating this equation today, we get

$$\sum_i \Omega_i + \Omega_k = 1 . \quad (1.11)$$

This has a simple consequence: if the curvature of the universe is observationally very small, that means that

$$\sum_i \Omega_i \equiv \Omega \approx 1 . \quad (1.12)$$

Writing the equations in terms of Ω will prove to be particularly useful when discussing the flatness problem of the Hot Big Bang paradigm.

Conformal time.—It is often convenient to define conformal time

$$\tau = \int \frac{dt}{a(t)} , \quad (1.13)$$

which runs from $-\infty$ to 0. In these coordinates, the beginning of time $t = 0$ corresponds to taking the limit when τ tends to $-\infty$. In terms of this time variable, the comoving distance travelled by a particle corresponds to the distance measured as if we neglected the expansion of the universe. Light rays will propagate in straight lines in the (τ, \mathbf{x}) space at 45° . In this case, the geometry in flat FLRW space becomes much simpler

$$ds^2 = a^2(\tau)(-d\tau^2 + d\mathbf{x}^2) . \quad (1.14)$$

We see that the metric tensor $g^{\mu\nu}$ is conformally related to the Minkowski metric, $\eta^{\mu\nu}$, via the scale factor, a , which is evolving in time.

In conformal time, Friedmann's equation becomes

$$\mathcal{H}^2 \equiv a^2 H^2 = a^2 \left(\frac{\rho}{3} - \frac{k}{a^2} \right) , \quad (1.15)$$

and Raychaudhuri's equation can be written as

$$\mathcal{H}' = -\frac{\rho a^2}{3}(1 + 3w) , \quad (1.16)$$

where the prime denotes derivative with respect to conformal time and \mathcal{H} is the Hubble parameter defined in conformal time.

1.2 Big Bang Model

Homogeneity and isotropy offer a very simple description of the universe on large scales. However, it brings conceptual problems to the Hot Big Bang paradigm when the universe is composed by conventional sources of matter, which we briefly describe next.

The flatness problem.—Cosmological observations show that the universe is approximately flat today, with k being almost zero. What are the implications of this observation? From Eq. (1.15) we find

$$\Omega - 1 = k\mathcal{H}^{-2} . \quad (1.17)$$

We can show that the density parameter obeys the differential equation

$$\frac{d\Omega}{dt} = 2Hq(\Omega - 1) , \quad (1.18)$$

where $q \equiv -\ddot{a}/\dot{a}^2$ is the deceleration parameter. This equation governs the time evolution of the density parameter, which for non-vanishing values of H and q , indicates that Ω will generically be different from unity, unless $\Omega = 1$ exactly always. Also, differentiating Eq. (1.17) with respect to conformal time and using Eq. (1.16), we obtain

$$\frac{d \ln \Omega}{d\tau} = (1 + 3w)\mathcal{H}(\Omega - 1) . \quad (1.19)$$

Since Ω today is very close to 1, writing $\Omega = 1 + \delta$, with $|\delta| \ll 1$, the last equation takes the

form

$$\frac{d \ln \delta}{d\tau} = (1 + 3w)\mathcal{H} . \quad (1.20)$$

The solution to this equation is

$$\delta(\tau) = \delta_0 \exp \left\{ (1 + 3w) \int_{\tau_0}^{\tau} \mathcal{H}(\tilde{\tau}) d\tilde{\tau} \right\} . \quad (1.21)$$

For fluids with $w > -1/3$, which in fact correspond to the baryonic matter and radiation we are familiar with, a universe with vanishing curvature presents a serious initial value problem— $k = 0$ is not an attractor solution. With Ω diverging exponentially from unity, there is nothing that stops the universe from having a large curvature.

Another way of looking at this problem is to rewrite Eq. (1.17) as

$$\Omega^{-1} = 1 - \frac{3k}{\rho a^2} = 1 - \frac{3k}{\rho_0} a^{1+3w}(t) . \quad (1.22)$$

We observe that Ω indeed grows away from unity unless k is fine-tuned to be extremely close to 1 initially (under the assumption that the strong energy condition³, $w > -1/3$, is obeyed). A conservative approach based on observations of our universe today, suggests that at the time of the Big Bang nucleosynthesis [16]

$$|\Omega_{BBN} - 1| \lesssim 10^{-16} .$$

Whilst it is possible that Ω started extraordinarily close to 1, it does require fine-tuning if the universe is dominated by baryonic matter and radiation—this is the essence of the *flatness problem*.

The horizon problem.—Wherever we look in the sky, the temperature is almost the same, up to very small differences. But why? Looking at two points which are separated by an angular distance larger than 2° , these points could not have been in causal contact and therefore they

³The strong energy condition asserts that $\rho + 3p > 0$.

could have not shared any information. Yet, their temperature is almost the same.

To understand this problem better, it is useful to phrase the discussion in terms of the *comoving particle horizon*. This is defined as the maximum comoving distance light could have travelled since the universe was born, when $\tau \rightarrow -\infty$:

$$d_{ph} = \int_0^t \frac{d\tilde{t}}{a(\tilde{t})} = \int_0^a \frac{d\tilde{a}}{\tilde{a}^2 H} . \quad (1.23)$$

It follows that events cannot be in causal contact when their distance is larger than the diameter of the comoving particle horizon. For the discussion that follows, it is useful to write the comoving particle horizon in terms of the comoving Hubble radius, which evolves in time. We rewrite Eq. (1.23) as

$$d_{ph} = \int_0^a d \ln \tilde{a} (\tilde{a} H)^{-1} . \quad (1.24)$$

From Eq. (1.10), we observe that d_{ph} increases monotonically in time for $w > -1/3$:

$$d_{ph} \sim a^{\frac{1}{2}(1+3w)} .$$

This has a puzzling consequence: scales which are entering the horizon now, were far outside the horizon when the universe became transparent—so, how can causally independent regions have the same temperature? This is the *horizon problem*.

The relics problem.—We know the early universe consisted of a hot, dense plasma, which was first dominated by radiation, and latter by baryonic matter. Tracing back the history of the universe, we would expect all the fundamental forces in Nature—electromagnetic, gravitational, weak and strong—to be unified. As the temperature dropped, presumably a GUT phase transition would occur, which would break the symmetry amongst all the forces in Nature. Such transition would have occurred at energies of order 10^{16} GeV, at which topological defects would have been produced. These would have an energy density at present far higher than that observed.

Since this expectation is in conflict with observations, monopoles and cosmic strings are usually called unwanted relics. We would therefore like to explain how these relics became so extraordinarily diluted.

1.3 Inflationland

Although there is still some debate about the origin of perturbations, inflation is the most popular description of what we believe was a dramatic event in the history of the universe. In the inflationary picture, when the universe was just a small fraction of a second old, it underwent a spectacular expansion phase, which pushed cosmological scales far outside the horizon. During this period space itself was expanding at a speed greater than that of the light. This simple idea has important insights when we try to explain the temperature distribution in the microwave sky.

So why is inflation such a good idea? Inflation not only provides a mechanism by which the problems of the standard cosmological model are ameliorated. When combined with Quantum Mechanics, it also explains the origin of the temperature perturbations in the sky and the seeds of large scale structure. It relates the physics of the very small and the very large. It does this by assuming a very simple hypothesis: if the expansion rate of the universe was accelerated,

$$\ddot{a} > 0 , \tag{1.25}$$

for at least 60 e-folds, then the comoving Hubble radius decreased in time:

$$\frac{d}{dt}(aH)^{-1} < 0 . \tag{1.26}$$

Therefore the observable universe went from being inside to outside the horizon by the time inflation ends.

To understand how inflation worked, we focus our attention in Eq. (1.23). If, during infla-

tion, the Hubble parameter H is roughly constant, then the comoving Hubble radius $(aH)^{-1}$ decreases in time. The largest contribution to the integrand in Eq. (1.23) arises at early times, when scales were in causal contact, although they do not appear in causal contact now.

We see that the accelerated expansion of the universe requires the strong energy condition to be broken, and that at those early times the energy density in the universe was dominated by a fluid with equation of state

$$w \equiv \frac{p}{\rho} < -1/3 .$$

The original formulation of inflation was put forth by Alan Guth in 1980 [17] and marks an exploration into ‘inflationland.’ Let us see how it can ameliorate the problems in the cosmological model.

First, the flatness problem. From Eq. (1.22) it follows that if $w < -1/3$, then the evolution of Ω dictates it should reach the attractor solution $\Omega \rightarrow 1$. Even if the curvature in the early universe was large, it would be greatly diluted away by the accelerated expansion.

Second, the horizon problem. This puzzle is resolved when we use the fact that the comoving Hubble radius decreased during inflation. This means that scales that re-enter the horizon after inflation ended, were *once* inside the horizon—they were therefore once in causal contact. With this assumption, there is no surprise in the universe being composed of incredibly homogeneous patches even at large angular separations.

Finally, with inflation relics are naturally diluted away since the accelerated expansion induces a dramatic decrease in the energy density of relic particles and topological defects.

With this positive outcome of assuming that a period of inflation took place in the early universe, let us explore this epoch more deeply. If the Hubble parameter H varies very slowly in time, then a period of quasi-de Sitter inflation is possible. In the limit when H is strictly a constant, it follows that

$$a \sim e^{Ht} . \tag{1.27}$$

This can be described by a fluid with equation of state $w = -1$, and the scalar field associated

with it is called the *inflaton*. The inflaton is a field whose energy density dominates the total energy density in the early universe, and generates an exponential expansion of the scale factor. To describe such period one usually introduces a slow-roll parameter, defined by

$$\varepsilon \equiv -\frac{\dot{H}}{H^2} , \quad (1.28)$$

which must obey $\varepsilon \ll 1$. For inflation to be efficient, one generically requires at least 60 e-folds of expansion, where the e-folding number

$$N \equiv \int_{a_i}^{a_f} d \ln a = \int_{t_i}^{t_f} H(t) dt \quad (1.29)$$

is a measure of the expansion of the size of the universe, from a_i to a_f . Its usefulness as a unit of time was first noticed in a paper by Sasaki & Tanaka [18]. To ensure that ε stays very small during inflation, one introduces a further slow-roll parameter

$$\eta \equiv \frac{\dot{\varepsilon}}{\varepsilon H} , \quad (1.30)$$

which is required to obey $|\eta| \ll 1$.

1.3.1 A simple inflation model

Which fluid with negative pressure could have sourced inflation? It certainly could not have been radiation or baryonic matter, for which the pressure is positive definite. To answer this question, let us take the simplest inflation model, involving only one scalar field, the inflaton, which we assume is homogeneous. This model is described by

$$S = \int d^4x \sqrt{-g} \left\{ \frac{1}{2} R - \frac{1}{2} (\partial \phi)^2 - V(\phi) \right\} . \quad (1.31)$$

In this action ϕ is only minimally coupled to the curvature of space-time. The scalar field has a canonical kinetic term and is subject to a self-interacting potential, $V(\phi)$. Different models have different potentials. For now, we will assume an arbitrary $V(\phi)$.

A typical example is depicted in the following schematics.

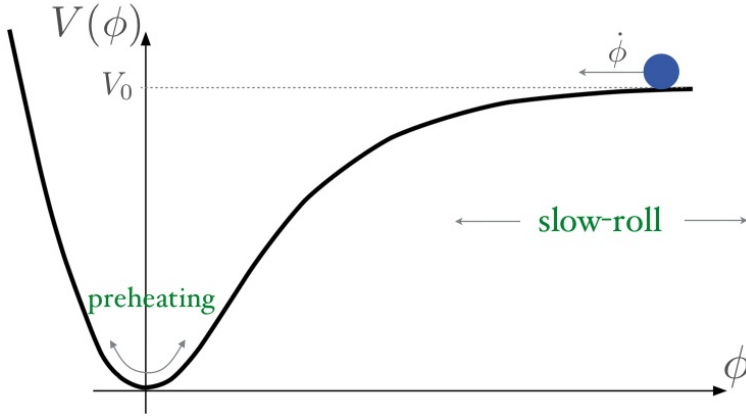


Figure 1.4: Simple (small-field) inflation potential and the dynamics of inflation.

During the slow-roll phase, the universe is inflating, and the potential is roughly constant, V_0 . This will be true until the potential energy of the scalar field ϕ no longer dominates the energy density in the universe, and is unable to source an accelerated expansion.

When this happens, the inflaton field speeds up and approaches the minimum of the potential. It then starts oscillating about the minimum, producing matter particles in the process, if it is coupled to other degrees of freedom. This process is called *reheating*, and we will study it in detail in chapter 6. To understand the slow-roll approximation better, we write the equations of motion for the scalar field. Assuming an FLRW background (1.1), these are

$$\ddot{\phi} + 3H\dot{\phi} + \frac{\partial V}{\partial \phi} = 0 . \quad (1.32)$$

The energy-momentum tensor can be found by varying the action (1.31) with respect to the metric tensor, giving

$$T_{\mu\nu} = \partial_\mu \phi \partial_\nu \phi - g_{\mu\nu} \left\{ \frac{1}{2} (\partial \phi)^2 - V(\phi) \right\} . \quad (1.33)$$

Interpreting the components of the energy-momentum tensor as those of a fluid, we find that

the energy density and pressure are given by

$$\rho = \frac{1}{2}\dot{\phi}^2 + V(\phi) \quad (1.34a)$$

$$p = \frac{1}{2}\dot{\phi}^2 - V(\phi) . \quad (1.34b)$$

As a result, the fluid has equation of state $w = -1$ if one neglects the kinetic energy compared to the potential energy. Moreover, if the potential is approximately constant then the energy density in Friedmann's equation (1.6) is roughly constant, sourcing a de Sitter universe, and

$$3H^2 \simeq V_0 . \quad (1.35)$$

This can be interpreted upon inspection of the action (1.31). If $V(\phi) \simeq V_0$ the energy density of the fluid acts as a cosmological constant and effectively sources inflationary expansion. Guth referred to this as the “ultimate free lunch” since despite the expansion of the universe, the energy density of the fluid was kept constant, as if it were sourcing it out of nothing.

The slow-roll approximation asserts that we can neglect the second time derivative of the field in Eq. (1.32) compared to the first time-derivative. Then

$$\ddot{\phi} \approx -\frac{1}{3H} \frac{\partial V}{\partial \phi} . \quad (1.36)$$

In terms of the features of the potential, we can also define the slow-roll parameters as follows:

$$\epsilon_V = \frac{1}{2} \left(\frac{\partial V / \partial \phi}{V} \right)^2 \quad \text{and} \quad (1.37a)$$

$$\eta_V = \frac{\partial^2 V}{\partial \phi^2} . \quad (1.37b)$$

These coincide with the definitions (1.28) and (1.30) up to slow-roll corrections. We observe that the requirements $\epsilon, |\eta| \ll 1$ translate into a potential that is almost flat for a large range

of ϕ , making its curvature very small. This is the slow-roll period illustrated in figure 1.4.

Slow-roll inflation lasts until $\varepsilon \sim 1$ and the kinetic energy of the scalar field becomes comparable to the potential energy—the potential becomes steeper and the scalar field speeds up, as described above. It is during the slow-roll phase that the scalar field fluctuations become imprinted in the CMBR—we will discuss this in detail in §1.3.3.

1.3.2 Beyond the simplest inflation models

Inflation offers a simple, dynamical solution to the cosmological problems, but the exact mechanism driving the process of inflationary expansion is still rather speculative. This is because the precise physics of inflation is essentially unknown and it is a matter of dispute whether we will ever be able to fully understand it.

Traditionally, we start with the simplest scenarios, like the action (1.31). We then add more ingredients to the action and try to understand their distinctive signatures in the CMBR in the hope to be able to distinguish between them once appropriate observational data is available. There are a number of ways of generalising the action (1.31). In what follows we mention some of the possible extensions.

- i. *inflation with modified gravity*. This can be achieved by assuming a non-minimal coupling to the curvature scalar. These are the so called scalar-tensor theories, described by

$$S = \int d^4x \sqrt{-g} \left\{ \frac{f(\phi)}{2} R - \frac{1}{2} (\partial\phi)^2 - V(\phi) - \mathcal{L}_{mat} \right\}, \quad (1.38)$$

where \mathcal{L}_{mat} defines the Lagrangian density of the matter sector. This action can be rewritten in the form of Einstein's gravity by performing a conformal transformation

$$g_{\mu\nu} \rightarrow \Omega^2(t, \mathbf{x}) g_{\mu\nu}$$

where the conformal factor is appropriately chosen [19]

$$\Omega^2 = f(\phi) .$$

After applying this transformation to the action (1.38), we say the theory of gravity is written in the Einstein frame. With this transformation, the space-time curvature is modified and the Ricci scalar becomes [20]

$$R \rightarrow \frac{1}{\Omega^2} \left\{ R + 6 \frac{\square \Omega}{\Omega} \right\} ,$$

with \square being the d'Alembertian, $\square \equiv \frac{1}{\sqrt{-g}} \partial_\mu (\sqrt{-g} g^{\mu\nu} \partial_\nu)$. To write the action in a more canonical way, we can further apply field redefinitions

$$d\phi \rightarrow \sqrt{\frac{2f + 3f'^2}{4f^2}} d\phi \quad \text{and} \quad V \rightarrow \frac{V}{f^2} ,$$

where $f' \equiv \partial f / \partial \phi$. Given these transformations, the action becomes

$$S = \int d^4x \sqrt{-g} \left\{ \frac{1}{2} R - \frac{1}{2} (\partial \phi)^2 - V(\phi) - \tilde{\mathcal{L}}_{mat} \right\} , \quad (1.39)$$

with $\tilde{\mathcal{L}}_{mat}$ denoting the modified matter Lagrangian density. Therefore, the modification of gravity observed in the action through the function $f(\phi)$ appears in the Einstein frame as a modification of the original Lagrangian of the matter sector. Nevertheless, whatever frame is chosen, the physics should stay the same. These theories have gained interest in recent years in the light of chameleon field theories (see, for example, Ref. [21]).

Other possibilities which fall under this class exist: Jordan–Brans–Dicke theory of gravity [22] (which also includes non-canonically normalized scalar fields), $f(R)$ gravity [23] (which can include higher powers of the Ricci scalar), and modified gravity in braneworld scenarios [24]. For a recent review on modified gravity theories and its cosmological

implications see Ref. [25].

- ii. *inflation with non-canonical kinetic terms*. This class of theories also goes by the name of k -inflation [26]. In contrast with the action (1.31) it is not the potential energy of ϕ that supports a de Sitter phase, but rather the non-canonical structure of the kinetic term. The action takes the form

$$S = \int d^4x \sqrt{-g} \left\{ \frac{1}{2} R + P(X, \phi) \right\}, \quad (1.40)$$

and it was initially proposed by Armendáriz-Picón, Damour & Mukhanov. Here $P(X, \phi)$ is an arbitrary function of the field profile ϕ and its first derivatives through $X \equiv -(\partial\phi)^2$. We recover action (1.31) by choosing $P(X, \phi) = -1/2(\partial\phi)^2 - V(\phi)$; more generically this action reproduces different models for different choices of the function $P(X, \phi)$. Without loss of generality, we can write

$$P(X, \phi) = \sum_n c_n(\phi) \frac{X^n}{\Lambda^{4n-4}}, \quad (1.41)$$

where Λ denotes some high-energy scale. Slow-roll inflation is obtained when $\Lambda^4 \gg X$.

This action will play an important rôle in this thesis and we will explore its phenomenology in detail in the subsequent chapters. Here, we shall only mention that it can support inflation even in the presence of very steep potentials. The most striking general feature of the non-canonical models, however, is that the inflationary dynamics and the consequences for observables becomes quite non-trivial. This corresponds to the limit $\Lambda^4 \sim X$ in Eq. (1.41). This limit raises one concern: radiative corrections can induce large renormalizations of the coefficients $c_n(\phi)$, which can lead to a ill-defined quantum field theory. In this case, only if the theory is equipped with a protective symmetry can we escape the problem of radiative instability. Of all the higher derivative single-field models, Dirac–Born–Infeld [27] and galileon inflation [28] are the only established examples where non-renormalization theorems apply. We will be more precise about this statement in the subsequent chapters.

Whether these are the only radiatively stable models is a very different query—we have nothing to say about this in this thesis. We are rather interested in understanding what are the consequences for observables of taking a generalised $P(X, \phi)$ action.

iii. *multi-field inflation*. In this case, there are multiple sectors in the action in addition to the inflaton field. This is a generic feature of the theory when embedding inflation in a more fundamental parent framework, like string theory. Indeed, effective field theories (examples of work in this area are Refs. [29, 30, 31]) and supergravity theories (see, for example, Refs. [32, 33]) usually contain multiple degrees of freedom. If all the fields play a rôle in the inflationary dynamics, then a single-field effective picture is not possible and the dynamics becomes more intricate than any single-field inflation model. Early studies of models involving more than one degree of freedom include works by Linde [34], Kofman & Linde [35], and Silk & Turner [36].

In this thesis we will focus on the perturbation theory of generalised single-field models, starting from the action (1.40). We will not attempt to investigate multi-field inflation models or modified gravity models in the sense described above, although galileon models arise naturally in the decoupling limit of massive gravities [37, 38, 39]—we will discuss these in chapters 3 and 4.

1.3.3 Seeding perturbations

We now turn to the question of how inflation can microscopically explain the origin of Large Scale Structure (LSS). For this we need to consider the quantum-mechanical behaviour of the ‘single-clock’ in the universe during inflation. Such rôle is played by the inflaton field which sets the initial conditions for the evolution of perturbations, as originally explained by Guth & Pi [40], Hawking [41], and Bardeen, Steinhardt & Turner [42].

Let us first revisit figure 1.4 of a typical schematics of a single-field inflationary model.

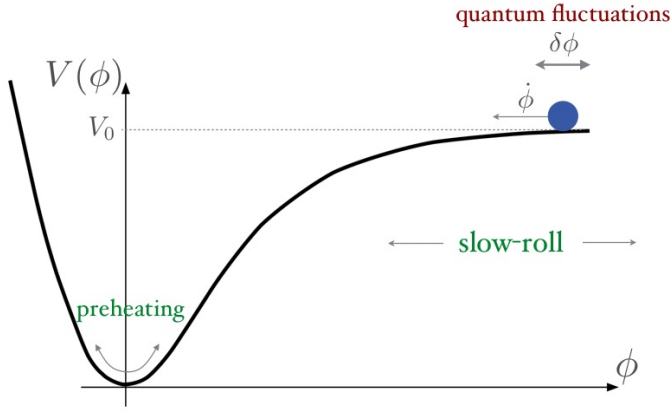


Figure 1.5: As inflation proceeds, the inflaton undergoes quantum fluctuations which are the seeds for density perturbations.

Going back to the idea that during inflation the comoving Hubble radius decreases, then quantum fluctuations with origin on sub-horizon scales will exit the horizon. While on super-horizon scales, such fluctuations freeze until they are able to re-enter the horizon at late times.

So how do the quantum fluctuations translate into fluctuations in the density field, which can then respond to the gravitational pull and form bound structures? Once created, the small, inhomogeneous inflaton perturbations, $\delta\phi(t, \mathbf{x})$, will induce slightly different arrival times of the expectation value ϕ at the bottom of the potential $V(\phi)$. As can be seen in the figure, regions in space where $\delta\phi$ is positive will remain potentially dominated for longer, whereas regions where $\delta\phi$ is negative will stop inflating sooner. Since ϕ is the only available clock in the universe (in single-field models), we can say that fluctuations $\delta\phi$ control the time differences at which inflation ends through

$$\delta t = \frac{\delta\phi}{\dot{\phi}} \sim \frac{H}{\dot{\phi}}, \quad (1.42)$$

where hypersurfaces of constant time are also hypersurfaces of constant energy density, and therefore constant H . After inflation ends and reheating proceeds, $H \sim 1/t$, and fluctuations in the expansion rate of the universe are mapped into density inhomogeneities, as follows

$$\frac{\delta t}{t} \sim \frac{\delta H}{H} \sim \frac{\delta\rho}{\rho} \sim H \frac{H}{\dot{\phi}}. \quad (1.43)$$

This way, the inflaton quantum perturbations seeded structure during the early universe,

which have later grown to form galaxies and clusters. What is most impressive still is that the small inhomogeneities produced during inflation were imprinted in the early plasma, which cooled down and became the CMBR after photon decoupling. Today we observe these imprints in the microwave sky as temperature anisotropies, which produce the beautiful map depicted in figure 1.2.

1.4 Λ CDM: the concordance model

Measuring observables faces a tremendous challenge: degeneracy. Given a set of data, different observables can compete and their effect might be so tied up in our measurements, that it is hard to find constraints for each individual observable. To attempt to solve for this pressing problem, cosmologists need to have access to various, often complementary, sets of data.

The BOOMERanG (Balloon Observations Of Millimetric Extragalactic Radiation and Geophysics) experiment⁴ measured in 1997 the CMBR anisotropies, determining the value of Hubble's constant, H , and the fractional density of the universe, Ω . It has also provided evidence in agreement with supernovae data on the present accelerated expansion, as announced in Refs. [43, 44]. Other experiments include SDSS (Sloan Digital Sky Survey)⁵, which is a ground-based telescope, that targets quasars and galaxies distributions, and places constraints on the cosmological parameters.

The best fit for the content of the universe today given by *WMAP* and BAO⁶ data [6, 7] is in table 1.1. The concordance model results from a significant component of the energy density in the universe being a cosmological constant, hence the name Λ CDM.

Observations indicate that the universe is made up of four basic components: radiation, dark matter, baryonic matter, and cosmological constant (or dark energy). The largest component is dark energy with a proportion of about 73% of all there is. Most of the universe is

⁴<http://cmb.phys.cwru.edu/boomerang/>, April 2012.

⁵<http://www.sdss.org/>, April 2012.

⁶BAO stands for Baryonic Acoustic Oscillations.

made up of something we cannot see and do not understand—we are only familiar with 4% of the entire universe’s budget. All the matter, m , in the universe is either baryonic matter, b , or cold dark matter c :

$$\Omega_m = \Omega_b + \Omega_c .$$

Including supernovae data, cosmologists have learnt that the dark energy has equation of state

$$w_\Lambda = -0.980 \pm 0.053 .$$

The data undeniably points to a flat universe.

parameter	best fit (mean)
Ω_b	0.0458 ± 0.0016
Ω_c	0.229 ± 0.015
$\Omega_\Lambda h^2$	0.725 ± 0.016
Ω_k	$-0.0133 - 0.0084$
$\Omega_m h^2$	0.1352 ± 0.0036
H_0	$070.2 \pm 1.4 km/s/Mpc$
t_0	$13.76 \pm 0.11 Gyr$

Table 1.1: The content of the universe given by direct measurements and induced parameter values obtained from *WMAP* & BAO data [6, 7]. t_0 denotes the age of the universe.

We have intentionally removed all the data related to the CMB anisotropies since we will discuss it in the next chapters.

1.5 *Planck*: the ultimate ‘thermometer’

As described before, the last few decades have seen remarkable advances in cosmology. These were only made possible owing to an unparalleled progress in observational cosmology. In May 2009 the *Planck* satellite⁷ was launched in an attempt to exhaust the amount of information one could extract from the CMB.

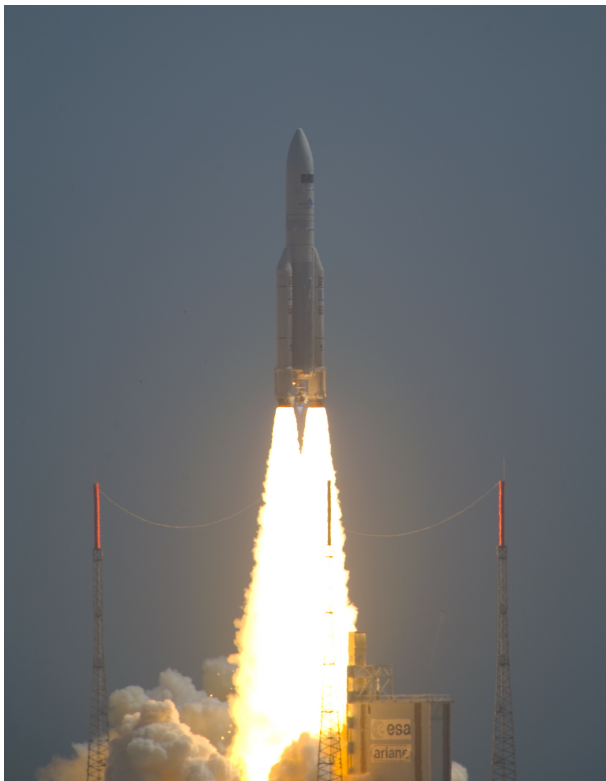


Figure 1.6: The launch of the *Planck* satellite and the Herschel telescope by Ariane 5 (image courtesy of ESA-CNES-Arianespace, Optique Vidéo du CSG, P Baudon).

One of the main objectives of this mission was to enable a rigorous test of the early universe models against observation. The sensitivity of the temperature measurements that *Planck* offers is simply staggering: one part in one million. Having a direct focus on the detection of primordial gravitational waves and specification of its spectrum, *Planck* will also allow the most detailed study of the scalar spectrum of perturbations yet performed. In particular, with *Planck* we expect to obtain very precise data on the higher-point correlations of the temperature field, which we can map backwards to draw the features of the primordial curvature perturbation.

It is anticipated that the major problem in analysing data will be to efficiently remove the foreground. It is therefore quite likely that *Planck* will turn out to be the end of the line in the generation of high-precision satellites. *Planck* will be able to distinguish between different types of inflationary models, and it is the most promising guide to understand the early

⁷<http://www.esa.int/SPECIALS/Planck/index.html>, April 2012.

universe. Among its many goals, it aims at unveiling the microphysics of inflation, understanding what are the high-energy theories beyond those imprinted in the CMBR fluctuations, and learning more about dark energy. In particular, and focusing on inflation theories, it might measure non-zero non-gaussianity, which is a key observational feature since it works as a discriminator of microphysics.

The main object of study in the next four chapters will be the bispectrum, which is the lowest-order non-gaussian statistics component, and therefore potentially easier to observe (than higher-point statistics).

1.6 Summary of the outline of the thesis

In this thesis we explore the inflationary signatures of single-field models, and study how the universe would have reheated after a Dirac–Born–Infeld inflation phase. One of the key questions we aim to address is: how can we efficiently use *Planck*'s data to solve for the degeneracy in the inflationary models? By this we mean that several, distinct sets of parameters in a given theory can combine in such a way so as to produce the same predictions for observables. What we would like to know is how to build an efficient dictionary between observations and parameters of a theory.

We start by reviewing non-gaussianities in chapter 2, explaining how they encode blueprints of the inflationary models. We first focus on $P(X, \phi)$ theories and compute the amplitude of their bispectrum to next-order in slow-roll. We later generalise our results to the Horndeski class of models, which includes all theories that do not have propagating ghosts.

For some time now we suspect that the theoretical uncertainty in estimating the bispectrum is larger than the experimental errors [45]. If we expect to constrain the parameters of the theory using *Planck*'s data, one necessarily needs to push the theory-error down, otherwise the advantages of having high-precision measurements are not met. This can be done in much the same way as electroweak precision tests some decades ago, when physicists realised that

they had to control the theoretical inaccuracy of their calculations to be able to keep pace with the precision of their experiments (see, for example, the review by Altarelli et al. [46]). In chapter 3 we give a more accurate estimate of the bispectrum, by reducing the maximum theory-error by several tens of percent (around 95% in most cases).

In chapter 4 we present a careful analysis of the scale and shape-dependences of the bispectrum and we elaborate on its discriminatory power to tell inflationary models apart. We focus on bispectrum shapes, rather than the amplitude of the bispectrum, to make a most efficient use of empirical evidence of inflationary theories. In chapter 2 we will see that the bispectrum depends only on a handful of parameters, which requires finding an efficient algorithm to solve for this degeneracy. We argue that using templates (as commonly done in CMBR data analysis) might not be the most promising strategy to understand the early universe microphysics.

In chapter 5 we go beyond the slow-roll approximation, and ask the following question: what if inflation was not close to de Sitter? In that case, one could wonder whether the inflationary signatures in the CMBR would be different from those obtained and discussed in chapters 2, 3 and 4. We obtain estimates for the bispectrum under the assumption that the spectrum of perturbations is approximately flat, consistent with observational data. We comment on the implications for the scale-dependence of the bispectrum in these theories, and argue this behaviour can be explored using complementary observational tests.

Chapter 6 focuses on the study of preheating after a period of Dirac–Born–Infeld inflation. We study how matter particles could have been created and efficiently repopulated the universe. We comment on the implications of the reheating temperature in such theories.

Finally, in chapter 7 we review the main findings of this thesis and point out to possible extensions to future work. The appendices collect important material for the developments of the chapters in the main body of this thesis.

Part I
The Physics at Early Times

We choose to go to the moon in this decade and do the other things, not because they are easy, but because they are hard, because that goal will serve to organise and measure the best of our energies and skills, because that challenge is one that we are willing to accept, one we are unwilling to postpone [...]

John F. Kennedy

2

Non-Gaussianity in Inflationland

For a long time theoretical cosmology’s only exercise was to develop theoretical models which would one day be put to scrutiny against observations as working models of the early universe. We are living in an exciting era of precision cosmology where, perhaps for the first time, we can gather enough data with the appropriate resolution to test those models. This data might not be able to rule out some inflation models completely, as some degree of fine-tuning in model building can accommodate even unfavourable data. Nevertheless, it will certainly put some models under moderately high pressure. We will ultimately want to know what was the physics behind inflation, if inflation did indeed happen. Our best hope to learn about this mechanism is through non-gaussianities.

Outline.— We start by reviewing in §2.1 the work that has been done on non-gaussianities, regarded as the most promising discriminator of microphysics. This chapter therefore contains important review material, but also original work. In §2.2 we discuss the background model and specify our version of the slow-roll approximation. Results involving the lowest powers in slow-roll parameters will be called “leading-order,” whereas those involving one extra power in slow-roll will be referred to as “next-order,” and so forth. Our initial discussion will be focused on $P(X, \phi)$ models. In §2.2.2 we recapitulate the computation of the two-point function of

perturbations (including its explicit scale-dependence). We discuss the derivation of the third-order action for the primordial perturbation in §2.3, and based on recent developments, we extend our calculation to *all* single-field models which *do not* contain ghost-like instabilities. We give in §2.3.2 a brief description of the “in-in” (or Schwinger–Keldysh) formulation for expectation values, necessary to compute correlation functions.

This chapter includes material based on work done in collaboration with Clare Burrage and David Seery, published in Ref. [1].

2.1 Understanding non-gaussianities

As we discussed in the introduction to this thesis, our picture of the early universe has become much more precise with access to data with unparalleled sensitivity. This has been made possible with the advent of high-precision satellites, like *WMAP* and more recently *Planck*. If the temperature in the microwave sky was *perfectly* homogeneous, there would be little to know about the CMB, except that its spectrum was that of blackbody radiation. Fortunately this is not the case. Below is the microwave sky as seen by the *WMAP* satellite.

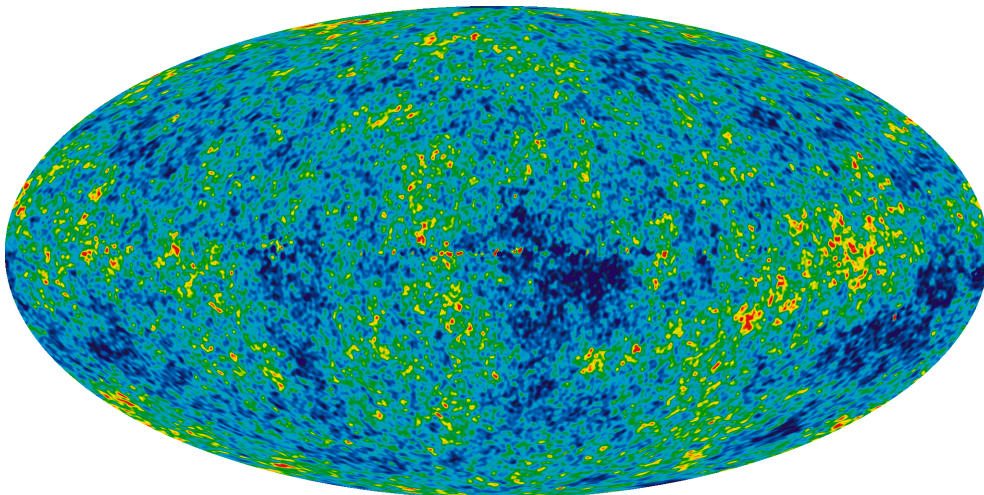


Figure 2.1: Detailed map of the microwave sky as seen by *WMAP*. This is a snapshot of the universe when it was only 380,000 years old.

The colours in this picture not only say that the microwave sky does not have the same temperature everywhere. They mainly tell us that there is a wealth of information encoded in the CMBR which is sensitive to the microphysics during inflation. It is in the way that the temperature in one point correlates with that in other points that we can learn about the inflationary mechanism. But how?

The CMBR is usually thought to have its origins in a primordial era [47] governed by quantum fluctuations. For a review on the numerous mechanisms for generation of quantum fluctuations during inflation see, for example, the book by Lyth & Liddle [16]. During inflation, cosmological scales were pushed outside the observable horizon. At the same time, quantum fluctuations were allowed to grow to later become classical far outside the horizon. In its simplest implementation, inflation forecasts an approximately scale-invariant, Gaussian distribution of perturbations [42, 48]. This means that fluctuations are only slightly stronger on larger scales (since the spectrum is red-tilted), and they are completely characterised by their two-point correlations (the power spectrum of perturbations). Although minimalist, these predictions are in good agreement with present-day observations, including *WMAP* 7-year data [49, 7, 6].

Given the recent improvement and sophistication of CMB experiments, we might now be able to detect non-zero three- and higher n -point correlations [50, 51]. These are globally known as *non-gaussianities* and they can be thought of as including important information about interactions within the inflaton sector, and others, during inflation. They are an intricate product of whatever inflationary process occurred in the early universe. Understanding and identifying the non-gaussian signatures in each inflationary model is comparable to producing an inflationary fingerprint, which can be later identified in the microwave sky. On the other hand, other constraints will soon emerge from the non-gaussian statistics of collapsed objects, using LSS data [52]. We therefore expect non-gaussianity constraints to arrive from different sets of data.

In principle, valuable information is encoded in each n -point function. In practice, ex-

tracting information from the four-point function is computationally challenging, as described in Refs. [53, 54]; it is also unclear whether data constraints associated with higher n -point functions can ever be used efficiently as model discriminators. For this reason, attention has focused on the three-point correlations, also known as the *bispectrum*. These are most usually cited in terms of a rescaled amplitude, f_{NL} [50, 51], although as we shall see in this thesis, there is a lot more information on the bispectrum, which can and should be used to draw constraints.¹ For a Gaussian field there is no extra information on higher n -point correlators, besides the one provided by the power spectrum, and $f_{\text{NL}} = 0$. This is the least desirable situation, which is also not excluded from present-day data.

Our work assumes there was only one active single scalar field, ϕ , during inflation and that its quantum fluctuations, $\delta\phi$, became imprinted in the CMB. The mapping we want to establish is that between a microphysical Lagrangian of perturbations and its correlation functions, $\langle\delta\phi^3\rangle$. Early references are the works by Starobinsky [55], Sasaki & Stewart [56] and Lyth & Rodríguez [57]. We now review some of the notable developments in this area.

2.1.1 Historical developments

The first calculations of correlators of quantum fluctuations $\delta\phi$ were presented shortly after the inflationary paradigm was proposed [42, 40, 41, 58, 59, 60, 61]. Results were obtained for the two-point functions of single-field inflation theories with canonical kinetic terms.

The possibility of producing non-gaussian fluctuations during inflation was first investigated by Allen, Grinstein & Wise in 1987 [62]. The first calculation of the three-point correlator of the temperature anisotropy dates as early as 1992 by Falk, Rangarajan & Srednicki [63], followed by other partial results [64, 65]. The complete three-point function was laid down in 2002 by Maldacena [66], in a paper which set up all the subsequent calculations of the bispectrum. Three-point correlators originated from multiple fields were originally calculated

¹The definition of f_{NL} will be presented in §3.1. For now it suffices to know that f_{NL} is a rescaled magnitude of the bispectrum.

by Seery & Lidsey [67]. Calculations of four-point correlations first appeared in Ref. [68] by Seery, Lidsey & Sloth, and Ref. [69] by Seery, Sloth & Vernizzi.

Maldacena’s epic calculation showed that f_{NL} would be unobservably small in single-field models with canonical kinetic terms. More precisely, $f_{\text{NL}} \sim r$, where r is the tensor-to-scalar ratio, constrained by observation to satisfy $r \lesssim 0.2$ [6]. Soon cosmologists turned their attention to more complicated realizations of single-field theories of inflation. Two classes of possibilities emerged: in effective field theories (see, for example, Ref. [70]) Lagrangians naturally contained high-order operators of derivatives of the scalar field, suppressed by some high-energy scale; in other theories the scalar field ϕ was not canonically normalised.

The first class of these was studied by Creminelli in 2003 [71], who concluded that if the dominant kinetic operator for the slowly rolling background field was of the form $(\partial\phi)^2$, then the three-point correlations of its perturbations were effectively indistinguishable from Maldacena’s simplest model [71]. This analysis relied on the slow-roll approximation. The result was that non-gaussianities in these models would disappointingly have negligible amplitude, and could not be used as a diagnostic tool.

Non-canonical models.—In theories where other operators than $(\partial\phi)^2$ are dominant, however, f_{NL} can become quite significant, depending on the precise form of the Lagrangian of the background theory. Examples of these more complicated scenarios are “ghost inflation” [72, 73], and Dirac–Born–Infeld (DBI) action [74]. In these models the scalar field action governing the dynamics of both background and perturbations can be written as

$$S = \frac{1}{2} \int d^4x \sqrt{-g} \left\{ R + 2P(X, \phi) \right\} , \quad (2.1)$$

where $X \equiv -(\partial\phi)^2$. The first term is the Einstein-Hilbert action involving the space-time Ricci scalar R , and $P(X, \phi)$ is an arbitrary function of ϕ and its first-derivatives through X . Because of the arbitrariness of P , these models can accommodate non-canonical kinetic structures.

In ghost-inflation, the kinetic term of ϕ has the wrong sign and the action contains several

$P(X, \phi)$ contributions among higher-order derivatives of ϕ , as follows

$$S = \int d^4x \sqrt{-g} \left\{ M^4 P_1(X) + M^2 P_2(X) (\Box \phi)^2 + M^2 P_3(X) \partial^\mu \partial^\nu \phi \partial_\mu \partial_\nu \phi + \dots \right\} ,$$

where P_1 , P_2 and P_3 are dimensionless functions of X (which is also dimensionless), M is some mass-scale and \dots represent higher derivative operators acting on ϕ . Since this action contains operators with more than one derivative acting on the scalar field, it gives rise to equations of motion which contain at least third-order derivatives of ϕ , signalling a ghost instability. Arkani-Hamed et al. showed that the solution of interest takes the form

$$\phi = ct ,$$

where c is some dimensionless constant. They also showed that this solution protects the theory against radiative corrections, even though the action contains non-renormalisable operators.

In contrast, in DBI inflation it is the presence of a higher-dimensional boost that protects the coefficients of the single derivative operators from large renormalisations. The action for the background field in this model takes the form

$$P(X, \phi) = -\frac{1}{f(\phi)} \left\{ \sqrt{1 - f(\phi) X} - 1 \right\} - V(\phi) ,$$

where $f(\phi)$ has units of $[\text{mass}]^{-4}$. The kinetic structure of ϕ is embedded in the non-analytic square root, which allows to sum an infinite number of powers of single derivative operators. We will review this inflation model in §3.4.1, and again in §6.2 from a brane-world perspective.

Related models based on “galileon” actions have also been obtained [28, 75, 76, 11]. “One of the reasons why these models raised so much interest was because they might leave fingerprints in the CMBR [77, 78]. ” A galileon singlet owes its name to invariance under the

transformation

$$\phi(x) \rightarrow \phi(x) + b_\mu x^\mu + c, \quad (2.2)$$

for constant b_μ and c , under which gradients of ϕ are shifted by a constant. Eq. (2.2) is a space-time version of a galilean transformation, first noticed in the Dvali–Gabadadze–Porrati (DGP) model [79, 80].

Galileons have recently become popular since they can be interpreted as longitudinal graviton modes near the decoupling limit of massive gravity, when $M_p \rightarrow \infty$, while the cutoff of the theory remains fixed [37, 38, 39]. From Eq. (2.2) we see that the galilean symmetry contains the shift symmetry $\phi \rightarrow \phi + c$, which means that if the background supports a de Sitter solution, then inflation can last for many e-folds, which can be problematic. For inflation to last 60 e-folds, the shift symmetry needs to be broken (even if only mildly). This is typically achieved by adding a potential. However, introducing a potential such as $V \sim m^2 \phi^2$ will manifestly break the galilean symmetry we started with. The absence of this special symmetry implies that the Lagrangian of the theory is no longer protected from other galilean violating terms generated via radiative corrections. As a result, one loses the motivation of starting with a Lagrangian which obeys the galilean symmetry in the first place. Nevertheless, it was shown by Burrage et al. [28] that a non-renormalisation theorem still operates, making the dangerous radiative corrections small. Therefore, despite these potential problems, galileon inflation sits, alongside DBI inflation, as one of the few known examples of a radiatively stable theory of inflation.

More recently a number of authors have rather focused on the much milder requirement that the Lagrangian preserved unitarity. The result would be a sensible quantum field theory [81, 75, 76, 82, 83, 84], where the Lagrangian operators give rise to equations of motion which are at most second-order in derivatives of the field. In these theories the galilean symmetry is lost [85] because it can no longer be realised in a generic space-time. These theories go often by the name “G–inflation,” although as we shall see in the end of this chapter, they can also be called “Horndeski” models.

Models in which the dominant operator of the background kinetic structure is different from $(\partial\phi)^2$ generically fall under the name of *non-canonical* theories. Eq. (2.1) was first suggested in 1999 by Armendáriz-Picón, Damour & Mukhanov [26], who named it “*k*-inflation” when applied to inflationary cosmologies. The corresponding two-point function for scalar perturbations was obtained in the same year by Garriga & Mukhanov [86]. Three-point correlations induced by (2.1) were investigated in 2004 by Gruzinov in a decoupling limit where the mixing with gravity fluctuations could be neglected [87]; gravitational interactions were included in the following year by Seery & Lidsey [88]. The bispectrum of these theories was given in generality by Chen et al. [45], followed by extensions to multiple fields [89, 90, 91]. The four-point function was also computed by a number of authors [92, 93, 94, 95, 96, 97].

2.1.2 Non-gaussianities in slow-roll inflation

In this chapter we revisit actions of the form (2.1) and reconsider the three-point function under the slow-roll approximation. We do this for two reasons: first, we review our present understanding of the bispectrum in $P(X, \phi)$ theories; second, we ask whether the estimates described in the literature are precise enough to be comparable with the high-sensitivity data soon to be delivered by *Planck*.

The analyses of the n -point correlators mentioned above assumed some sort of *slow-roll approximation* to control their calculations, usually by restricting their results to lowest powers of $\varepsilon \equiv -\dot{H}/H^2$ (or other quantities of similar magnitude, such as $\eta \equiv \dot{\varepsilon}/\varepsilon H$). We generically expect this procedure to yield estimates accurate to a fractional error of order ε , which in some models could be as large as 10^{-1} to 10^{-2} .² Whenever f_{NL} is small, as Maldacena showed in canonical models, this is indeed a very good approximation.

However, in models where f_{NL} is numerically large this might not be the case—a fractional error of order ε may be comparable to the sensitivity of *Planck*’s data, especially if the $\mathcal{O}(\varepsilon)$

²In Ref. [98] (see also Ref. [99]) the authors have studied the most likely values for ε and η in the context of brane inflation models. There $\varepsilon \lesssim 10^{-13}$. We will assume ε can be as large as 10^{-2} for the purposes of illustrating how large the slow-roll corrections to the bispectrum can become.

terms enter with a relatively large coefficient. We will show this is generically what happens in $P(X, \phi)$ theories. In the equilateral configuration³, *Planck* will measure f_{NL} with an error bar $\Delta f_{\text{NL}} \in [25 - 30]$; future CMB experiments such as *CMBPol* or *CoRE* may even achieve $\Delta f_{\text{NL}} \approx 10$ [100, 101]. Ideally, we would like the theoretical uncertainty in our predictions to fall *below* this threshold.

Next-order corrections.—In comparison to the bispectrum of perturbations, corrections to the power spectrum at subleading order in ϵ are well-understood. Stewart & Lyth [102] were the first to obtain the propagator for scalar fluctuations up to second-order terms in the slow-roll approximation.⁴ Gong & Stewart [104, 105] obtained results valid to cubic order in ϵ . In what follows we apply the notation introduced by Lidsey et al. in Ref. [106]: results involving the least powers in slow-roll parameters contribute at *leading-order*, followed by *next-order terms* which contain contributions with one extra power in slow-roll, and so forth.

Partial results generalising Stewart & Lyth’s calculation to non-canonical models were presented by Wei, Cai & Wang in Ref. [107]. Chen et al. [45] computed the power spectrum to next-order in slow-roll. How relevant are the slow-roll corrections to the bispectrum? Chen et al. [45] calculated the bispectrum to leading-order in the slow-roll approximation. Next-order contributions to the bispectrum were identified and presented in terms of quadratures, which made it hard to evaluate the corrections to f_{NL} at next-order in slow-roll.

Nevertheless, the cubic action for perturbations derived by Seery & Lidsey [88] was perturbative in the amplitude of fluctuations around the background field, but *exact* in slow-roll quantities. The coefficients of each operator in the action were shown to be slow-roll suppressed, but the derivation did *not* rely on the slow-roll approximation. It follows that to get an estimate of how much next-order terms can change the amplitude f_{NL} , one can evaluate a subset of such corrections present in the coefficients of the cubic operators. If these corrections

³We will be more precise about what we mean by equilateral configuration or template in chapter 4.

⁴Stewart & Lyth were obliged to assume that the slow-roll parameter $\epsilon = -\dot{H}/H^2$ was small, thereby truncating the slow-roll approximation accordingly. On the other hand, Grivell & Liddle [103] dropped this assumption but were unable to obtain analytic solutions. Their numerical results confirmed that the Stewart–Lyth formulae were valid within a small fractional error.

are to be representative of the typical magnitude of next-order terms, then this estimate can be trusted.

What do we find? In the case of DBI inflation [27, 74], the next-order corrections entering the coefficients of the cubic operators in the action for perturbations, generates a fractional correction of $101\varepsilon/7 \simeq 14\varepsilon$ in the equilateral limit. How large can this be? For $\varepsilon \simeq 1/20$ (suggested by Alishahiha, Silverstein & Tong [74]) this can be of order 70%.⁵ This implies that next-order corrections to DBI can be as large as 70%. If f_{NL} is observationally large in the equilateral mode, say between 50 and 250 (in agreement with current bounds), then the corrections can shift f_{NL} as much as $\Delta f_{\text{NL}} \in [40, 200]$ —this window is well within reach of *Planck*'s sensitivity.⁶

Are there other compelling reasons to evaluate these corrections? So far we described how large an effect next-order corrections can have on the *amplitude* of the bispectrum. The bispectrum, however, is a much richer object. Are there different shapes arising at next-order? Can they be realised in an inflation model without requiring serious fine-tuning? If so, the appearance of new shapes could provide strong evidence in favour of $P(X, \phi)$ theories controlling the inflationary dynamics. Can we use next-order results to learn more about inflation?

In this chapter we introduce a precise, accurate calculation of the slow-roll corrections. Our ultimate goal is to resolve the large theoretical uncertainties which do not meet the high-sensitivity standards imposed by *Planck*. Although next-order calculations are likely to be sufficient for *Planck*, our findings suggest that next-next-order results could be in principle required by a fourth-generation satellite such as *CMBPol* or *CoRE*. We do not attempt this here.

⁵Baumann & McAllister later suggested that the Lyth bound [108] placed a limit on ε [109]. Lidsey & Huston [110] argued that in combination with the large value of ε implied by Alishahiha, Silverstein & Tong [74] (see also Ref. [111]) this made the ‘UV’ version of the DBI model microscopically inviable. The UV model has other difficulties. Bean et al. [112] noted that backreaction could invalidate the probe brane approximation, spoiling inflation. Moreover, we recall from Refs. [98, 99] that in brane inflation scenarios, numerical simulations show that values of ε are typically much smaller than one, and so assuming $\varepsilon \sim 10^{-2}$ can be too optimistic. For the purposes of making an estimate we are ignoring these details—here, we are interested in gauging the impact of these corrections in the results of the bispectrum.

⁶In this estimate we are discarding for simplicity the sign of f_{NL} .

2.2 Single-field inflation: an overview

We consider the theory (2.1)

$$S = \frac{1}{2} \int d^4x \sqrt{-g} \{R + 2P(X, \phi)\} ,$$

with a homogeneous background solution given by the FLRW metric (1.2). The corresponding Friedmann equations are

$$3H^2 = 2XP_{,X} - P \quad \text{and} \quad 2\dot{H} + 3H^2 = -P , \quad (2.3)$$

where $P_{,X} \equiv \partial P / \partial X$. The nontrivial kinetic structure of P causes fluctuations of the scalar field ϕ to propagate with phase velocity, c_s , different from that of light:

$$c_s^2 = \frac{P_{,X}}{P_{,X} + 2XP_{,XX}} . \quad (2.4)$$

In what follows we shall refer to the phase speed of fluctuations simply as “sound speed,” although these are generically different as explained by Christopherson & Malik in Ref. [113]. In the special case of a canonically normalized field, we have $P = X/2 - V(\phi)$ and the fluctuations in ϕ propagate at the speed of light. We see that in these circumstances, the function P is actually the pressure of the fluid associated with the scalar field ϕ [cf. Eq. (1.34b)].

2.2.1 Fluctuations

During inflation the universe quickly becomes smooth and isotropic, making ϕ spatially homogeneous to a good approximation. At the same time, quantum fluctuations generate small perturbations, $\delta\phi$, whose statistics we want to calculate. Since ϕ is the only scalar field in our model, its fluctuations must be communicated to the metric. Therefore, for consistency we also need to study the metric fluctuations.

Our freedom to make coordinate redefinitions allows the metric and field fluctuations to be studied in a variety of gauges [114, 115]. Whatever choice of gauge (corresponding to a threading and slicing of space-time) we should recover the unperturbed FLRW line element in the limit of vanishing perturbations.

There is always enough freedom to write the perturbed metric in terms of the Arnowitt–Deser–Misner (ADM) metric [116],

$$ds^2 = -N^2 dt^2 + h_{ij} (dx^i + N^i dt)(dx^j + N^j dt), \quad (2.5)$$

where N is the lapse, N^i is the shift function, and h^{ij} is the intrinsic metric on spacelike hypersurfaces of constant time t . The ADM formalism is sometimes called the Hamiltonian formulation of General Relativity, which was nicely reviewed by D’Eath in Ref. [117]. In the absence of perturbations $N = 1$ and $N^i = 0$, and Eq. (2.5) reduces to the background FLRW metric (1.2), if the spatial metric is flat, $h^{ij} = a^2(t)\delta^{ij}$. The usefulness of this space-time foliation is that N and N_i do not support propagating modes, which are restricted to ϕ and the spatial metric h_{ij} only. There are three scalar⁷ and two tensor modes, of which one scalar can be gauged away by choice of spatial coordinates and another by choice of time.

At quadratic order the tensor modes decouple from the scalar fluctuations. This has a simple consequence: when computing the quadratic action for the tensor fluctuations, the scalar field contributions $\delta\phi$ will not contribute to the answer. At tree-level the tensor fluctuations only start contributing to the four-point function [93, 69]. The contributions of the tensor modes to the bispectrum arise only at loop level, generated by insertion of vertices with extra factors of the fluctuations. Such diagrammatic expansion is in powers of $H^2/M_p^2 \approx 10^{-10}$, which is negligible compared to the contributions from tree-level diagrams. In what follows we shall work at tree-level,⁸ and we therefore discard in what follows the tensor modes. We

⁷These originate from the field perturbation $\delta\phi$, and the scalar components of h^{ij} which are proportional to $a\delta^{ij}$ and $\partial^i\partial^jb$ (any metric can be decomposed into these scalar components, and others).

⁸Weinberg [118, 8, 119] and van der Meulen & Smit [120] have investigated when loop diagrams are subdominant compared to tree-level diagrams.

will compute in §3.5 the spectrum of tensor perturbations.

Regardless of whether or not we take the tensor fluctuations into account, we use constraint equations to find the lapse and the shift as functions of the propagating modes. This is because N and N^i are, in fact, Lagrange multipliers in the action. While N is associated with the freedom of choosing time reparametrizations, N^i is associated with spatial coordinates reparametrizations. Alternatively, we could adopt the path integral formulation for inflationary perturbations proposed in [121], which does not solve for these constraint equations; rather the constraints are imposed by introducing auxiliary, non-dynamical fields. In this thesis, however, we shall adopt the traditional route and solve for the constraint equations.

The choice of gauge depends essentially on the model we want to study. If there are multiple fields in the action then it is common to adopt the *uniform-curvature gauge*, whereas in single-field models it is traditional to work in the *comoving gauge*. In the latter the three-dimensional surfaces are chosen so that ϕ is perfectly homogeneous and there exists only one propagating scalar mode—this is absorbed by ζ in the spatially flat metric h_{ij} , via

$$h_{ij} = a^2(t) e^{2\zeta} \delta_{ij} . \quad (2.6)$$

From this equation we read that ζ is the perturbation of the locally defined scale factor, which encodes the expansion history of the universe [42, 122]. Using the definition of the number of e-folds in Eq. (1.29), it follows that

$$\zeta = \delta N . \quad (2.7)$$

This equation is the essence of the “ δN ” or “gradient expansion” formalism, which is a popular approach for computing the correlation functions of ζ , and therefore non-gaussianity—see, for example, Refs. [123, 57].

Notation.—At this point we comment on the notation for the comoving curvature perturbation used in this thesis, which agrees with the more recent literature, including Refs. [124, 66, 45,

125, 11, 126]. Historically, the perturbation in the comoving gauge was initially denoted by \mathcal{R} —see, for example, the early papers in Refs. [127, 128, 48]. The letter ζ had often been reserved to denote the perturbation in the uniform density gauge. In either case, in single-field inflation for adiabatic, super-horizon perturbations, the comoving and uniform density slicings coincide—up to a(n) (irrelevant) sign convention—as showed by Wands et al. [48]. It then follows that for super-horizon evolution (or rather, lack of), we can write

$$\zeta = \mathcal{R} \ ,$$

and the letters can be interchanged without harm. Throughout this thesis we employ the notation that ζ is the comoving curvature perturbation.

Slow-variation parameters.—Our first goal is to deduce the action for the small, inhomogeneous perturbations, ζ . It is in this sense that we work perturbatively in ζ . This is *independent* of assuming a slow-roll approximation.

As we have discussed in §1.3, one typically assumes that inflation is described by a de Sitter expansion, when the Hubble parameter, H , is constant. To quantitatively describe how far away inflation can occur from a purely de Sitter epoch, one typically introduces slow-roll parameters, as defined in Eqs. (1.28) and (1.30):

$$\varepsilon \equiv -\frac{d \ln H}{dN} = -\frac{\dot{H}}{H^2} \quad \text{and} \quad \eta \equiv \frac{d \ln \varepsilon}{dN} = \frac{\dot{\varepsilon}}{H\varepsilon} \ . \quad (2.8)$$

To parametrize the time evolution of the sound speed for perturbations we further introduce

$$s \equiv \frac{d \ln c_s}{dN} = \frac{\dot{c}_s}{Hc_s} \ . \quad (2.9)$$

For inflation to occur we expect background quantities to be slowly varying, and to satisfy

$$\varepsilon, |\eta|, |s| \ll 1 \ .$$

This is the *slow-roll approximation*.

Action and constraints.—Writing the action (2.1) in terms of the ADM variables in Eq. (2.5), we obtain

$$S = \frac{1}{2} \int d^4x \sqrt{h} N \{R^{(3)} + 2P(X, \phi)\} + \frac{1}{2} \int d^4x \sqrt{h} N^{-1} \{E_{ij}E^{ij} - E^2\} , \quad (2.10)$$

where E_{ij} satisfies

$$E_{ij} = \frac{1}{2} \left(\dot{h}_{ij} - N_{(i|j)} \right) . \quad (2.11)$$

Here $|$ denotes a covariant derivative with respect to h_{ij} , and symmetrized indices are enclosed in brackets (\dots) . The extrinsic curvature of spatial slices, K_{ij} , is related to E_{ij} via the shift function, $K_{ij} = N^{-1}E_{ij}$.

The (non-dynamical) constraint equations are obtained by varying the action with respect to N and N_i [88]. We find

$$R^{(3)} + 2P - 4P_{,X} \left(X + h^{ij} \partial_i \phi \partial_j \phi \right) - \frac{1}{N^2} \left(E_{ij}E^{ij} - E^2 \right) = 0 , \quad (2.12a)$$

and

$$\nabla^j \left[\frac{1}{N} \left(E_{ij} - E h_{ij} \right) \right] = \frac{2P_{,X}}{N} \left(\dot{\phi} \partial_i \phi - N^j \partial_i \phi \partial_j \phi \right) . \quad (2.12b)$$

Eqs. (2.12a)–(2.12b) are to be solved order-by-order. To do so, we write

$$N = 1 + \alpha ,$$

where α is some expandable function in powers of the perturbation ζ . Likewise, the shift vector can be decomposed into its irrotational and divergent-free parts,

$$N_i = \partial_i \theta + \beta_i ,$$

where β_i satisfies $\partial_i \beta_i = 0$, by assumption. We also expand θ and β_i perturbatively in powers of ζ , writing the terms of n^{th} order as α_n , β_{ni} and θ_n . As discussed in Refs. [66, 45], it turns out we only need to solve the constraints to first-order to study the three-point correlations.⁹

To first-order, we find

$$\alpha_1 = \frac{\dot{\zeta}}{H}, \quad \beta_{1i} = 0, \quad \text{and} \quad \theta_1 = -\frac{\zeta}{H} + \frac{a^2 \Sigma}{H^2} \partial^{-2} \dot{\zeta}, \quad (2.13)$$

where we have introduced quantities measuring derivatives of P [88]:

$$\Sigma \equiv X P_{,X} + 2X^2 P_{,XX} = \frac{\varepsilon H^2}{c_s^2} \quad \text{and} \quad (2.14a)$$

$$\lambda \equiv X^2 P_{,XX} + \frac{2}{3} X^3 P_{,XXX}. \quad (2.14b)$$

Some of our formulae will be expressed in terms of these variables.

2.2.2 Two-point correlations

To compute the two-point statistics of the comoving curvature perturbation we first need to obtain the action (2.10) to second-order in ζ . This was first done for $P(X, \phi)$ theories by Garriga & Mukhanov [86], who have found

$$S^{(2)} = \int d^3x d\tau a^2 z \{ (\zeta')^2 - c_s^2 (\partial \zeta)^2 \}, \quad (2.15)$$

where $z \equiv \varepsilon / c_s^2$. The form of this action is actually quite general, and we will see it applies to all single-field models of interest. To make the comparison with extensions of this chapter easier, we will leave z explicit in our formulae. Accordingly, we define the corresponding slow-variation parameter,

$$v \equiv \frac{d \ln z}{dN} = \frac{\dot{z}}{Hz} = \eta - 2s. \quad (2.16)$$

⁹To be more precise, in general to obtain the m -point correlator, we only need to solve the Euler-Lagrange equations to $(m-2)^{\text{th}}$ -order.

The last equality applies to $P(X, \phi)$ models only. For more complicated theories, such as galileon inflation, this shall not be the case and v can have a rather complicated expression. The only requirement we impose on z is that it must be positive so that the fluctuations are not ghost-like, and its first-derivative must be well-defined.

To simplify some intermediate expressions, it will be necessary to have an expression for the variation $\delta S^{(2)}/\delta\zeta$:

$$\delta S^{(2)} = \int d^4x \frac{\partial \mathcal{L}^{(2)}}{\partial \zeta} \delta \zeta .$$

We find

$$\frac{\partial S^{(2)}}{\partial \zeta} = -2aH\partial^2\chi - 2a\partial^2\dot{\chi} + 2\varepsilon a\partial^2\zeta , \quad (2.17)$$

where χ satisfies

$$\partial^2\chi = \frac{\varepsilon a^2}{c_s^2}\dot{\zeta} . \quad (2.18)$$

The equation of motion for ζ follows by setting $\delta S_2/\delta\zeta = 0$ in (2.17)—we say ζ is *on-shell*.

Slow-variation approximation.—Although Eqs. (2.15) and (2.17)–(2.18) are exact at linear order in ζ , it is not known how to solve the equation of motion (2.17) for arbitrary backgrounds in conformal time variables, when $\{\varepsilon, \eta, s\}$ might be non-perturbative. We will show how this can be done using different time coordinates in §5.1.

As an alternative approach, Lidsey et al. [106] noted that the time-derivative of each slow-variation parameter is proportional to a sum of products of slow-variation parameters, overall contributing at next-order in slow-roll. Therefore, assuming

$$0 < \varepsilon \ll 1, \quad |\eta| \ll 1, \quad |s| \ll 1 \quad \text{and} \quad |v| \ll 1, \quad (2.19)$$

and working to first-order in these quantities, we may formally treat them as constants. The calculation will then be organised in increasing powers of these quantities. Corrections contributing at or higher-order than next-to-next order will not be kept, since we expect them to be strongly subdominant. Indeed, in general we expect next-to-next order terms to be sup-

pressed compared to next-order corrections by the same amount that next-order terms are corrections to leading-order results.

The expansion of a general background quantity under the slow-variation approximation above works as follows. Take the Hubble parameter, $H(t)$, to be a representative background quantity. Expanding this variable up to next-order in slow-roll around a reference time, t_* , yields

$$H(t) \simeq H(t_*) \{1 + \varepsilon_* \Delta N_*(t) + \dots\}, \quad (2.20)$$

where $\Delta N_*(t) = N(t) - N(t_*)$ denotes the number of elapsed e-folds since the reference time. The reference time is just a pivot scale and we anticipate that physical quantities (that is, *observables*) cannot depend on the arbitrary reference scale t_* , or equivalently ΔN_* . This is precisely equivalent to what happens in renormalisation techniques in quantum field theory. We expect Eq. (2.20) to yield a good approximation to the full time evolution whenever $|\varepsilon_* \Delta N_*(t)| \ll 1$ [104, 105, 129]. We see that this approximation fails when $\Delta N_*(t) \sim 1/\varepsilon_*$; also, if some of the slow-variation parameters become (even) temporarily large around the time of horizon crossing, as in “feature models” [130, 131, 132, 133, 134], then this approximation breaks down. It follows that the approximation (2.20) can only be trusted a few e-folds after the reference scale has exited the horizon.

How can we then study the super-horizon evolution of the perturbations if the approximation (2.20) does not seem to apply in this asymptotic limit? The super-horizon limit corresponds to *many* e-folds after horizon crossing, when typically one needs to apply an improved formulation of perturbation theory obtained by resumming powers of ΔN [135, 136, 137] (various such formalisms are in use [57, 138, 139, 140, 141]). This is usually the case in multi-field inflation, when ordinary perturbation theory breaks down because of large ε and η , and one needs to invoke some sort of renormalisation technique. In single-field inflation, however, this difficulty does not arise—this is because on super-horizon scales, when spatial gradients can safely be neglected, ζ is conserved [142, 123, 143]. We expect that the same

conservation theorem applies to the correlation functions of ζ .¹⁰ We will comment on the time-independence of the two-point correlator shortly.

Two-point function.—The time-ordered two-point function is the Feynman propagator,

$$\langle T \zeta(\tau, \mathbf{x}_1) \zeta(\tau', \mathbf{x}_2) \rangle = G(\tau, \tau'; |\mathbf{x}_1 - \mathbf{x}_2|) ,$$

which depends on the 3-dimensional invariant $|\mathbf{x}_1 - \mathbf{x}_2|$. Moving to Fourier space variables $G = \int d^3q (2\pi)^{-3} G_q(\tau, \tau') e^{i\mathbf{q}\cdot(\mathbf{x}_1 - \mathbf{x}_2)}$, we can write

$$\langle T \zeta(\mathbf{k}_1, \tau) \zeta(\mathbf{k}_2, \tau') \rangle = (2\pi)^3 \delta(\mathbf{k}_1 + \mathbf{k}_2) G_k(\tau, \tau') . \quad (2.21)$$

The δ -distribution enforces conservation of three-momentum, and therefore $k = |\mathbf{k}_1| = |\mathbf{k}_2|$. Breaking up the propagator into elementary wavefunctions of the primordial perturbation

$$G_k(\tau, \tau') = \begin{cases} \zeta_k(\tau) \zeta_k^*(\tau') & \text{if } \tau < \tau' \\ \zeta_k^*(\tau) \zeta_k(\tau') & \text{if } \tau' < \tau \end{cases} . \quad (2.22)$$

The elementary wavefunction ζ_k is a positive frequency solution of (2.15) with the on-shell requirement $\delta S_2 / \delta \zeta = 0$. Working to next-order in the slow-variation approximation (2.19), we find the time evolution for the perturbation modes

$$\zeta_k(\tau) = \frac{\sqrt{\pi}}{2\sqrt{2}} \frac{1}{a(\tau)} \sqrt{\frac{-(1+s)\tau}{z(\tau)}} H_{\frac{3}{2}+\varpi}^{(2)} [-kc_s(1+s)\tau] , \quad (2.23)$$

with $H_\nu^{(2)}$ being the Hankel function of the second kind of order ν , and $\varpi \equiv \varepsilon + \nu/2 + 3s/2$. At sufficiently early times when the modes are well within the horizon, $|kc_s\tau| \gg 1$, they cannot feel the curvature of space-time, and Eq. (2.23) describes the time evolution of the perturbations in Minkowski space [144].

¹⁰We will show that the three-point correlator is time-independent on super-horizon scales for all the single-field models studied in this thesis.

Power spectrum.—The two-point function at equal times defines the power spectrum $P(k, \tau)$

$$P(k, \tau) = G_k(\tau, \tau) .^{11} \quad (2.24)$$

In general, the power spectrum evolves in time, and one needs to specify the time at which it is to be evaluated. Using Eq. (2.22) for $\tau' \rightarrow \tau$, working in the super-horizon limit $|kc_s \tau| \rightarrow 0$ and expanding all the background quantities uniformly around a reference time τ_* , we can safely neglect the decaying mode and approximate the time evolution of the perturbations by the growing mode. We find

$$P(k) = \frac{H_*^2}{4z_* c_{s*}^3} \frac{1}{k^3} \left[1 + 2 \left\{ \varpi_* \left(2 - \gamma_E - \ln \frac{2k}{k_*} \right) - \varepsilon_* - s_* \right\} \right] . \quad (2.25)$$

The Euler–Mascheroni constant is $\gamma_E \approx 0.577$. We have introduced a quantity k_* satisfying $|k_* c_{s*} \tau_*| = 1$. Since to leading-order in slow-roll, $|k_* c_{s*} \tau_*| \simeq |k_* c_{s*} / a_* H_*|$, we describe τ_* as the horizon-crossing time associated with the wavenumber k_* .¹² The leading-order result in slow-roll is the first coefficient in between the square bracket $[\dots]$, and the “next-order” correction arises from the remaining terms which are one higher-order in the slow-roll expansion. Eq. (2.25) therefore satisfies the organisational scheme of the slow-roll approximation used throughout this thesis.

The formula for the power spectrum (2.25) allows for a clear statement of the time-independence of the two-point correlator. We note that our calculation started with an expansion of *all* the background quantities around some reference time τ_* , or equivalently, some reference scale k_* . Nevertheless, Eq. (2.25) does *not* depend on ΔN_* and therefore becomes time-independent once the scale k has crossed outside the sound-horizon. This is a special property of single-field inflation. In classical perturbation theory ζ becomes constant and it

¹¹ P here denotes the power spectrum of perturbations and should not be confused with the function $P(X, \phi)$ used to specify non-canonical theories.

¹²Chen et al. [45] adopted a definition in terms of $|k_*/a_* H_*|$, but the content of their results is identical to ours.

appears that, in all the examples in the literature, the correlation functions are explicitly time-independent as well. We will return to this issue in §2.3.1 when we discuss the three-point correlator in detail.

Scale-dependence.—We have observed that the power spectrum (2.25) is time-independent on super-horizon scales. Moreover it exhibits a weak scale-dependence through the logarithmic term in $P(k)$. We conclude that the quantitative predictive power of (2.25) is limited for scales obeying $|\ln(2k/k_*)| \lesssim 1$. Because k_* is an arbitrary scale, we always have the freedom to choose $k \sim k_*$. To compute the scaling of the power spectrum, one introduces its “dimensionless” version \mathcal{P} by the rule $\mathcal{P} = k^3 P(k)/2\pi^2$. We define the spectral index (assuming $k = k_*$) as

$$n_s - 1 = \frac{d \ln \mathcal{P}}{d \ln k} = -2\varpi_* , \quad (2.26)$$

which is valid to lowest-order in slow-roll [102]. We see that by fixing the scale, one can no longer work with constant background quantities, and their time-dependence needs to be taken into account. Alternatively, one could have left the scale-dependence arbitrary, and extracted the coefficients multiplying $\ln k$ directly. The spectral index is therefore the logarithmic scale-dependence of the power spectrum. Given the alternative ways of computing the spectral index under the slow-roll approximation, it follows that Eq. (2.26) can be interpreted as a renormalisation group equation in quantum field theory describing the flow of \mathcal{P} with k , where

$$\beta_{\mathcal{P}} \equiv (n_s - 1)\mathcal{P}$$

plays the rôle of the β -function.

The computation of correlation functions of ζ is indeed strongly related to renormalisation group techniques popular in quantum field theory. The comoving curvature perturbation is related to the field fluctuation via the one-to-one mapping

$$\zeta = \frac{H}{\dot{\phi}} \delta\phi .$$

It thus follows that

$$\langle \delta\phi \delta\phi \rangle = \left(\frac{H}{\dot{\phi}} \right)^{-2} \langle \zeta\zeta \rangle , \quad (2.27)$$

where we have defined $\langle \delta\phi \delta\phi \rangle = (2\pi)^3 \delta(\mathbf{k}_1 + \mathbf{k}_2) P_{\delta\phi}(k)$. Considering a canonically normalized scalar field and using the scalar field equations of motion under the slow-roll approximation, we can write

$$\left(\frac{\dot{\phi}}{H} \right)^2 \simeq 2\varepsilon_* \left\{ 1 - \eta_* \ln(-k_* \tau) \right\} ,$$

where the second term in brackets captures the next-order corrections. Replacing Eq. (2.25) in Eq. (2.27), we find that

$$\langle \delta\phi \delta\phi \rangle = \frac{H_*^2}{2k_*^3 c_{s*}^2} \left\{ 1 + 2\varpi_* \left[2 - \gamma_E - \ln \left(\frac{2k}{k_*} \right) \right] - 2\varepsilon_* - 2s_* - \eta_* \ln(-k_* \tau) \right\} . \quad (2.28)$$

Applying the Callan–Symanzik equation

$$\left\{ \frac{\partial}{\partial \ln k_*} + \beta_\phi \frac{\partial}{\partial \phi} \right\} \langle \delta\phi \delta\phi \rangle = 0 , \quad (2.29)$$

with $\beta_\phi \equiv \partial\phi / \partial \ln k_*$, we find that

$$\beta_\phi = -\frac{\partial\phi}{\partial N} = \sqrt{2\varepsilon_*} , \quad (2.30)$$

where we have used $\Delta N = -\ln(-k_* \tau)$. We conclude that using renormalisation groups techniques applied to slow-roll inflation can be used to understand how the correlators run with scale. Furthermore, a generalisation to multi-field inflation can prove useful in understanding the time and scale-dependences of the correlators. We do not attempt this here.

To complete the presentation of the slow-variation catalogue, we define additional slow-variation parameters to control the expansion,

$$\xi \equiv \frac{\dot{\eta}}{H\eta} , \quad t \equiv \frac{\dot{s}}{Hs} , \quad \text{and} \quad w \equiv \frac{\dot{v}}{Hv} . \quad (2.31)$$

Table 2.1 collects the results for the spectral index valid at leading and next-order for different single-field theories. As argued above, in multi-field models the spectral index will have a super-horizon evolution, and will therefore depend on time—see, for example, Ref. [145].

model	lowest-order	next-order
arbitrary	$-2\varepsilon_\star - \nu_\star - 3s_\star$	$-2\varepsilon_\star^2 + \varepsilon_\star\eta_\star \left(2 - 2\gamma_E - 2\ln\frac{2k}{k_\star}\right) + s_\star t_\star \left(4 - 3\gamma_E - 3\ln\frac{2k}{k_\star}\right) - 5\varepsilon_\star s_\star - 3s_\star^2 - \nu_\star(\varepsilon_\star + s_\star) + \nu_\star w_\star \left(2 - \gamma_E - \ln\frac{2k}{k_\star}\right)$
canonical	$-2\varepsilon_\star - \eta_\star$	$-2\varepsilon_\star^2 + \varepsilon_\star\eta_\star \left(1 - 2\gamma_E - 2\ln\frac{2k}{k_\star}\right) + \eta_\star\xi_\star \left(2 - \gamma_E - \ln\frac{2k}{k_\star}\right)$
$P(X, \phi)$	$-2\varepsilon_\star - \eta_\star - s_\star$	$-2\varepsilon_\star^2 + \varepsilon_\star\eta_\star \left(1 - 2\gamma_E - 2\ln\frac{2k}{k_\star}\right) - s_\star t_\star \left(\gamma_E + \ln\frac{2k}{k_\star}\right) + \eta_\star\xi_\star \left(2 - \gamma_E - \ln\frac{2k}{k_\star}\right) - s_\star^2 - 3\varepsilon_\star s_\star - s_\star\eta_\star$

Table 2.1: $n_s - 1$ at lowest and next-order in the slow-roll approximation. The first row applies for arbitrary positive, smooth z , as explained below Eq. (2.16). We assume this is the case throughout this thesis.

2.3 Three-point correlations

To compute non-gaussianities, we need the cubic action for ζ . For the action (2.1) this calculation was first done by Seery & Lidsey in Ref. [88], where a partial result for the three-point function was obtained. The full three-point function was later obtained by Chen et al. [45].

2.3.1 Third-order action

We briefly describe the algorithm for computing the cubic action of ζ here. After expanding the action perturbatively in ζ to third-order, applying numerous integration by parts, using

Eqs. (2.3) and (2.13), we get

$$S^{(3)} \supseteq \frac{1}{2} \int d^3x dt a^3 \left\{ -2 \frac{\varepsilon}{a^2} \zeta (\partial \zeta)^2 + 6 \frac{\Sigma}{H^2} \zeta \dot{\zeta}^2 - 2 \frac{\Sigma + 2\lambda}{H^3} \dot{\zeta}^3 - \frac{4}{a^4} \partial^2 \theta_1 \partial_j \theta_1 \partial_j \zeta \right. \\ \left. + \frac{1}{a^4} \left(\frac{\dot{\zeta}}{H} - 3\zeta \right) \partial^2 \theta_1 \partial^2 \theta_1 - \frac{1}{a^4} \left(\frac{\dot{\zeta}}{H} - 3\zeta \right) \partial_i \partial_j \theta_1 \partial_i \partial_j \theta_1 \right\}. \quad (2.32)$$

We recall that λ and Σ were defined in Eqs. (2.14a) and (2.14b). In addition we find the boundary contribution to the action:

$$S^{(3)} \supseteq \int_{\partial} d^3x a^3 \left\{ -9H\zeta^3 + \frac{1}{a^2 H} \zeta (\partial \zeta)^2 \right\}. \quad (2.33)$$

The action given by the combination of Eqs. (2.32) and (2.33) can be further simplified by performing integration by parts. Combining Eqs. (2.13) and (2.17) with Eq. (2.18), one finds

$$S^{(3)} \supseteq \frac{1}{2} \int d^3x dt a^3 \left\{ \frac{2}{c_s^2 a^2} \left\{ \varepsilon (1 - c_s^2) + \eta \varepsilon + \varepsilon^2 + \varepsilon \eta - 2\varepsilon s \right\} \zeta (\partial \zeta)^2 \right. \\ \left. + \frac{1}{c_s^4} \left\{ 6\varepsilon (c_s^2 - 1) + 2\varepsilon^2 - 2\varepsilon \eta \right\} \zeta \dot{\zeta}^2 \right. \\ \left. + \frac{1}{H} \left(2 \frac{\varepsilon}{c_s^4} (1 - c_s^2) - 4 \frac{\lambda}{H^2} \right) \dot{\zeta}^3 \right. \\ \left. + \frac{\varepsilon}{2a^4} \partial^2 \zeta (\partial \chi)^2 + \frac{\varepsilon - 4}{a^4} \partial^2 \chi \partial_j \zeta \partial_j \chi + \frac{2f}{a^3} \frac{\delta S_2}{\delta \zeta} \right\}, \quad (2.34)$$

to which we should add the contributions from the boundary terms as follows

$$S^{(3)} \supseteq \frac{1}{2} \int_{\partial} d^3x a^3 \left\{ -18H^3 \zeta^3 + \frac{2}{a^2 H} \left(1 - \frac{\varepsilon}{c_s^2} \right) \zeta (\partial \zeta)^2 - \frac{1}{2a^4 H^3} \partial^2 \zeta (\partial \zeta)^2 - \frac{2\varepsilon}{H c_s^4} \zeta \dot{\zeta}^2 \right. \\ \left. - \frac{1}{a^4 H} \partial^2 \chi \partial_j \chi \partial_j \zeta - \frac{1}{2a^4 H} \partial^2 \zeta (\partial \chi)^2 + \frac{1}{a^4 H^2} \partial^2 \zeta \partial_j \chi \partial_j \zeta \right. \\ \left. + \frac{1}{2a^4 H^2} \partial^2 \chi (\partial \zeta)^2 \right\}. \quad (2.35)$$

In Eq. (2.34) we have defined f to satisfy

$$f \equiv -\frac{1}{Hc_s^2}\zeta\dot{\zeta}^2 + \frac{1}{4a^2H^2}(\partial\zeta)^2 - \frac{1}{4a^2H^2}\partial_j\zeta\partial_j\chi - \frac{1}{4a^2H^2}\partial^{-2}\{\partial_i\partial_j(\partial_i\zeta\partial_j\zeta)\} \\ + \frac{1}{4a^2H}\partial^{-2}\partial_j\{\partial^2\zeta\partial_j\chi + \partial^2\chi\partial_j\zeta\} . \quad (2.36)$$

On-shell, we observe that the cubic action for perturbations (2.34) is given by *five* Lagrangian operators only. This seems to differ in appearance from the actions obtained in Refs. [88, 45]. There, a further transformation was made to rewrite the terms proportional to the slow-variation parameter η . Using the field equation (2.17) and integrating by parts, this procedure gives rise to new contributions both to f and to the boundary term. Moreover, it also generates one extra operator $\zeta^2\dot{\zeta}$, which does *not* appear in Eq. (2.34).

In this thesis we will work with the action (2.34) for the following reasons. First, as we shall shortly see, to compute the full three-point correlation function, we require the contributions arising from each Lagrangian operator separately. Therefore the more operators in the cubic action, the more individual contributions one needs to compute. Second, after making the additional transformation, the boundary terms will now contribute to the three-point function. To consolidate their contribution one now requires an appropriate field redefinition, that generates an auxiliary field $\tilde{\zeta}$. This redefinition must eventually be reversed to obtain the correlation functions of the physical field ζ . As we explain below, leaving the action in the form of (2.34) renders such field redefinition unnecessary.

Boundary terms.—The boundary terms defined in a three-dimensional hypersurface in Eqs. (2.33) and (2.35) arise in the cubic action from integration by parts with respect to time. They were not quoted in the original calculation by Maldacena [66], neither in subsequent calculations by Seery & Lidsey [88], and Chen et al. [45]. These calculations explicitly discarded all boundary terms, retaining only contributions proportional to $\delta S^{(2)}/\delta\zeta$ in the action (2.34). The $\delta S^{(2)}/\delta\zeta$ terms were then subtracted by making a field redefinition.

This procedure can be misleading. The terms proportional to $\delta S^{(2)}/\delta\zeta$ give no contribution

to any Feynman diagram at any order in perturbation theory, because $\delta S^{(2)}/\delta\zeta$ is zero by construction when evaluated on a propagator—this is the on-shell evaluation we mentioned before. The final answer should therefore be the same whether these terms are subtracted or not. On the other hand, if a field redefinition is performed, then we expect the correlator to be modified accordingly.

Under what conditions is this subtraction procedure correct then? It will yield the correct answer if and only if it reproduces the contribution of the boundary component in (2.35). This argument was first given in Ref. [67], and later in more detail in Refs. [146, 137], but it was applied to the third-order action for field fluctuations in the spatially flat gauge. In this gauge only a few integrations by parts are required. The boundary term is not complicated and the subtraction procedure works as intended. In the present case, however, it appears impossible that the subtraction procedure could be correct, because the boundary action (2.35) contains operators such as ζ^3 which are not present in f . Indeed, because ζ becomes constant at late times, the ζ^3 term seems to diverge which should manifest itself as a rapidly evolving contribution to the three-point function outside the horizon. As we pointed out earlier, this is forbidden in single-field inflation.

This potential problem can be seen most clearly after making the redefinition $\zeta \rightarrow \pi - f$ under which the quadratic action transforms as

$$S^{(2)}[\zeta] \rightarrow S^{(2)}[\pi] - 2 \int_{\partial} d^3x a^3 \frac{\varepsilon}{c_s^2} \dot{\pi} f - \int d^3x d\tau f \frac{\delta S^{(2)}}{\delta \zeta} . \quad (2.37)$$

The bulk term proportional to $\delta S^{(2)}/\delta\zeta$ disappears by construction. After the transformation above, the boundary term becomes

$$S^{(3)} \supseteq \frac{1}{2} \int_{\partial} d^3x a^3 \left\{ -18H\pi^3 + \frac{2}{a^2H} \left(1 - \frac{\varepsilon}{c_s^2}\right) \pi(\partial\pi)^2 - \frac{1}{2a^4H^3} \partial^2\pi(\partial\pi)^2 + \frac{2\varepsilon}{Hc_s^4} \pi\dot{\pi}^2 + \frac{1}{aH} \partial^2\pi(\partial\chi)^2 - \frac{1}{aH} \partial_i\partial_j\pi\partial_i\chi\partial_j\chi \right\} , \quad (2.38)$$

in which χ is to be interpreted as a function of π [cf. Eq. (2.18)].

The subtraction procedure has produced Eq. (2.38) which is not zero. This result only leaves the conclusions of Refs. [66, 88, 45] unchanged if Eq. (2.38) does *not* contribute to the three-point correlator. We will see that this is guaranteed by conservation of ζ on super-horizon scales. Before doing so, we need to briefly recapitulate the *in-in* formalism necessary to compute the correlation functions. We will then return to the issue of the contributions to the three-point function from the boundary terms in §2.3.3.

2.3.2 Schwinger–Keldysh’s *in-in* formalism

The correlation functions we want to study are equal-time expectation values taken in the state corresponding to the vacuum at past infinity. They are different from the “in-out” calculations performed in particle physics which determine the probability of some *in* state (defined at past infinity) becoming an *out* state at future infinity. Quantum field theory correlation functions were initially studied by Schwinger [147] and Keldysh [148] in the 60s, and later applied to cosmology by Jordan [149] and Calzetta & Hu [150]. But it was only with Maldacena’s epic publication in 2002 [66] that the applications of the *in-in* formalism to non-gaussianity were made more clear, together with a pair of papers by Weinberg [8, 119]. This formalism is the appropriate construction to compute expectation values on a time-dependent background, and we briefly summarise its basic ideas in what follows (there are a number of papers which review the *in-in* formalism—see, for example, Refs. [68, 151, 152]).

We will be interested in computing three-point correlation functions at tree-level in the interactions of ζ .

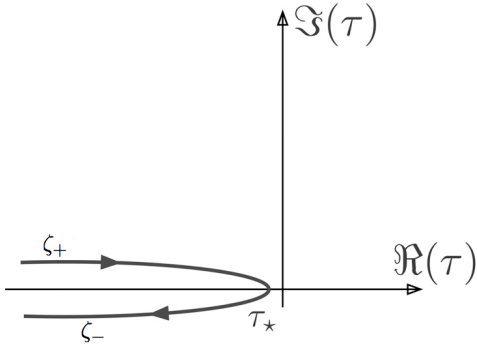


Figure 2.2: Integration contour for the Feynman path integral.

In terms of the Argand diagram in complex conformal time τ , these correlations are obtained by performing a path integral from the true vacuum of the theory, at $\tau \rightarrow -\infty$, to the time of interest when we compute the expectation value, τ_* . To this we add the path integral performed backwards, which returns to the vacuum at $\tau \rightarrow -\infty$.

Schematically, this can be translated into the functional integral

$$\langle \zeta(\mathbf{k}_1)\zeta(\mathbf{k}_2)\zeta(\mathbf{k}_3) \rangle = \int [d\zeta_+ d\zeta_-] \zeta_+(\mathbf{k}_1)\zeta_+(\mathbf{k}_2)\zeta_+(\mathbf{k}_3) e^{iS[\zeta_+] - iS[\zeta_-]} \delta[\zeta_+(\tau_*) - \zeta_-(\tau_*)] , \quad (2.39)$$

where the forward path integral is labelled by the fields ζ_+ , whereas the backwards path integral is labelled by the fields ζ_- . This is *Schwinger's formula*. In practice, to project onto the true vacuum of the interacting theory, one needs to translate the integration contour to be slightly above and below the negative real axis of conformal time—this is shown in figure 2.2. This prescription is in many ways similar to the $i\epsilon$ trick recurrent in quantum field theory and ensures the convergence of the integral above. The fields ζ_+ and ζ_- are constrained (by the δ -distribution) to agree at any one time *later* than that of the observation, so that the path integrals are evaluated with an integration contour necessarily turning and crossing the (negative) real τ -axis.

The correlation function can be interpreted in terms of Feynman diagrams: at tree-level and to leading order in the interactions, the three-point correlator is the sum of two Feynman diagrams, depicted in figure 2.3, corresponding to the two integrations in Eq. (2.39).

Each diagram has three legs with momentum labels \mathbf{k}_i , and at the “core” the vertices are

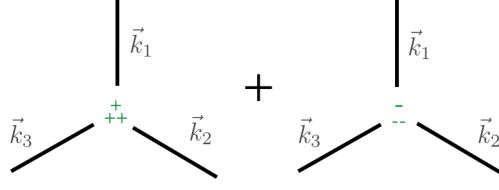


Figure 2.3: Tree-level Feynman diagrams associated with the three-point correlator.

evaluated using either the labels ζ_+ or ζ_- . The external legs are to be evaluated at a later time, whereas the internal lines are associated to earlier times. Each diagram will give a contribution which is precisely the complex conjugate of the other—this means we only need to compute *one* of these diagrams for each operator in Eq. (2.34). In total, there will be *five* such calculations to produce the overall bispectrum.

So how are the elementary wavefunctions used to construct the bispectrum? To answer this let us first look at an explicit calculation of a three-point correlator following Schwinger’s formula (2.39). Focusing on one Feynman diagram and losing the field label to simplify the notation, we write

$$\langle \zeta(\mathbf{k}_1)\zeta(\mathbf{k}_2)\zeta(\mathbf{k}_3) \rangle = \int [d\zeta] \zeta(\mathbf{k}_1)\zeta(\mathbf{k}_2)\zeta(\mathbf{k}_3) e^{iS^{(2)}+iS^{(3)}} .$$

Expanding the cubic action of ζ in the interactions, and moving to Fourier space, we get

$$\langle \zeta(\mathbf{k}_1)\zeta(\mathbf{k}_2)\zeta(\mathbf{k}_3) \rangle = \int [d\zeta] \zeta(\mathbf{k}_1)\zeta(\mathbf{k}_2)\zeta(\mathbf{k}_3) e^{iS^{(2)}} \times \left\{ 1 + i \int d^3x d\tau \frac{d^3q_1 d^3q_2 d^3q_3}{(2\pi)^9} \mathcal{O}[\zeta^3(\mathbf{q}_i)] e^{i\mathbf{x} \cdot \sum_i \mathbf{q}_i} + \dots \right\} , \quad (2.40)$$

where \dots represent higher-order, slow-roll suppressed contributions, and $\mathcal{O}[\zeta^3]$ denotes one of the five cubic operators, which contain at least one (time or spatial) differentiated field. For the purposes of illustrating how the calculation of the three-point correlator works though, it suffices to consider $\mathcal{O}[\zeta^3]$ an arbitrary cubic operator in ζ .

The first term in curly brackets offers no contribution to the three-point function because

it involves an odd number of fields ζ weighted by a Gaussian measure $e^{iS^{(2)}}$, which give unsuccessful Wick contractions. Performing the integration in the spatial coordinates \mathbf{x} , we are left with

$$\langle \zeta(\mathbf{k}_1)\zeta(\mathbf{k}_2)\zeta(\mathbf{k}_3) \rangle = i(2\pi)^3 \int d\tau \frac{d^3q_1 d^3q_2 d^3q_3}{(2\pi)^9} \delta\left(\sum_i \mathbf{q}_i\right) \times \int [d\zeta] \zeta(\mathbf{k}_1)\zeta(\mathbf{k}_2)\zeta(\mathbf{k}_3) e^{iS^{(2)}} \mathcal{O}[\zeta^3(\mathbf{q}_i)] + \dots \quad (2.41)$$

where the δ -distribution enforces the conservation of 3-momentum.

At this point we invoke a standard, useful result in quantum field theory. Let A be a $n \times n$ symmetric, positive-definite matrix. Then

$$\int d^n x e^{-\frac{1}{2} \mathbf{x} A \mathbf{x}} = \frac{(2\pi)^{n/2}}{\sqrt{\det A}} .$$

It follows that for an expectation value, say the two-point correlator

$$\langle x_i x_j \rangle = A_{ij}^{-1} ,$$

where the inverse satisfies $A_{ij} A^{jk} = \delta_i^k$. Now, for a free field theory

$$e^{iS^{(2)}} = e^{-\frac{1}{2} \int dz \Phi(z) \tilde{Q} \Phi(z)} ,$$

where \tilde{Q} satisfies $(\square + m^2)\tilde{Q} = \delta(\mathbf{z} - \mathbf{z}')$, in which m is the mass of the field Φ . \tilde{Q} is the inverse of the propagator, and the Green's function of the operator $(\square + m^2)$. We learn that

$$\int [d\zeta_i d\zeta_j] \zeta_m(\mathbf{k}_1)\zeta_n(\mathbf{q}_1) e^{-\frac{1}{2} \int dz \zeta_i(z) \tilde{Q}_{ij} \zeta_j(z)} = (\tilde{Q}_{mn}^{-1})(\mathbf{k}_1, \mathbf{q}_1) . \quad (2.42)$$

An integration involving one pair of fields gives rise to a propagator, which is built from the elementary wavefunctions as defined in Eq. (2.22). For each three-point correlator we will

require *three* pairs of *two* wavefunctions, each defined at a different time, and the result is

$$\int [d\zeta_i d\zeta_j] \zeta_m(\mathbf{k}_1)\zeta_n(\mathbf{q}_1) \zeta_a(\mathbf{k}_2)\zeta_b(\mathbf{q}_2) \zeta_c(\mathbf{k}_3)\zeta_d(\mathbf{q}_3) e^{-\frac{1}{2} \int dz \zeta_i(z) \tilde{Q}_{ij} \zeta_j(z)} = \quad (2.43)$$

$$(\tilde{Q}_{mn}^{-1})(\mathbf{k}_1, \mathbf{q}_1) (\tilde{Q}_{ab}^{-1})(\mathbf{k}_2, \mathbf{q}_2) (\tilde{Q}_{cd}^{-1})(\mathbf{k}_3, \mathbf{q}_3) .$$

Our calculation will be a direct application of this formula.

2.3.3 Boundary terms removed

The boundary terms in Eq. (2.38) were generated from performing integration by parts, using the equations of motion and the field redefinition described in Eq. (2.37). They appear in Eq. (2.39) as part of the action S with support at past infinity and at $\tau = \tau_*$. The deformed contour of integration makes any contribution from past infinity highly suppressed, leaving a boundary term evaluated precisely at $\tau = \tau_*$. Because the δ -distribution in Eq. (2.39) constrains the fields to agree, it follows that any boundary Lagrangian operators not involving *time* derivatives produce only a phase which cancels between the $+$ and $-$ contours. This implies that operators involving an admixture of fields and spatial-derivatives of fields give no contribution either. We conclude that, in principle, only time-differentiated operators can contribute to the three-point function.

Revisiting the definition of χ in Eq. (2.18), we understand that the entire first line of operators in (2.38) does not contribute to the answer we are seeking. The argument we have given before that the fields ζ_+ and ζ_- are constrained to agree at $\tau = \tau_*$ (enforced by the δ -distribution), does not apply to their time-derivatives. We therefore focus on the last three operators of the boundary action (2.38).

Inspection of Eq. (2.38) shows that the time-derivative operators are of the schematic form $\pi \dot{\pi}^2$, and therefore lead to a field redefinition of the form

$$\zeta \rightarrow \pi + \pi \dot{\pi} .$$

This generates operators which have two time-derivatives. We now argue that boundary operators with two or more time-derivatives are irrelevant on super-horizon scales. Using the schematic field redefinition, the three-point correlation functions of ζ and π are related by $\langle \zeta^3 \rangle = \langle \pi^3 \rangle + 3\langle \pi^2 \rangle \langle \pi \dot{\pi} \rangle$ plus higher-order contributions. However, because Eq. (2.25) implies that the two-point correlator is time-independent on super-horizon scales, then $\langle \pi \dot{\pi} \rangle \rightarrow 0$ and therefore we can write $\langle \zeta^3 \rangle = \langle \pi^3 \rangle$, up to an irrelevant decaying mode.

Therefore, on super-horizon scales, the correlation functions of the original and redefined fields agree, and after subtraction by a field redefinition, the unwanted boundary terms in Eq. (2.38) can be ignored. We can also see that the contributions given by time-differentiated operators of order two or higher are zero because of conservation of ζ . We conclude that time-differentiated operators can be discarded from the three-point functions calculations.

We observe that the only problematic field redefinitions are of the schematic form $\zeta \rightarrow \pi + \pi^2$, which arise from boundary operators containing a *single* time-derivative. Eq. (2.38) contains no such operators, and therefore we can discard all the boundary action in what follows. We note, however, that this was not guaranteed to be the case, and that a careful analysis of the boundary terms must, in general, be performed. Shortly before Ref. [1] was submitted for publication, a preprint by Arroja & Tanaka appeared [153] presenting arguments regarding the rôle of boundary terms which are equivalent to those of this section.

2.4 Beyond $P(X, \phi)$ and towards Horndeski theories

We conclude that the relevant operators in our calculation of the three-point function in $P(X, \phi)$ theories are

$$S^{(3)} = \int d^3x d\tau \left\{ a g_1 \zeta'^3 + a^2 g_2 \zeta \zeta'^2 + a^2 g_3 \zeta (\partial \zeta)^2 + a^2 g_4 \zeta' \partial_i \zeta \partial^i (\partial^{-2} \zeta') + a^2 g_5 \partial^2 \zeta (\partial_i \partial^{-2} \zeta')^2 \right\}. \quad (2.44)$$

The interaction coefficients g_i can be read from Eq. (2.34).

The calculation we have described above follows the traditional methodology to compute the bispectrum in a given inflationary theory: starting from the action for the background field ϕ we have applied perturbation theory to derive the action for the perturbation ζ .

However, recent developments have simplified this procedure. First, Gao & Steer [84] and De Felice & Tsujikawa [154] (see also Ref. [155]) obtained the universal action for perturbations in stable single-field models involving what we call *Horndeski operators* [156] (cubic operators in ζ). Over thirty years ago, Horndeski had already written the most general action involving one single scalar field yielding equations of motion which were at most second-order in derivatives [157]. This action has the following structure

$$S = \int d^4x \sqrt{-g} \left\{ \frac{R}{2} + P_1(X, \phi) - P_2(X, \phi) \square \phi + \mathcal{L}_3 + \mathcal{L}_4 \right\}, \quad (2.45)$$

where

$$\mathcal{L}_3 = P_3(X, \phi)R + P_{3,X} \left[(\square \phi)^2 - (\nabla_\mu \nabla_\nu \phi) (\nabla^\mu \nabla^\nu \phi) \right] \quad (2.46a)$$

$$\mathcal{L}_4 = P_4(X, \phi)G_{\mu\nu}(\nabla^\mu \nabla^\nu \phi) - \frac{1}{6}P_{4,X} \left[(\square \phi)^3 - 3\square \phi (\nabla_\mu \nabla_\nu \phi) (\nabla^\mu \nabla^\nu \phi) + 2(\nabla^\mu \nabla_\alpha \phi) (\nabla^\alpha \nabla_\beta \phi) (\nabla^\beta \nabla_\mu \phi) \right], \quad (2.46b)$$

in which P_1, \dots, P_4 are arbitrary functions of ϕ and X , $P_{i,X} \equiv \partial P_i / \partial X$ and $G_{\mu\nu} \equiv R_{\mu\nu} - \frac{1}{2}Rg_{\mu\nu}$ is the Einstein tensor. Although the action involves high-order derivatives, the non-minimal couplings to the curvature ensure that the resulting Euler-Lagrange equations for ϕ are at most second-order in derivatives. This is an essential requirement for the theory to respect unitarity. Recently there has been renewed interest in these theories in the context of DGP theories [79], and gravity theories based on galileon models (see, for example, Refs. [158, 85, 159, 160]; see also Ref. [161]).

Unless an additional symmetry is imposed on these theories (for example, through the specific form of the functions $P_i(X, \phi)$), they will not be stable against radiative corrections.

Among higher-derivative theories, a notable exception is DBI inflation [27], where a higher dimensional boost protects the coefficients in the function $P(X, \phi)$ from receiving large radiative corrections. If we, however, relax this requirement, we conclude that any healthy, single-field inflation model can be written in the form (2.45). The only model dependent features in the action would reside in different coefficients chosen in the functions $P_i(X, \phi)$.

Second, it was shown in Ref. [155] that the cubic action for ζ has a minimal representation in terms of only *five* of these Horndeski operators. This action was originally derived in Ref. [1], on which this chapter is based. It is our Eq. (2.44).

With these latest developments we arrive at a universal methodology to compute the bispectrum of *all* single-field models, with the cubic action for ζ being always of the form

$$S^{(3)} = \int d^3x d\tau \left\{ a\Lambda_1 \zeta'^3 + a^2\Lambda_2 \zeta \zeta'^2 + a^2\Lambda_3 \zeta (\partial \zeta)^2 + a^2\Lambda_4 \zeta' \partial_i \zeta \partial^i (\partial^{-2} \zeta') + a^2\Lambda_5 \partial^2 \zeta (\partial_i \partial^{-2} \zeta')^2 \right\}. \quad (2.47)$$

The model-dependent imprints will be encoded in each of the *five* coefficients Λ_i of the Horndeski operators. There is a priori *no* hierarchy between these coefficients, although specialization to different models can impose specific ratios between Λ_i (as in DBI inflation). The action above will be our starting point in computing the bispectrum for all single-field models, whether or not the slow-roll approximation is invoked. This is because the action (2.47) is *perturbative* in ζ , but *exact* in slow-roll.

God does not care about our mathematical difficulties. He integrates empirically.

Albert Einstein

3

Microphysics in Non-Gaussianity

In the previous chapter we revisited the computation of the two-point correlator and briefly reviewed the “in-in” formalism for correlation functions. We have initiated the calculation of the bispectrum of single-field inflation theories and have argued that the cubic action for perturbations is simplest written in terms of five bulk operators, given in Eq. (2.47). The calculation we are about to describe applies to *any* single-field inflation model where the equations of motion are at most second-order in derivatives of the field. For the purposes of understanding the implications of our results, however, we will specify the coefficients Λ_i to certain models of interest.

Outline.—In this chapter we report a calculation of the next-order corrections to the bispectrum. We break up the next-order bispectrum in its magnitude, f_{NL} , and its shape and scale-dependences. In this chapter we shall focus on its magnitude, whereas §§4.1–4.2 of chapter 4 will be devoted to the scale and shape-dependences of the bispectrum.

Applications of our results to a collection of models are displayed in §§3.3–3.4. §3.3 focuses on canonical single-field inflation models with an arbitrary potential, whilst §3.4 explores models which can imprint a significant non-gaussian signature because of their non-canonical structure—of these we focus on DBI inflation and k -inflation. In §3.4.1 we discuss an im-

important consequence of obtaining next-order corrections for f_{NL} in generalised DBI inflation model. Through such corrections we gain access to compactification data, such as the shape of the potential and the warp factor, for the first time. Not only does this calculation decrease the theory error associated with previous estimates of the bispectrum, but it also allows access to important information encoded in the CMB which can reveal data inaccessible by other means.

In §3.5 we turn to the set of observables related to tensor fluctuations. Primordial gravitational waves are a generic prediction of inflationary models. We briefly review the next-order computation of the power spectrum for tensor fluctuations: we compute the tensor-to-scalar ratio, r , and the scaling of the tensor perturbations through the tensor spectral index, n_t .

Finally, we summarise our findings in §3.6. Appendix A supports the findings of this chapter. In A.1 we give details of the derivation of the next-order corrections to the scalar propagator. We collect in Appendices A.2–A.3 mathematical details of certain integrals needed for presenting the next-order bispectrum in closed form. This appendix extends what had been originally obtained by Chen et al. in Ref. [45].

This chapter is based on work done in collaboration with Clare Burrage and David Seery, published in Ref. [1].

3.1 The bispectrum beyond lowest-order

We define the bispectrum, B , in terms of the three-point function¹

$$\langle \zeta(\mathbf{k}_1)\zeta(\mathbf{k}_2)\zeta(\mathbf{k}_3) \rangle = (2\pi)^3 \delta(\mathbf{k}_1 + \mathbf{k}_2 + \mathbf{k}_3) B(k_1, k_2, k_3) . \quad (3.1)$$

¹This definition may differ from other notations in the literature, such as that in Ref. [45], by numerical factors of 2π .

It turns out to be useful to define the *reduced bispectrum*, f_{NL} , which satisfies [51, 57]

$$f_{\text{NL}} \equiv \frac{5}{6} \frac{B(k_1, k_2, k_3)}{P(k_1)P(k_2) + P(k_1)P(k_3) + P(k_2)P(k_3)} . \quad (3.2)$$

Observational constraints are typically quoted in terms of f_{NL} evaluated in certain bispectrum *templates* often used in CMB analysis to compare the measured bispectrum with the bispectrum predicted by the theory. We discuss them in §4.2.1. Each template can be thought of as being related to a specific triangular configuration, although this need not be the case. Current constraints on f_{NL} in the simplest inflationary models have been discussed by Senatore et al. in Ref. [162]. Tighter constraints are expected to be placed in the upcoming year using *Planck's* data.

3.1.1 Sources of next-order corrections

We are now in a position to compute the three-point function of Eq. (2.34) to next-order in the slow-roll approximation. As we discussed in §2.3.3, the boundary action and $\delta S^{(2)}/\delta\zeta$ contributions can be discarded by construction of the *in-in* formalism and because the propagators are evaluated on-shell.

Next-order terms arise in the bulk operators from a variety of sources. First, the coefficients of each interaction vertex in Eq. (2.34) contain an admixture of leading and next-order contributions in the slow-roll approximation. This allowed us to anticipate an estimate of the next-order contributions to three-point correlator in §2.1.2. Second, the leading-order part of each vertex is a (slowly) time-dependent quantity which must be expanded around a reference time or scale, as in Eq. (2.20), producing next-order terms. Third, there are next-order corrections to the propagator, obtained by expanding Eqs. (2.22)–(2.23) around the reference time. Propagator corrections appear on both the external and internal legs of the diagram. The external legs corrections correspond to the propagator arising at late times, when we take $|\tau| \rightarrow 0$; the internal legs corrections arise from the expansion of the order of the Hankel

functions in Eq (2.23).

It may be useful to identify these corrections in the Feynman diagram as follows

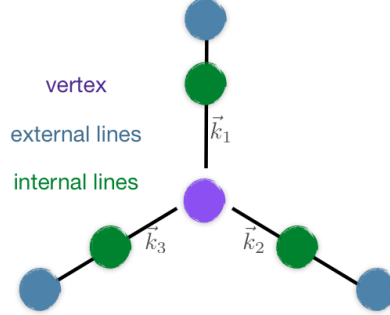


Figure 3.1: Sources of next-order corrections in slow-roll in the tree-level Feynman diagram.

3.1.2 Reference time, factorisation scale

To proceed, we must choose a reference point τ_* around which to expand time-dependent quantities. Such reference point is arbitrary by construction, but some choices might be more useful than others. Take an arbitrary correlation function of fields $\zeta(\mathbf{k}_i)$ (not necessarily a three-point correlator). Whatever our choice of τ_* , the result (2.25) for the power spectrum shows that we must expect logarithms of the form $\ln(k_i/k_*)$ which compensate for the difference in time of horizon crossing between the mode k_i and the reference scale k_* . To obtain a reliable answer we should attempt to minimise these logarithms.

What typical values do the logarithmic terms have? Consider an arbitrary three or higher order correlator. If all fields participating in the correlation function carry momenta of approximately common magnitude $k_i \sim k$ —described as the “equilateral limit”—the logarithm will be small when $k_* \sim k$. The logarithmic term will, in general, be less or of order unity, and it will multiply a slow-variation parameter, or a linear combination of these. In this case, naïve perturbation theory is not spoiled by the appearance of large logarithms.

In the opposite limit, one or more fields have “soft” momenta of order k_{IR} which are much smaller than the remaining “hard” momenta of order k_{UV} , $k_{\text{IR}} \ll k_{\text{UV}}$. When $k_{\text{IR}}/k_{\text{UV}} \rightarrow 0$ it

will not be possible to find a choice of k_* which keeps *all* logarithms small; while we might be able to minimise one of these, say $\ln(k_{\text{IR}}/k_*)$, the hierarchy between k_{IR} and k_{UV} modes makes $\ln(k_{\text{UV}}/k_*)$ inevitably very large. Said differently, a reference scale appropriate for small scale physics will produce sizeable corrections to large scale physics and the calculation passes outside the validity of ordinary perturbation theory. At this point one requires a resummation technique to deal with large logarithmic terms. We have encountered the problem of large logarithms which led to the renormalisation group formalism of Gell-Mann & Low [163].

In the study of inflationary correlation functions, configurations mixing hard and soft momenta with $k_{\text{IR}} \ll k_{\text{UV}}$ are referred to as “squeezed.” For this configuration of momenta, the bispectrum for canonical inflation reaches its maximum magnitude [66]. Given the analogy with ordinary processes in quantum chromodynamics (QCD) [164], one could study the behaviour of a correlation function as its momenta are squeezed by setting up an appropriate renormalisation group analysis [165]. But this is more complicated than necessary.

Maldacena argued that, as the momentum carried by one operator becomes soft, the three-point function factorises into the two-point correlation between the remaining hard operators on a background created by the soft operator [66]. Because of the δ -distribution in the bispectrum (3.1), the two hard operators are described by the same energy scale. f_{NL} arises naturally as the appropriate observable quantity since the bispectrum factorises into two copies of the power spectrum multiplied by $n_s - 1$ (as we shall see in §3.2.2). Factorization of this kind is typical in the infrared dynamics of gauge theories such as QCD, where it plays an important rôle in extracting observational predictions. The various factorisation theorems for QCD correlation functions have been comprehensively reviewed by Collins, Soper & Sterman [166].

The concept of factorisation is not new in cosmology. Indeed, the separate universe method can be thought of as a factorisation theorem for time-dependent logarithms $\sim \ln|kc_s\tau|$. The δN rules which translate correlation functions of the field perturbations, $\delta\phi$, into correlation functions of ζ are an important special case, and they allow for the summation of large logarithms. In this sense, factorisation is as important in extracting observable quantities for

inflation as it is for QCD. Maldacena’s argument was later generalised by Creminelli & Zaldarriaga [167]. The factorisation property can be illustrated by an explicit decomposition of the field into hard and soft modes—see Refs. [168, 169].

Because the squeezed limit can be described by Maldacena’s technique, the outcome of this discussion is that the reference scale should usually be chosen to minimise the logarithms when all momenta are comparable. In the remainder of this chapter we quote results for arbitrary k_* for full generality, but frequently adopt the symmetric choice $k_* = k_1 + k_2 + k_3$ when citing numerical results.² Having done so, we will be formally unable to describe the squeezed limit. Nevertheless, we will be able to verify the correctness of our calculation at the onset of factorisation in appropriate circumstances—a property usually referred to as Maldacena’s *consistency relation*.³

3.1.3 Horndeski operators

In chapter 2 we obtained the cubic action (2.44) for the comoving curvature perturbation

$$S^{(3)} = \int d^3x d\tau a^2 \left\{ \frac{g_1}{a} \zeta'^3 + g_2 \zeta \zeta'^2 + g_3 \zeta (\partial \zeta)^2 + g_4 \zeta' \partial_j \zeta \partial_j \partial^{-2} \zeta' + g_5 \partial^2 \zeta (\partial_j \partial^{-2} \zeta') (\partial_j \partial^{-2} \zeta') \right\}. \quad (3.3)$$

In a $P(X, \phi)$ model the interaction vertices are

$$\begin{aligned} g_1 &= \frac{\varepsilon}{H c_s^4} \left(1 - c_s^2 - 2 \frac{\lambda c_s^2}{\Sigma} \right), & g_2 &= \frac{\varepsilon}{c_s^4} \left[-3(1 - c_s^2) + \varepsilon - \eta \right], \\ g_3 &= \frac{\varepsilon}{c_s^2} \left[(1 - c_s^2) + \varepsilon + \eta - 2s \right], & g_4 &= \frac{\varepsilon^2}{2c_s^4} (\varepsilon - 4), & g_5 &= \frac{\varepsilon^3}{4c_s^4}, \end{aligned} \quad (3.4)$$

but our calculation will apply for arbitrary coefficients g_i . Therefore, unless explicitly written otherwise, the results that follow hold for any Horndeski theory.

²In the gauge theory language discussed above, the scale k_* can be thought of as the factorisation scale. Operators carrying momentum $k \ll k_*$ should not be included as part of the hard subprocess, but factorised into the background.

³See Renaux-Petel [169] for a recent discussion of Maldacena’s condition applied to $P(X, \phi)$ models.

Although ζ is dimensionless by construction, it is helpful to think about it as a field of engineering dimension [mass], obtained after division by the Hubble rate H . In this counting scheme, the ζ'^3 operator is dimension-6, whereas the remaining four operators are dimension-5. At low energies one would naïvely expect the dimension-6 operator to be irrelevant in comparison to those of dimension-5. Nevertheless, the dimension-5 operators are suppressed by the scale H making all contributions equally relevant in the action (3.3). This manifests itself as an extra power of H in the denominator of g_1 , which will appear in our results. Estimates of the magnitude of next-order corrections described in §2.1.2 are based on the interactions (3.4)—we will discuss this in more detail in §3.4.

As we discussed in §3.1.1, the vertex factors g_i are time-dependent background quantities. We can therefore introduce slow-variation parameters h_i which measure their rate of change per e-fold,

$$h_i \equiv \frac{\dot{g}_i}{H g_i} ; \quad (3.5)$$

we take these to be $O(\varepsilon)$ in the slow-variation approximation, that is, $|h_i| \ll 1$.

3.2 Three-point correlations

We use these conventions to compute the bispectra at next-order in slow-roll for each operator in the action (3.3). The resulting three-point functions are intricate objects of momenta, and when quoting their magnitudes it is often helpful to adopt an organizing principle. We divide the possible contributions into two natural classes. In the first class, labelled ‘a,’ we collect

- i. the leading-order bispectrum,
- ii. effects arising from corrections to the wavefunctions associated with external lines, and
- iii. effects arising from the time variation of the vertices.

In the second class, labelled ‘b,’ we focus on internal legs corrections to the Feynman diagrams. These classes are qualitatively different in character because wavefunctions associated with

the internal lines are integrated over time.

Large logarithms, infrared singularities.—In our answers, we expect at least three species of large logarithms to appear, disrupting ordinary perturbation theory. We carefully track the contribution from each species. The most familiar types, already encountered in the two-point function, measure time- and scale-dependences. A third type of large logarithm is associated with the far infrared limit $k_{\text{IR}}/k_{\text{UV}} \rightarrow 0$ discussed in §3.1—this is Maldacena’s “squeezed” limit, in which the behaviour of the three-point function obeys a factorisation principle. We will show that the various large logarithms arrange themselves in such a way that they can be absorbed into the scale-dependence of background quantities.

Time-dependent logarithms appear after expanding background quantities near a fixed reference scale, as in Eq. (2.20), where at conformal time τ the number of elapsed e-folds counts $N_* = \ln |k_* c_s \tau|$. In §2.2.2 we explained that the correlation functions of ζ are expected to become time-independent far outside the horizon. Therefore there cannot be any time-dependence in our final result.

How do the $\ln|\tau|$ terms disappear from the answer? Some N_* -type logarithms cancel amongst themselves, but others cancel with time-dependent logarithms arising from wave-function corrections associated with internal lines. The internal lines⁴ are only aware of the intrinsic geometrical scale $k_t \equiv k_1 + k_2 + k_3$ and cannot depend on the arbitrary reference scale k_* —this results in a residue of the form $\ln(k_t/k_*)$. These are scaling logarithms describing variation of the three-point function with the geometrical scale k_t . They appeared before in the power spectrum (2.25), and they are easily distinguishable from other species of logarithms for they contain k_* . Scale logarithms can also occur in the form $\ln(k_i/k_*)$.

The third logarithm species takes the form $\ln(k_i/k_t)$ and first emerges in the three-point function; this is related to the hierarchy of momentum scales we discussed in §3.1.2. Each side of the triangle must scale linearly with the perimeter, so despite appearances these have no dependence on k_t —they are unaffected by rigid rescalings of the momentum triangle. To

⁴This is explained in detail in §A.1.

better understand this, one can write k_i in terms of the perimeter, k_t , and two additional coordinates, describing the angular dependence. This implies that $\ln(k_i/k_t)$ is effectively only a function of the angular coordinates, and it is therefore responsible for the shape-dependence of the bispectrum. The ‘pure’ shape logarithms become large in the squeezed limit $k_i/k_t \rightarrow 0$.

We will discuss the appearance of these logarithmic species in detail next.

3.2.1 The bispectra

a-type bispectrum.—Collecting the a -type contributions to the bispectrum, we find it can be written as follows

$$\begin{aligned}
 B^a = \frac{H_\star^4}{2^4 c_{s\star}^6} \frac{g_{i\star}}{z_\star^3} \frac{T^a(k_1)}{k_t^2 \prod_i k_i^3} \left\{ \begin{aligned}
 & - \varpi_\star U^a(k_1) \ln \frac{k_1 k_2 k_3}{k_\star^3} \\
 & + 2V^a(k_1) \varepsilon_\star \ln \frac{k_t}{k_\star} + W^a(k_1) h_{i\star} \ln \frac{k_t}{k_\star} \\
 & + X^a(k_1) (1 + 3E_\star) + 2Y^a(k_1) \varepsilon_\star + Z^a(k_1) h_{i\star} \end{aligned} \right\} \quad (3.6) \\
 + \text{cyclic permutations} .
 \end{aligned}$$

The coefficients $T^a(k_1)$, $U^a(k_1)$, $V^a(k_1)$, $W^a(k_1)$, $X^a(k_1)$, $Y^a(k_1)$, and $Z^a(k_1)$ are functions of all three momenta k_i and are symmetric under the exchange $k_2 \leftrightarrow k_3$. We adopt the convention, used through the remainder of this thesis, of writing only the asymmetric momentum explicitly. The notation ‘cyclic permutations’ denotes addition of the preceding term under cyclic permutations of the k_i , that is, $k_1 \rightarrow k_2 \rightarrow k_3$. The result is symmetric under interchange of any two momenta by construction.

We give explicit expressions for the coefficient of these functions in Table 3.1. The quantity E is a linear combination of slow-variation parameters, $E = \varpi(2 - \gamma_E - \ln 2) - \varepsilon - s$, and it has also appeared in the power spectrum (2.25). The term in $X^a(k_1)$ includes the entire leading-order bispectrum.

	operator				
	ζ'^3	$\zeta\zeta'^2$	$\zeta(\partial\zeta)^2$	$\zeta'\partial_j\zeta\partial_j\partial^{-2}\zeta'$	$\partial^2\zeta(\partial_j\partial^{-2}\zeta')^2$
$T^a(k_1)$	$6H_*\frac{k_1^2k_2^2k_3^2}{k_t}$	$k_2^2k_3^2(k_1+k_t)$	$\frac{k_t}{c_{s*}^4}(\mathbf{k}_2\cdot\mathbf{k}_3)$	$\frac{k_1^2}{2}(\mathbf{k}_2\cdot\mathbf{k}_3)$	$k_1^2(\mathbf{k}_2\cdot\mathbf{k}_3)$ $\times(k_1+k_t)$
$U^a(k_1)$	1	1	$c_{s*}^2\left(K^2-k_t^2+\frac{k_1k_2k_3}{k_t}\right)$	$3k_t-k_1$	1
$V^a(k_1)$	1	1	$-c_{s*}^2\left(k_t^2-K^2-\frac{k_1k_2k_3}{k_t}\right)$	$3k_t-k_1$	1
$W^a(k_1)$	1	1	$3c_{s*}^2\left(K^2-k_t^2+\frac{k_1k_2k_3}{k_t}\right)$	$3k_t-k_1$	1
$X^a(k_1)$	1	1	$c_{s*}^2\left(K^2-k_t^2+\frac{k_1k_2k_3}{k_t}\right)$	$3k_t-k_1$	1
$Y^a(k_1)$	$\gamma_E-\frac{1}{2}$	$\gamma_E+\frac{k_t}{k_1+k_t}$	$c_{s*}^2\left[K^2-\gamma_E\left(k_t^2-K^2-\frac{k_1k_2k_3}{k_t}\right)\right]$	$(3k_t-k_1)\gamma_E+2k_t$	$\gamma_E+\frac{k_t}{k_1+k_t}$
$Z^a(k_1)$	$\gamma_E-\frac{3}{2}$	$\gamma_E-\frac{k_1}{k_1+k_t}$	$3c_{s*}^2\left[\gamma_EK^2+(1-\gamma_E)\left(k_t^2-\frac{k_1k_2k_3}{k_t}\right)\right]$	$(3k_t-k_1)\gamma_E+k_1-k_t$	$\gamma_E-\frac{k_1}{k_1+k_t}$

Table 3.1: Coefficients of the leading-order bispectrum, where $K^2 \equiv k_1k_2 + k_1k_3 + k_2k_3$.

b-type bispectrum.—The *b*-type bispectrum must be added to the *a*-type terms. It contributes at next-order *only* and can be written as

$$B^b = \frac{H_*^4}{2^4 c_{s*}^6} \frac{g_{i*}}{z_*^3} \frac{T^b(k_1)}{k_t^2 \prod_i k_i^3} \left\{ \varpi_* \sum_{i=1}^3 \left(k_t U^b(k_i) J_0(k_i) + V_i^b(k_1) J_1(k_i) + k_t^2 W^b(k_i) \ln \frac{2k_i}{k_*} \right) \right. \\ \left. + \varpi_* \left(X^b J_2(k_1) + Y^b k_t^3 \ln \frac{k_t}{k_*} \right) + Z^b + c_{s*} k_t^2 \operatorname{Re}(\mathcal{J}_*) \right\} \quad (3.7)$$

+ cyclic permutations .

The same convention applies to the arguments of the coefficient functions $T^b(k_1)$, $U^b(k_i)$, $V_i^b(k_1)$, $W^b(k_i)$, X^b , Y^b and Z^b ; explicit expressions are provided in Table 3.2. As before, ‘cyclic permutations’ entails addition of the preceding term under cyclic permutations of the k_i .

We observe that the type-*b* bispectrum (3.7) depends on three logarithmic functions J_i (which are *not* Bessel functions) defined by

$$\vartheta_i J_0(k_i) = \ln \frac{2k_i}{k_t} , \quad (3.8a)$$

$$\vartheta_i^2 J_1(k_i) = \vartheta_i + \ln \frac{2k_i}{k_t} , \quad (3.8b)$$

$$\vartheta_i^3 J_2(k_i) = \vartheta_i(2 + \vartheta_i) + 2 \ln \frac{2k_i}{k_t} , \quad (3.8c)$$

where $\vartheta_i = 1 - 2k_i/k_t$. These exhaust the ‘pure’ shape logarithms of the form $\ln(k_i/k_t)$, discussed above. It transpires from Eqs. (3.8) that there is an obvious logarithmic divergence in the squeezed limit $k_i \rightarrow 0$, which we will show to be responsible for factorisation of the correlation function. There is potentially a power-law divergence in the limit $k_t \rightarrow 2k_i$. This is *also* a squeezed limit, in which the i^{th} side stays fixed while $k_j \rightarrow 0$. In this limit $\vartheta_i \rightarrow 0$, making the J_i naïvely divergent. If present, such power-law divergences would be puzzling. However, it can be checked that, in combination with the logarithm, each J_i is finite. This infrared-safe behaviour relies on a resummation procedure reached by analytic continuation—

see Appendix A.2 for more details.

The function \mathcal{J}_* in Eq. (3.7) satisfies

$$\mathcal{J}_* = \frac{1}{k_t c_{s*}} \left\{ \gamma_0 - \frac{\gamma_1 + \delta_1}{k_t} - \frac{2\gamma_2 + 3\delta_2}{k_t^2} + \frac{6\gamma_3 + 11\delta_3}{k_t^3} + \frac{24\gamma_4 + 50\delta_4}{k_t^4} \right. \\ \left. - \left(\gamma_E + \ln \frac{k_t}{k_*} + i \frac{\pi}{2} \right) \left(\delta_0 - \frac{\delta_1}{k_t} - 2 \frac{\delta_2}{k_t^2} + 6 \frac{\delta_3}{k_t^3} + 24 \frac{\delta_4}{k_t^4} \right) \right\}. \quad (3.9)$$

This function is discussed in Appendix A.3. The coefficients $\gamma_0, \dots, \gamma_3$, and $\delta_0, \dots, \delta_3$ depend on the operator under consideration, and they are quoted in Table 3.3.

	operator				
	ζ^3	$\zeta\zeta'^2$	$\zeta(\partial\zeta)^2$	$\zeta'\partial_j\zeta\partial_j\partial^{-2}\zeta'$	$\partial^2\zeta(\partial_j\partial^{-2}\zeta')^2$
$T^b(k_1)$	$-\frac{3}{2}H_*c_{s*}^2k_1^2k_2^2k_3^2$	k_1^2	$\frac{1}{c_{s*}^2}(\mathbf{k}_2 \cdot \mathbf{k}_3)$	$k_1^2(\mathbf{k}_2 \cdot \mathbf{k}_3)$	$k_1^2(\mathbf{k}_2 \cdot \mathbf{k}_3)$
$U^b(k_i)$		-1	$2k_ik_t - 2k_i^2 - K^2$	$c_{s*}k_t$	$c_{s*}k_t$
$V_1^b(k_1)$		k_1	$k_1k_2k_3$	$-\frac{1}{2}(k_2 + k_3)$	k_1
$V_2^b(k_1)$		$-k_1$	$k_1k_2k_3$	$\frac{1}{2}(k_2 - k_3)$	$-k_1$
$V_3^b(k_2)$		$-k_1$	$k_1k_2k_3$	$\frac{1}{2}(k_3 - k_2)$	$-k_1$
$W^b(k_i)$			$k_t - 2k_i$		
X^b	$\frac{1}{c_{s*}^2k_t}$				
$Y^{(b)}$			2		
Z^b			$k_t^3[2\varpi_{1*} - 3\text{Re}(\mu_{0*}) + 3\gamma_E\varpi_{1*}]$		

Table 3.2: Coefficients of the subleading corrections to the bispectrum, where $K^2 \equiv k_1k_2 + k_1k_3 + k_2k_3$.

	operator				
	ζ'^3	$\zeta\zeta'^2$	$\zeta(\partial\zeta)^2$	$\zeta'\partial_j\zeta\partial_j\partial^{-2}\zeta'$	$\partial^2\zeta(\partial_j\partial^{-2}\zeta')^2$
γ_0		$\mu_{0*} + 2s_* - 2\mu_{1*}$	$s_*k_1^2 + k_1\mu_{1*}(k_2 + k_3) - \mu_{0*}k_2k_3$	$\mu_{0*} + 2s_* - 2\mu_{1*}$	$\mu_{0*} + 2s_* - 2\mu_{1*}$
γ_1		$3k_1\mu_{1*} + k_t s_*$ $- 3k_1 s_*$	$-s_*k_1^2(k_2 + k_3) - \mu_{1*}k_1k_2k_3$	$k_t s_* - 3k_2 s_*$ $+ 3\mu_{1*}k_2$	$k_t s_* - 3k_1 s_*$ $+ 3\mu_{1*}k_1$
γ_2	$\frac{s_* - \mu_{1*}}{c_{s_*}^2}$	$k_1 k_t s_*$	$-s_*k_1^2 k_2 k_3$	$k_2 k_t s_*$	$k_1 k_t s_*$
γ_3	$k_1 \frac{s_*}{c_{s_*}^2}$				
δ_0		$3\varpi_{1*} - 4s_*$	$-s_*k_1^2 - K^2\varpi_{1*}$	$3\varpi_{1*} - 4s_*$	$3\varpi_{1*} - 4s_*$
δ_1		$-k_t s_* + 5k_1 s_*$ $- 3k_1 \varpi_{1*}$	$s_*k_1^2(k_2 + k_3) + \varpi_{1*}k_1k_2k_3$	$-k_t s_* + 5k_2 s_*$ $- 3k_2 \varpi_{1*}$	$-k_t s_* + 5k_1 s_*$ $- 3k_1 \varpi_{1*}$
δ_2	$\frac{\varpi_{1*} - 2s_*}{c_{s_*}^2}$	$-s_*k_1 k_t$	$s_*k_1^2 k_2 k_3$	$-k_2 k_t s_*$	$-k_1 k_t s_*$
δ_3	$-k_1 \frac{s_*}{c_{s_*}^2}$				

Table 3.3: Coefficients appearing in the function \mathcal{J} for each operators. Note that the γ_i contain complex numbers. The imaginary part is cancelled on addition of the + and - Feynman diagrams, and only the real part of these coefficients contribute. In an intermediate step for the three-point function of $\zeta(\partial\zeta)^2$, the cancellation of power-law divergences in τ (required by Weinberg's theorem [8]) depends on a real contribution generated from the product of two imaginary terms.

Comments on the calculation.—The operators $\zeta\zeta'^2$, $\zeta'\partial_j\zeta\partial^{-2}\partial_j\zeta$ and $\partial^2\zeta(\partial^{-2}\partial_j\zeta')^2$ are all dimension-5, and differ only in the arrangement of spatial gradients. For arbitrary shapes their three-point functions will not coincide, but for equilateral triangles the arrangement of gradients is irrelevant and the resulting f_{NL} should agree. This can be confirmed upon inspection of the respective coefficients quoted in tables 3.1, 3.2, and 3.3. This represents a minimal check of our expressions. We will carry out further checks in §§3.3–3.4 and §4.1 using Maldacena’s consistency condition.

Bispectra a and b are computed using the same *in-in* formalism rules briefly reviewed in §2.3.2. The third Horndeski operator, $\zeta(\partial\zeta)^2$, presents an additional degree of complexity compared to the others.⁵ We briefly mention the technicalities of this calculation here.

Starting from action (3.3), we note this operator is undifferentiated, making the integral, at least, power-law divergent. This is because there will be insufficient powers of conformal time τ , to counteract those in denominator from $a(\tau)$ in the integrand. As a result the integrand behaves, at leading-order, as $a^2 \sim 1/\tau^2$. At the same time, next-order corrections will add logarithmic terms to the integrand. This has serious repercussions in the final result because it can potentially lead to spurious power-law and logarithmic divergences in τ when one takes the limit $|\tau| \rightarrow 0$ —these are *dangerous interactions*, as named by Weinberg [8].

In order to ensure that the real part of the correlation function converges in the asymptotic limit, one needs to carefully isolate the primitively divergent contributions: either power-laws like $|\tau|^{-\alpha}$, with $\alpha > 0$, or logarithmic terms $\ln(-\tau)$. This is done by integrating all divergent integrals by parts an appropriate number of times. Only two situations occur as a result:

- i. the isolated divergent terms contribute with a purely imaginary part to the correlation function. In this case, this divergence becomes irrelevant since the total correlation function is given by the sum of two path integrals which are complex conjugates;
- ii. the isolated divergent contributions are real and contribute to the final answer. When we sum type a and type b bispectra, however, we verify that these divergent contributions

⁵This difficulty will also appear in chapter 5.

precisely cancel out amongst themselves and the final result is finite.

It is crucial to take these two possibilities into account to obtain a correct result: first, to ensure that the correlation functions do not diverge in their asymptotic limit (at late times); and second, to guarantee that the calculation contains all the necessary convergent contributions to the overall bispectrum. This is particularly important when checking whether our results are consistent with Maldacena’s factorisation theorem [66, 167].

Next-order corrections.—A subset of next-order corrections to the bispectrum were calculated by Chen et al. [45]. Our calculations are different in two aspects. First, Chen et al. worked to fixed order in slow-roll quantities, keeping terms of $O(\varepsilon)$ only. In a model where $c_s \ll 1$ they reproduce the next-order corrections. However, in a model where $c_s \sim 1$ the leading terms are themselves $O(\varepsilon)$ and the formulae of Chen et al. reduce to these leading contributions. In our calculation, we work *uniformly to next-order* rather than at fixed order in powers of ε . When $c_s \ll 1$ our next-order corrections are $O(\varepsilon)$, and we have verified that they agree with those computed in Ref. [45]. When $c_s \sim 1$ the next-order corrections are $O(\varepsilon^2)$. These were not included in the formulae quoted in Ref. [45].

Second, we retain a floating reference scale k_* , chosen to be $k_* = k_t$ in Ref. [45]. Retaining this scale allows us to extract the scale- and shape-dependences of f_{NL} —see §§4.1–4.2.

3.2.2 Formulae for f_{NL}

The individual bispectra, with their detailed shape-dependence, are the principal observable objects containing a wealth of information about the microphysics during inflation. However, for simple model comparisons it is helpful and quite popular to have an explicit expression for the nonlinearity parameter f_{NL} defined in Eq. (3.2). Accounting for scale-dependent logarithms present in the power spectrum (2.25), one finds

$$f_{\text{NL}} = \frac{5}{6} \left(\frac{4z_* c_{s*}^3}{H_*^2} \right)^2 \frac{B(k_1, k_2, k_3) \prod_i k_i^3}{\sum_i k_i^3 \left\{ 1 + 4E_* - 2\varpi_{1*} \ln(k_i^{-1} k_t^{-2} \prod_j k_j) \right\}} . \quad (3.10)$$

This expression is to be expanded uniformly to $O(\varepsilon)$ in slow-variation parameters. It is therefore valid up to next-order corrections in the slow-variation approximation.

There is another reason to study f_{NL} , which is related to Maldacena's factorisation rule. We have explained that large logarithms of the form $\ln(k_i/k_*)$ or $\ln(k_i/k_t)$ are to be expected in the squeezed limit $k_i \rightarrow 0$, describing variation of the bispectrum with shape. The power spectrum $P(k)$ contains similar large logarithms. Since copies of the power spectrum must be factored out to obtain f_{NL} , one may anticipate it to be more regular in the squeezed limit. Indeed, a more precise statement is possible. Partitioning the momenta into a single soft mode of order k_{IR} and two hard modes both of order k_{UV} , Maldacena's consistency condition requires [66]

$$f_{\text{NL}} \longrightarrow -\frac{5}{12}(n_s - 1)|_{k_{\text{UV}}}, \quad (3.11)$$

as $k_{\text{IR}} \rightarrow 0$, where the right-hand side is to be evaluated at horizon exit for the mode k_{UV} . It is clear from Eq. (3.11) that, in this limit, two and three-point correlators talk to each other. Both sides of Eq. (3.11) are finite and independent of any logarithms associated with the squeezed limit; this factorisation procedure absorbs all the power-law and logarithmic divergences.

For each operator i , we write the corresponding f_{NL} as $f_{\text{NL}i}$ and quote it in the form

$$f_{\text{NL}i} = f_{\text{NL}}|_{i0} \{1 + \kappa_{h|i} h_{i*} + \kappa_{v|i} v_{i*} + \kappa_{s|i} s_{i*} + \kappa_{\varepsilon|i} \varepsilon_{i*}\}. \quad (3.12)$$

In Tables 3.4 and 3.5 we give explicit expressions for the coefficient functions $f_{\text{NL}}|_{i0}$ and κ_i specialised for equilateral⁶ and squeezed triangular configurations. Table 3.5 confirms that f_{NL} in Eq. (3.12) is finite in the squeezed limit, as required.

In the next sections we explore our calculation of the bispectrum. We start by applying our results to popular single-field models.

⁶The quoted quantity is $f_{\text{NL}}(k, k, k)$, which is *not* the same as $f_{\text{NL}}^{(\text{equilateral})}$ for which constraints are typically given [162, 6]. To obtain $f_{\text{NL}}^{(\text{equilateral})}$, one should take an appropriately normalised inner product (see §4.2 for a simple example) between the full next-order bispectrum shape and the equilateral template [170, 171].

	operator				
	ζ^3	$\zeta\zeta'^2$	$\zeta(\partial\zeta)^2$	$\zeta'\partial_j\zeta\partial_j\partial^{-2}\zeta'$	$\partial^2\zeta(\partial_j\partial^{-2}\zeta')^2$
$f_{\text{NL} i0}$	$\frac{5}{81} \frac{g_{1*} H_*}{z_*}$	$\frac{10}{27} \frac{g_{2*}}{z_*}$	$\frac{85}{108} \frac{g_{3*}}{z_* c_s^2}$	$-\frac{5}{27} \frac{g_{4*}}{z_*}$	$\frac{10}{27} \frac{g_{5*}}{z_*}$
$\kappa_{\text{hl} i}$	$\gamma_E - \frac{3}{2} + \ln \frac{3k}{k_*}$ -0.922784^a	$\gamma_E - \frac{1}{4} + \ln \frac{3k}{k_*}$ 0.327216^a	$\gamma_E - \frac{26}{17} + \ln \frac{3k}{k_*}$ -0.952196^a	$\gamma_E - \frac{1}{4} + \ln \frac{3k}{k_*}$ 0.327216^a	$\gamma_E - \frac{1}{4} + \ln \frac{3k}{k_*}$ 0.327216^a
$\kappa_{\text{vl} i}$	$-\gamma_E - \frac{29}{2} + 78\omega - \ln \frac{2k}{k_*}$ 1.14139^a	$-\gamma_E - \frac{1}{4} + 6\omega - \ln \frac{2k}{k_*}$ 0.794645^a	$-\gamma_E + \frac{22}{17} + \frac{30}{17}\omega - \ln \frac{2k}{k_*}$ 1.48013^a	$-\gamma_E - \frac{1}{4} + 6\omega - \ln \frac{2k}{k_*}$ 0.794645^a	$-\gamma_E - \frac{1}{4} + 6\omega - \ln \frac{2k}{k_*}$ 0.794645^a
$\kappa_{\text{sl} i}$	$-49 + 240\omega$ -0.344187^a	$-\frac{3}{2} + 24\omega$ 3.36558^a	$-2\gamma_E + \frac{40}{17} + \frac{124}{17}\omega - 2\ln \frac{2k}{k_*}$ 3.4882^a	$-\frac{3}{2} + 24\omega$ 3.36558^a	$-\frac{3}{2} + 24\omega$ 3.36558^a
$\kappa_{\text{el} i}$	$-\gamma_E - \frac{63}{2} + 158\omega - \ln \frac{2k}{k_*}$ 0.359993^a	$-1 + 16\omega$ 2.24372^a	$-\frac{8}{17} + \frac{128}{17}\omega$ 1.05587^a	$-1 + 16\omega$ 2.24372^a	$-1 + 16\omega$ 2.24372^a

^a Evaluated at the conventional reference scale $k_* = k_t$ for a quantitative result.

Table 3.4: Equilateral limit of f_{NL} at leading and next-order in the slow-roll approximation. The numerical constant ω satisfies $\omega = \frac{1}{2} \ln \frac{3}{2} = \coth^{-1} 5$.

	operator			
	ζ'^3	$\zeta\zeta'^2$	$\zeta(\partial\zeta)^2$	$\zeta'\partial_j\zeta\partial_j\partial^{-2}\zeta'$ $\partial^2\zeta(\partial_j\partial^{-2}\zeta')^2$
$f_{\text{NL}} _{i0}$		$\frac{5}{24} \frac{g_{1*}}{z_*}$	$\frac{5}{8} \frac{g_{2*}}{z_* c_{s*}^2}$	
$\kappa_{h i}$		$\gamma_E + \ln \frac{2k}{k_*}$ 0.577216 ^a	$\gamma_E - \frac{4}{3} + \ln \frac{2k}{k_*}$ -0.756118 ^a	
$\kappa_{v i}$		$-\gamma_E + 1 - \ln \frac{2k}{k_*}$ 0.422784 ^a	$-\gamma_E + \frac{5}{3} - \ln \frac{2k}{k_*}$ 1.08945 ^a	
$\kappa_{s i}$		3	$-2\gamma_E + \frac{11}{3} - 2 \ln \frac{2k}{k_*}$ 2.51224 ^a	
$\kappa_{\varepsilon i}$		2	$\frac{2}{3}$ 0.666667	

^a Evaluated at the reference scale $k_* = 2k_{\text{UV}}$ for a quantitative result, where k_{UV} is the common hard momentum.

Table 3.5: f_{NL} in the squeezed limit at leading and next-order in the slow-roll approximation.

3.3 Canonical single-field inflation

The simplest model of inflation is that of a single, canonical scalar field dominating the inflation era. Maldacena showed that the fluctuations in this model are almost Gaussian, with f_{NL} being unobservably small [66]. In a canonical model, scalar field fluctuations propagate at the speed of light, $c_s = 1$.

Nonlinearity parameter.—To calculate f_{NL} we need to know the expressions for the flow parameters h_i , which measure the time-dependence in g_i of Eq. (3.4). These are

$$\begin{aligned} h_1 &= 0 \quad , & h_2 &= \frac{\eta(2\varepsilon - \eta - \xi)}{\varepsilon - \eta} \quad , \\ h_3 &= \frac{\eta(2\varepsilon + \eta + \xi)}{\varepsilon + \eta} \quad , & h_4 &= \frac{\eta(8 - \varepsilon)}{4} \quad , & h_5 &= 3\eta \quad . \end{aligned} \quad (3.13)$$

In this model the time-dependence of z is described by $v = \eta$. Collecting contributions from Table 3.4, we find the equilateral limit of f_{NL} , which we shall denote by $f_{\text{NL}}^{(\text{equilateral})}$, is

$$\begin{aligned} f_{\text{NL}}^{(\text{equilateral})} \rightarrow \frac{5}{36} \left\{ 11\varepsilon_* + 3\eta_* + \frac{35\varepsilon_*^2}{216} \left(768\omega - 54 \right) + \frac{35\eta_*\xi_*}{36} \left(3\gamma_E - 8 + 3 \ln \frac{3k}{k_*} \right) \right. \\ \left. + \frac{35\varepsilon_*\eta_*}{36} \left(11\gamma_E - 14 + 64\omega + 11 \ln \frac{3k}{k_*} \right) \right\} \quad , \end{aligned} \quad (3.14)$$

where we have used the numerical constant $\omega = \coth^{-1} 5$, and k is the common momentum scale, $k_i = k$. Likewise, the squeezed limit may be recovered from Table 3.5. We find

$$f_{\text{NL}}^{(\text{squeezed})} \rightarrow \frac{5}{12} \left\{ 2\varepsilon_* + \eta_* + 2\varepsilon_*^2 + \eta_*\xi_* \left(\gamma_E - 2 + \ln \frac{2k}{k_*} \right) + \varepsilon_*\eta_* \left(2\gamma_E - 1 + 2 \ln \frac{2k}{k_*} \right) \right\} \quad , \quad (3.15)$$

where k is now the scale of the hard momenta, k_{UV} . In §3.2.2 we emphasized that f_{NL} should be finite in this limit, containing no large logarithms, because these factorise into the power spectrum and are subtracted upon division. The surviving logarithms [the $\ln(2k/k_*)$ terms in Eq. (3.15)] track the dependence of f_{NL} on the hard scale, and will be studied below. Using

Eq. (3.11) and comparing with the spectral indices quoted in Table 2.1, it is easy to check that our formula correctly reproduces Maldacena's limit.

3.4 Non-canonical single-field inflation

For the non-canonical action (2.1), the h_i can be written as

$$\begin{aligned}
 h_1 &= \varepsilon + \eta - 2s + \frac{\frac{2\lambda}{\Sigma}(\eta - 2\varepsilon - 2s - \ell) - \frac{2}{c_s^2}s}{\frac{1-c_s^2}{c_s^2} - \frac{2\lambda}{\Sigma}} , & h_2 &= \eta - 4s + \frac{\eta(\varepsilon - \xi) + 6c_s^2s}{\eta - \varepsilon - 3(1 - c_s^2)} , \\
 h_3 &= \eta - 2s + \frac{\eta(\varepsilon + \xi) - 2s(t - c_s^2)}{\varepsilon + \eta - 2s + (1 - c_s^2)} , & h_4 &= 2\eta - 4s - \frac{\eta\varepsilon}{4 - \varepsilon} , \\
 h_5 &= 3\eta - 4s , & &
 \end{aligned} \tag{3.16}$$

where we have defined $\xi \equiv \dot{\eta}/H\eta$, $\ell \equiv \dot{\lambda}/H\lambda$ [45], and $t \equiv \dot{s}/Hs$.

In the canonical case, it was possible to verify Maldacena's consistency condition to next-order. In the non-canonical case this is not possible without a next-next-order calculation, because for $c_s \neq 1$ the leading contribution to f_{NL} is first-order in the slow-variation expansion. Therefore our calculation of subleading corrections produces a result valid to $O(\varepsilon)$, which is short of the $O(\varepsilon^2)$ accuracy required to verify the consistency condition at next-order. Chen et al. gave the subleading corrections in terms of undetermined integrals [45]. Expanding these asymptotically, they argued that the consistency relation would be satisfied at lowest-order. More recently, Renaux-Petel [169] gave an equivalent demonstration. Here, we have knowledge of the full bispectrum to subleading order. Using Eq. (3.16), it can be verified that in the squeezed limit, and expanding around a reference scale k_* ,

$$f_{\text{NL}}^{(\text{squeezed})} \rightarrow \frac{5}{12} (2\varepsilon_* + \eta_* + s_*) . \tag{3.17}$$

One may check that this agrees with Eq. (3.11) and Table 2.1.

3.4.1 Asymptotically power-law models

Power-law inflationary models were introduced by Lucchin & Matarrese [172, 173], who studied potentials producing an expansion history of the form $a(t) \propto t^{1/p}$, where $p < 1$ is a constant. This describes an inflating solution. Exact solutions can be found in the canonical case, upon which the next-order calculation was based [106].

In this section we study two examples which are asymptotically described by non-canonical power-law inflation at late times. The first is Dirac–Born–Infeld (DBI) inflation, which produces a scale-invariant power spectrum of perturbations at leading-order. Departures from scale-invariance appear at next-order in the slow-roll approximation. This special property implies that we can compare our results to a formula of Khoury & Piazza which was obtained without invoking the slow-roll approximation, but where a scale-invariant spectrum was imposed [174]. Here we expand the discussion initiated in §1.3.2. Our second example is k -inflation, for which the power spectrum is not scale-invariant at lowest-order, and to which Khoury & Piazza’s result does not apply.

Dirac–Born–Infeld inflation

The DBI action is a low-energy effective theory which describes a D3-brane moving in warped space. It was proposed as a model of inflation by Silverstein & Tong [27], and subsequently developed with Alishahiha [74]. The action is of the form (2.1), with $P(X, \phi)$ satisfying

$$P(X, \phi) = -\frac{1}{f(\phi)} \left\{ \sqrt{1 - f(\phi) X} - 1 \right\} - V(\phi) , \quad (3.18)$$

where f is an arbitrary function of ϕ known as the warp factor, and $V(\phi)$ is the potential arising from couplings between the brane and other degrees of freedom. The DBI Lagrangian is non-analytical but algebraically special [111, 160, 175]. It enjoys a number of remarkable properties, including a form of non-renormalisation theorem [176, 177, 178]; its invariance under a higher-dimensional boost makes DBI one rare example of a radiatively stable higher-

derivative model against quantum corrections.

In principle in the DBI action non-minimal curvature couplings can be present, of the form $R\phi^2$, which spoil inflation [179]. This gives a form of the η -problem, and we assume such terms to be negligible.

It is conventional to define a Lorentz factor as follows

$$\gamma \equiv (1 - f \dot{\phi}^2)^{-1/2} . \quad (3.19)$$

When $\gamma \sim 1$ the motion of the brane in the warped throat is nonrelativistic. When $\gamma \gg 1$, the brane is moving close to the speed limit. The Lorentz factor is related to the speed of sound of perturbations by $c_s = \gamma^{-1}$. In the limit $\gamma \gg 1$, the scalar fluctuations around background solutions of the action (3.18) propagate at small sound speed, which is related to large non-gaussianities. The square root in Eq. (3.18) must be real, imposing a dynamical speed limit for ϕ .

Eq. (3.18) makes $2\lambda/\Sigma = (1 - c_s^2)/c_s^2$, which requires $g_1 \rightarrow 0$ but causes the denominator of h_1 given in Eq. (3.16) to diverge. Only the finite combination $g_1 h_1$ appears in the physical, observable quantity f_{NL} , and it can indeed be checked that $g_1 h_1 \rightarrow 0$ as required.

“Traditional” DBI inflation scenario.—Silverstein & Tong [27] obtained attractor solutions supported by (3.18) and specific forms of the potential and warping, which were described at late times by power-law inflation. In this limit, the slow-variation parameters ε and s are constant, with $\eta = \xi = t = 0$, but ℓ does not vanish. Variation of the sound speed gives $s = -2\varepsilon$, making $\varpi = 0$ and yielding scale-invariant fluctuations at leading-order in slow-roll [cf. Eq. (2.26)] [174]. In the equilateral limit,⁷ we find

$$f_{\text{NL}}^{(\text{equilateral})} \rightarrow -\frac{35}{108} (\gamma_\star^2 - 1) \left\{ 1 - \frac{\gamma_\star^2}{\gamma_\star^2 - 1} (3 - 4\gamma_{\text{E}}) \varepsilon + \mathcal{O}(\gamma_\star^{-2}) \right\} . \quad (3.20)$$

In §2.1 we have estimated the relative uncertainty in f_{NL} to be $\sim 14\varepsilon$, working in the limit

⁷Recall that the equilateral limit is $f_{\text{NL}}(k, k, k)$, and not the quantity constrained by experiment.

$\gamma \gg 1$, based on $O(\varepsilon)$ terms from the vertices (3.4) only. Eq. (3.20) shows that, because of an apparently fortuitous cancellation, this large contribution is almost completely subtracted, leaving a small fractional correction of only $\sim 0.69\varepsilon$.

In the squeezed limit we find

$$f_{\text{NL}}^{(\text{squeezed})} \rightarrow \frac{10\gamma_*^2}{3}\varepsilon^2 \left\{ 4\gamma_E - 5 + 4\ln \frac{4k}{k_*} \right\} . \quad (3.21)$$

which is $O(\varepsilon^2)$, as predicted by Maldacena's condition (3.11) and the property $\varpi = 0$ [74].

Comparison with previous results.—Khoury & Piazza estimated the bispectrum in a power-law inflationary model satisfying exact scale-invariance, $\varpi = 0$, without invoking an expansion in slow-variation parameters [174]. They quoted their results in terms of a quantity f_X which replaces λ , as follows

$$\lambda \equiv \frac{\Sigma}{6} \left(\frac{2f_X + 1}{c_s^2} - 1 \right) . \quad (3.22)$$

For the DBI model, $f_X = 1 - c_s^2$. They assumed constant f_X , making their result valid to all orders in ε but only lowest-order in the time dependence of f_X . Working in the equilateral limit for arbitrary but constant f_X , we find

$$\begin{aligned} f_{\text{NL}}^{(\text{equilateral})} \rightarrow & -\frac{5}{972c_{s^*}^2} \left\{ 55(1 - c_{s^*}^2) + 8f_X \right\} \\ & + \frac{5\varepsilon}{972c_{s^*}^2} \left\{ 149 - 8c_{s^*}^2 - 220\gamma_E - 220\ln \frac{3k}{k_*} + f_X \left(40 - 32\gamma_E - 32\ln \frac{3k}{k_*} \right) \right\} . \end{aligned} \quad (3.23)$$

Adopting the evaluation point $k_* = 3k$, this precisely reproduces Khoury & Piazza's Eq. (8.4) [174] when expanded to first-order in ε . Although Eq. (3.23) does not rigorously apply to DBI, where c_s and thus f_X are changing, it can be checked that effects due to the time-dependence of f_X do not appear at next-order. Indeed, Eq. (3.23) yields Eq. (3.20) when $f_X = 1 - \gamma^{-2}$.

Generalized DBI inflation.—The analysis above was restricted to the asymptotic power-law regime first obtained by Silverstein & Tong [27], but this is not required. Using an arbitrary

potential $V(\phi)$ in the action (3.18) one can in principle construct a generic quasi-de Sitter background. Many of their properties, including the attractor behaviour, were studied by Franche et al. in Ref. [180].

How can we learn about the shape of the potential from observables such as f_{NL} ? We will show that through the next-order terms in f_{NL} we will be able to estimate corrections arising from the shape of $V(\phi)$ or $f(\phi)$. Analogous effects have been computed for galileon inflation [28], but our computation enables us to determine them in the DBI scenario for the first time. This is particularly relevant since the motivation behind DBI lies in brane inflation scenarios, and we can now gain access to compactification data which was previously hard, or even impossible to obtain by other means.

For $\gamma \gg 1$ the non-canonical structure suppresses the background dependence on details of the potential. But small fluctuations around the background cannot be shielded from these details, which induce three-body interactions whether or not they are relevant for supporting the quasi-de Sitter epoch. These interactions generate relatively unsuppressed contributions to the three-point function.

We adapt the notation of Franche et al. [180], who defined quantities measuring the shape of the potential $V(\phi)$ and the warping $f(\phi)$ ⁸

$$\varepsilon_v \equiv \frac{1}{2} \left(\frac{V'}{V} \right)^2, \quad \eta_v \equiv \frac{V''}{V}, \quad \text{and} \quad \Delta \equiv \text{sgn}(\dot{\phi} f^{1/2}) \frac{f'}{f^{3/2}} \frac{1}{3H}. \quad (3.24)$$

The same branch of $f^{1/2}$ should be chosen in computing $f^{3/2}$ and $\text{sgn}(\dot{\phi} f^{1/2})$. Note that these shape parameters do *not* coincide with the ‘global’ slow-variation parameters ε and η defined in Eq. (2.8). Franche et al. argued that $\Delta \ll 1$ was required to obtain attractor solutions, which we will assume to be satisfied in what follows. In addition, we work in the equilateral limit and take $\gamma \gg 1$, which is the regime of principal interest for observationally large f_{NL} .

⁸The factor $\text{sgn}(\dot{\phi} f^{1/2})$ was not used by Franche et al. [180], but is necessary here because the relativistic background solution requires $fX = 1 + \mathcal{O}(\gamma^{-2})$ up to corrections suppressed by $\mathcal{O}(\varepsilon)$, which are higher-order than those we retain. Depending on the direction of motion, this yields $\dot{\phi} = \pm f^{-1/2} + \mathcal{O}(\gamma^{-2})$. The choice of sign is important in obtaining the correct mapping between ε and ε_v , and others.

With these assumptions we find

$$\varepsilon \rightarrow \frac{\varepsilon_v}{\gamma}, \quad \eta \rightarrow 3 \frac{\varepsilon_v}{\gamma} - \frac{\eta_v}{\gamma} - \frac{3}{2} \Delta, \quad \text{and} \quad s \rightarrow -\frac{\varepsilon_v}{\gamma} + \frac{\eta_v}{\gamma} - \frac{3}{2} \Delta. \quad (3.25)$$

The leading-order term of Eq. (3.20) is unchanged, but the subleading terms are dominated by shape-dependent corrections, as follows:

$$f_{\text{NL}}^{(\text{equilateral})} \rightarrow -\frac{35\gamma_*^2}{108} \left\{ 1 + \frac{3\Delta_*}{14} \left(31 + 14\gamma_E - 228\omega + 14 \ln \frac{2k}{k_*} \right) + \frac{\eta_{v*}}{7\gamma_*} \left(3 - 14\gamma_E - 14 \ln \frac{3k}{k_*} \right) - \frac{2\varepsilon_{v*}}{7\gamma_*} \left(43 - 7\gamma_E - 256\omega - 7 \ln \frac{3k}{k_*} \right) + \mathcal{O}(\gamma_*^{-2}) \right\}. \quad (3.26)$$

These subleading terms are more important than those present in Eq. (3.20), which began at relative order γ_*^{-2} and are therefore strongly suppressed for $\gamma \gg 1$. Moreover, upon inspection of Eq. (3.25), inflation can occur even for relatively large values of ε_v and η_v , roughly whenever $\varepsilon_v/\gamma < 1$ —hence these corrections need *not* be extremely small.

For large $|f_{\text{NL}}^{(\text{equilateral})}|$, we estimate the relative correction to the leading-order $f_{\text{NL}}^{(\text{equilateral})}$ to be

$$\frac{\Delta f_{\text{NL}}^{(\text{equilateral})}}{f_{\text{NL}}^{(\text{equilateral})}} \simeq -2.75\Delta_* + \frac{2.10\varepsilon_{v*} - 0.41\eta_{v*}}{|f_{\text{NL}}^{(\text{equilateral})}|^{1/2}}. \quad (3.27)$$

For negative equilateral f_{NL} , current constraints roughly require $|f_{\text{NL}}|^{1/2} \lesssim 12$ [6]. Therefore, these corrections can be rather important unless the potential is tuned to be flat, although some cancellation occurs because ε_v and η_v enter with opposite signs.

To obtain an estimate, we suppose for simplicity that Δ_* is negligible. Taking the extreme 95%-confidence value $f_{\text{NL}} = -151$ [6], and $\varepsilon_v \simeq |\eta_v| \sim 1$ for a “generic” potential, the correction is of order 14% if $\eta_v > 0$ and 20% if $\eta_v < 0$. To reduce these shifts we might be prepared to assume $\varepsilon_v \simeq |\eta_v| \sim 0.1$, which suppresses the correction to the percent level. Nevertheless, the corrections grow with decreasing $|f_{\text{NL}}|$. Keeping the generic estimate $\varepsilon_v \simeq |\eta_v| \sim 1$, and

using $|f_{\text{NL}}| \approx 50$,⁹ we find the corrections to be of order 24% for $\eta_v > 0$ and 36% for $\eta_v < 0$.¹⁰ These are significant and cannot be ignored.

Although Franche et al. argued that Δ_* must be small to obtain attractor behaviour, it need not be entirely negligible. In such cases it introduces a dependence on the shape of the warp factor in addition to the shape of the potential. This may be positive or negative. If the Δ_* and ε_* terms add constructively, the next-order correction can become rather large. This, however, will be very model-dependent.

Infrared model.—The DBI scenario can be realized in several ways. The original “ultraviolet” model is now disfavoured by microscopic considerations [109, 111]. Chen introduced an alternative “infrared” implementation [181, 182, 183] which evades these constraints and remains compatible with observation [112, 184, 185, 186]. In this infrared version of DBI inflation, the warp factor $f(\phi)$ is that of an AdS throat λ/ϕ^4 , where λ is a dimensionless parameter. The potential is given by

$$V(\phi) = V_0 - \beta^2 H^2 \phi^2 / 2 ,$$

in which the mass is expressed as a fraction $\beta^{1/2}$ of the Hubble scale. The constant term V_0 dominates, making ε negligible, but the remaining slow-variation parameters need not be small. It is convenient to express our results in terms of the number e-folds to the end of inflation, N_e , which satisfies $\gamma \simeq \beta N_e / 3$. Background quantities evaluated at this time carry a subscript ‘e.’

Evaluating Eq. (3.25) for these choices of V and f , we obtain

$$\eta_e \simeq 3/N_e \quad \text{and} \quad s_e \simeq 1/N_e . \quad (3.28)$$

⁹For these values $\gamma \approx 10$ and the approximation $\gamma \gg 1$ used to derive Eq. (3.27) is at the limit of its applicability.

¹⁰In producing these estimates we are discarding constraints arising from the normalisation of the power spectrum.

The infrared model is an example where $\Delta_e \sim 1/N_e$ is not negligibly small. Using Eq. (3.27), we find

$$\frac{\Delta f_{\text{NL}}}{f_{\text{NL}}} \simeq -\frac{1}{7N_e} \left\{ 65 + 14\gamma_E - 484\omega + 14 \ln \frac{2k}{k_*} \right\} \simeq \frac{4.39}{N_e}, \quad (3.29)$$

where we have chosen $k_* = 3k$ in the final step. Adopting the best-fit value $N_e \approx 38$ suggested by Bean et al. [112], we find the fractional correction is of order 12%. This relatively small correction is a consequence of the negligible value of ε in this model. Keeping $N_e \approx 38$ and using the maximum likelihood value $\beta = 1.77$ quoted by Bean et al., we find $\Delta f_{\text{NL}} \approx -19$. The corresponding shift is from $f_{\text{NL}} \approx -163$ without next-order corrections to $f_{\text{NL}} \approx -182$ with next-order corrections included. This can be measured by *Planck*.

We conclude that next-order corrections not only need to be taken into account to keep the theory-error below *Planck*'s sensitivity, but they can also reveal important details about the potential and warping in DBI inflation scenarios.

***k*-inflation**

Another model that admits power-law solutions was proposed by Armendáriz-Picón, Damour & Mukhanov [26], and is known as *k*-inflation. The action is

$$P(X, \phi) = \frac{4}{9} \frac{4 - 3\gamma}{\gamma^2} \frac{X^2 - X}{\phi^2}, \quad (3.30)$$

where γ is some constant, no longer related to the speed of sound by the formula $c_s = \gamma^{-1}$ which applied for DBI. Unlike the DBI Lagrangian, Eq. (3.30) is not radiatively stable and its microscopic motivation is uncertain. Nevertheless, non-gaussian properties of the inflationary fluctuations in this toy model were studied by Chen et al. [45].

There exists a solution of the action (3.30) with

$$X = \frac{2 - \gamma}{4 - 3\gamma}, \quad (3.31)$$

making $\varepsilon = 3\gamma/2$ and c_s constant. Therefore this model has $\eta = s = 0$, but non-vanishing ε , and is thus not scale-invariant. Inflation occurs in the regime for which $0 < \gamma < 2/3$. This already requires a relatively tight constraint on the allowed values for γ . The leading-order contribution to f_{NL} is of order $1/\gamma$, making the next-order term of order unity. A next-next-order calculation would be required to accurately estimate the term of order γ .

In the equilateral limit, Chen et al. [45] quoted the leading-order result

$$f_{\text{NL}}^{(\text{equilateral})} \simeq -170/81 \gamma .$$

Proceeding as in §2.1 by focusing on the interaction vertices g_i given in Eq. (3.4), one can estimate the fractional theoretical uncertainty in this prediction to be $\sim 9\gamma$, or roughly ± 20 . This is comparable to *Planck*'s error bar, and is likely to exceed the error bar achieved by a subsequent CMB satellite. Still working in the equilateral limit, we find

$$f_{\text{NL}}^{(\text{equilateral})} \rightarrow -\frac{170}{81\gamma} \left\{ 1 - \frac{\gamma}{34} \left(61 - 192 \ln \frac{3}{2} \right) + \mathcal{O}(\gamma^2) \right\} . \quad (3.32)$$

Like for DBI inflation, a fortuitous cancellation brings the fractional correction down from our initial estimate $\sim 9\gamma$ to $\sim 0.5\gamma$ with all the next-order corrections taken into account. It was not necessary to choose a reference scale k_* in order to evaluate Eq. (3.32); in k -inflation, f_{NL} is scale-invariant even though the power spectrum is not.

Comparison with previous results.—Because $\varpi \neq 0$ in this model, the analysis of Khoury & Piazza does not apply. In another paper, however, Noller & Magueijo presented a generalisation which was intended to be valid for constant, but otherwise arbitrary ε and s , and small ϖ [187]. Their analysis also assumes constant f_X , which is not a good approximation in the regime of rapidly varying speed of sound. For comparison, we set the reference scale to be

$k_* = 3k$ and work in the equilateral limit for arbitrary constant f_X . One finds

$$\begin{aligned}
f_{\text{NL}}^{(\text{equilateral})} \rightarrow & -\frac{5}{972c_{s^*}^2} \left\{ 55(1 - c_{s^*}^2) + 8f_X \right\} \\
& + \frac{5\varepsilon}{972c_{s^*}^2} \left\{ 177 + 120c_{s^*}^2 - 1024\omega(1 - c_{s^*}^2) + f_X(264 - 1280\omega) \right\} \\
& + \frac{5s}{486c_{s^*}^2} \left\{ 7 + 55\gamma_E + 32c_{s^*}^2 - 256\omega(1 - c_{s^*}^2) + f_X(56 + 8\gamma_E - 320\omega) \right\} .
\end{aligned} \tag{3.33}$$

For $s = -2\varepsilon$, both Eq. (3.33) and Noller & Magueijo's formula (A.15) reduce to Eq. (3.23).

For $s \neq -2\varepsilon$, Eq. (3.33) disagrees with Noller & Magueijo's result. This occurs partially because they approximate the propagator (2.24) using the elementary wavefunction (2.23) in the super-horizon limit $|kc_s\tau| \ll 1$; in this limit details of the interference between growing and decaying modes around the time of horizon exit are lost. For example, their approximation discards the Ei-contributions of Eq. (A.2) although these are $O(\varpi)$ and as large as other contributions which are retained. But were these terms kept, the super-horizon limit $|kc_s\tau| \ll 1$ could not be used to estimate them. Infrared safety of the J_i integrals in Eqs. (3.8) is spoiled if truncated at any finite order, causing incorrect divergences in the squeezed limit $\vartheta_i \rightarrow 0$ and a spurious contribution to the bispectrum with a local shape. As we explain in Appendices A.1 and A.2, it appears that—as a point of principle—if $\varpi \neq 0$ corrections are kept, then the shape of the bispectrum can be accurately determined only if the *full time-dependence* of each wavefunction around the time of horizon exit is retained.

Another reason for the discrepancy with our results lies in the dynamics assumed for the scale factor. Even though Ref. [187] assumed small deviations from a perfectly scale-invariant spectrum of perturbations, their analysis used a scale-invariant evolution for the scale factor. As a result, their calculation dismisses contributions to the background dynamics as relevant as others kept in the evolution of the wavefunctions.

3.5 Tensor modes

We conclude our report on slow-roll corrections by studying the implications to tensor modes. Inflation has inevitably produced tensor fluctuations to accompany the scalar fluctuation ζ . Detecting the B-mode polarisation signal produced by these fluctuations is a major aim of the *Planck* satellite and future CMB experiments [188]. If measured, this signal will provide important constraints on the energy scale of inflation. Above all, it will be a strong indication that an inflationary period took place in the early universe.

In certain models the tensor sector provides sufficient observables to allow one or more quantities, such as f_{NL} , to be written in terms of other observables. These *consistency relations* were introduced by Copeland et al. [189, 190], and are completely decoupled of the way we choose to parametrise the theory. To be used effectively with the next-order results obtained in this chapter, we will require next-order predictions for the tensor modes. These were first obtained by Stewart & Lyth [102], and are unchanged by the non-canonical action (2.1) for the scalar field.

The tensor fluctuation is a propagating spin-2 mode which belongs to h_{ij} of the ADM metric (2.5). We write

$$h_{ij} = a^2 e^{2\zeta} (e^\gamma)_{ij} ,$$

where $\text{tr} \gamma_{ij} = 0$. At quadratic order, the action for tensor fluctuations is [191]

$$S_g^{(2)} = \frac{1}{8} \int d^3x d\tau a^2 \left\{ \gamma'_{ij} \gamma'_{ij} - \partial_k \gamma_{ij} \partial_k \gamma_{ij} \right\} . \quad (3.34)$$

As described in §2.2.1, the tensor perturbations decouple, at quadratic order, from the scalar modes. There are two polarisations, traditionally denoted ‘+’ and ‘×,’ making γ_{ij} transverse, $\partial_i \gamma_{ij} = 0$. Introducing a reference scale k_* as in §2.2.2 and adding both polarisations, the

resulting dimensionless spectrum can be written [102]

$$\mathcal{P}_g = \frac{2H_*^2}{\pi^2} \left\{ 1 + 2\varepsilon_* \left(1 - \gamma_E - \ln \frac{2k}{k_*} \right) \right\} . \quad (3.35)$$

This result is equal to the sum of two copies of the power spectrum for a massless scalar field with $c_s = 1$, and so \mathcal{P}_g is also conserved on super-horizon scales (there is no residual time-dependence in the answer). Including next-order corrections and for arbitrary k_* , the scale-dependence of \mathcal{P}_g is measured by the tilt n_t ,

$$n_{t*} \equiv \frac{d \ln \mathcal{P}_g}{d \ln k} = -2\varepsilon_* \left\{ 1 + \varepsilon_* - \eta_* \left(1 - \gamma_E - \ln \frac{2k}{k_*} \right) \right\} . \quad (3.36)$$

It is conventional to measure the amplitude of tensor fluctuations relative to ζ . One defines the tensor-to-scalar ratio, r , by the rule [190]

$$r \equiv \frac{\mathcal{P}_g}{\mathcal{P}} , \quad (3.37)$$

where \mathcal{P} is the dimensionless version of the scalar power spectrum (2.25). We find

$$r_* \simeq 16\varepsilon_* c_{s*} \left\{ 1 - 2\eta_* + (s_* + \eta_*) \left(\gamma_E + \ln \frac{2k}{k_*} \right) \right\} . \quad (3.38)$$

In canonical models, r can be written purely in terms of observable quantities. In the non-canonical case this is not automatically possible without the addition of new observables. In general,

$$r_* \simeq -8n_{t*} c_{s*} \left\{ 1 - \varepsilon_* - \eta_* + s_* \left(\gamma_E + \ln \frac{2k}{k_*} \right) \right\} . \quad (3.39)$$

One may use the lowest-order result for n_t to eliminate ε . To eliminate η would require the scalar spectral index, n_s . It is possible to use f_{NL} to rewrite c_s in the prefactor [111], but in doing so one introduces dependence on the parameter ℓ . Therefore at least two extra observables would be required to eliminate the dependence on s and ℓ . If these depend on t ,

ξ or similar parameters, then further observables could be required.

We conclude that at next-order in slow-roll, for a general $P(X, \phi)$ Lagrangian, the observables $\{r, n_s, n_t, f_{\text{NL}}\}$ do not form a closed set. As we shall see in §4.3.2, the consistency relations derived after modal decomposition of the bispectrum are able to circumvent this degeneracy, provided a sufficient number of observables (with comparable accuracy) is available.

3.6 Main results

This chapter is one of the main backbones of this thesis, which we attempt to summarise here. In the (very) near future, we expect key cosmological observables to be determined to high-precision. In particular, *Planck* is expected to deliver data in less than one year's time, and may determine the scalar spectral index n_s to an accuracy of roughly one part in 10^3 [192]. The level of precision reached by the present CMB experiments can only be exploited effectively if our theoretical predictions keep pace. In this chapter we have focused on three essential questions:

- i. How accurate are the theoretical estimates of the bispectrum?
- ii. How can we reduce the theory-error of our estimates to be in line with the sensitivity set by *Planck*?
- iii. How can we efficiently explore *Planck*'s data on the primordial bispectrum, and therefore learn more about the microphysics of the early universe?

The first two questions, and partly the last one, have been addressed in this chapter. The last question will be explored in detail in chapter 4.

Almost twenty years ago, Stewart & Lyth [102] obtained analytic formulae for the two-point function accurate to next-order in the slow-roll parameter $\varepsilon \equiv -\dot{H}/H^2$. Subsequent observational developments have restricted attention to a region of the parameters space where $\varepsilon \ll 1$ is a good approximation, making the leading-order prediction for the power spectrum

an accurate match for experiment. There is no reason to believe the same will remain true for three- and higher n -point correlations, which will be experimentally probed with *Planck*.

The results of §3.4 show that next-order corrections to f_{NL} in the equilateral mode may be comparable to *Planck*'s observational precision. For a future CMB satellite it is actually conceivable that the data will be more precise than a leading-order estimate. In this chapter we have reported a next-order calculation of the bispectrum in the slow-roll approximation applicable to all single-field inflationary models: those belonging to the Horndeski class, which includes models described by a Lagrangian of the form $P(X, \phi)$, where $X = (\partial\phi)^2$. Our calculation has so far focused on the magnitude of the bispectrum, f_{NL} , and in many models it provides a much more precise estimate than the lowest-order result.

Our major results can be categorised into two groups, as follows.

Accuracy and precision

Except in special cases where exact results are possible,¹¹ predictions for observable quantities have so far been presented with a theory-error encapsulating uncertainty due to small contributions which had not been calculated. For inflationary observables the typical scale of the theory-error is set by the accuracy of the slow-variation approximation, where the dimensionless quantities $\varepsilon \equiv -\dot{H}/H^2$, $\eta \equiv \dot{\varepsilon}/H\varepsilon$, $s \equiv \dot{c}_s/Hc_s$ (and others) are taken to be small. These are the assumptions of the slow-roll approximation, on which the results of this chapter are based. To obtain numerical estimates, we have applied our results to some models.

Power-law DBI inflation and k -inflation.—In §2.1 and §§3.4.1–3.4.1 we estimated the *precision* which could be ascribed to the leading-order formula for f_{NL} in the absence of a complete calculation of next-order effects. Using the next-order contributions from the vertices g_i in Eqs. (3.4), which can be obtained without detailed calculation, we estimated the fractional uncertainty to be of order 14ε (or as large as 70%) for DBI and 9γ (or as large as 6%) for k -inflation.

¹¹Amongst such exceptions are the results of Khoury & Piazza for constant f_X discussed in §3.4, and the calculation described in chapter 5.

The prospect of such large uncertainties, also pointed out by Adshead et al. [193], demands carrying out the full computation of all next-order terms in the slow-roll approximation.

In DBI and k -inflation scenarios, we find the terms omitted from these estimates generate large cancellations, in each case reducing the next-order contribution by roughly 95%. This is similar to what was observed by Gong & Stewart in their calculation of next-next-order corrections to the power spectrum [104]. Having done this calculation, it seems reasonable to infer that the contributions from g_i systematically overpredict the next-order terms. But this could not have been anticipated without a calculation of all next-order effects. Therefore, for power-law DBI and k -inflation models we conclude that the leading-order calculation is unexpectedly accurate.

Generalised DBI inflation.—The situation is different for a generalised DBI model with arbitrary potential $V(\phi)$ and warp factor $f(\phi)$. The largest next-order corrections measure a qualitatively new effect, not included in the power-law solution, arising from the shape of V and f . The fractional shift was quoted in Eq. (3.27) and can be large, because the DBI action supports inflation even on relatively steep potentials, for which ε_V and η_V may not be very small. Indeed, if one were to tune the potential to be flat, say $\varepsilon_v \sim |\eta_v| \lesssim 10^{-2}$, then much of the motivation for a higher-derivative model would have been lost. Even for rather large values of $|f_{\text{NL}}|$, the correction can be several tens of percent for an “untuned” potential with $\varepsilon_v \sim |\eta_v| \sim 1$ (maintaining ε and η small). For slightly smaller values of $|f_{\text{NL}}|$, the correction is increasingly significant, perhaps growing to $\sim 35\%$. The formulae quoted in §3.4.1 assume $\gamma \gg 1$ and would require modification for very small f_{NL} where $O(\gamma^{-1})$ corrections need not be negligible. If desired, these can be obtained from our full formulae tabulated in §3.1.

Infrared DBI inflation.—In the infrared DBI scenario proposed by Chen [181, 182, 183], we find the correction to be $\sim 12\%$ for parameter values currently favoured by observation, which translates to reasonably large shifts in f_{NL} . For the maximum-likelihood parameter values suggested by the analysis of Bean et al. [184], we find that next-order corrections increase the magnitude of f_{NL} by a shift $|\Delta f_{\text{NL}}| \simeq 19$. This is a little smaller than the error bar which

Planck is expected to achieve, but nevertheless of comparable magnitude. We conclude that a next-order calculation will be adequate for *Planck*, but if the model is not subsequently ruled out, a next-next-order calculation may be desirable for a *CMBPol*- or *CoRE*-type satellite.

Technical results

Our calculation includes a number of more technical results, listed below.

Treatment of boundary terms.—In §2.3.1 we gave a systematic treatment of boundary terms in the third-order action for ζ . Although these terms were properly accounted for in previous results [66, 88, 45], these calculations used a field redefinition which was not *guaranteed* to remove all terms in the boundary action.

Our calculation has also shown how the cubic action could be written in terms of a minimal number of *five* Horndeski operators, given in Eq. (3.3).

Pure shape logarithms.—The subleading correction to the propagator contains an exponential integral contribution whose time-dependence cannot be described by elementary functions [104, 45, 28]. This term contributes at the level of the internal legs of the Feynman diagram. We argue that it must be handled carefully to avoid unphysical infrared divergences in the squeezed limit, where one momentum goes to zero. In Appendix A.2 we describe how this contribution yields the J_i functions given in Eqs. (3.8). These are obtained using resummation and analytic continuation techniques introduced in Ref. [28].

The possibility of spurious divergences in the squeezed limit shows that, as a matter of principle, one should be cautious when determining the shape of the bispectrum generated by an approximation to the elementary wavefunctions. Obtaining the quantitatively correct *momentum* behaviour requires all details of the interference in *time* between growing and decaying modes near horizon exit. The possibility of such interference effects, absent in classical mechanics, is a typical feature of quantum mechanical processes. This interference correctly resolves the unwanted divergences in the infrared limit $k_j \rightarrow 0$ with $j \neq i$, as discussed in

detail in Appendices [A.1](#) and [A.2](#).

Comparison with known results.—We have verified Maldacena’s consistency condition (3.11) to next-order in canonical models by doing an explicit calculation of the full bispectrum. This agrees with a recent calculation by Renaux-Petel [169]. This matching depends carefully on keeping track of the scale and shape logarithms available in the next-order terms in slow-roll.

In the case of power-law inflation with a scale-invariant spectrum of scalar perturbations, $\varpi = 0$, and constant ε and s , we reproduce a known result derived by Khoury & Piazza [174]. A subset of our corrections was computed by Chen et al. [45]. Up to first-order terms in powers of slow-roll quantities—where our results can be compared—we find exact agreement.

Mystery creates wonder and wonder is the basis of man's desire to understand.

Albert Einstein

4

Decoding the Bispectrum of Single-Field Inflation

This chapter reports a thorough investigation of the properties of the bispectrum in single-field inflation, based on the results obtained in chapter 3. The main object of study will be the scale and the shape-dependences of the bispectrum. They offer very insightful information about the microphysics of the early universe, and together with the amplitude f_{NL} , they fully characterise the bispectrum as an intricate ‘three-dimensional’ object. This chapter is therefore complementary to chapter 3.

Outline.—We obtain in §4.1 a generic formula for the overall running of f_{NL} with scale in single-field inflation theories. This is particularly important if we want to use data collected at different scales—the ability to use different sets of data makes the constraints on the parameters of the theory tighter [194].

In §4.2 we catalogue the Horndeski shapes appearing at leading and next-order in the slow-roll approximation. We identify what appears to be a ‘new’ bispectrum shape uncorrelated with the common templates used in CMB analysis. This shape can show up both at leading and at next-order in the slow-roll approximation, and it had appeared before in a galileon model

constructed by Creminelli et al. [11]. To explain the recurrent emergence of this shape we decompose in §4.3 the primordial bispectrum into fundamental harmonics. We elaborate on the consistency relations obtained between the amplitudes of each fundamental eigenmode, and discuss their usefulness. We present in §4.4 a summary of our findings.

This chapter contains material discussed in Ref. [1] in collaboration with Clare Burrage & David Seery, and Ref. [2] in collaboration with David Seery.

4.1 Scale-dependence

As we discussed in §3.2, we can use the logarithms $\ln(k_i/k_*)$ and $\ln(k_t/k_*)$ to study the scale-dependence of the three-point function. In the squeezed limit this is determined by Maldacena’s consistency condition (3.11). The only scale which survives the factorisation procedure is the common hard momentum k_{UV} , and the variation of f_{NL} with this scale is dictated by the variation of $(n_s - 1)$. This is typically called the *running with scale* of the scalar spectral index [195]. It follows that the running of Eq. (3.11) leads to a further consistency relation inherited from Maldacena’s.¹ In the case of single-field canonical inflation, studied in §3.3, we were able to verify this explicitly.

Away from the squeezed limit, deformations of the momentum triangle may change either its shape or scale. Scale dependence appears in all models, for the same reason that the spectrum \mathcal{P} and spectral index n_s depend on scale [57, 66, 88, 67, 45].

As the spectral index measures the running of the power spectrum with scale, one can similarly apply the same technique to the bispectrum. Chen [183] introduced a tilt of f_{NL} , denoted by $n_{f_{NL}}$ and defined by²

$$n_{f_{NL}} \equiv \frac{df_{NL}}{d \ln k_t} . \quad (4.1)$$

¹In general, a hierarchy of such consistency equations can be generated by taking an arbitrary number of derivatives of both sides of Eq. (3.11)—this has been investigated in Ref. [196]. However, so far only the first of such derivatives has been the subject of investigation.

²Chen implicitly worked in the equilateral limit $k_i = k$, for which $k_t = 3k$ and $d \ln k_t = d \ln k$. We are defining $n_{f_{NL}}$ to be the variation of f_{NL} with the perimeter of an arbitrary triangular configuration with fixed shape.

For a fixed triangular shape, this measures changes in f_{NL} as the perimeter varies. Scale-dependence of this type was subsequently studied by several authors [197, 175]. Observational constraints have been determined by Sefusatti et al. [198]. Byrnes et al. performed a similar analysis in multiple-field models producing a local bispectrum [199, 200]. They allowed for deformations of the momentum triangle including a change of shape, but found these to be less important than rescalings of k_t .

As we shall see in the next section, shape-dependence is often substantially more complicated than scale-dependence. By construction, Eq. (3.2) makes f_{NL} dimensionless, but contains both powers and logarithms of the momenta k_i . The powers occur as dimensionless ratios in which k_t does not appear, but the shape-dependence remains. The argument of each logarithmic term is also a dimensionless ratio, but an extra scale becomes available: the reference scale k_* . When present, this gives rise to the scaling logarithms $\ln(k_i/k_*)$ and $\ln(k_t/k_*)$, which depend on k_t as well as the shape. In particular we observe that any $\ln k_t$ appears in the form $\ln(k_t/k_*)$; said differently, all the dependence of the triangle with scale is rescaled with respect to the pivot scale, k_* .

It follows that a simple way to track the k_t -dependence of f_{NL} is through the k_* -logarithms:

$$n_{f_{\text{NL}}} = -\frac{df_{\text{NL}}}{d \ln k_*} . \quad (4.2)$$

For an arbitrary Horndeski model, $n_{f_{\text{NL}}}$ can be written

$$\begin{aligned} n_{f_{\text{NL}}} \rightarrow \frac{5}{24z_*} & \left\{ g_{1*} H_* (h_{1*} - \varepsilon_* - \nu_*) f_1(k_i) + g_{2*} (h_{2*} - \nu_*) f_2(k_i) \right. \\ & + \frac{g_{3*}}{c_{s*}^2} (h_{3*} - \nu_* - 2s_*) f_3(k_i) + \frac{g_{4*}}{c_{s*}^2} (h_{4*} - \nu_*) f_4(k_i) \\ & \left. + \frac{g_{5*}}{c_{s*}^2} (h_{5*} - \nu_*) f_5(k_i) \right\} , \end{aligned} \quad (4.3)$$

where the functions $f_m(k_i)$ correspond to dimensionless ratios of polynomials of k_i and are listed in Table 4.1.

$f_1(k_i)$	$\frac{24k_1^2k_2^2k_3^3}{k_1^3(k_1^3+k_2^3+k_3^3)}$
$f_2(k_i)$	$\frac{4[k_1^2k_2^2(k_1+k_2)+2k_1^2k_2^2k_3+(k_1+k_2)(k_1^2+k_1k_2+k_2^2)k_3^2+(k_1^2+k_2^2)k_3^3]}{k_1^2(k_1^3+k_2^3+k_3^3)}$
$f_3(k_i)$	$\frac{2(k_1^2+k_2^2+k_3^2)[k_1^3+2k_1^2(k-2+k_3)+2k_1(k_2^2+k_2k_3+k_3^2)+(k-2+k_3)(k_2^2+k_2k_3+k_3^2)]}{k_1^2(k_1^3+k_2^3+k_3^3)}$
$f_4(k_i)$	$\frac{2k_1^5+3k_1^4(k_2+k_3)+(k_2-k_3)^2(k_2+k_3)(2k_2+k_3)(k_2+2k_3)+3k_1(k_2^2-k_3^2)^2-5k_1^3(k_2^2+k_3^2)-k_1^2(k_2+k_3)(5k_2^2+k_2k_3+5k_3^2)}{k_1^2(k_1^3+k_2^3+k_3^3)}$
$f_5(k_i)$	$\frac{2k_1^5+k_1^4(k_2+k_3)+k_1(k_2^2-k_3^2)^2-3k_1^3(k_2^2+k_3^2)+(k_2-k_3)^2(k_2+k_3)(2k_2^2+3k_2k_3+2k_3^2)}{k_1^2(k_1^3+k_2^3+k_3^3)}$

Table 4.1: Functions $f_m(k_i)$ determining the momentum dependence of the running of f_{NL} in Eq. (4.3).

Squeezed and equilateral limits.—In the equilateral limit, we find

$$n_{f_{\text{NL}}} \rightarrow -\frac{5}{81z_*} \left\{ g_{1*} H(\varepsilon_* + \nu_* - h_{1*}) + 3g_{2*}(\nu_* - h_{2*}) + \frac{51g_{3*}}{4c_{s*}^2}(\nu_* + 2s_* - h_{3*}) + \frac{12g_{4*}}{4c_{s*}^2}(h_{4*} - \nu_*) + \frac{12g_{5*}}{4c_{s*}^2}(h_{5*} - \nu_*) \right\} . \quad (4.4)$$

The squeezed limit gives a simpler result,

$$n_{f_{\text{NL}}} \rightarrow \frac{5}{24z_*} \left\{ g_{2*}(h_{2*} - \nu_*) + \frac{3g_{3*}}{c_{s*}^2}(h_{3*} - 2s_* - \nu_*) \right\} . \quad (4.5)$$

To illustrate an application of the hierarchy condition deduced from Maldacena's consistency condition (3.11), we define the running of the spectral index, α_s , by [195]

$$\alpha_s = \frac{d(n_s - 1)}{d \ln k} . \quad (4.6)$$

Compatibility with Eq. (3.11) in the squeezed limit requires

$$n_{f_{\text{NL}}} \rightarrow -\frac{5}{12} \alpha_s \Big|_{k_{\text{UV}}} . \quad (4.7)$$

For canonical single field inflation, discussed in §3.3, specializing to the equilateral limit of $n_{f_{\text{NL}}}$, we find

$$n_{f_{\text{NL}}}^{(\text{equilateral})} \rightarrow \frac{5}{216} \eta_*(66\varepsilon_* + 18\xi_*) . \quad (4.8)$$

In the squeezed limit one obtains

$$n_{f_{\text{NL}}}^{(\text{squeezed})} \rightarrow \frac{5}{12} \eta_*(2\varepsilon_* + \xi_*) = -\frac{5}{12} \alpha_{s*} , \quad (4.9)$$

which describes the running of the scalar spectral index, α_{s*} , in agreement with Eq. (3.11). The consistency conditions (3.15) and (4.9) represent a nontrivial check on the correctness of our calculation. Throughout the calculation we have carefully separated the conceptually

different scales k_t and k_* . Therefore the correct formula (4.9) is *not* simply a consequence of obtaining the correct leading-order terms in Eq. (3.15). It rather depends on a careful matching between the spectral index and f_{NL} in this limit.

As anticipated, $n_{f_{\text{NL}}}^{(\text{squeezed})} = \mathcal{O}(\varepsilon^2)$ in non-canonical models. Therefore a next-next-order calculation is required to estimate the running of f_{NL} in these models; this will be slow-roll suppressed compared to f_{NL} itself.

4.2 Shape-dependence

In the early days of computing next-order corrections to the power spectrum, pioneered by Stewart & Lyth [102], the main purpose was to obtain an accurate estimate of its amplitude.

In comparison, next-order corrections to the bispectrum can be relevant for at least three reasons. First, they can change the amplitude of three-point correlations beyond *Planck*'s experimental sensitivity. Second, as we have seen in the previous section, next-order corrections allow us to investigate the scale-dependence of the bispectrum. Third, they could potentially lead to the appearance of new “shapes,” by which we mean the momentum dependence of $B(k_1, k_2, k_3)$ [10], defined in Eq. (3.1). In principle, all these three effects are measurable.

The plots and overlapping cosines included in this chapter were produced by David Seery and originally presented in Refs. [1, 2].

4.2.1 Inner product and cosine

How similar, or dissimilar, are two given bispectrum shapes? Conservation of 3-momentum in the bispectrum requires that the momenta \mathbf{k}_i form a triangle in momentum space. The bispectrum is a function on this space of triangles. Babich et al. [10] described its functional form as the “shape” of the bispectrum and introduced a measure to distinguish *qualitatively*

different shapes. We briefly recall their method. We define the shape S_i as

$$S_i \equiv (k_1 k_2 k_3)^2 B_i . \quad (4.10)$$

One can introduce a formal “cosine” which may be used as a *quantitative* measure of similarity in shape between different bispectra. The inner product between two bispectra is defined by

$$B_1 \cdot B_2 \equiv \int_{\text{triangles}} dk_1 dk_2 dk_3 S_1(k_1, k_2, k_3) S_2(k_1, k_2, k_3) , \quad (4.11)$$

where the integral is to be taken over all triangular configurations of momenta \mathbf{k}_i . The cosine between B_1 and B_2 is given by

$$\cos(B_1, B_2) \equiv \frac{B_1 \cdot B_2}{(B_1 \cdot B_1)^{1/2} (B_2 \cdot B_2)^{1/2}} . \quad (4.12)$$

These expressions require some care. In certain cases the result may be infinite, requiring the integral to be regulated. This is usually the case when one of the bispectra peaks in the squeezed configuration. We will comment on how to deal with these cases next.

Parametrisations.—One can represent each shape S_i as a function of the three momenta, k_i , subject to the δ -distribution, that constrains only two of these to be linearly independent. Take k_3 to be the privileged scale in the triangle. Then k_1 and k_2 can be rescaled with respect to k_3 , and S_i can be represented in terms of k_1/k_3 and k_2/k_3 . This is the Babich et al. parametrisation [10], where the shape function is given by

$$S_i \rightarrow \left(\frac{k_1}{k_3} \right)^2 \left(\frac{k_2}{k_3} \right)^2 B_i \left(\frac{k_1}{k_3}, \frac{k_2}{k_3}, 1 \right) .$$

There is another useful parametrisation which enhances the symmetry in surfaces of the shape with equal magnitude. This is the parametrisation proposed by Fergusson & Shellard

[9], in which the momenta k_i in the inner product (4.11) can be parametrized geometrically in terms of the perimeter, k_t (which becomes the privileged scale), and two dimensionless ratios. As a result, for scale-invariant correlators only two variables, denoted α and β , are linearly independent, and these are defined by [9]

$$k_1 = \frac{k_t}{4} (1 + \alpha + \beta) \quad (4.13a)$$

$$k_2 = \frac{k_t}{4} (1 - \alpha + \beta) \quad (4.13b)$$

$$k_3 = \frac{k_t}{2} (1 - \beta) , \quad (4.13c)$$

where $0 \leq \beta \leq 1$ and $\beta - 1 \leq \alpha \leq 1 - \beta$. The shape function is given by the combination

$$S \rightarrow k_1^2 k_2^2 k_3^2 B(k_1, k_2, k_3) .$$

The measure $dk_1 dk_2 dk_3$ in the integrand of Eq. (4.11) is proportional to $k_t^2 dk_t d\alpha d\beta$. Therefore we can write

$$B_1 \cdot B_2 = N \int_{\substack{0 \leq \beta \leq 1 \\ \beta - 1 \leq \alpha \leq 1 - \beta}} d\alpha d\beta (1 - \beta)(1 + \alpha + \beta)(1 - \alpha + \beta) S_1(\alpha, \beta) S_2(\alpha, \beta) , \quad (4.14)$$

where N is a harmless normalisation which can be divided out. With this understanding we use Eq. (4.14) to determine the cosine in Eq. (4.12).

In practice, our bispectra are not scale-invariant and therefore Eq. (4.14) does not strictly apply. However, as we have already studied in §4.1 the violations of scale-invariance are small, and to a good approximation Eq. (4.14) can be used.

Divergences.—As mentioned before, the cosine defined in Eq. (4.12) requires some care. In particular, Eq. (4.14) may be infinite. For example, the well-studied local bispectrum diverges

like $(1 + \alpha + \beta)^{-2}$ or $(1 - \alpha + \beta)^{-2}$ in the limit $\beta \rightarrow 0$, $\alpha \rightarrow \pm 1$, or like $(1 - \beta)^{-2}$ in the limit $\beta \rightarrow 1$, $\alpha \rightarrow 0$ [10]. These correspond to the squeezed limits discussed in §3.1. Eq. (4.14) therefore exhibits power-law divergences on the boundaries of the region of integration, and in such cases the integral must be regulated to obtain a finite answer. For simplicity, we adopt a sharp cutoff which requires $k_i/k_t > \delta_{\min}$. As $\delta_{\min} \rightarrow 0$ the cosine (4.12) may converge to a nonzero limit if $B_1 \cdot B_2$, $B_1 \cdot B_1$ and $B_2 \cdot B_2$ diverge at the same rate.

For this reason, where divergences exist, the value assigned to $\cos(B_1, B_2)$ is largely a matter of convention, and should be interpreted as an indicative number. Nevertheless, to resolve the practical question of whether two shapes can be distinguished by observation it should be remembered that experiments cannot measure arbitrarily small wavenumbers [16]. Therefore their ability to distinguish shapes peaking in the squeezed limit is limited. In this case, to obtain accurate forecasts of what can be distinguished (especially today in anticipation to *Planck's* results), one should restore the k_t -dependence in (4.14) and restrict the integration to observable wavenumbers, yielding a manifestly finite answer [9, 201]. We do not attempt this here.

Template Shapes

It is often useful to compare the bispectrum shapes in a given model with certain templates. There are essentially four main templates used in CMB analysis: local³, equilateral⁴, orthogonal and enfolded⁵. At this point there is a potential issue with the notation used in this thesis. To distinguish between the equilateral *template* and the bispectrum shapes which can *peak at the equilateral limit*, we use a different font for the templates. A shape which peaks in the equilateral limit need not be 100% correlated with the equilateral template.

The name attributed to the templates is usually related to the triangular configuration which maximises the amplitude of the bispectrum, that is, f_{NL} . However, that need not be the

³See Komatsu & Spergel [51] and Babich et al. [10].

⁴See Babich et al. [10].

⁵See Meerburg et al. [202] and Senatore et al. [162].

case. For example, the orthogonal shape was proposed by Senatore, Smith & Zaldarriaga [162] (also see Chen [203] for a review), and it is constructed so as to peak both in the equilateral and flattened configurations (when two of the sides of the triangle are equal to half the third side).

We quote on table 4.2 the overlap cosines between the four templates mentioned above. The templates have variable overlap amongst themselves. For example, the local template overlaps mildly with the equilateral ($\sim 34\%$) template, but significantly with the orthogonal ($\sim 49\%$) and the enfolded ($\sim 60\%$) templates. The equilateral template is practically uncorrelated with the orthogonal, by construction, but overlaps roughly 51% with the enfolded template. Finally, the orthogonal template is correlated with the enfolded template roughly 85%.

	local	equilateral	orthogonal	enfolded
local	1.00			
equilateral	0.34	1.00		
orthogonal	0.49	0.03	1.00	
enfolded	0.60	0.51	0.85	1.00

Table 4.2: Overlap cosines between common templates, depicted in Table 4.3.

In table 4.3 we depict the four templates in the two different parametrisations.

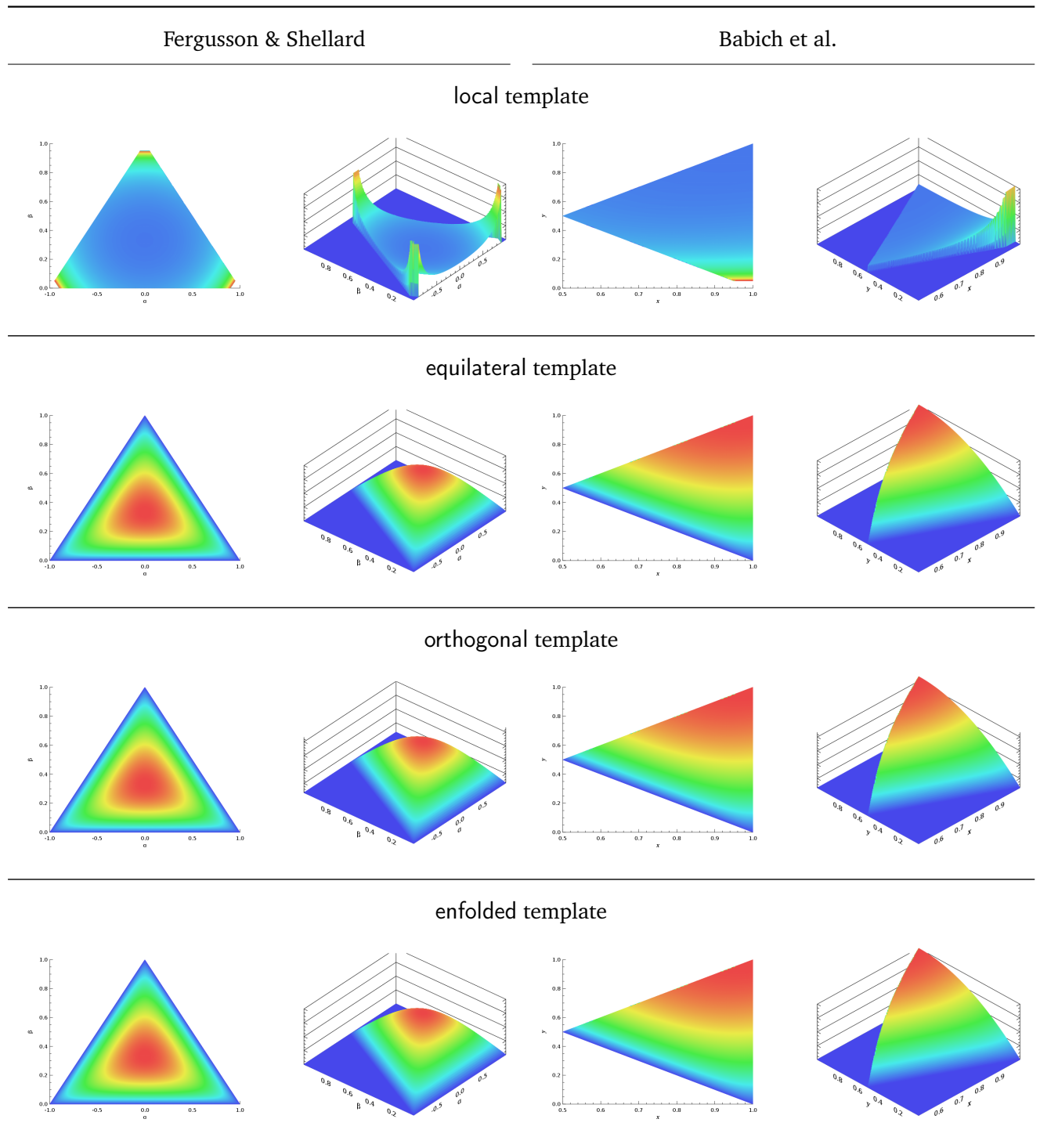


Table 4.3: The bispectrum templates used in CMB analysis in the Fergusson & Shellard [9], and Babich et al. [10] parametrisations. We see that the first parametrisation enhances the symmetry of the shape in $\{\alpha, \beta\}$ space.

4.2.2 Bispectrum shapes from slow-variation parameters

In a model with arbitrary interaction vertices g_i , the bispectrum is a linear combination of the shapes produced by the five operators in the action (3.3):

$$B = (k_1 k_2 k_3)^{-2} \sum_{i=1}^5 S_i, \quad (4.15)$$

where each operator i yields a shape S_i . We will now examine in detail the shapes arising at leading and next-order in the slow-variation approximation.

Leading-order shapes.—We quote the cosines of the shapes S_i , computed at lowest-order in the slow-roll approximation, with the common templates in table 4.4. We also plot the shapes S_i in table 4.5, using the two different parametrisations mentioned in §4.2.1. The ζ'^3 , $\zeta' \partial \zeta \partial \partial^{-2} \zeta'$ and $\partial^2 \zeta (\partial \partial^{-2} \zeta')^2$ shapes are largely correlated with the equilateral template. The $\zeta \zeta'^2$ and $\zeta (\partial \zeta)^2$ shapes are in turn correlated with the local template. In most cases there is a moderate overlap with the enfolded template, as we would expect from the correlations between the templates—see table 4.2.

	shapes at leading-order in slow-roll				
	$S_{\zeta'^3}$	$S_{\zeta \zeta'^2}$	$S_{\zeta (\partial \zeta)^2}$	$S_{\zeta' \partial_i \zeta \partial^i (\partial^{-2} \zeta')}$	$S_{\partial^2 \zeta (\partial_i \partial^{-2} \zeta')^2}$
local	0.42	0.99	1.00	0.35	0.31
equilateral	0.94	0.44	0.38	1.00	0.99
orthogonal	0.29	0.50	0.49	0.02	0.12
enfolded	0.75	0.65	0.62	0.55	0.43

Table 4.4: Cosines between the leading-order shapes and the common templates.

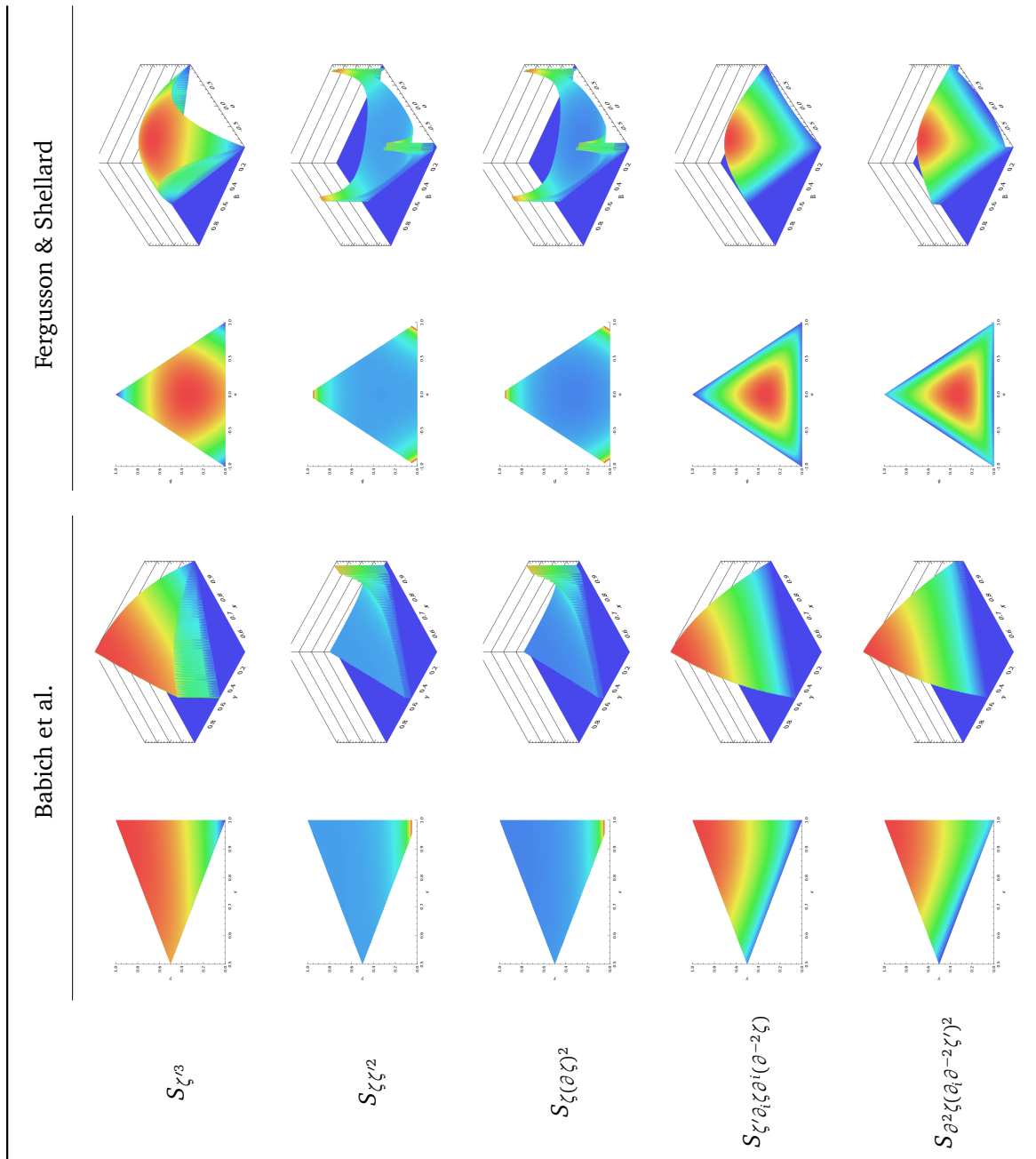


Table 4.5: Bispectrum shapes at leading-order in slow-roll for the operators in the action (3.3), using the Babich et al. [10], and Fergusson-Shellard [9] parametrisations.

A ‘new’ shape emerges at leading-order.—What is the overall bispectrum shape at leading-order? Factoring out an overall normalisation, the shape S of the bispectrum can be written

$$S \propto \alpha S_{\zeta^3} + \beta S_{\zeta\zeta^2} + \gamma S_{\zeta(\partial\zeta)^2} + \delta S_{\zeta'\partial_i\zeta\partial^i(\partial^{-2}\zeta')} + \omega S_{\partial^2\zeta(\partial_i\partial^{-2}\zeta')^2} , \quad (4.16)$$

where $\alpha, \beta, \gamma, \delta, \omega$ are rescaled versions of the interactions g_i .⁶ In a generic model we could perhaps expect all these ratios to be order unity.

We assume arbitrary g_i . By adjusting these coefficients it is possible to find a “critical surface” in the space of bispectrum shapes on which B becomes orthogonal to the set $Z = \{\text{equilateral, local, enfolded}\}$. The bispectrum can then be written in the form

$$S \propto \begin{pmatrix} \delta & \omega \end{pmatrix} \cdot \begin{pmatrix} S_\delta \\ S_\omega \end{pmatrix} + \begin{pmatrix} a & b & c \end{pmatrix} \cdot \begin{pmatrix} S_{\zeta^3} \\ S_{\zeta\zeta^2} \\ S_{\zeta(\partial\zeta)^2} \end{pmatrix} , \quad (4.17)$$

where the shapes S_δ and S_ω are orthogonal to each template in Z . The coefficients δ and ω act as coordinates on the subspace of bispectra orthogonal to these templates, whereas a , b and c are coordinates labelling departures from this critical surface. The appropriate choice is

$$\alpha \simeq 2.394\delta + 2.208\omega + a \quad (4.18a)$$

$$\beta \simeq 0.473\delta + 0.642\omega + b \quad (4.18b)$$

$$\gamma \simeq -0.183\delta - 0.248\omega + c . \quad (4.18c)$$

⁶ α and β here should not be confused with the $\{\alpha, \beta\}$ parameters in the Fergusson-Shellard parametrisation.

The shapes S_δ and S_ω then satisfy

$$S_\delta \simeq 2.394S_{\zeta'^3} + 0.473S_{\zeta\zeta'^2} - 0.183S_{\zeta(\partial\zeta)^2} + S_{\zeta'\partial_i\zeta\partial^i(\partial^{-2}\zeta')} \quad (4.19a)$$

$$S_\omega \simeq 2.208S_{\zeta'^3} + 0.642S_{\zeta\zeta'^2} - 0.248S_{\zeta(\partial\zeta)^2} + S_{\partial^2\zeta(\partial_i\partial^{-2}\zeta')^2} . \quad (4.19b)$$

Although we did not require it, these shapes have negligible overlap with the orthogonal template. But they *need not* be orthogonal amongst themselves. To measure *independent* combinations from data typically requires a dedicated template which has negligible overlap with other combinations. We follow the procedure of Refs. [162, 203]. The inner product matrix is $C_{ij} \equiv S_i \cdot S_j$. It is diagonalized by an orthogonal matrix \mathbf{P} whose columns are formed from the eigenvectors of \mathbf{C} . Setting $a = b = c = 0$ so that the bispectrum shape lies within the required critical surface, we write $\mathbf{x} = (\delta \ \omega)$, and $\mathbf{S} = (S_\delta \ S_\omega)^T$. The part of the bispectrum on the critical subspace can be written as $B^\parallel \propto \mathbf{q}\mathbf{H}$, where $\mathbf{q} \equiv \mathbf{x}\mathbf{P}$ and $\mathbf{H} \equiv \mathbf{P}^T\mathbf{S}$.

The shapes $S_{\zeta\zeta'^2}$ and $S_{\zeta(\partial\zeta)^2}$ have local-type divergences, which can be subtracted out by taking a suitable linear combination. This leaves four independent terms, from which we wish to construct a linear combination orthogonal to the three templates. We should expect a unique solution. This can be extracted from \mathbf{H} , and is given by

$$S_H = -0.805S_\delta + 0.593S_\omega . \quad (4.20)$$

This procedure discards the independent linear combination of $S_{\zeta\zeta'^2}$ and $S_{\zeta(\partial\zeta)^2}$. For practical purposes, we expect its divergence in the squeezed limit to make it almost indistinguishable from the local template. We ignore it in the equations which follow, although in principle one should remember that it is present. S_H is sometimes confusingly referred to in the literature as “orthogonal” since it results from an *orthogonalisation* procedure. We shall rather describe the shapes constructed this way as orthogonally designed.

We quote the overlap cosines between S_H and the templates in table 4.6. In table 4.7 we plot S_H in the Fergusson & Shellard parametrisation. Given that this parametrisation highlights

the symmetry of the surface of the shape, it will be very useful in what follows. As a function of the k_i there are multiple peaks in the critical surface, and therefore S_H is not maximised on a unique type of triangle.

local ^a	equilateral	orthogonal	enfolding
0.02	0.00	0.00	0.00

Table 4.6: Cosines between the S_H -shape (4.20) and common templates.

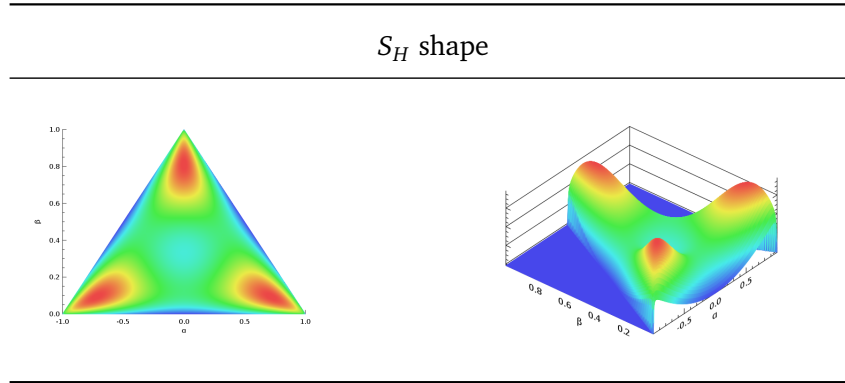


Table 4.7: The S_H -shape in the Fergusson & Shellard parametrisation.

The shape S_H smoothly converges to zero in the squeezed limit but exhibits a distinctive drumlin-shaped features near the corners of the triangle. This shape will occur in a typical bispectrum with coefficients which depend on ω and δ . We find

$$S = (0.593\omega - 0.805\delta)S_H + \begin{pmatrix} \alpha - 2.394\delta - 2.208\omega \\ \beta - 0.473\delta - 0.642\omega \\ \gamma + 0.183\delta + 0.248\omega \end{pmatrix} \cdot \begin{pmatrix} S_{\zeta^3} \\ S_{\zeta\zeta^2} \\ S_{\zeta(\partial\zeta)^2} \end{pmatrix}. \quad (4.21)$$

How significant is its contribution to the overall bispectrum shape? Since all prefactors will generically be of order unity, by assumption of a generic Horndeski model, the question re-

duces to the relative magnitudes of S_H and S_{ζ^3} , $S_{\zeta\zeta^2}$ and $S_{\zeta(\partial\zeta)^2}$. We find $\|S_H\| \sim 10^{-2}$, whereas $\|S_{\zeta^3}\| \sim 1$. The precise values assigned to $\|S_{\zeta\zeta^2}\|$ and $\|S_{\zeta(\partial\zeta)^2}\|$ depend on how their squeezed divergences are regulated, but generically we find $\|S_{\zeta\zeta^2}\|$ and $\|S_{\zeta(\partial\zeta)^2}\| \sim 10^1 - 10^2$. We conclude that S_H has an amplitude suppressed by roughly 10^3 to 10^4 compared with the leading-order shapes, all of which are well-matched by the standard templates. For the ‘new’ shape S_H to be visible requires *either*:

- i. the leading-order shapes to be suppressed, so that $a \simeq b \simeq c \simeq 0$ to an accuracy of a few parts in 10^3 to 10^4 . This could happen in a specific model, but requires fine-tuning.
- ii. the overall amplitude of the bispectrum to be sufficiently large so that the suppressed S_H is visible. Without a dedicated analysis of the signal-to-noise available in the S_H -channel for a CMB survey, it is not possible to know how large the bispectrum must be. However, it is unlikely that the signal to noise for S_H will be dramatically better than that for the equilateral template. Therefore, it seems reasonable to suggest that the leading-order operators would have to produce $|f_{\text{NL}}^{\text{equilateral}}| \gtrsim 100$ in order for the S_H -shape to be visible. This is presently under stress by experimental sensitivity [170, 171, 162, 6].

We conclude that it is both theoretically and observationally hard to realise S_H . There is another curious feature about this shape: it is extraordinarily similar to a shape encountered by Creminelli et al. [11], and which we plot on table 4.8. We will return to this issue in §4.3.

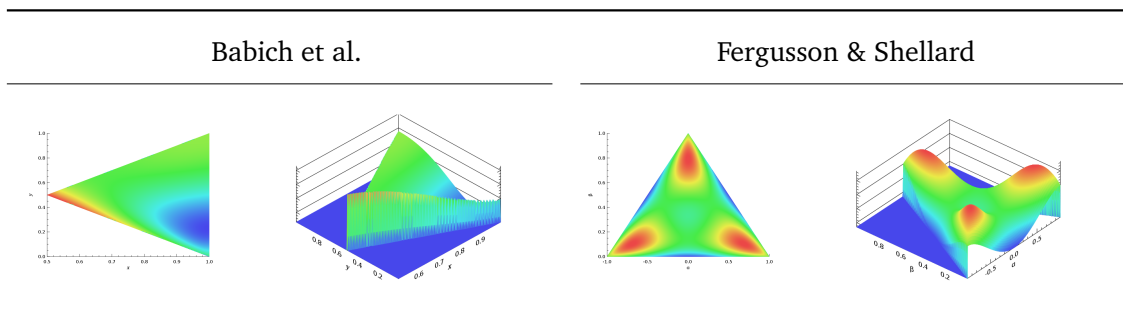


Table 4.8: Highly orthogonally designed shape constructed by Creminelli et al. [11].

Enhanced leading-order shapes by a reduced sound speed.—As discussed in §3.1.3, a $P(X, \phi)$

theory imposes strong correlations amongst the g_i . In this sense it is not as generic as an arbitrary Horndeski model, and we might not be able to finely tune the g_i to produce a ‘new,’ exotic bispectrum shape. In particular, at leading-order, g_4 and g_5 do not contribute.

We focus on a model with small sound speed, $c_s \ll 1$, in which next-order corrections are most likely to be observable, and retain only contributions enhanced by c_s^{-2} . The remaining three operators organise themselves into a family of shapes of the form $S_1 + \tilde{\alpha}S_2$, where S_2 arises only from ζ'^3 , but S_1 is a linear combination of the shapes produced by ζ'^3 , $\zeta\zeta'^2$ and $\zeta(\partial\zeta)^2$. The parameter $\tilde{\alpha}$ is the enhanced part of λ/Σ , that is

$$\frac{\lambda}{\Sigma} = \frac{\tilde{\alpha}}{c_s^2} + \text{O}(1) \quad \text{for } c_s \ll 1. \quad (4.22)$$

In the DBI model $\tilde{\alpha} = 1/2$. We plot the shapes S_1 and S_2 in Table 4.9.

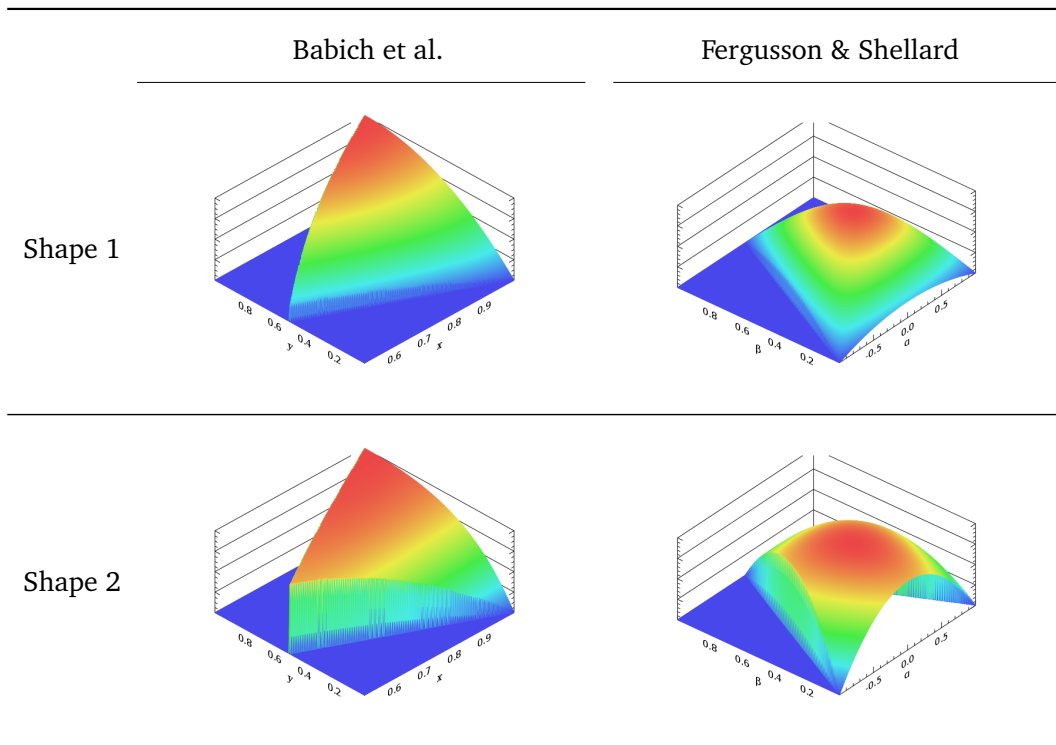


Table 4.9: Lowest-order bispectrum shapes enhanced by c_s^{-2} in $P(X, \phi)$ models.

Note that although S_1 involves a linear combination of the local-shape operators $\zeta\zeta'^2$ and

$\zeta(\partial\zeta)^2$, the $P(X, \phi)$ Lagrangian correlates their amplitudes in such a way that there is no divergence in the squeezed limit. Both S_1 and S_2 are strongly correlated with the equilateral template. They are similar to the M_1 - and M_2 -shapes studied by Creminelli et al. [11].

Next-order shapes.—Even though most next-order shapes are largely correlated with their parent leading-order shape, more shapes become available at next-order. Naïvely, the family of enhanced bispectra is labelled by ε , η , s , and also ℓ . In practice there is some degeneracy, because the shapes corresponding to these independent parameters may be strongly correlated. We will see these degeneracies emerge naturally in our analysis.

The c_s^{-2} -enhanced next-order shape can be written as a linear-combination of shapes proportional to the ε , η , s and ℓ parameters, modulated by $\tilde{\alpha}$,

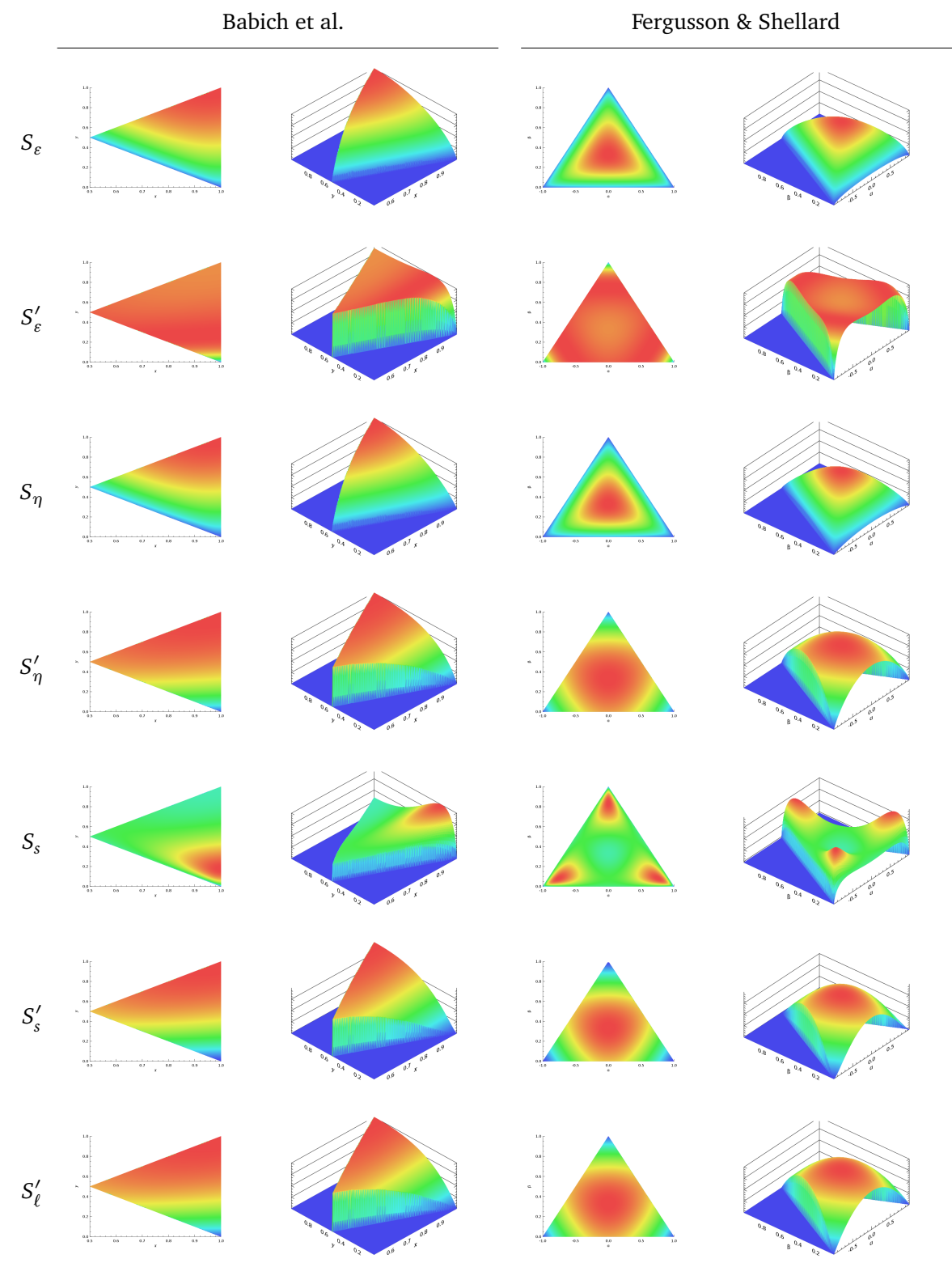
$$S_{\text{next-order}} \sim \varepsilon S_\varepsilon + \eta S_\eta + s S_s + \tilde{\alpha} \left(\varepsilon S'_\varepsilon + \eta S'_\eta + s S'_s + \ell S'_\ell \right) . \quad (4.23)$$

Primed shapes are enhanced by a small sound speed since they multiply $\tilde{\alpha}$ (prime here just denotes the c_s^{-2} -enhanced next-order shapes). We give overlap cosines between S_i and S'_i with the standard templates in Table 4.10 and plot them in Table 4.11.

	S_ε	S'_ε	S_η	S'_η	S_s	S'_s	S'_ℓ
local	0.38 ^a	0.50 ^a	0.37 ^a	0.43 ^a	0.54 ^a	0.39 ^a	0.42 ^a
equilateral	0.99	0.87	1.00	0.93	0.80	0.94	0.94
orthogonal	0.084	0.46	0.065	0.31	0.52	0.25	0.29
enfolding	0.60	0.86	0.59	0.77	0.87	0.72	0.75

^a The **local** template, and the operators $\zeta\zeta'^2$ and $\zeta(\partial\zeta)^2$, are strongly peaked in the “squeezed” limit where one momentum becomes much softer than the other two. For these shapes the inner product which defines the cosine is divergent, and must be regulated. The resulting cosines are almost entirely regulator-dependent. See the discussion in §4.2. The values we quote are meaningful only for our choice of regulator. For the values quoted above we used $\delta_{\min} = k/k_t = 10^{-3}$, where δ_{\min} is defined in the main text.

Table 4.10: Overlap cosines for the bispectrum shape proportional to each slow-variation parameter. Sign information has been discarded.

Table 4.11: Bispectrum shapes enhanced by c_s^{-2} at next-order in a $P(X, \phi)$ model.

Overall these shapes have strong overlaps with the equilateral template. However, two are quite different in appearance and have a slightly smaller cosine ~ 0.85 with this mode: these are S'_ε and S_s . We fix two coefficients in (4.23) by choosing a linear combination orthogonal to both S_1 and S_2 . Without loss of generality we can choose these to be η and s . We find the required orthogonal combination is

$$\eta \simeq \frac{0.12\tilde{\alpha}\ell(\tilde{\alpha} + 0.72)(\tilde{\alpha} + 1.82) - 0.88\varepsilon(\tilde{\alpha} - 9.15)(\tilde{\alpha} - 0.22)(\tilde{\alpha} + 1.82)}{(\tilde{\alpha} - 10.24)(\tilde{\alpha} - 0.23)(\tilde{\alpha} + 1.82)} \quad \text{and} \quad (4.24a)$$

$$s \simeq \frac{\tilde{\alpha}\ell(3.88 - 0.12\tilde{\alpha}) - 1.12\varepsilon(\tilde{\alpha} - 8.51)(\tilde{\alpha} - 0.08)}{(\tilde{\alpha} - 10.24)(\tilde{\alpha} - 0.23)}. \quad (4.24b)$$

It is possible this procedure is stronger than necessary. Both S_1 and S_2 are correlated with the equilateral template, and it may be sufficient to find a linear combination orthogonal to that. In what follows, however, we insist on orthogonality with S_1 and S_2 . For certain values of $\tilde{\alpha}$ the denominator of both η and s may simultaneously vanish, making the required η and s very large. This implies that, near these values of $\tilde{\alpha}$, no shape orthogonal to both S_1 and S_2 can be found within the validity of next-order perturbation theory. Therefore, we restrict attention to those $\tilde{\alpha}$ which allow acceptably small η and s .

This process leaves two linear combinations proportional to ε and ℓ . In principle these can be diagonalized, yielding a *pair* of shapes orthogonal to each other and $\{S_1, S_2\}$. However, the 2×2 matrix of inner products between these linear combinations is degenerate. Therefore, only *one* member of this pair is physical and can be realised in a $P(X, \phi)$ model. The other is not: it has zero inner product with the shape (4.23), and is impossible to realise because of enforced correlations between coefficients.

We denote the physical orthogonal combination O . It has a vanishing component proportional to ℓ . This was expected, because the shape S'_ℓ is the same as S_2 . For this reason, Chen et al. [45] absorbed ℓ into a redefined λ/Σ . It is indistinguishable from the lowest-order prediction and could never be observed separately, which is the origin of the degeneracy. We could have arrived at the same O by excluding S'_ℓ from (4.23). Demanding the inner product with S_1

and S_2 to be zero reproduces the physical linear combination obtained from diagonalisation.

We plot the shape of O in Table 4.12. Again, it is very similar to the highly orthogonal shape constructed by Creminelli et al. [11] plotted in table 4.13. Its dependence on $\tilde{\alpha}$ is modest. For comparison, we quote the cosine between O and the Creminelli et al. shape in Table 4.6. For varying $\tilde{\alpha}$ we find a cosine in the range 0.8 – 0.9, which indicates it would be observationally difficult to distinguish between these shapes.

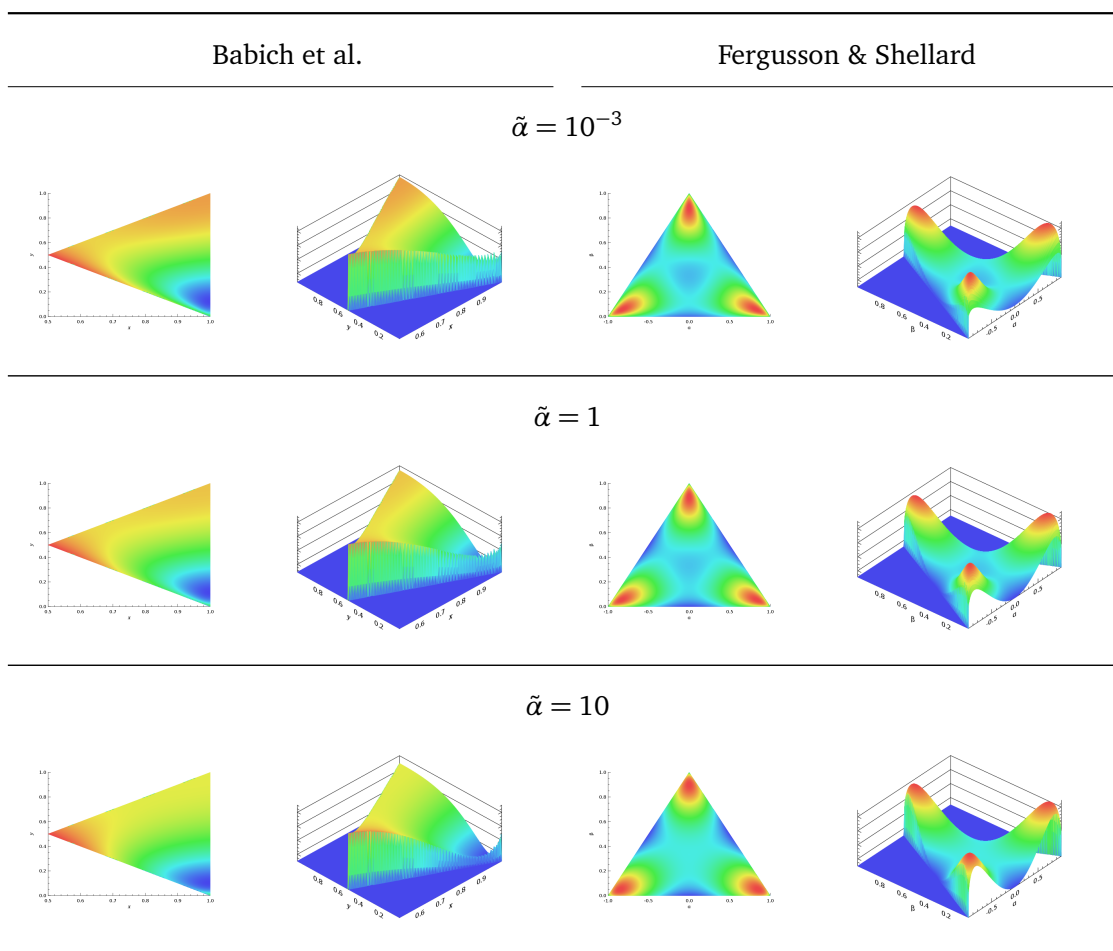


Table 4.12: The “orthogonal” shape O has zero overlap with both the shapes S_1 and S_2 .

In Table 4.13 we also give the overlap cosine with the common templates. The leading-order shapes S_1 and S_2 are strongly correlated with the equilateral template, and since O is orthogonal to these by construction, it also has small cosines with the equilateral template,

of order 10^{-2} . There is a moderate cosine with the local template of order $\sim 0.3 - 0.4$. The precise value depends on our choice of δ_{\min} , but the dependence is not dramatic. In Table 4.13 we have used $\delta_{\min} = 10^{-3}$. For $\delta_{\min} = 10^{-5}$ the local cosines change by roughly 25%, but overlaps with the remaining templates remain stable. O has a cosine of order $0.36 - 0.40$ with the orthogonal template, and of order $0.32 - 0.35$ with the enfolded template. We conclude that O it is not strongly correlated with any of the standard templates used in CMB analysis.

$\tilde{\alpha}$	local	equilateral	orthogonal	enfolded	Creminelli et al.
10^{-3}	0.35 ^a	0.012	0.36	0.32	0.89
1	0.38 ^a	0.012	0.38	0.33	0.86
10	0.41 ^a	0.011	0.40	0.35	0.81

^a Our choice of regulator is $\delta_{\min} = k/k_t = 10^{-3}$, where δ_{\min} was defined in §4.2.

Table 4.13: Overlap cosines between the orthogonal shape O and common templates.

For completeness and to facilitate the comparison, we include here the plots of all the orthogonally designed bispectrum shapes. Even if they could be realised in an inflationary model with severe fine-tuning, they could not be used to support one theory over another. From the shapes in table 4.14, shape O is the one which exhibits sharper features, with a steeper drumlin base. The remaining shapes appear to be slightly smoother.

These bispectrum shapes are incredibly similar, with an overlapping cosine in excess of roughly 85%. This raises the question of why a linear combination of dome-like shapes can always give rise to a drumlin-shape, with much more structure. We will investigate this in the next section.

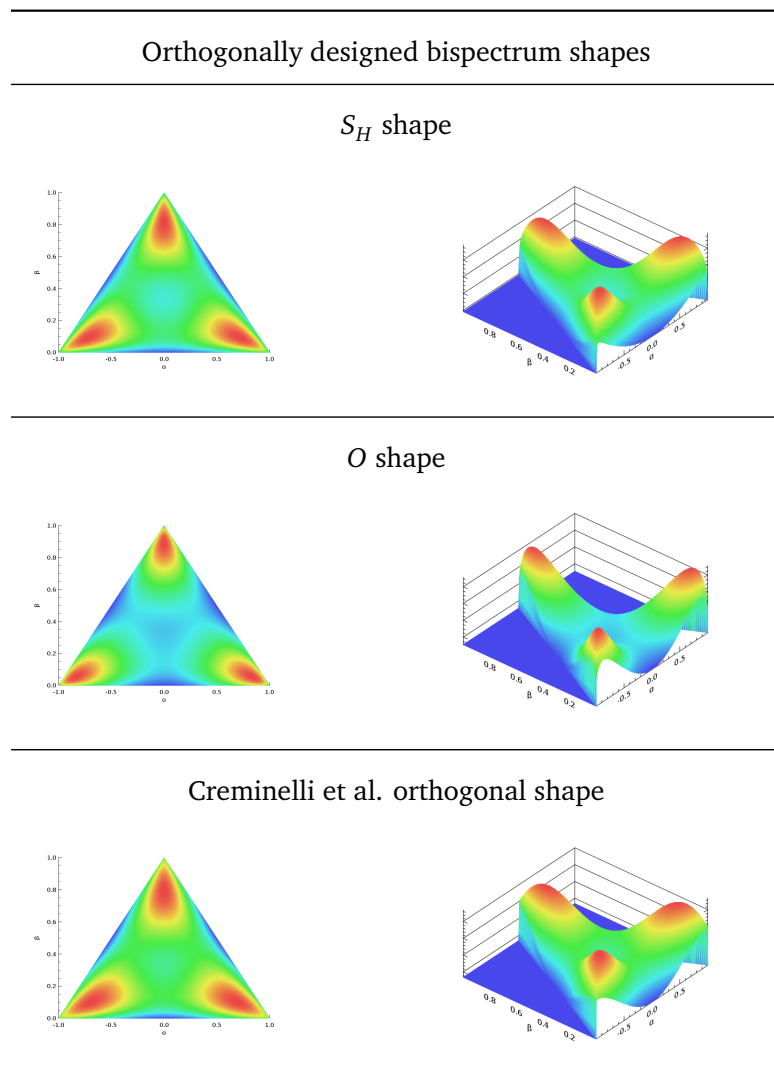


Table 4.14: The bispectrum shapes S_H , O and the one found by Creminelli et al. [11].

4.3 Resolving the “drumlin” bispectrum shape

The plots in table 4.14 make it clear that the ‘new,’ orthogonally designed shape cannot be used as a diagnostic tool to distinguish between models. However, why is this shape recurrent in the orthogonalisation procedure?

The drumlin structure increases the number of nodes/anti-nodes in the bispectrum. One can think of the orthogonalisation procedure as taking two almost pure Fourier harmonics and constructing an orthogonal function. The result will be approximately the next available Fourier harmonic, which by construction will not correlate with the fundamental modes. This suggests that to understand the appearance of these shapes, it might be helpful to decompose the bispectrum into some analogue of Fourier modes. The underlying triangular geometry is different to the flat intervals which yield Fourier harmonics, so the appropriate analogue will be a generalised partial wave, though we might refer to them as fundamental harmonics.

4.3.1 Harmonic decomposition

Although partial-wave decompositions have been usefully applied to quantum field theory, so far they have not been very popular in inflationary correlations. Recently, Fergusson et al. [9, 201] introduced an eigenmode decomposition, and emphasised its computational efficiency. We largely follow their method and notation. Physical conclusions must be independent of the basis, but the analysis may be made simpler by an appropriate choice.⁷

Fergusson et al. suggested writing each shape function in the form

$$S(k_1, k_2, k_3) = \sum_n \alpha_n \mathcal{R}'_n(k_1, k_2, k_3) , \quad (4.25)$$

for some coefficients α_n (not to be confused with $\tilde{\alpha}$ in §4.2.2) and a set of dimensionless basis functions \mathcal{R}'_n which are orthonormal in the inner product (4.11). The functions \mathcal{R}'_n are a subset

⁷ For comparison with the Fergusson et al. basis, we have repeated the analysis using Bessel functions [9]. With this choice, convergence is much slower. A different decomposition was used by Meerburg [204].

of those constructed by Fergusson et al. [9, 201] and labelled \mathcal{R}_n . The \mathcal{R}'_n form a basis on a fixed slice at constant k_t , suitable for an approximately scale-invariant primordial bispectrum. Fergusson et al.'s \mathcal{R}_n are not scale-invariant and are orthonormal in a three-dimensional inner product which accounts for variation in k_t . Our \mathcal{R}'_n are constructed using precisely the same procedure, but because many of the \mathcal{R}'_n are degenerate purely as a function of shape (but not scale) they are projected out of the \mathcal{R}'_n . It is in this sense that the \mathcal{R}'_n form a subset of the \mathcal{R}_n .

The choice of \mathcal{R}'_n was motivated by numerical considerations, as follows. Define a complete set of orthonormal polynomials $q_p(x)$ on the unit interval $x \in [0, 1]$ with measure $w(x)$ and introduce separable quantities $\mathcal{Q}_{(p,q,r)}$ satisfying

$$\mathcal{Q}_{(p,q,r)} = q_p(2k_1/k_t)q_q(2k_2/k_t)q_r(2k_3/k_t) + 5 \text{ permutations} . \quad (4.26)$$

Fergusson et al. chose w to cancel an unwanted growth in the bispectrum at large k ; for all details and the construction of the $q_p(x)$ we refer to the original literature [9, 201]. One may impose a fixed normalisation for the $\mathcal{Q}_{(p,q,r)}$ if desired. They can be ordered by defining $\rho^2 = p^2 + q^2 + r^2$ and sorting the $\mathcal{Q}_{(p,q,r)}$ in ascending order of ρ .

Finally, the \mathcal{R}'_n are constructed by Gram–Schmidt orthonormalisation of the ordered $\mathcal{Q}_{(p,q,r)}$, resulting in a linear combination of separable functions. This leads to efficiencies in computation, which was the principal motivation for Refs. [9, 201]. One can obtain the expansion coefficients α_n for any bispectrum B using the inner product (4.11)

$$\alpha_n = \langle \mathcal{R}'_n, B \rangle . \quad (4.27)$$

Since $\|B\|^2 = \sum_n \alpha_n^2$, then α_n^2/α_m^2 measures the relative importance of the m^{th} and n^{th} modes.

We plot the first few \mathcal{R}'_n in Table 4.15. The $n = 0$ mode is a constant. The $n = 1, 2$ modes are a good match for the overall shape of both the equilateral and orthogonal templates. Strong features in the corners of the triangle, characteristic of the local shape, appear at higher n . Generically speaking, from $n = 4$ onwards there is more structure in each harmonic basis.

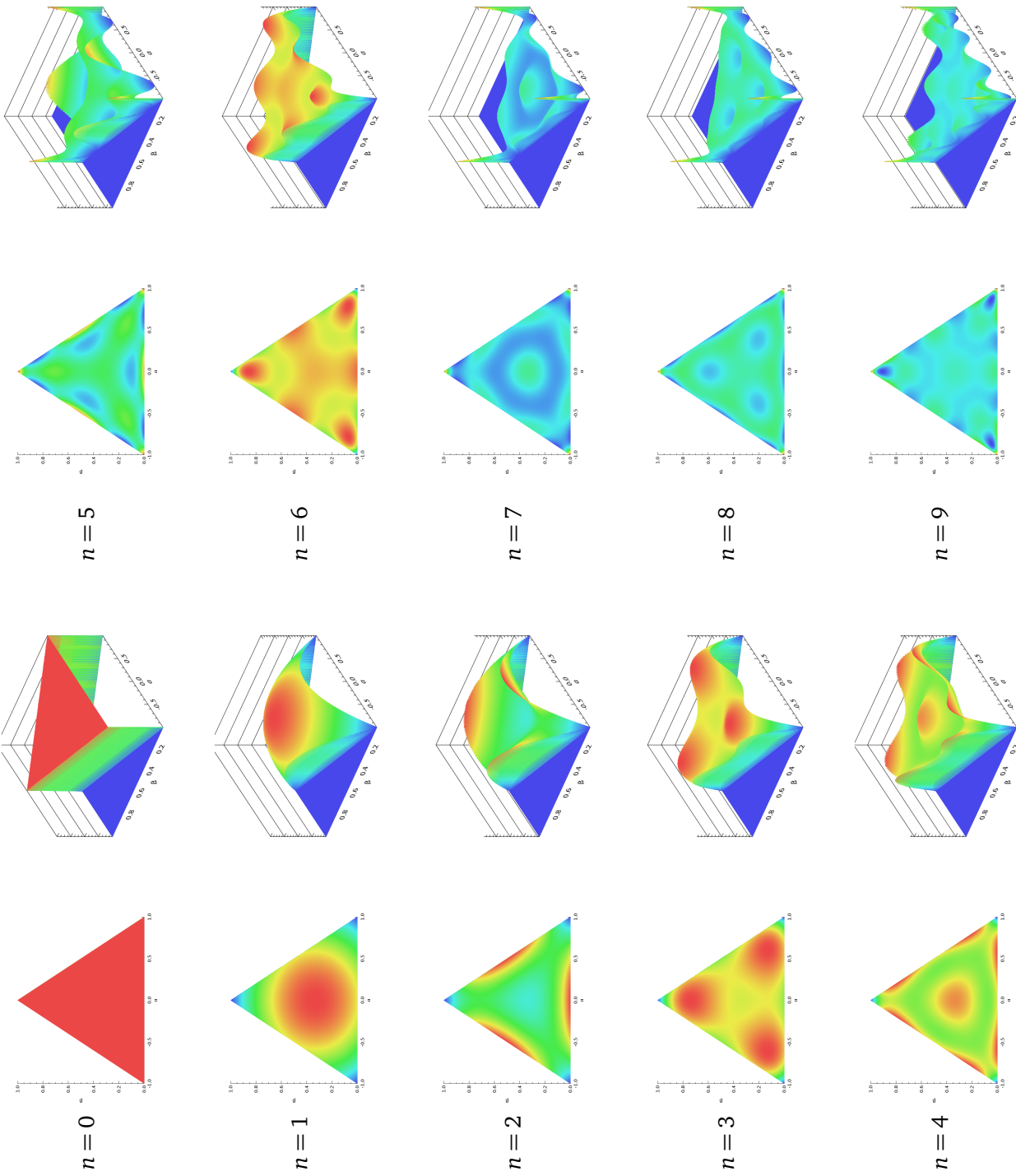


Table 4.15: Bispectrum basis shapes \mathcal{B}'_n in 2d and 3d plots up to $n = 9$.

Any arbitrary bispectrum shape will thus be the product of a linear combination of the fundamental \mathcal{R}'_n basis:

$$\begin{aligned}
 S(k_1, k_2, k_3) = & \alpha_0 \text{ [shape 0]} + \alpha_1 \text{ [shape 1]} + \alpha_2 \text{ [shape 2]} \\
 & + \alpha_3 \text{ [shape 3]} + \alpha_4 \text{ [shape 4]} + \alpha_5 \text{ [shape 5]} \\
 & + \dots
 \end{aligned}$$

Figure 4.1: An arbitrary bispectrum built as a linear combination of fundamental harmonic shapes.

Orthogonal combinations

That we can expand a bispectrum shape in fundamental, orthogonalised harmonics is not surprising. This is *always* permissible. For our purposes, however, the \mathcal{R}'_n depicted in the table 4.15 are particularly useful since the first three partial waves provide a very good description of the equilateral, orthogonal and enfolded templates. Indeed, these can all be obtained by shifting the equilateral shape by a constant [162, 203]. The \mathcal{R}'_0 shape is the constant shift. The “first harmonic,” \mathcal{R}'_1 , peaks in the equilateral limit, whereas \mathcal{R}'_2 peaks in the *flattened* configuration, where $\alpha = \beta = 0$ (this makes $k_i = k_j = k_k/2$).

We quote the expansion coefficients α_n for the common templates in table 4.16, obtained using Eq. (4.27). For the reasons we have explained, the equilateral, orthogonal and enfolded templates are dominated by $\{\mathcal{R}'_0, \mathcal{R}'_1, \mathcal{R}'_2\}$, and for higher n we observe the corresponding α_n decrease. This explains why the shapes S_H in Eq. (4.20) and O depicted in table 4.12 have negligible overlap with the orthogonal template, even though this was not guaranteed by its

construction. On the other hand, the local shape does not have a rapidly convergent expansion because its squeezed divergence requires a comparatively larger admixture of modes with $n \gg 1$. As a result the \mathcal{R}'_n -basis is particularly well-adapted for an efficient description of the higher-derivative self-interactions of ζ , like those arising in DBI inflation, which typically do not generate such divergences.

	α_0	α_1	α_2	α_3	α_4	α_5	α_6	α_7	α_8	α_9
local	-2.16	1.78	0.75	-1.21	0.79	-0.49	0.85	1.01	-0.53	-0.55
equilateral	0.52	0.23	-0.16	-0.03	-0.01	0.02	0.00	0.05	0.02	-0.01
orthogonal	-0.44	0.68	-0.49	-0.10	-0.04	0.07	0.01	0.13	0.05	-0.03
enfolding	0.48	-0.23	0.16	0.03	0.01	-0.02	0.00	-0.04	-0.02	0.01

Table 4.16: Expansion of common templates in terms of the \mathcal{R}'_n basis.

The idea that the orthogonalisation method suppresses, by construction, the coefficients of the first fundamental harmonics $\{\mathcal{R}'_0, \mathcal{R}'_1, \mathcal{R}'_2\}$, emerges from the discussion above. We give α_n for the various ‘new,’ orthogonally designed shapes discussed in §4.2.2 on table 4.17. We observe that the \mathcal{R}'_0 shape is projected out entirely both for the shape of Creminelli et al. and the S_H -shape in Eq. (4.20). The situation for the O shape seems more complicated, as previously anticipated, and we exclude it from our analysis for simplicity. For the other two shapes, the $n = 1, 2$ harmonics are not completely removed but their amplitudes are significantly damped. The largest individual term in each orthogonalised shape is a nearby higher mode—in this case, the $n = 3$ term. (This is the next highest, although recall that the precise ordering of the \mathcal{R}'_n is somewhat arbitrary.) There is an admixture of the other harmonics with smaller amplitudes. Comparison with table 4.15 shows that the large $n = 3$ contribution is essentially responsible for the common appearance of drumlin features.

	α_0	α_1	α_2	α_3	α_4	α_5	α_6	α_7	α_8	α_9
S_H -shape	0.000	0.006	0.006	0.010	0.005	-0.002	-0.002	-0.005	-0.003	0.002
O-shape	0.047	-0.190	-0.100	-0.107	-0.024	0.026	0.028	0.043	0.024	-0.019
Creminelli et al. shape	0.000	0.015	0.019	0.024	0.011	-0.006	-0.002	-0.012	-0.006	0.003

Table 4.17: Expansion of the S_H -shape (defined at leading-order in slow-roll), the O-shape (defined at next-order in slow-roll) [1] and the Creminelli et al. shape [11] in terms of the \mathcal{R}'_r basis.

In table 4.18, the right-hand columns give an approximation to each exact shape, built from the first ten \mathcal{R}'_n . We quote the corresponding cosines in table 4.19. The approximations are rather good, resulting in cosines in excess of 0.99. Given a set of trial shapes, which could presumably be generated by considering arbitrarily exotic higher-derivative operators in the Lagrangian, this basis could be constructed precisely by the Gram–Schmidt procedure described in §4.2.2.

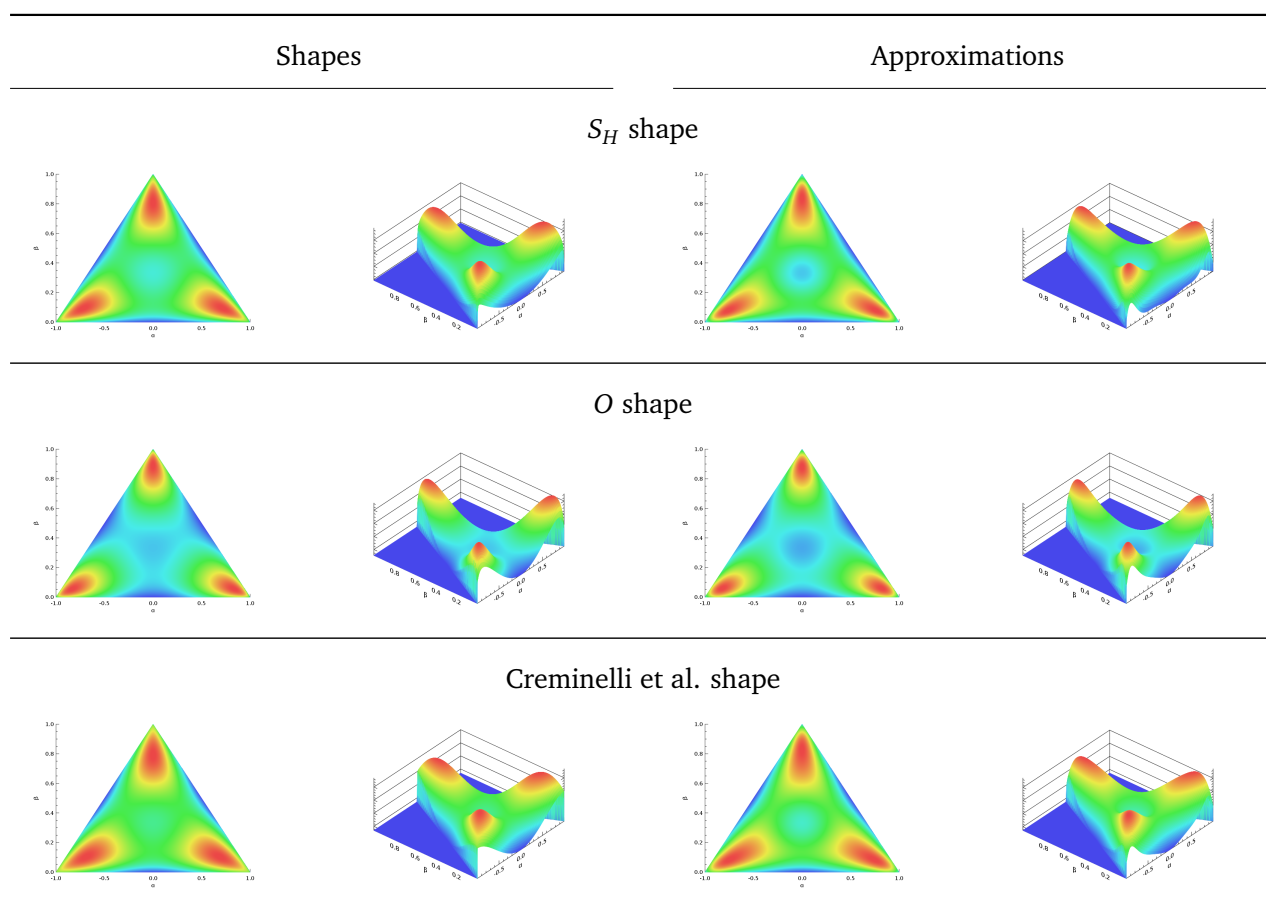


Table 4.18: Approximations to the S_H -shape and similar bispectra, up to the first ten harmonics in the \mathcal{R}_n expansion. The coefficients α_n are listed in table 4.17.

4.3.2 Distinguishing microphysics

The discussion above implies that, instead of obtaining orthogonal combinations from the terms in Eq. (4.16), it may be possible to do just as well with the \mathcal{R}'_n themselves.

	Approximations to orthogonal shapes		
	S_H shape	Creminelli et al. shape	O shape
S_H shape	0.99	0.98	0.89
Creminelli et al. shape	0.97	0.99	0.88
O shape	0.82	0.83	1.00

Table 4.19: Cosines between \mathcal{R}'_n -approximations to the orthogonal shapes depicted in table 4.18 and the corresponding exact shape.

As we concluded in the last section, the recurrent appearance of the drumlin-like shape in table 4.14 suggests that the *shape* of the bispectrum itself will not serve as a sensitive discriminant of microphysics. Most of all, it may not be an appropriate diagnostic tool compared with the unprecedented sensitivity of *Planck*'s data. A significant local mode will favour dominantly local interactions, driven by gravitational evolution—usually this is related with a strong coupling between scalar field fluctuations and the gravity sector. On the other hand, a significant equilateral mode will favour strong, higher-derivative self-interactions. However, it seems difficult to be more precise. Instead of focusing on shapes, it may be more profitable to study relations between their fundamental *amplitudes* in order to distinguish amongst competing inflationary scenarios.

Partial-wave amplitudes

To proceed, we define a set of dimensionless amplitudes β_n for an arbitrary bispectrum B ,

$$\langle B_{k_*}, \mathcal{R}'_n \rangle \equiv \beta_n \mathcal{P}^2(k_*) , \quad (4.28)$$

where \mathcal{P} is the dimensionless power spectrum of the primordial curvature perturbation. We will elaborate on the scale k_* below. The β_n are similar to the amplitudes f_{NL} , but they are

rather defined with respect to an inner product.

Any predictive Lagrangian will depend on only a *finite* number of unknown parameters. If enough β_n can be estimated from data, then Eq. (4.28) allows these parameters to be expressed in terms of measurable quantities. The remaining relations in Eq. (4.28), when expressed in terms of these measurable quantities, constitute predictions of the theory. In the inflationary literature such relationships are typically known as *consistency relations*, and were introduced by Copeland et al. in 1993 [189, 190]. In the language of particle physics they are “observables in terms of observables”—predictions which are independent on the parametrisation of the theory, and which the renormalisation programme has taught us represent the physical (not the bare) content of any quantum field theory. Their power lies precisely in providing important tests of entire classes of models. These consistency relations are analogous to the ones derived in §3.5 on tensor modes.

In practice, the precise β_n depend on the definition of the inner product, and indeed will vary between experiments. To perform a satisfactory analysis, one should obtain survey-dependent predictions for the β_n . The primordial bispectrum should be propagated to the surface of last scattering and projected on to the sky, and the β_n should be computed in the resulting two-dimensional inner product. The set of basis shapes should be orthogonal when measured using the experiment in question, and may not be directly related to the \mathcal{R}'_n . This will lead to numerically different β_n for each survey. Conversely, one can evolve the CMB bispectrum extracted from the data and the β_n backwards, to obtain the respective primordial objects, and then compare them with the theoretical estimates. In either case, a more precise analysis than the one we attempt to produce here would have to be performed.

In what follows, we work for illustrative purposes with the primordial, three-dimensional bispectrum rather than the projected bispectrum. We make a number of simplifications. We use the inner product (4.11) in a scale-invariant approximation, in the sense described in §3.4.1. In evaluating $\langle B, \mathcal{R}'_n \rangle$ one must choose a reference scale, k_* , at which B is evaluated. The bispectrum then contains scale-dependent logarithms of the form $\ln(k/k_*)$, as discussed

in §3.2, making $\langle B, \mathcal{R}'_n \rangle$ also a function of k_* . The (dimensionless) power spectrum on the right-hand side of Eq. (4.28) is meant to be evaluated at k_* as well. Because our implementation of the inner product does not retain scale information, we cannot apply this prescription precisely. We replace such logarithms by $\ln(k/k_t)$, where k_t is the perimeter of the triangle. This is likely to make an impact on β_n at next-order, which should therefore be considered approximate. However, for the purposes of illustrating the construction of the coefficients β_n , these assumptions are not restrictive.

We apply the method described above to two different models.

Case study: DBI inflation

As an illustration, we consider DBI inflation governed by the action

$$S = \int d^4x \sqrt{-g} \left\{ -\frac{1}{f(\phi)} \left[\sqrt{1 - f(\phi) X} - 1 \right] - V(\phi) \right\}, \quad (4.29)$$

where $X = -(\partial\phi)^2$. We discussed this model in §3.4.1. This is a special action in the Horndeski class, and it is known to lead to strong non-gaussianities if $\gamma \gtrsim 1$ [74, 45], where $\gamma \equiv (1 - f\dot{\phi}^2)^{-1/2}$. In what follows we will be interested in the case where γ is, at least, moderate. The algebraically special structure of the action makes the coefficients of the Lagrangian operators stable against quantum corrections.

The inflationary fluctuations in this model depend on the parameters defined in Eq. (3.24) [180], which we recall here

$$\varepsilon_V = \frac{1}{2} \left(\frac{V'}{V} \right)^2, \quad \eta_V = \frac{V''}{V}, \quad \text{and} \quad \Delta = \text{sgn}(\dot{\phi} f^{1/2}) \frac{f'}{f^{3/2}} \frac{1}{3H}, \quad (4.30)$$

where primed quantities are differentiated with respect to ϕ (and not conformal time). Typically, these must be small. The bispectrum was determined to $\mathcal{O}(\varepsilon, \eta, \Delta)$ in §3.4.1, to which we refer the reader for details.

The Lagrangian depends on the three parameters in Eq. (4.30) and γ . We will therefore

require *four* observables to fix them. A further *fifth* observable enables the theory to be tested. The presently well-measured parameters are only the amplitude, \mathcal{P} , and tilt, n_s , of the scalar power spectrum. There are relatively weak constraints on a few modes of the bispectrum. In the future, possibly with *Planck*, we might be able to detect the tensor amplitude \mathcal{P}_t . Assuming it will eventually be possible to measure β_0 and β_1 together with the tensor-to-scalar ratio, $r \equiv \mathcal{P}_t/\mathcal{P}$, then using the results of §3.4.1, we find

$$\left(2.88 \frac{\beta_1}{\beta_0} - 1\right) = 1.93(n_s - 1) + 0.03r \sqrt{-\beta_0} + 2.87 \left(6.60 \frac{\beta_2}{\beta_0} + 1\right) . \quad (4.31)$$

One of the results from our analysis is that the DBI model predicts $\beta_0 < 0$ if the bispectrum is large enough to be observable, as we will explain below. If r cannot be measured, or only with poor accuracy, then it will be necessary to use β_3 as a substitute. In this case, we find

$$\left(2.88 \frac{\beta_1}{\beta_0} - 1\right) = 0.65(n_s - 1) - 0.02 \left(6.60 \frac{\beta_2}{\beta_0} + 1\right) - 0.17 \left(34.98 \frac{\beta_3}{\beta_0} + 1\right) . \quad (4.32)$$

In Eqs. (4.31)–(4.32) we must recall that observables (such as the β_n) may mix Lagrangian *parameters* at lowest-order, next-order and possibly other higher-orders. The β_n begin at lowest-order, whereas $(n_s - 1)$ and r begin at next-order in slow-roll. Indeed, we find this is the case. This can be seen from inspection of Eqs. (4.31)–(4.32): the numerical coefficients multiplying $(n_s - 1)$ and β_2/β_0 differ in both equations.

In obtaining these equations we have assumed that each term in Eq. (4.32) is roughly of the same order of magnitude, that is

$$\left|2.88 \frac{\beta_1}{\beta_0} - 1\right| \sim \left|6.60 \frac{\beta_2}{\beta_0} + 1\right| \lesssim |n_s - 1| \sim r . \quad (4.33)$$

Which of these two equations, (4.31) or (4.32), is more useful will depend on the relative difficulty of measuring r and β_3 . These expressions constitute a *model-independent* test of the DBI framework: they hold for any DBI action, up to $O(\varepsilon, \eta, \Delta)$, no matter what potential or

warp factor is chosen. They are written in terms of observables only. By showing that relations such as (4.31) or (4.32) are not satisfied, one could rule out the DBI action as the origin of the inflationary perturbations.

Unfortunately, there is no one-to-one mapping from models to consistency relations such as (4.31)–(4.32), and determining that any such equation is satisfied does not provide decisive evidence in favour of a model. The utility of such equations lies, on the other hand, with their power to rule models out. Showing that the β_n satisfy a hierarchy of consistency equations derived from some Lagrangian would, nevertheless, be circumstantial evidence in favour of that model, especially if the agreement persists to large n .

As mentioned above, Eqs. (4.31)–(4.32) are analogues of the “next-order” consistency equations for the tensor tilt, n_t [cf. Eqs. (5.6)–(5.7) of Lidsey et al. [106]]. If the β_n cannot be determined with sufficient accuracy to test these equations, we can obtain a simpler set of “lowest-order” relations obtained by systematically neglecting next-order terms in the slow-roll approximation. This entails assuming $(n_s - 1) \simeq r \simeq 0$ in Eq. (4.33). Together with (4.31)–(4.32), Eq. (4.33) then implies

$$2.88 \frac{\beta_1}{\beta_0} \simeq -6.60 \frac{\beta_2}{\beta_0} \approx 1. \quad (4.34)$$

Even more simply, Eq. (4.34) requires β_0 and β_1 to have the same sign, and β_2 to have the opposite sign. By consulting the individual expressions for the β_n , it follows that β_0 and β_1 must be negative, but β_2 should be positive whenever γ is moderately large. This more primitive test of the consistency relations is applicable even if the β_n cannot be determined accurately. In the present framework, it is a manifestation of the well-known result that the DBI model produces $f_{\text{NL}}^{(\text{equilateral})} < 0$, whereas WMAP data favour $f_{\text{NL}}^{(\text{equilateral})} \gtrsim 0$. For this reason, present-day observations are already sufficient to disfavour DBI inflation.

We note that Eq. (4.34), and similar expressions for β_n with $n > 2$, express the expected decrease in amplitude of $\langle B, \mathcal{R}'_n \rangle$ with increasing n . The decrease is not monotonic, because

the spikes which appear in \mathcal{R}'_n at larger n cause a small enhancement. However, the $n = 0, 1, 2$ harmonics are larger than the rest, which is required by the analysis of §4.3.1.

Case study: k -inflation

For comparison, consider the power-law k -inflation model of Armendáriz-Picón, Dalmour & Mukhanov [26], which we discussed in §3.4.1. The action for this model satisfies

$$S = \int d^4x \sqrt{-g} \frac{4}{9} \frac{4 - 3\gamma}{\gamma^2} \frac{X^2 - X}{\phi^2} . \quad (4.35)$$

It admits an inflationary solution for $X = (2 - \gamma)/(4 - 3\gamma)$ provided $0 < \gamma < 2/3$, unrelated to the Lorentz factor in the DBI model. In the limit $\gamma \ll 1$, and keeping only leading-order terms, this model predicts

$$2.61 \frac{\beta_1}{\beta_0} = -4.80 \frac{\beta_2}{\beta_0} = 1 . \quad (4.36)$$

Comparison with Eq. (4.34) for the DBI consistency relations shows that it would be necessary to measure β_0/β_1 to about 10% in order to distinguish these models. A sufficiently accurate measurement of β_2 would make the test considerably easier to apply. Just like for DBI, β_0 is also negative for k -inflation.

This method is closely related to a trispectrum-based test for single-field inflation proposed by Smidt et al. [53]. The trispectrum contains contributions from two different ‘local’ shapes, with amplitudes parametrized by τ_{NL} and g_{NL} [205, 206, 207]. The τ_{NL} contribution obeys the Suyama–Yamaguchi inequality $\tau_{\text{NL}} \geq (6f_{\text{NL}}^{\text{local}}/5)^2$ [208, 209], where the equality applies to single-source models. Smidt et al. suggested studying $A = \tau_{\text{NL}}/(6f_{\text{NL}}^{\text{local}}/5)^2$, which is analogous to the ratios β_n/β_0 introduced above. Their analysis suggested that *Planck* may be able to measure A to ± 1.0 at 1σ , and a future CMB satellite may even be able to achieve ± 0.3 with the same significance. An accurate measurement of $A > 1$ would be sufficient to rule out single-field scenarios.

In summary, like the well-known standard inflationary consistency relations, whether re-

lations such as Eqs. (4.31)–(4.34) and Eq. (4.36) are useful in practice will depend on the accuracy with which each component can be measured. This depends on the signal-to-noise associated with each harmonic shape. However, the method we have described can be implemented with *any* suitable basis; it is not restricted to the \mathcal{R}'_n functions described above. Nevertheless, our choice of \mathcal{R}'_n makes it transparent that one can think about the templates used in the CMB analysis arising as the first harmonics. After applying the orthogonalisation procedure, a shape given by higher-order harmonics emerges as a result.

4.4 Summary of results

In this chapter we have explored the scale and shape-dependences of the bispectrum in single-field inflation models. Our main findings are summarised as follows.

“New” bispectrum shapes

Our results capture the shape-dependence of the bispectrum even in the squeezed limit. Therefore, we are able to fully determine the relationship between the leading and next-order shapes in the slow-roll approximation, discussed in §4.2.

Working in a $P(X, \phi)$ model, the enhanced part of the leading-order bispectrum is well-known to correlate with the equilateral template. Only two shapes are available, plotted in Table 4.9, and the bispectrum is a linear combination of these. If enough fine-tuning is allowed, one is able to produce a distinctive shape, at leading-order, which does not correlate with the typical templates used in CMB analysis. This shape is very similar to a ‘new’ shape constructed by Creminelli et al. [11], working in an entirely different model—a galilean shift-invariant Lagrangian with at least two derivatives applied to the field.

The next-order bispectrum is a linear combination of *seven* different shapes, although these cannot be varied independently: strong correlations among their coefficients are imposed by the $P(X, \phi)$ Lagrangian. Many of these shapes also correlate with the equilateral mode, but

two of them are different: in the language of §4.2, these are S'_ϵ and S_s . For typical values of $\tilde{\alpha}$ (which is the c_s^{-2} -enhanced part of λ/Σ), one can obtain a linear combination of the next-order shapes orthogonal to both lowest-order shapes. This is the orthogonal shape O in Table 4.12.

We conclude that provided we are willing to tolerate a large fine-tuning of the coefficients g_i (or a large overall amplitude of the primordial bispectrum), this ‘new’-shape can always be produced in the bispectrum of any single-field theory. Therefore, the presence of this shape cannot be used as a diagnostic tool to support a specific model. This suggests performing a different kind of analysis to the bispectrum shapes.

Insights from the modal decomposition

Motivated by the recurrent presence of the shape with drumlin features, we have turned in §4.3 to the modal decomposition of the CMB bispectrum, originally proposed by Fergusson & Shellard [9, 201]. The decomposition into fundamental harmonics is naturally designed to study correlations among the amplitudes of shapes which *are* present in the primordial bispectrum. A given Lagrangian will typically generate fluctuations which depend on a finite number of parameters. If enough modes of the bispectrum can be determined with sufficient accuracy, these parameters can be written in terms of observable quantities. Further observations then constitute tests of a particular theory, and can ultimately allow us to reduce the number of competing inflationary models.

As an illustration, we have applied our method to DBI inflation with an arbitrary potential and warp factor. We compared the resulting consistency relations with the ones obtained in the k -inflation scenario. With sufficiently accurate observations it may be possible to distinguish these models. Similar tests can be devised for any single-field inflationary model.

For an arbitrary Horndeski model, only *five* measurements of the correlations between the primordial bispectrum and the (first five) fundamental harmonics are required to know the coefficients g_i . Further measurements break the degeneracy amongst the dynamical quantities

from which each g_i is built, and also allow us to test the theory against observations.

Real science is a revision in progress, always.

It proceeds in fits and starts of ignorance.

Stuart Firestein, in *Ignorance: How It Drives Science*

5

Inflationary Signatures of Single-Field Models Beyond Slow-Roll

As we have seen in the previous two chapters, until recently to compute the bispectrum we started from the action for the comoving curvature perturbation, ζ , for each model independently. However, recent developments have taught us that, in single-field models without ghost-like instabilities, the cubic action for ζ can always be written in the form

$$S^{(3)} = \int d^3x d\tau \left\{ a\Lambda_1 \zeta'^3 + a^2\Lambda_2 \zeta \zeta'^2 + a^2\Lambda_3 \zeta (\partial\zeta)^2 + a^2\Lambda_4 \dot{\zeta} \partial_i \zeta \partial^i (\partial^{-2} \zeta') + a^2\Lambda_5 \partial^2 \zeta (\partial_i \partial^{-2} \zeta')^2 \right\}. \quad (5.1)$$

The model-dependent imprints are encoded in each of the *five* coefficients Λ_i of the Horndeski operators. This action will be our starting point to compute the bispectrum in this chapter.

Many authors have focused on the study of the action (5.1) under the assumption of slow-roll regime in which the inflationary expansion is quasi-de Sitter, whilst allowing for a small variation of the sound speed of perturbations. In this approximation, $\varepsilon \equiv -d \ln H / dN$, $\eta \equiv d \ln \varepsilon / dN$ and $s \equiv d \ln c_s / dN$ all obey $\varepsilon, |\eta|, |s| \ll 1$. Examples of such works include Refs. [88, 45, 28], and the calculation introduced in chapter 2. But, what if inflation was *not* very

close to de Sitter, and these parameters cannot be treated perturbatively? Khoury & Piazza [174] showed that this scenario was still compatible with a perfectly scale-invariant spectrum of perturbations, in fair agreement with observations [7], provided the relation $s = -2\varepsilon$ was satisfied in $P(X, \phi)$ models.¹

We know that both ε and $|\eta|$ must be small to allow for a successful period of inflation. But *how small* are they required to be? If ε is not much smaller than 1, then a calculation beyond slow-roll is technically required, especially to fit in the current era of precision cosmology. Previous works which have attempted to study correlations beyond the slow-roll regime include corrections to the power spectrum in canonical models worked out by Steward & Lyth [102]; moreover, Gong & Stewart [104] (see also Ref. [129]) used the Green's function method to obtain the propagator of scalar fluctuations to next-next-order in slow-roll. This terminology has been explained in §2.1.2. This was later generalised by Wei et al. [107] who considered models with a varying speed of sound of perturbations. Additionally Bartolo et al. [213] calculated the power spectrum beyond leading-order in the context of effective field theories of inflation [125, 214].

In this chapter we will be interested in models where the spectrum is almost scale-invariant, so that the condition found by Khoury & Piazza is mildly broken, and becomes

$$s = -2\varepsilon + \delta .$$

This requires working to *all* orders in ε and s , but *perturbatively* in δ , in deviations of the spectral index from unity, $n_s - 1 \ll 1$, and time variations of ε and s . This last assumption ensures that the conditions $\varepsilon, |s| < 1$ are preserved for a sufficiently large number of e-folds, which is a primary requisite for inflation to last at least 60 e-folds.² In this sense, this is a calculation *beyond* the slow-roll approximation, which works as a resummation technique applied to the

¹These authors have also considered solutions within the ekpyrotic mechanism (see Ref. [210] for a review, and also Refs. [211, 212]). Here, however, we focus on the inflationary scenario.

²This work explicitly excludes models with features in the potentials, which can trigger the slow-roll parameters to temporarily grow during inflation (see, for example, the review by Chen [203]).

non-perturbative parameters ε and s . We refer to it as *scale-invariant approximation*. Starting from the action (5.1), the calculation is immediately applicable to all Horndeski models. For this reason we will work with arbitrary interaction coefficients Λ_i —assignments to these coefficients will correspond to specific models.

We organise the calculation in increasing powers in the hierarchy of slow-variation parameters, focusing on leading and next-order contributions. Leading-order results involve the least power of perturbative parameters, and correspond to results obtained assuming a perfectly scale-invariant spectrum of perturbations. Next-order corrections contain small deviations from this which are parametrised by $n_s - 1$, and therefore involve terms with one extra power in the perturbative parameters. This organisational scheme follows the one used throughout Refs. [28, 1, 45] and the previous chapter, which nevertheless applied to the slow-roll approximation. On the other hand, our calculation relies on the *scale-invariant approximation* and generalises their results up to next-order in scale-invariance.

Outline.—This chapter is organised as follows. In §5.1 we obtain the dynamical behaviour of the scale factor and the other relevant background quantities in the scale-invariant approximation. The dynamical behaviour is exact in ε and s , and perturbative in the time variation of these parameters, δ and $n_s - 1$. In §5.1.1 we obtain the power spectrum for scalar fluctuations, and we derive in §5.1.2 formulae for the elementary wavefunctions from which the scalar propagator is built to next-order in scale-invariance.

We use these results to compute the bispectrum of perturbations in §5.2 and comment on the differences when using the slow-roll approximation. We conclude in §5.3. Appendix B collects useful formulae and detailed expressions of recurring integrals necessary to produce closed form bispectra. Some of these are strongly related to those investigated in Appendix A. However, for completeness, and because (as we shall see) these integrals are performed in a different time variable, we include them in Appendix B as well.

This chapter is strongly based on Ref. [3].

5.1 Background evolution beyond exact scale-invariance

We are interested in nearly scale-invariant models which fall under the class of Horndeski theories. As argued in Ref. [174] a scale-invariant spectrum for perturbations can be accommodated by a background where both the Hubble parameter and the speed of sound of perturbations vary significantly in time, provided they obey the *exact* relation $s = -2\varepsilon$.

We start with an arbitrary single-field theory for a homogeneous scalar field, on which small, inhomogeneous perturbations, $\delta\phi$, develop. All we require is the spectrum of perturbations to be *quasi* scale-invariant. For all inflation models involving one single clock in the universe, the quadratic action for the primordial comoving perturbation, ζ , can be written as

$$S^{(2)} = \frac{1}{2} \int d^3x d\tau a^2 z \left\{ \zeta'^2 - c_s^2 (\partial\zeta)^2 \right\}, \quad (5.2)$$

where z is required to be a well defined, differentiable function of the background dynamics and Lagrangian parameters, but is otherwise arbitrary.³ We have seen this action before in Eq. (2.15). The time evolution of $z(y)$ will be parametrised by $w \equiv d \ln z / dN$. For consistency, we also work to all orders in w . For an arbitrary w , Khoury & Piazza's relation between ε and s required for scale-invariance, is generalised to⁴

$$3s = -2\varepsilon - w.$$

This formula reduces to $s = -2\varepsilon$ for $P(X, \phi)$ models. As we discuss in Appendix B.1, it is more convenient to study the dynamics of background quantities as a function of y , satisfying $dy = c_s d\tau$, rather than conformal time, τ . In this new time-coordinate, the action (5.2) becomes

$$S^{(2)} = \frac{1}{2} \int d^3x dy q^2 \left\{ \left(\frac{\partial\zeta}{\partial y} \right)^2 - (\partial\zeta)^2 \right\}, \quad (5.3)$$

³For $P(X, \phi)$ models, $z = \varepsilon / c_s^2$ [1], but the same need not be true for other models, such as galileon inflation theories [28]. We will come back to this point in §5.1.2. We note that z here is not the usual z for k -inflation defined in Ref. [86].

⁴We refer the reader to Eq. (B.5) in appendix B.2 for details on the derivation of this formula.

with $q = a\sqrt{z}c_s$. Introducing the canonically normalised field $v_k = q\zeta_k$, where the subscript k specifies the Fourier mode, and changing variables to $v_k = A_k\sqrt{-ky}$, we find that the modes A_k obey a Bessel equation of the form

$$A_k'' + \frac{1}{y}A_k' + A_k \left\{ k^2 - \left(\frac{q''}{q} + \frac{1}{4y^2} \right) \right\} = 0 .$$

The solution to this equation is a linear combination of Hankel functions, $H_\nu^{(1)}(-ky)$ and $H_\nu^{(2)}(-ky)$, with order

$$\nu = \frac{3}{2} - \frac{n_s - 1}{2} .$$

For a perfectly scale-invariant spectrum of perturbations, then $\nu_0 = 3/2$ and the spectral index is unity. This results in the power being constant in all scales. We refer the reader to Appendix B.2 for details of how the spectral index relates to the background quantities, although the precise formula will be unimportant in what follows, as we shall see.

Agreement with the appropriate normalization of the propagator gives the overall evolution of the elementary wavefunction as follows

$$\zeta_k = \sqrt{\frac{\pi}{8k}} \frac{\sqrt{-ky}}{a\sqrt{z}c_s} H_\nu^{(1)}(-ky) . \quad (5.4)$$

Finally, the power spectrum of perturbations can be obtained by evaluating the scalar propagator at equal times [cf. Eq. (2.24)], yielding

$$\langle \zeta(\mathbf{k}_1)\zeta(\mathbf{k}_2) \rangle = (2\pi)^3 \delta^{(3)}(\mathbf{k}_1 + \mathbf{k}_2) \frac{\pi}{8} \frac{(-y)}{a^2(y)z(y)c_s(y)} \left| H_\nu^{(1)}(-ky) \right|^2 . \quad (5.5)$$

To further simplify this expression we will require the evolution of the scale factor a in y -coordinates. In order to do so, we specify the parameters in the slow-variation catalogue, which will allow us to perform a uniform expansion up to next-order terms in the scale-

invariant approximation.

Slow-variation catalogue.—To obtain the dynamical evolution of the scale factor in a background where ε and s are smaller than 1 (but not necessarily *much smaller* than 1), we introduce the following slow-variation parameters:

$$\eta \equiv \frac{d \ln \varepsilon}{dN} \quad \text{and} \quad t \equiv \frac{d \ln s}{dN} . \quad (5.6)$$

We assume these parameters satisfy $|\eta|, |t| \ll 1$. Our results rely on the scale-invariant expansion, and are organised in leading-order contributions, and terms contributing at next-order only. Leading-order results are the lowest-order terms which are compatible with a perfectly scale-invariant power spectrum of perturbations, whereas next-order terms are corrections parametrising the deviation from $n_s - 1 = 0$. This organisational scheme is motivated by the cosmological data that suggests that $n_s - 1$ is very small, and can therefore be treated perturbatively.

To determine the behaviour of the scale factor, we start by integrating $c_s d\tau$ to compute y . Working *perturbatively* in η and t , but to *all* orders in ε and s , we find

$$y = -\frac{c_s}{aH} \sum_{m=0}^{+\infty} \left\{ (\varepsilon + s)^m + (\varepsilon + s)^{m-1} \sum_{k=0}^m k (ts + \varepsilon\eta) \right\} .$$

These sums converge and give

$$a(y) = -\frac{c_s}{Hy(1-\varepsilon-s)} \left\{ 1 + \frac{\varepsilon\eta + ts}{(1-\varepsilon-s)^2} \right\} . \quad (5.7)$$

This result was first obtained by Khoury & Piazza in Ref. [174]. Using Eq. (5.7) we can further simplify the two-point correlator (5.5) in y -time, which becomes

$$\langle \zeta(\mathbf{k}_1) \zeta(\mathbf{k}_2) \rangle = (2\pi)^3 \delta^{(3)}(\mathbf{k}_1 + \mathbf{k}_2) \frac{\pi H^2(y) (-y)^3 (1-\varepsilon-s)^2}{8 z(y) c_s^3(y)} \left\{ 1 - 2 \frac{\varepsilon\eta + ts}{(1-\varepsilon-s)^2} \right\} |H_v^{(1)}(-ky)|^2 . \quad (5.8)$$

In a generic model, the two-point correlator will evolve in time. However, for a single-field model, by virtue of conservation of ζ on super-horizon scales [59, 48], it follows that the power spectrum will rapidly converge to its asymptotic value.⁵ We have also seen this explicitly in §2.2.2.

Therefore, we can focus our calculation a few e-folds after horizon crossing for a given scale, k_* . This has become the standard approach when calculating the asymptotic limit of the power spectrum. This remains true even in multi-field inflation, where this procedure sets the appropriate initial conditions for evolving correlation functions after horizon crossing, using techniques such as δN [57], transport equations [138, 139], or transfer matrices [216] (see, for example, Refs. [217, 218, 219, 140, 220, 221]). The advantages of applying this approach are twofold: on one hand, at this point in the evolution the elementary wavefunction is completely characterised by the growing mode, since the decaying mode has become negligible; on the other hand, the power spectrum obtained in this way is already the asymptotic value, at late times. Said differently, at this point of evaluation ζ has *become classical* [59, 222].

With this methodology in mind, and working perturbatively in η and t we obtain

$$\varepsilon \simeq \varepsilon_* \left\{ 1 - \frac{\eta_*}{1 - \varepsilon_* - s_*} \ln(-k_* y) \right\} \quad \text{and} \quad (5.9a)$$

$$s \simeq s_* \left\{ 1 - \frac{t_*}{1 - \varepsilon_* - s_*} \ln(-k_* y) \right\} \quad (5.9b)$$

to next-order in the scale-invariant approximation. As before, starred quantities are to be evaluated when some scale, k_* , has exited the y -horizon, so that $k_* y_* = -1$. It is important to leave this scale arbitrary since this generates the scale-dependence of the correlation functions. The appearance of the logarithmic term corresponds precisely to the number of e-folds, N_* , measured in y -coordinates, which have elapsed since the scale k_* has exited the horizon. The expansion in Eqs. (5.9) is only valid up to a few e-folds outside the horizon, when one can

⁵See Ref. [215] for comments on the number of e-folds necessary for such asymptotic behaviour to be reached after horizon crossing. There, the authors studied a two-field inflation model, but the same conclusions apply to single-field models.

trust the expansion in Taylor series to first-order. We note that quasi scale-invariance demands $\eta_* = t_*$, up to next-next-order corrections, which we do not keep in our calculation.

Given the individual dynamics of $c_s(y)$ and $H(y)$ derived in Eqs. (B.11) and (B.13) of Appendix B.3, we can replace for the evolution of the scale factor in Eq. (5.7). We find:

$$a(y) = \frac{c_{s*}(-k_*y)^{-\frac{s_*+\varepsilon_*}{1-\varepsilon_*-s_*}}}{H_*(1-\varepsilon_*-s_*)(-y)} \left\{ 1 + \beta_* - \left[\frac{\beta_*}{1-\varepsilon_*-s_*} \right] \ln(-k_*y) + \left[\frac{\alpha_*(\varepsilon_*+s_*)}{2(1-\varepsilon_*-s_*)} \right] (\ln(-k_*y))^2 \right\}, \quad (5.10)$$

where the next-order parameters α and β are defined in Eqs. (B.10).⁶ Despite its complicated structure, Eq. (5.10) correctly reproduces the results of chapter 2 and Ref. [174] when we take the limit of *exact* scale-invariance, for which $\eta_* = t_* = 0$, resulting in vanishing α_* and β_* [cf. Eqs. (B.10)]. The extra terms in between brackets in Eq. (5.10) are precisely the corrections to a pure, dominant power-law evolution.

5.1.1 The scalar power spectrum

The power spectrum $P(k)$ defined by

$$\langle \zeta(\mathbf{k}_1)\zeta(\mathbf{k}_2) \rangle = (2\pi)^3 \delta^{(3)}(\mathbf{k}_1 + \mathbf{k}_2) P(k) \quad (5.11)$$

where $k = |\mathbf{k}| = |\mathbf{k}_1| = |\mathbf{k}_2|$, will in general depend on time. Taking the super-horizon limit, $|ky| \rightarrow 0$, we find that the dominant contribution arising from the Hankel function in Eq. (5.8) is given by

$$\left| H_\nu^{(1)}(-ky) \right|^2 \longrightarrow -\frac{2}{\pi k^3 y^3} \left\{ 1 + (n_s - 1) \left[-2 + \gamma_E + \ln(-2ky) \right] \right\}.$$

Whatever y -evolution the remaining terms in Eq. (5.8) have in *this* limit, they should precisely cancel the y -dependence of the Hankel function. This is a requirement imposed by conser-

⁶ α and β here are not to be confused with the parameters referred to by the same letters in the previous chapters.

vation of ζ on super-horizon scales in single-field models. This allows us to readily write the power spectrum as

$$P(k) = \frac{H_*^2 (1 - \varepsilon_* - s_*)^2}{4z_* (k c_{s*})^3} \left\{ 1 + 2E_* + (n_s - 1) \ln(k/k_*) \right\} , \quad (5.12)$$

where we have defined

$$E_* = -\beta_* + \frac{n_s - 1}{2} \{ -2 + \gamma_E + \ln 2 \} . \quad (5.13)$$

This is the power spectrum for a nearly scale-invariant Horndeski theory. To recover the perfectly scale-invariant formula obtained by Khoury & Piazza [174], we simply set E_* and $n_s - 1$ to zero, since these enter the power spectrum as next-order corrections in scale-invariance. Whilst being time-independent, Eq. (5.12) correctly reproduces the expected logarithmic scale-dependence in the limit when the slow-roll regime applies, in which ε and s are slow-roll parameters [cf. Eq. (2.25)]. Indeed, we can check that defining the dimensionless version of the power spectrum using the usual rule $\mathcal{P} = k^3 P(k)/2\pi^2$, Eq. (5.12) gives

$$n_s - 1 = \frac{d \ln \mathcal{P}}{d \ln k} .$$

Again, the explicit expression for $n_s - 1$ will not be required in any stage of the calculation, but we refer the reader to Appendix B.2 where its formula is derived. It suffices to treat it as an arbitrary next-order quantity.

5.1.2 Obtaining next-order corrections to the wavefunctions, ζ_k

Our ultimate interest lies in obtaining the bispectrum of perturbations starting from the action (5.1). We will rely on the scale-invariant approximation introduced in this chapter. Since we will keep corrections up to next-order, we also require corrections to the elementary wavefunctions up to the same order, for consistency. We have already explained them in detail in

§3.1.1, but we enumerate them here for completeness.

External legs.—The corrections to the external lines of the Feynman diagram correspond to evaluating the propagator in the asymptotic regime, when $|ky| \rightarrow 0$. From Eq. (5.12) we can read off the corrections to the external legs

$$\zeta_k(y)^{(\text{background+external})} = \frac{i H_*(1 - \varepsilon_* - s_*)}{2 \sqrt{z_*} (k c_{s_*})^{3/2}} \left\{ 1 + E_* + \frac{n_s - 1}{2} \ln(k/k_*) \right\}. \quad (5.14)$$

As argued in §5.1.1, the time-independence of this is guaranteed because the primordial perturbation ζ is conserved on super-horizon scales in single-field models.

From this it also follows that whatever function is assigned to $z(y)$, it must generically behave, at leading-order in scale-invariance, as

$$z(y) \sim (-k_* y)^{\frac{2\varepsilon_* + 3s_*}{1 - \varepsilon_* - s_*}}. \quad (5.15)$$

This imposes a mild requirement on an otherwise arbitrary, but smooth function $z(y)$. We check that for $P(X, \phi)$ models, where $z = \varepsilon/c_s^2$, this behaviour is consistent with Eqs. (5.9) and (B.11), supplemented by the condition $s_* = -2\varepsilon_*$ (which holds at leading-order in the scale-invariant approximation scheme). If in a given model z has a different evolution from that of Eq. (5.15), it leads to a background where ζ is evolving on super-horizon scales, which is incompatible with the single-field inflation scenario.

Internal legs.—This correction is a result of the spectrum being slightly tilted. Using Eq. (5.7), we rewrite, for clarity, Eq. (5.4) for the elementary wavefunction as

$$\zeta_k(y) = \sqrt{\frac{\pi}{8}} \frac{H(y)(-y)^{3/2}(1 - \varepsilon - s)}{\sqrt{z(y)} c_s^{3/2}(y)} \left\{ 1 - \frac{\varepsilon\eta + ts}{(1 - \varepsilon - s)^2} \right\} H_\nu^{(1)}(-ky). \quad (5.16)$$

The order of the Hankel function, ν , differs from $3/2$ by next-order corrections proportional to $(n_s - 1)$. To evaluate corrections to ζ_k we start by Taylor expanding the Hankel function around order $\nu_0 = 3/2$. Following Refs. [45, 28], we find the background evolution of the

wavefunctions is given by

$$\zeta_k(y)^{\text{(background)}} = \frac{iH_*(1 - \varepsilon_* - s_*)}{2\sqrt{z_*}(kc_{s_*})^{3/2}} (1 -iky) e^{iky} , \quad (5.17)$$

which gives the leading-order behaviour of Eq. (5.14) in the limit $|ky| \rightarrow 0$. The next-order corrections arising from $\delta\nu = \nu - 3/2 = -(n_s - 1)/2$ and the slow-variation of the background quantities in (5.16) organise themselves into the internal leg corrections:

$$\begin{aligned} \delta\zeta_k(y)^{\text{(internal)}} = \frac{iH_*(1 - \varepsilon_* - s_*)}{2\sqrt{z_*}(kc_{s_*})^{3/2}} \left\{ -e^{iky}(1 -iky) \left[\beta_* + \frac{n_s - 1}{2} \ln(-k_*y) \right] \right. \\ \left. + \frac{n_s - 1}{2} \left[e^{-iky}(1 +iky) \int_{-\infty}^y \frac{e^{2ik\xi}}{\xi} d\xi - 2e^{iky} - i\frac{\pi}{2} e^{iky}(1 -iky) \right] \right\} . \end{aligned} \quad (5.18)$$

The integral representation on the second line above corresponds to the exponential integral function, $\text{Ei}(-ky)$, defined for real, non-zero argument

$$\text{Ei}(x) = \int_{-\infty}^x \frac{e^t}{t} dt ,$$

which was discussed in detail in Appendix A.1. The time-dependence of the internal leg corrections is fairly intricate and we verify that there are no divergences in Eq. (5.18) when we take the limit $|ky| \rightarrow 0$. This represents a minimal check on this result. Expressions for the time-derivatives of the wavefunctions can be found in Appendix B.3.

Corrections arising from evolving interaction vertices.—The interaction coefficients Λ_i can generically evolve very fast, and one expects their time evolution to be of the form

$$\Lambda_i \simeq \Lambda_{i*}(-ky)^n \left\{ 1 + \tilde{a} \ln(-k_*y) + \tilde{b} (\ln(-k_*y))^2 \right\} , \quad (5.19)$$

with the power n depending on the exact expression of Λ_i , and \tilde{a} and \tilde{b} being next-order terms in the scale-invariant approximation. This power-law dependence needs to be taken

into account for consistency with the scale-invariant approximation—we will study an explicit example in §5.2.2. There, we explain in detail that the behaviour in Eq. (5.19) can potentially bring problems to the convergence of the integral in the formula for the bispectrum. In particular, there might be values of ε for which one is unable to perform the calculation, because they would lead to a time-dependent three-point function.

Mainly to simplify our results, we assume the interaction vertices to have a very smooth and slow evolution in y -time. To this end, we introduce a supplementary slow-variation parameter

$$h_i \equiv \frac{1}{\Lambda_i H} \frac{d\Lambda_i}{dt} , \quad (5.20)$$

which satisfies $|h_i| \ll 1$. We expect this approximation to be valid for all Horndeski models whenever the interaction vertices are slowly evolving in time. As described in §5.2.2, the methods developed in this chapter can still be used to compute n -point correlation functions in models where this assumption fails. We conclude that, if Λ_i is slowly varying, then each interaction vertex evolves as

$$\Lambda_i \simeq \Lambda_{i^*} \left\{ 1 - \frac{h_{i^*}}{1 - \varepsilon_* - s_*} \ln(-k_* y) \right\} . \quad (5.21)$$

This means that for simplicity in the remainder of this chapter we will set $n = 0$ and $\tilde{b} = 0$ in Eq. (5.19), but we will show how to deal with $n \neq 0$ in one simple example in §5.2.2. This assumption concludes the presentation of the slow-variation catalogue, which is therefore composed by the set $\{n_s - 1, \delta, \eta, t, h_i\}$.

Simplifying our results.—We note that a further simplification to the background dynamics follows from inspection of Eqs. (5.14) and (5.18). The variable w that parametrises the variation of z , does not appear in our formulae. Indeed such term is only present implicitly since it is encapsulated in the spectral index $(n_s - 1)$ [cf. Eq. (B.5)]. Therefore the calculation is explicitly *independent* of our choice of w . As a consequence, we can effectively reduce the relation we found between ε , s and w , to one which only involves the first two variables. To

this end, we take the relation between ε and s to be

$$s = -2\varepsilon + \delta ,$$

where δ is a next-order parameter in the scale-invariant approximation. We emphasize that this procedure in no way lacks generality: the calculation is still non-perturbative in both ε and s . The formula above generalises the regime studied in Ref. [174] by considering a nearly scale-invariant spectrum. This also implies that $t = \eta$ at next-order in the scale-invariant approximation, which is in agreement with the observations in §5.1.

This procedure dramatically simplifies our formulae and reduces the slow-variation catalogue to a minimum of parameters, which we choose to be $\{n_s - 1, \delta, \eta, h_i\}$. At the same time, our results will be displayed in terms of only one non-perturbative parameter, which we choose to be ε .⁷ We note that this will imply some conceptual restructuring of our formulae. In particular, Eq. (5.17) now contains leading *and* next-order contributions in δ_* , which can now be interpreted as an extra contribution to the external legs at next-order in Eq. (5.14).

Eqs. (5.14), (5.18), and (5.21) combine amongst themselves to produce the overall corrections required to write the bispectrum at next-order in the scale-invariant approximation. They naturally combine to produce two separate contributions to the bispectrum: the background contributions and next-order corrections arising from the vertex and external legs; and the next-order contributions arising from the internal legs of the Feynman diagram. We will use this way of partitioning the bispectrum to present our results for the bispectrum in §5.2.1 by labelling the first contributions as *type-a bispectrum*, and the second as *type-b bispectrum*. This is the same notation defined in §3.2.1.

⁷ Our calculation is non-perturbative in *both* ε and s . By noting that we can write $s = -2\varepsilon + \delta$, we can replace the non-perturbative parameter s by the perturbative parameter δ . In the remainder of the text, the dependence in s is absorbed by δ .

5.2 Non-gaussianity in the bispectrum

As we have seen in the last chapters, non-gaussian signatures encoded in the CMBR work as a powerful discriminant between inflationary models. We compute the bispectrum in nearly scale-invariant theories using the same *in-in* rules reviewed in §2.3.2. The study of shapes is, however, beyond the scope of this work, and we leave it to forthcoming investigation. We illustrate our results by specifying estimates of f_{NL} in some useful limits.

5.2.1 Bispectrum of Horndeski theories

As argued before, it will be convenient to write the action for perturbations in y -coordinates. From Eq. (5.1) this is given by

$$S^{(3)} = \int d^3x dy a^2 \left\{ \frac{c_s^2}{a} \Lambda_1 \left(\frac{\partial \zeta}{\partial y} \right)^3 + c_s \Lambda_2 \zeta \left(\frac{\partial \zeta}{\partial y} \right)^2 + \frac{1}{c_s} \Lambda_3 \zeta (\partial_i \zeta)^2 \right. \\ \left. + c_s \Lambda_4 \left(\frac{\partial \zeta}{\partial y} \right) \partial_i \zeta \partial^i \left(\partial^{-2} \frac{\partial \zeta}{\partial y} \right) + c_s \Lambda_5 \partial^2 \zeta \left(\partial_i \partial^{-2} \frac{\partial \zeta}{\partial y} \right)^2 \right\}. \quad (5.22)$$

Our calculation is organised as follows:

Bispectrum type a.—The leading contributions and the corrections arising from the slow-variation of the interaction vertices and external legs can be written in the general form

$$B^a = \frac{\Lambda_{i*} H_*^4 (1 + \varepsilon_*)^4}{2^6 c_{s*}^6 z_*^3 \prod_i k_i^3} N^a(k_1) \left\{ \text{Re} \left(P^a(k_1) \tilde{J}_\gamma \right) + \text{Re} \left(Q^a(k_1) \tilde{J}_{\gamma+1} \right) + T^a(k_1) \right\} + \text{cyclic permutations}, \quad (5.23)$$

where the addition of cyclic permutations entails the symmetric exchange of momenta $k_1 \rightarrow k_2 \rightarrow k_3$. The functions $N^a(k_1)$, $P^a(k_1)$, $Q^a(k_1)$ and $T^a(k_1)$ are listed in table 5.1. The functions \tilde{J}_γ are studied in Appendix B.4 and defined by

$$\tilde{J}_\gamma \equiv (ik_t)^{1+\gamma} \int_{-\infty}^0 dy e^{ik_t y} (-y)^\gamma \left\{ A_* + B_* \ln(-k_* y) + C_* (\ln(-k_* y))^2 \right\}. \quad (5.24)$$

Table 5.2 contains the assignments A_* , B_* and C_* for the functions \tilde{J}_γ . We note that the co-

efficients for the operators $\zeta\zeta'^2$, $\zeta'\partial_j\zeta\partial_j\partial^{-2}\zeta'$, and $\partial^2\zeta(\partial_j\partial^{-2}\zeta')^2$ are the same. Having done the calculation independently for each operator, this is a minimal check of the correctness of our results. This happens because these operators have the same time-derivative structure, and differ only in the arrangement of spatial-derivatives, and therefore, in the momentum dependence.

Bispectrum type b.—Likewise, the contributions from the propagator in the internal lines of the Feynman diagram can be consolidated for all operators in the form

$$\begin{aligned}
B^b = \frac{\Lambda_{i_*} H_*^4 (1 + \varepsilon_*)^4}{2^6 c_{s_*}^6 z_*^3 \prod_i k_i^3} N^b(k_1) & \left\{ (n_s - 1) \sum_i \left[\operatorname{Re} \left(P_i^b(k_1) \right) \tilde{I}_\gamma(k_i) + \operatorname{Re} \left(Q_i^b(k_1) \right) \tilde{I}_{\gamma+1}(k_i) \right] \right. \\
& + \operatorname{Re} \left(R^b(k_1) \tilde{J}_\gamma \right) + \operatorname{Re} \left(S^b(k_1) \tilde{J}_{\gamma+1} \right) + (n_s - 1) T^b(k_1) \left. \right\} \\
& + \text{cyclic permutations} \ ,
\end{aligned} \tag{5.25}$$

where again the addition of cyclic permutations entails the symmetric exchange of momenta $k_1 \rightarrow k_2 \rightarrow k_3$. The functions $N^b(k_1)$, $P_i^b(k_1)$, $Q_i^b(k_1)$, $R^b(k_1)$, $S^b(k_1)$ and $T^b(k_1)$ are listed in tables 5.3, 5.4 and 5.5. Table 5.6 contains the assignments A_* , B_* and C_* for the functions \tilde{J}_γ . The functions $\tilde{I}_\gamma(k_i)$ are defined by

$$\tilde{I}_\gamma(k_3) \equiv (i\vartheta_3 k_t)^{\gamma+1} \int_{-\infty}^0 dy \left\{ (-y)^\gamma e^{i(k_1+k_2-k_3)y} \int_{-\infty}^y \frac{d\xi}{\xi} e^{2ik_3\xi} \right\} \ , \tag{5.26}$$

where $\vartheta_3 = (k_t - 2k_3)/k_t$. We refer the reader to Appendix B.4 for details on the evaluation of these functions.

operator	contributions to B^a			
	$N^a(k_1)$	$P^a(k_1)$	$Q^a(k_1)$	
ζ'^3	$12H_*(1+\epsilon_*) \prod_i k_i^2 k_*^{\frac{5\epsilon_*}{1+\epsilon_*}}$	$-i \left(\frac{1}{ik_t} \right)^{3+\frac{5\epsilon_*}{1+\epsilon_*}}$		
$\zeta\zeta'^2$	$4k_2^2 k_3^2 k_*^{\frac{4\epsilon_*}{1+\epsilon_*}}$	$i \left(\frac{1}{ik_t} \right)^{1+\frac{4\epsilon_*}{1+\epsilon_*}}$	$-k_1 \left(\frac{1}{ik_t} \right)^{2+\frac{4\epsilon_*}{1+\epsilon_*}}$	
$\zeta(\partial\zeta)^2$	$\frac{4(\mathbf{k}_2 \cdot \mathbf{k}_3)}{c_{S^*}^2}$			$\Omega_{1^*} \vec{k}$ $+ \Omega_{2^*} \left(-k_t + \frac{k_1 k_2 k_3}{k_t^2} \right)$ $- \Omega_{2^*} \left(\gamma_E - \ln \frac{k_*}{k_t} \right) \vec{k}$
$\zeta' \partial_j \zeta \partial_j \partial^{-2} \zeta'$	$2k_1^2 (\mathbf{k}_2 \cdot \mathbf{k}_3) k_*^{\frac{4\epsilon_*}{1+\epsilon_*}}$	$2i \left(\frac{1}{ik_t} \right)^{1+\frac{4\epsilon_*}{1+\epsilon_*}}$	$-(k_2 + k_3) \left(\frac{1}{ik_t} \right)^{2+\frac{4\epsilon_*}{1+\epsilon_*}}$	
$\partial^2 \zeta (\partial_j \partial^{-2} \zeta')^2$	$4k_1^2 (\mathbf{k}_2 \cdot \mathbf{k}_3) k_*^{\frac{4\epsilon_*}{1+\epsilon_*}}$	$i \left(\frac{1}{ik_t} \right)^{1+\frac{4\epsilon_*}{1+\epsilon_*}}$	$-k_1 \left(\frac{1}{ik_t} \right)^{2+\frac{4\epsilon_*}{1+\epsilon_*}}$	

Table 5.1: Coefficients of the functions appearing in the B^a bispectrum. For simplicity of notation, we define the quantities \vec{k} , Ω_1 and Ω_2 in table B.1 of Appendix B.5.

operator	assignments to \tilde{J}_γ in B^a			
	γ	A_*	B_*	C_*
ζ'^3	$2 + \frac{5\varepsilon_*}{1 + \varepsilon_*}$	Ω_{3*}	$-\frac{h_{1*} - 5\beta_*\varepsilon_*}{1 + \varepsilon_*} + \frac{\delta_*(2\varepsilon_* - 3) + \varepsilon_*\eta_*}{(1 + \varepsilon_*)^2}$	$-\frac{5}{2} \frac{\alpha_*\varepsilon_*}{1 + \varepsilon_*}$
$\zeta\zeta'^2$	$\frac{4\varepsilon_*}{1 + \varepsilon_*}$	Ω_{1*}	$-\frac{h_{2*} - 4\beta_*\varepsilon_*}{1 + \varepsilon_*} + \frac{\delta_*(\varepsilon_* - 3) + 2\varepsilon_*\eta_*}{(1 + \varepsilon_*)^2}$	$-2 \frac{\alpha_*\varepsilon_*}{1 + \varepsilon_*}$
$\zeta(\partial\zeta)^2$	not applicable			
$\zeta'\partial_j\zeta\partial_j\partial^{-2}\zeta'$	$\frac{4\varepsilon_*}{1 + \varepsilon_*}$	Ω_{1*}	$-\frac{h_{4*} - 4\beta_*\varepsilon_*}{1 + \varepsilon_*} + \frac{\delta_*(\varepsilon_* - 3) + 2\varepsilon_*\eta_*}{(1 + \varepsilon_*)^2}$	$-2 \frac{\alpha_*\varepsilon_*}{1 + \varepsilon_*}$
$\partial^2\zeta(\partial_j\partial^{-2}\zeta')^2$	$\frac{4\varepsilon_*}{1 + \varepsilon_*}$	Ω_{1*}	$-\frac{h_{5*} - 4\beta_*\varepsilon_*}{1 + \varepsilon_*} + \frac{\delta_*(\varepsilon_* - 3) + 2\varepsilon_*\eta_*}{(1 + \varepsilon_*)^2}$	$-2 \frac{\alpha_*\varepsilon_*}{1 + \varepsilon_*}$

Table 5.2: Coefficients of the functions \tilde{J}_γ appearing in the B^a bispectrum, where Ω_{1*} and Ω_{3*} are defined in table B.1 of Appendix B.5. The functions \tilde{J}_γ are defined in Eq. (5.24) and discussed in detail in Appendix B.4.

function	operator		
	$\zeta^{\prime 3}$	$\zeta \zeta^{\prime 2}$	$\zeta (\partial \zeta)^2$
$N^b(k_1)$	$4H_*(1+\epsilon_*) \prod_i k_i^{2\epsilon_*}$	$4k_2^2 k_3^2 k_*^{4\epsilon_*}$	$\frac{2(\mathbf{k}_2 \cdot \mathbf{k}_3)}{c_{s*}^2}$
$P_1^b(k_1)$	$\frac{1}{2} \left(\frac{1}{\vartheta_1 k_t} \right)^{3+\frac{5\epsilon_*}{1+\epsilon_*}} \cos \left[\frac{5\pi\epsilon_*}{2(1+\epsilon_*)} \right]$	$\frac{1}{2} \left(\frac{1}{\vartheta_1 k_t} \right)^{1+\frac{4\epsilon_*}{1+\epsilon_*}} \cos \left[\frac{2\pi\epsilon_*}{1+\epsilon_*} \right]$	$-\frac{1}{2k_t} (k_1 k_2 + k_1 k_3 - k_2 k_3)$
$P_2^b(k_1)$	$\frac{1}{2} \left(\frac{1}{\vartheta_2 k_t} \right)^{3+\frac{5\epsilon_*}{1+\epsilon_*}} \cos \left[\frac{5\pi\epsilon_*}{2(1+\epsilon_*)} \right]$	$\frac{1}{2} \left(\frac{1}{\vartheta_2 k_t} \right)^{1+\frac{4\epsilon_*}{1+\epsilon_*}} \cos \left[\frac{2\pi\epsilon_*}{1+\epsilon_*} \right]$	$-\frac{1}{2k_t} (k_1 k_2 + k_2 k_3 - k_1 k_3)$
$P_3^b(k_1)$	$\frac{1}{2} \left(\frac{1}{\vartheta_3 k_t} \right)^{3+\frac{5\epsilon_*}{1+\epsilon_*}} \cos \left[\frac{5\pi\epsilon_*}{2(1+\epsilon_*)} \right]$	$\frac{1}{2} \left(\frac{1}{\vartheta_3 k_t} \right)^{1+\frac{4\epsilon_*}{1+\epsilon_*}} \cos \left[\frac{2\pi\epsilon_*}{1+\epsilon_*} \right]$	$-\frac{1}{2k_t} (k_1 k_3 + k_2 k_3 - k_1 k_2)$
$Q_1^b(k_1)$		$-\frac{k_1}{2} \left(\frac{1}{\vartheta_1 k_t} \right)^{2+\frac{4\epsilon_*}{1+\epsilon_*}} \cos \left[\frac{2\pi\epsilon_*}{1+\epsilon_*} \right]$	$-\frac{k_1 k_2 k_3}{k_t^2}$
$Q_2^b(k_1)$		$\frac{k_1}{2} \left(\frac{1}{\vartheta_2 k_t} \right)^{2+\frac{4\epsilon_*}{1+\epsilon_*}} \cos \left[\frac{2\pi\epsilon_*}{1+\epsilon_*} \right]$	$-\frac{k_1 k_2 k_3}{k_t^2}$
$Q_3^b(k_1)$		$\frac{k_1}{2} \left(\frac{1}{\vartheta_3 k_t} \right)^{2+\frac{4\epsilon_*}{1+\epsilon_*}} \cos \left[\frac{2\pi\epsilon_*}{1+\epsilon_*} \right]$	$-\frac{k_1 k_2 k_3}{k_t^2}$

Table 5.3: Coefficients of the functions appearing in the B^b bispectrum for the first three operators, where $\vartheta_i = \frac{1}{k_i} (k_i - 2k_j)$, and Ξ and $f(k_1, k_2, k_3)$ are defined in table B.1 of Appendix B.5.

function	operator		
	ζ'^3	$\zeta\zeta'^2$	$\zeta(\partial\zeta)^2$
$R^b(k_1)$	$3i\left(\frac{1}{ik_t}\right)^{3+\frac{5\epsilon_*}{1+\epsilon_*}}$	$i\left(\frac{1}{ik_t}\right)^{1+\frac{4\epsilon_*}{1+\epsilon_*}}$	
$S^b(k_1)$		$-k_1\left(\frac{1}{ik_t}\right)^{2+\frac{4\epsilon_*}{1+\epsilon_*}}$	
$T^b(k_1)$		$-\left(\frac{1}{k_t}\right)^{1+\frac{4\epsilon_*}{1+\epsilon_*}}\Xi$	$f(k_1, k_2, k_3)$

Table 5.4: Coefficients of the functions appearing in the B^b bispectrum for the first three operators, where Ξ and $f(k_1, k_2, k_3)$ are defined in table B.1 of Appendix B.5.

function	operator	
	$\zeta' \partial_j \zeta \partial_j \partial^{-2} \zeta'$	$\partial^2 \zeta (\partial_j \partial^{-2} \zeta')^2$
N^b	$2k_1^2 (\mathbf{k}_2 \cdot \mathbf{k}_3) k_*^{\frac{4\epsilon_*}{1+\epsilon_*}}$	$4k_1^2 (\mathbf{k}_2 \cdot \mathbf{k}_3) k_*^{\frac{4\epsilon_*}{1+\epsilon_*}}$
P_1^b	$\left(\frac{1}{\vartheta_1 k_t}\right)^{1+\frac{4\epsilon_*}{1+\epsilon_*}} \cos\left[\frac{2\pi\epsilon_*}{1+\epsilon_*}\right]$	$\frac{1}{2} \left(\frac{1}{\vartheta_1 k_t}\right)^{1+\frac{4\epsilon_*}{1+\epsilon_*}} \cos\left[\frac{2\pi\epsilon_*}{1+\epsilon_*}\right]$
P_2^b	$\left(\frac{1}{\vartheta_2 k_t}\right)^{1+\frac{4\epsilon_*}{1+\epsilon_*}} \cos\left[\frac{2\pi\epsilon_*}{1+\epsilon_*}\right]$	$\frac{1}{2} \left(\frac{1}{\vartheta_2 k_t}\right)^{1+\frac{4\epsilon_*}{1+\epsilon_*}} \cos\left[\frac{2\pi\epsilon_*}{1+\epsilon_*}\right]$
P_3^b	$\left(\frac{1}{\vartheta_3 k_t}\right)^{1+\frac{4\epsilon_*}{1+\epsilon_*}} \cos\left[\frac{2\pi\epsilon_*}{1+\epsilon_*}\right]$	$\frac{1}{2} \left(\frac{1}{\vartheta_3 k_t}\right)^{1+\frac{4\epsilon_*}{1+\epsilon_*}} \cos\left[\frac{2\pi\epsilon_*}{1+\epsilon_*}\right]$
Q_1^b	$\frac{k_2 + k_3}{2} \left(\frac{1}{\vartheta_1 k_t}\right)^{2+\frac{4\epsilon_*}{1+\epsilon_*}} \cos\left[\frac{2\pi\epsilon_*}{1+\epsilon_*}\right]$	$\frac{k_1}{2} \left(\frac{1}{\vartheta_1 k_t}\right)^{2+\frac{4\epsilon_*}{1+\epsilon_*}} \cos\left[\frac{2\pi\epsilon_*}{1+\epsilon_*}\right]$
Q_2^b	$\frac{k_3 - k_2}{2} \left(\frac{1}{\vartheta_2 k_t}\right)^{2+\frac{4\epsilon_*}{1+\epsilon_*}} \cos\left[\frac{2\pi\epsilon_*}{1+\epsilon_*}\right]$	$-\frac{k_1}{2} \left(\frac{1}{\vartheta_2 k_t}\right)^{2+\frac{4\epsilon_*}{1+\epsilon_*}} \cos\left[\frac{2\pi\epsilon_*}{1+\epsilon_*}\right]$
Q_3^b	$\frac{k_2 - k_3}{2} \left(\frac{1}{\vartheta_3 k_t}\right)^{2+\frac{4\epsilon_*}{1+\epsilon_*}} \cos\left[\frac{2\pi\epsilon_*}{1+\epsilon_*}\right]$	$-\frac{k_1}{2} \left(\frac{1}{\vartheta_3 k_t}\right)^{2+\frac{4\epsilon_*}{1+\epsilon_*}} \cos\left[\frac{2\pi\epsilon_*}{1+\epsilon_*}\right]$
R^b	$-2i \left(\frac{1}{ik_t}\right)^{1+\frac{4\epsilon_*}{1+\epsilon_*}}$	$-i \left(\frac{1}{ik_t}\right)^{1+\frac{4\epsilon_*}{1+\epsilon_*}}$
S^b	$(k_2 + k_3) \left(\frac{1}{ik_t}\right)^{2+\frac{4\epsilon_*}{1+\epsilon_*}}$	$k_1 \left(\frac{1}{ik_t}\right)^{2+\frac{4\epsilon_*}{1+\epsilon_*}}$
T^b	$-2 \left(\frac{1}{k_t}\right)^{1+\frac{4\epsilon_*}{1+\epsilon_*}} \Xi$	$-\left(\frac{1}{k_t}\right)^{1+\frac{4\epsilon_*}{1+\epsilon_*}} \Xi$

Table 5.5: Coefficients of the functions appearing in the B^b bispectrum for the last two operators, where $\vartheta_i = \frac{1}{k_t}(k_t - 2k_i)$, and Ξ is defined in table B.1 of Appendix B.5.

operator	assignments to \tilde{J}_γ in B^b			
	γ	A_\star	B_\star	C_\star
ζ'^3	$2 + \frac{5\varepsilon_\star}{1 + \varepsilon_\star}$	$\frac{\delta_\star}{1 + \varepsilon_\star} - \frac{\varepsilon_\star \eta_\star}{(1 + \varepsilon_\star)^2} + \frac{i\pi}{4}(n_s - 1)$	$\frac{n_s - 1}{2}$	
$\zeta\zeta'^2$	$\frac{4\varepsilon_\star}{1 + \varepsilon_\star}$	$-\frac{3\delta_\star}{1 + \varepsilon_\star} + \frac{3\varepsilon_\star \eta_\star}{(1 + \varepsilon_\star)^2} - \frac{3\pi i}{4}(n_s - 1)$	$-\frac{3}{2}(n_s - 1)$	
$\zeta(\partial\zeta)^2$	0	not applicable		
$\zeta'\partial_j\zeta\partial_j\partial^{-2}\zeta'$	$\frac{4\varepsilon_\star}{1 + \varepsilon_\star}$	$\frac{3\delta_\star}{1 + \varepsilon_\star} - \frac{3\varepsilon_\star \eta_\star}{(1 + \varepsilon_\star)^2} + \frac{3\pi i}{4}(n_s - 1)$	$\frac{3}{2}(n_s - 1)$	
$\partial^2\zeta(\partial_j\partial^{-2}\zeta')^2$	$\frac{4\varepsilon_\star}{1 + \varepsilon_\star}$	$\frac{3\delta_\star}{1 + \varepsilon_\star} - \frac{3\varepsilon_\star \eta_\star}{(1 + \varepsilon_\star)^2} + \frac{3\pi i}{4}(n_s - 1)$	$\frac{3}{2}(n_s - 1)$	

Table 5.6: Coefficients of \tilde{J}_γ appearing in the B^b bispectrum. The functions \tilde{J}_γ are discussed in detail in Appendix B.4.

5.2.2 Features of the bispectrum of Horndeski theories

These results extend those obtained assuming a slow-roll inflationary phase in the early universe. We now comment on our results.

Enhancement of non-gaussianities.—It is apparent from our formulae that the enhancement of the bispectrum can be very different from the one found in models using the slow-roll approximation. This strictly depends on the expressions for the coefficients Λ_i . As observed in Ref. [28], if the interaction vertices in the action (5.1) do not contain enough powers in the speed of sound, then the overall dependence in c_s could be stronger than that commonly associated with DBI models $f_{\text{NL}} \sim c_s^{-2}$. Depending on z , there might exist models that reproduce such behaviour. To gauge whether this scenario would be permissible could involve applying the partial wave decomposition method to the Horndeski overall bispectrum shape, described in §4.2. Five measurements would be required to fix each of the Λ_i interactions, and a number of additional measurements to break the degeneracy in other parameters in Λ_i , such as ε and c_s . Ultimately this would allow us to place constraints on all the parameters of the theory. Only then would we be able to conclude whether there is enhancement of non-gaussianities in these models.

Logarithms.—Our formulae contain logarithms of momenta encoded, for example, in the master integral J_γ (defined in Eq. (B.23) of Appendix B.4). There are two varieties of logarithms as noted in §3.2: those which depend on the reference scale, $\ln(k_*/k_t)$, and those which depend on the perimeter momentum scale, $\ln(k_i/k_t)$. The first type of logarithms are clearly of the same nature as the ones identified in the power spectrum (5.12): they encode the scale-dependence of the bispectrum. One can choose the reference scale, k_* , so as to minimise these logarithms; alternatively, one can use this degree of freedom to measure primordial non-gaussianities on different scales. The last type of logarithms are responsible for the shape-dependence of the bispectrum.

Away from slow-roll.—If the inflationary background is almost de Sitter, so that $\varepsilon \ll 1$, it is

easy to see that the power-law behaviour $k_*^{\alpha \frac{\varepsilon_*}{1+\varepsilon_*}}$ (seen in table 5.1), where α is some integer, can be written as a next-order logarithmic correction. This can be checked by taking the limit of very small ε in the Taylor series expansion and comparing our results to §3.2.1. Away from the slow-roll regime, the dependence on the reference scale, k_* , arises from power-laws (whose Taylor expansion we cannot truncate) in addition to logarithmic contributions. For comparison, let us write the formula of the bispectrum *type-a* for one operator, say $(\partial\zeta/\partial y)^3$, which we shall call $B_a^{(a)}$. We find that:

$$B_a^{(a)} = \frac{12H_*^5 (1 + \varepsilon_*)^5 \Lambda_{1*}}{2^6 z_*^3 c_{s*}^6 k_t^3 \prod_i k_i} \left(\frac{k_*}{k_t} \right)^{\frac{5\varepsilon_*}{1+\varepsilon_*}} \Gamma(\xi) \left\{ \cos(\zeta) \left[A_* + \ln \frac{k_*}{k_t} \left(B_* + C_* \ln \frac{k_*}{k_t} \right) + C_* \psi^{(1)}(\xi) \right. \right. \\ \left. \left. + \psi^{(0)}(\xi) \left(B_* + 2C_* \ln \frac{k_*}{k_t} + C_* \psi^{(0)}(\xi) \right) \right] \right. \\ \left. - \frac{\pi}{2} \sin(\zeta) \left[B_* + C_* \ln \frac{k_*}{k_t} + \ln \frac{k_*}{k_t} + 2C_* \psi^{(0)}(\xi) \right] \right\} , \quad (5.27)$$

with $\xi \equiv 3 + \frac{5\varepsilon_*}{1+\varepsilon_*}$ and $\zeta \equiv \frac{5\pi\varepsilon_*}{2(1+\varepsilon_*)}$. This expression shows an unusual power-law dependence on the reference scale, k_* , which is absent from previous studies, where only the logarithmic contributions $\ln(k_*/k_t)$ were known [1]. By keeping the reference scale k_* arbitrary in our calculation, the scale-dependence of the bispectrum can be calculated. This will include the contribution of the power-law scaling as $k_t^{-3 - \frac{5\varepsilon_*}{1+\varepsilon_*}}$, which could receive large corrections from ε_* . In Ref. [174] Khoury & Piazza chose $k_* = k_t$, which masks the power-law effect.

Considering a slow-roll expansion, by which we take ε_* to be a slow-roll parameter [treating it on equal footing as δ and $(n_s - 1)$], Eq. (5.27) simplifies to

$$B_a^{(a)} \simeq \frac{3\Lambda_{1*} H_*^5}{8z_*^3 c_{s*}^6 \prod_i k_i k_t^3} \left\{ 1 + \frac{h_{1*}}{2} (-3 + 2\gamma_E) + \frac{3(n_s - 1)}{2} (-2 + \gamma_E) + \frac{\delta_*}{2} (-13 + 6\gamma_E) + \frac{\varepsilon_*}{2} (25 - 10\gamma_E) \right. \\ \left. + \frac{3(n_s - 1)}{2} \ln \left(\frac{2k_1 k_2 k_3}{k_*^3} \right) - (h_{1*} + 3\delta_* - 5\varepsilon_*) \ln \frac{k_*}{k_t} \right\} , \quad (5.28)$$

which resembles the bispectrum obtained in §3.2.1.⁸ We note that in Eq. (5.28) the dependence on k_* appears through logarithms, and the power-law behaviour has explicitly disappeared from the result. As advertised, by taking ε to be a small parameter, the power-law is well described, at next-order in the slow-roll approximation, by a logarithmic contribution. The reference scale, k_* , appears in the form of two logarithmic functions: $\ln(k_i/k_*)$ and $\ln(k_*/k_t)$. These species of logarithms were thoroughly studied in §3.2.1, to which we refer the reader for details. It is in this sense that our work generalises the calculations which have been performed assuming the slow-roll approximation.

The behaviour described above shows that whereas the power spectrum has a universal weak logarithmic scale-dependence [cf. Eq. (5.12)], the bispectrum of these theories beyond the slow-roll regime can have a much stronger scale-dependence. In principle, this could be used as a diagnostic tool from CMB ($k \lesssim 0.5h\text{Mpc}^{-1}$) to cluster scales ($k \gtrsim 0.5h\text{Mpc}^{-1}$), interpolating with scales probed by the galaxy bispectrum.

A number of authors have studied constraints on non-gaussianity arising from galaxy surveys [223, 52], including its relation with biasing [50]. The scale-dependence of the bispectrum was initially studied by Chen in an infrared model of DBI inflation [183], and later investigated in $P(X, \phi)$ models (a subset of the Horndeski class) by LoVerde et al. [197]. It is not the aim of this chapter to present a detailed analysis of the scale-dependence of the bispectrum. We rather want to offer an explicit example of theories which inherit a strong scale-dependence from the background dynamics.

Comparison with previous results

Khouri & Piazza.—Khouri & Piazza [174] calculated the bispectrum of $P(X, \phi)$ theories in an exactly scale-invariant background, in which $s_* = -2\varepsilon_*$. In this chapter we have extended this study in two ways: by performing the calculation perturbatively away from exact scale-

⁸To be more precise, we can indeed show that our results for the overall bispectrum agree (adding *type a* and *type b* bispectrum), including the explicit dependence on the reference scale, k_* .

invariance, as supported by observations, and applying it to the Horndeski class of models.

In particular, let us take a specific example for comparison. Focusing on the operator $\zeta(\partial\zeta/\partial y)^2$ and in the action studied by Khoury & Piazza, we take

$$\Lambda_2(y) = \frac{\varepsilon}{c_s^4} (\varepsilon - 3 + 3c_s^2) .$$

We note that $\Lambda_2(y)$ is rapidly varying in time and should therefore be placed inside the integral to compute the bispectrum, which we denote by B_b :

$$B_b^{(\text{leading})} \sim \int_{-\infty}^0 dy \Lambda_2(y) c_s(y) a^2(y) y^2 (1 - iky) , \quad (5.29)$$

where the factor y^2 comes from the two time-derivatives of the wavefunctions and the last one (between brackets) from the undifferentiated wavefunction. For comparison purposes, we only retain the contributions at leading-order in scale-invariance, which means setting all the next-order corrections we have carefully kept track in this chapter to zero.

Therefore, selecting only the leading-order contribution in Eq. (5.23), we find

$$\begin{aligned} B_b^{(\text{leading})} = & \frac{H_*^4 (1 + \varepsilon_*)^4 k_2^2 k_3^2}{16 c_{s*}^4 \varepsilon_*^2 \prod_i k_i^3 k_t^2} \left\{ 3c_{s*}^2 (k_1 + k_t) + \right. \\ & \left. + (\varepsilon_* - 3) \left(\frac{k_t}{k_*} \right)^{\frac{4\varepsilon_*}{1+\varepsilon_*}} \Gamma \left(1 - \frac{4\varepsilon_*}{1+\varepsilon_*} \right) \cos \left(\frac{2\pi\varepsilon_*}{1+\varepsilon_*} \right) (k_1 + k_t + \varepsilon_* (k_t - 3k_1)) \right\} \\ & + \text{cyclic permutations} , \end{aligned} \quad (5.30)$$

where we have retained the scale-dependence through k_* . This formula reproduces the results of Ref. [174] provided we choose the reference scale to satisfy $k_* = k_t$. Eq. (5.30) is the bispectrum of the operator $\zeta(\partial\zeta/\partial y)^2$ for a perfectly scale-invariant spectrum of perturbations.

Whenever comparison was possible our results reproduce those of Ref. [174].

Noller & Magueijo.—Second, in Ref. [187] *Noller & Magueijo* estimated the magnitude of the next-order corrections to the bispectrum in the scale-invariant approximation of $P(X, \phi)$ models. In comparison, our calculation extends to the larger Horndeski scalar field theories. Their estimate focused on a subset of next-order corrections important when $|ky| \rightarrow 0$.

However, as we pointed out in §3.4.1, there are other contributions which contribute equally to the bispectrum and are sensitive to the dynamics around horizon crossing, when the approximation $|ky| \rightarrow 0$ fails. As we have shown, these corrections can be obtained by evaluating the change in the Hankel function of order $\nu = 3/2 - (n_s - 1)/2$, rather than at the exact scale-invariant choice, $\nu = 3/2$. If these contributions are not taken into account then the details of the interference between growing and decaying modes around horizon-crossing are lost. As we have argued in the previous chapters, these details are very important for our results to obey Maldacena’s consistency condition.

Moreover, in our calculation we have performed a uniform expansion to next-order corrections in the scale-invariant approximation. In particular we used Eq. (5.10) for the scale factor, a , and Eq. (B.11) for c_s . Ref. [187] on the other hand assumed a perfectly scale-invariant background, on top of which perturbations would develop. This amounts to setting $\alpha_* = \beta_* = 0$ in our Eq. (5.10), even though their contribution is as important as terms linear in $(n_s - 1)$ —as we have previously argued, the scalar fluctuations are sensitive to the background dynamics, and in particular to the next-order corrections we have calculated in the scale-invariant approximation.

For completeness, we will investigate one particular limit in $P(X, \phi)$ theories (these include DBI inflation) studied in Ref. [187], when the speed of sound of fluctuations is small, $c_s \ll 1$. This regime is phenomenologically interesting since it is known to be related with large non-gaussianities [74], for which the dominant operator is $(\partial\zeta/\partial y)^3$. To make this application more explicit we apply the notation of §5.2.1, and also Refs. [1, 45]), and take the action

$$S^{(3)} \supseteq \int d^3x dy a \Lambda_1 c_s^2 \left(\frac{\partial\zeta}{\partial y} \right)^3, \quad (5.31)$$

with

$$\Lambda_1 = \frac{\varepsilon}{Hc_s^4} \left(1 - c_s^2 - 2c_s^2 \frac{\lambda}{\Sigma} \right)$$

where

$$\frac{\lambda}{\Sigma} \equiv \frac{1}{6} \left(\frac{2f_X + 1}{c_s^2} - 1 \right) .$$

We assume f_X is constant. In DBI models, $f_X = 1 - c_s^2$ and therefore one sees that we cannot require f_X to be constant given that we are interested precisely in the regime when c_s is rapidly varying. However, for the purposes of making this comparison more transparent, we assume this is the case, similarly to what was done in Refs. [174, 187, 1], and implemented in §3.4.1. Technically, a more precise estimate would have to take the time-dependence of f_X into account.

We can see that taking the limit of small c_s , corresponds to considering $\left| \frac{\lambda}{\Sigma} \right| \gg 1$, in which case the interaction vertex is well approximated by

$$\Lambda_1(y) \simeq -\frac{2}{3} \frac{\varepsilon f_X}{Hc_s^4} .$$

Inspection of this formula reveals that this interaction vertex is rapidly varying, by virtue of its time-dependence in ε , H and c_s , of which only ε is slowly varying.

Our formulae are easily adapted to the case of rapidly varying Λ_i . For Λ_1 we find

$$\Lambda_1(y) = \Lambda_{1*} (-k_* y)^{-\frac{9\varepsilon_*}{1+\varepsilon_*}} \left\{ 1 - \frac{1}{1+\varepsilon_*} \left[\eta_* + 9\varepsilon_* \beta_* + \frac{\varepsilon_* \delta_*}{1+\varepsilon_*} + \frac{4\varepsilon_* \delta_* (\varepsilon_* - 1)}{1+\varepsilon_*} \right] \ln(-k_* y) + \frac{9}{2} \frac{\alpha_* \varepsilon_*}{1+\varepsilon_*} (\ln(-k_* y))^2 \right\} , \quad (5.32)$$

up to next-order corrections in scale-invariance. These corrections can be absorbed into the coefficients A_* , B_* and C_* in table 5.2. This generalises Eq. (5.21) to rapidly varying interaction vertices. Since (5.32) adds power-law contributions to the integral in Eq. (5.31), one might worry that not all the previously allowed values of ε will make the final result converge—we recall that the overall power-law needs to decay faster than $(-y)^{-1}$ for convergence criteria

to be met. In the event this does not happen then one is required to perform integration by parts an appropriate number of times to isolate the primitively divergent contributions, in a completely analogous way as we have dealt with the operator $\zeta(\partial\zeta)^2$ in §3.2.1. A convergent answer should similarly place constraints on the allowed values of ε so that the correlators do not evolve in time, since this could signal a spurious divergence.

Nevertheless, for this operator the integral (B.23) is evaluated for $\gamma = 2 - 4\varepsilon_*/(1 + \varepsilon_*)$ and is therefore always convergent, since the condition $\text{Re}(\varepsilon_*/(1 + \varepsilon_*)) < 3/4$ is satisfied for all the range of $0 < \varepsilon_* < 1$. The calculation is carried out as described in §5.2.1. Using the definition of f_{NL} (3.2), we find that at leading-order in scale-invariance

$$f_{\text{NL}}^{\text{(leading, equilateral)}} = \frac{5f_X}{c_{s*}^2} \frac{\prod_i k_i^2}{\sum_i k_i^3} \left(\frac{k_*}{k_t}\right)^{\frac{3-\varepsilon_*}{1+\varepsilon_*}} k_*^{-3} (1 + \varepsilon_*) \Gamma(\Upsilon) \cos\left(\frac{\pi(1 - \varepsilon_*)}{1 + \varepsilon_*}\right), \quad (5.33)$$

where $\Upsilon = \frac{3-\varepsilon_*}{1+\varepsilon_*}$ is a non-negative constant. f_{NL} can change sign if $\varepsilon_* > 1/3$, when the argument of the trigonometric function changes from the first to the second quadrant. This would be important since WMAP constraints predict predominantly positive values for $f_{\text{NL}}^{\text{(equilateral)}}$, whereas the original DBI model, under the slow-roll approximation, gives negative $f_{\text{NL}}^{\text{(equilateral)}}$.

Including the next-order corrections, the result becomes substantially more complicated and in an attempt to simplify it as much as possible, we evaluate f_{NL} in the equilateral limit and when $k_* = k$. We organise the correction to the leading-order non-gaussianity, δf_{NL} , in terms proportional to the various slow-variation parameters, as follows:

$$\delta f_{\text{NL}}^{\text{(equilateral)}} = (n_s - 1)f_{\text{NL}}^{n_s-1} + \delta f_{\text{NL}}^\delta + \eta f_{\text{NL}}^\eta, \quad (5.34)$$

with

$$f_{\text{NL}}^{n_s-1} = \frac{5f_X k^{2+\frac{4}{1+\varepsilon_*}}}{2c_{s_*}^2(1+\varepsilon_*)^2} \left\{ 3^{-\frac{3-\varepsilon_*}{1+\varepsilon_*}} \cos\left(\frac{2\pi}{1+\varepsilon_*}\right) k^{-\frac{2(3+\varepsilon_*)}{1+\varepsilon_*}} (1+\varepsilon_*)^3 \Gamma(\Upsilon) \mathcal{H}_\varpi \right. \\ \left. - (1+\varepsilon_*)^3 3^{\frac{4\varepsilon_*}{1+\varepsilon_*}} k^{-\frac{2(3+\varepsilon_*)}{1+\varepsilon_*}} \Gamma(\Upsilon) \cos\left(\frac{2\pi}{1+\varepsilon_*}\right) \left(2+2\gamma_E + \ln\frac{27}{2}\right) \right. \\ \left. - (1+\varepsilon_*)^3 k^{-6+\frac{4\varepsilon_*}{1+\varepsilon_*}} \sin\left(\frac{2\pi\varepsilon_*}{1+\varepsilon_*}\right) \mathcal{J} \right\}, \quad (5.35a)$$

$$f_{\text{NL}}^\delta = -\frac{5 \times 3^{-\frac{4}{1+\varepsilon_*}}}{2c_{s_*}^2(1+\varepsilon_*)} f_X \Gamma(\Upsilon) \left\{ \cos\left(\frac{\pi}{2}\Upsilon\right) \pi(3+\varepsilon_*(-5+4\varepsilon_*)) \right. \\ \left. + \sin\left(\frac{\pi}{2}\Upsilon\right) \left[2\left[1+\varepsilon_* + \ln 3(-3+\varepsilon_*(5-4\varepsilon_*))\right] \right. \right. \\ \left. \left. + 2(3+\varepsilon_*(-5+4\varepsilon_*))\psi^{(0)}(\Upsilon) \right] \right\}, \quad \text{and} \quad (5.35b)$$

$$f_{\text{NL}}^\eta = \frac{5 \times 3^{-\frac{4\varepsilon_*}{1+\varepsilon_*}} k^{2+\frac{4}{1+\varepsilon_*}}}{2c_{s_*}^2(1+\varepsilon_*)^2} f_X \Gamma(\Upsilon) \left\{ \cos\left(\frac{\pi\varpi}{2}\right) k^{-\frac{2(3+\varepsilon_*)}{1+\varepsilon_*}} \left[-2\varepsilon_*(1+\varepsilon_*) + \ln 3(2+2\varepsilon_*(1+2\ln 3)) \right. \right. \\ \left. \left. - (2(1+\varepsilon_*) + 8\varepsilon_* \ln 3 - 4\varepsilon_* \psi^{(0)}(\Upsilon))\psi^{(0)}(\Upsilon) + 4\varepsilon_* \psi^{(1)}(\Upsilon) \right] \right. \\ \left. - 8 \cos\left(\frac{\pi\varpi}{2}\right) k^{-3-\frac{3-\varepsilon_*}{1+\varepsilon_*}} \varepsilon_*(1+\varepsilon_*) \right. \\ \left. + \frac{1}{2} \sin\left(\frac{\pi\varpi}{2}\right) k^{-\frac{2(3+\varepsilon_*)}{1+\varepsilon_*}} \left[\pi + 4\varepsilon_* \pi - 8\varepsilon_* \pi \psi^{(0)}(\Upsilon) \right] \right\}. \quad (5.35c)$$

where $\varpi \equiv 2(1-\varepsilon_*)/(1+\varepsilon_*)$. We note the dependence on the power-law in k , expected whenever the slow-roll approximation breaks down. The polygamma functions of order zero, $\psi^{(0)}$, were introduced in Eq. (B.20) in Appendix B.4. \mathcal{H}_m denotes the m^{th} -harmonic number which relates to $\psi^{(0)}$ via $\mathcal{H}_{m-1} = \psi^{(0)}(m) + \gamma_E$, and \mathcal{J} satisfies

$$\mathcal{J} = \Gamma(\Upsilon) \left[\gamma_E + \ln 2 + \psi^{(0)}(\Upsilon) \right] - 2\Gamma\left(\frac{4}{1+\varepsilon_*}\right) {}_3F_2\left(\left\{1, 1, \frac{4}{1+\varepsilon_*}\right\}, \{2, 2\}, -2\right),$$

using the results from Appendix B.4. Eq. (5.34) contains all the next-order contributions in

the scale-invariant approximation. Eqs. (5.33) and (5.34) are to be compared to Eq. (3.15) of Ref. [187].

As argued in chapter 3, there is no reason to believe these corrections will be negligible, but their magnitude will depend on the values of the parameters ε , η , δ , and $(n_s - 1)$. We do not attempt to produce an order of magnitude of these corrections here. We also notice that the dependence on the scale k vanishes in the slow-roll limit, when ε_* becomes a perturbative parameter, $\varepsilon \ll 1$. This observation is in line with our previous comments on the strong scale-dependence whenever there was an appreciable deviation from the slow-roll regime, and the scale-invariant approach became valid.

With this example, it becomes clear that the scale-invariant approximation allows resummation of all powers of ε and s in the slow-roll approximation, provided the spectrum of perturbations is nearly scale-invariant.

Burrage et al..—Finally, as previously discussed, our results extend what was obtained by Burrage et al. [1] (on which our chapters 2 and 3 are based), and also Chen et al. [45] who treated the variation of the speed of sound of scalar fluctuations, s , and the expansion rate, ε , as slowly varying in the $P(X, \phi)$ class of models. Taking the limit of small ε and restoring s in our formulae by setting $\delta = s + 2\varepsilon$, we find perfect agreement between our results to next-order in slow-roll, including the logarithmic corrections previously discussed. As emphasised before, these corrections are important to correctly evaluate the scale-dependence of the bispectrum. Moreover, their motivation is driven by data and they could contribute to our estimates of non-gaussianities with a precision level comparable to the sensitivity of *Planck*'s data. As a consequence, our results obey Maldacena's factorisation theorem [66, 167] in the limit when slow-roll is a good approximation, which represents a non trivial consistency check of our calculation. The results presented in §§4.1–4.2 regarding the scale and shape-dependences of the bispectrum apply to our analysis if the slow-roll approximation is valid. Whenever there is significant breaking of the slow-roll approximation, we expect different results.

5.3 Summary of results

Whereas most studies of the bispectrum assume slow-roll conditions, cosmological constraints still allow for a deviation from this regime, whilst being compatible with inflation [174]. In this chapter we studied the phenomenology of inflationary backgrounds where $\varepsilon, |s| < 1$, but are treated *non-perturbatively*. They are nevertheless combined to produce an almost scale-invariant spectrum of scalar perturbations. Under these assumptions, we have calculated the bispectrum for single-field Horndeski models *perturbatively* in $(n_s - 1)$, but to *all orders* in ε and s . We have found that the scale-dependence of the bispectrum is encapsulated not only in a logarithmic [cf. §3.2], but in a stronger, power-law form. The power-law behaviour is more relevant if the breaking from slow-roll is stronger, and the slow-roll approximation fails.

In an optimistic scenario, such behaviour can be used to constrain the parameters of a given theory more tightly, and potentially eliminate it from the list of sensible models against observations. It is quite likely that with *Planck* the amount of information one is able to extract from the CMBR about the early universe will come to an end. It is therefore important to be able to retain the scale-dependence of the bispectrum in our theoretical computations and estimations, so as to use results from the complementary smaller scales (LSS) [224, 225, 226, 227].

We have obtained the general expression for the bispectrum in Horndeski theories for both constant and rapidly varying interaction coefficients, Λ_i . This work should be regarded as a first step towards estimating observables on a background that does not obey the slow-roll regime. Because these theories have a strong scale-dependence, they are more vulnerable to data constraints arising from different scales.

We leave the study of decomposing bispectrum shapes into fundamental harmonics (basis shapes) for future work. This partial-wave decomposition is very important in distinguishing between models as discussed in Ref. [2] and throughout chapter 4. Also, it will be interesting to derive the consistency relations between the amplitudes of each harmonic. This could enable us to project out models whose dynamics is beyond slow-roll, if those relations were

not supported by data. If single field models are excluded by observations, we will have to embark on a multi-field inflation exploration, where the interplay between curvature and isocurvature modes can be quite intricate (see, for example, Refs. [200, 228, 141]) .

Part II
The Physics After Inflation

*The only mystery in the universe
Is that there is a mystery of the universe.
Yes, this Sun that unintentionally illuminates ...
Everything not even brings with it the explanation
Of existing, nor does it have mouth with which to speak.*

Fernando Pessoa, in *Fausto*



Preheating at the End of Inflation

In the first part of this thesis we have focused on the inflationary imprints on the CMBR. In particular, we have studied the bispectrum in single-field models both using and discarding the slow-roll approximation. Our calculation not only reduces the theory-error associated with previous estimates, but it also makes small steps towards developing a potentially more appropriate diagnostic tool that enables telling models apart.

Whatever the microphysical origin of the post-inflationary universe, we know that the universe was almost empty at the end of inflation, as the number density in particles was diluted away by the exponential expansion. We thus find ourselves with two conceptual problems. First, the inflaton is not observed today. Therefore, some mechanism must have caused its energy density to dissipate. Second, matter is abundant all around us. After all, we are made up of particles. So, how was the universe repopulated after inflation?

To answer these questions, we will discuss the phenomenology of preheating in a DBI model in this short chapter. It is certainly not intended to signify a full study of preheating in this model. We rather want to briefly analyse what are the main differences between preheating in canonical and non-canonical models. This chapter represents a departure from our previous programme of investigating non-gaussian features in the bispectrum. We regard it

as a transition from the study of the early universe during inflation, to the standard Big Bang model.

Outline.—We start by giving a short review of some relevant historical developments in the theory of preheating in §6.1, and briefly revisit the DBI model §6.2. In §6.3 we discuss a DBI toy model in which inflation ends as the brane settles to its final position in the warped background. We show that this model is comparable to chaotic inflation in a theory with canonical kinetic terms, and discuss the parametric resonance event.

In §6.4 we study the stage of perturbative reheating and provide an estimate for the reheating temperature in models driven by a DBI kinetic term. We give a summary of our findings in §6.5. Additional material related to this chapter is collected in Appendix C.

This chapter is the result of work done in collaboration with Nazim Bouatta, Anne-Christine Davis and David Seery, and published as Ref. [4].

6.1 Preheating: development of a theory

In this chapter we are interested in understanding how the universe could have reheated after a period of DBI inflation. The DBI inflation model was discussed in §3.4.1 from the point of view of an effective field theory. There, the inflaton was a scalar field whose dynamics was governed by the DBI action. Here, we review DBI from the brane world perspective, but perform our calculation from the quantum field theory point of view.

In the proposal set forth by Tong & Silverstein [27], and later elaborated in collaboration with Alishahiha [74], the DBI action describes the low-energy dynamics of a D3-brane moving in a warped background space-time. D-branes naturally arise in string theory and are extended objects in space-time where open strings can end—for a review of their properties see the classic textbook by Johnson [229]. Inflation in these models was discussed by Chen [182], and inflation in string cosmology has been reviewed by McAllister & Silverstein [230].

Reheating in related brane-world models has been studied in Refs. [231, 232, 233, 234,

[235]. Any inflationary theory needs to be completed through a reheating phase, which depends strongly on the details of the preceding inflationary phase as emphasised in Refs. [236, 237]. In principle, no two models find the same preheating phenomenology, by which the universe is repopulated with matter particles. Preheating is a subtle function of the underlying physics, probing information which can be regarded as complementary to the physics of the density fluctuation, studied in part I of this thesis. For this reason, competing inflationary models exhibit important differences in their preheating analysis. In particular, in this chapter we shall explore this process and display the main dissimilarities between DBI models and those with canonical kinetic terms. Here, the DBI model is to be regarded as representative of the non-canonical class.

Many authors have contributed to the theory of particle production, which is now well-developed in light of many authors' efforts [238, 239, 240, 241]. The theory of preheating has been reviewed by Bassett et al. [242]; see also Ref. [243]. We highlight the review by Kofman, Linde & Starobinsky [244], where a comprehensive study of preheating and reheating was presented. In *perturbative reheating*, the decay rate of inflaton particles into other species of the matter sector is calculated directly from an S -matrix. The calculation of this process follows the well-known *in-out* quantum field theory rules applied to scattering processes. By virtue of the perturbative nature of this process, reheating is not particularly efficient in producing a significant number density of particles.

It was later understood that it was possible that an enhancement of the perturbative decay described above could occur. This could be understood as a by-product of the accumulation of several previous decays, leading to a resonant phase of *non-equilibrium* production known as *preheating*. By this process, inflaton particles see their energy dumped into the matter sector, which one can interpret as an amplification in particles occupancy number. This will be the central topic in this chapter.

A different effect, named *tachyonic preheating* [245, 246, 247, 248], is associated with the end of inflation in certain models, usually when a spontaneous symmetry breaking oc-

curs. Unlike conventional preheating, this does not merely convert one species of particle into another, but (like any tachyonic instability) reflects a preference for converting one vacuum state into another, by the rapid accumulation and condensation of particles. This phenomenon happens, for example, in hybrid inflation models, initially proposed by Linde [249]. The delicate dynamics between this two-field inflation model makes preheating particularly hard to investigate, as documented by Lyth in Refs. [250, 251].

The general theory of preheating has been systematically applied to concrete models. In particular this was possible for some versions of brane inflation, where a careful interpretation was given [252, 253]; see also the review by Sen [254]. In these models, inflation ends when the mobile D3-brane becomes close to a parallel, fixed antibrane (a $\overline{D3}$ -brane), allowing open strings stretching between the D3- $\overline{D3}$ pair to form. The inflaton field in these models is the distance between the two branes. The open string states include a tachyon mode which develops for sufficiently close branes. This tachyonic instability is believed to induce fragmentation of the D3-brane into D0-branes (which pack together to form the D3-brane). The D0 fragments efficiently decay into closed string states, which are enumerated by the Kaluza-Klein (“KK”) modes of supergravity fields in the warped background. These KK modes subsequently decay into the species of matter and radiation which build up the standard model content of our universe [253].

In this chapter we shall focus on a much less dramatic version of post-inflationary dynamics. We work in a model where the D3-brane comes to rest near an edge of its warped background, the “tip of the throat.” As it settles on its resting-place it undergoes coherent oscillations, inducing growing, quantum fluctuations which fold and wrinkle the surface of the brane.

As we mentioned before, our interest lies in the *qualitative* differences which emerge between inflation models driven by canonical and non-canonical kinetic terms [255]. What is the effect of the extra non-linearities due to the DBI action on the preheating mechanism? Is the reheating temperature different? Focusing on the differences between these two classes

of models, we will mostly ignore their similarities. In particular, we acknowledge the use of perturbation theory in either case will break down when back-reaction becomes important, at which point the number density of the recently produced particles needs to be taken into account [241]. For this reason, our preheating analysis is restricted to times before the onset of back-reaction.

6.2 DBI dynamics

The DBI model was reviewed in §3.4.1, and we revisit it here in a different perspective: that of branes. In Ref. [27] Silverstein & Tong discussed the brane-world scenario where one or more D3-branes move in a warped throat, taken to be a six-dimensional elongated region in a higher dimensional world-volume. This is usually the AdS throat. Another possibility exists: the throat can be capped off in the infra-red limit of the underlying field theory.

A low-energy description of a D3-brane travelling in this warped throat is given by the Dirac–Born–Infeld action¹

$$S = \frac{1}{2} \int dx \sqrt{-g} \left\{ R + 2 \left[-\frac{1}{f(\phi)} \left[\sqrt{1 - f(\phi)X} - 1 \right] - V(\phi) \right] \right\}, \quad (6.1)$$

where $g_{\mu\nu}$ is the pull-back of the 10-dimensional metric to the brane world-volume, and R is the Ricci scalar constructed from $g_{\mu\nu}$. As usually in brane world scenarios, ϕ acts as a collective coordinate measuring the radial position of the brane within the throat, and V is the potential describing how the brane is attracted towards the bottom of the throat. The warp factor, $f(\phi)$, is in general a function of the radial coordinate. A more precise interpretation is possible: f^{-1} measures the tension of the D3-brane, redshifted by the warp factor, giving f canonical dimension $[\text{mass}]^{-4}$ (we are using units in which ϕ has dimensions $[\text{mass}]$).

If the throat is exactly anti-de Sitter, the result is a static BPS state in which the potential $V(\phi)$ is quartic at lowest-order in the field, because conformal invariance forbids the existence

¹See, for example, Refs. [256, 257, 258] for discussions on the DBI action.

of a mass term. If the throat is capped off, then conformal invariance is broken—a typical example is the Klebanov–Strassler throat [259]. In this case we expect a mass term to be generated which receives contributions from moduli stabilization and bulk fluxes [252, 260, 261, 262, 263, 264, 265]. In a general compactification, a spectrum of terms will be generated including a $\phi^{3/2}$ term which may lead to a phase of inflexion-point inflation. We assume this term is absent, or forbidden by a symmetry. Therefore, for small departures from the equilibrium point for ϕ , the potential attracting the brane towards the infrared tip of the throat is (to lowest order) quadratic [27],

$$V(\phi) = \frac{1}{2}m^2\phi^2 . \quad (6.2)$$

D-brane inflation with this potential is sometimes referred to as the “UV model.” A related small-field, IR model due to Chen [182] takes $V = V_0 - m^2\phi^2/2$ with V_0 dominant—we discussed its non-gaussian features in §3.4.1.

As the brane approaches the infrared tip of the throat, ϕ tends *slowly* to zero. In this limit $\dot{\phi}^2 \ll 1$ and the square root can be expanded in powers of X , reproducing the action for a canonically normalised scalar field with potential V . If, however, the brane is moving relativistically, then $X \sim 1$ and the square root in Eq. (6.1) is *non-expandable*. Said differently, in this case we are forced to retain an infinite set of non-renormalisable operators involving powers of $(\partial\phi)^2$ with pre-defined Taylor coefficients, but higher-order derivative operators do not arise. It is the algebraically special form of the action through $\sqrt{1-fX}$ which makes DBI satisfy a non-renormalisation theorem [27, 175, 266, 160] against large renormalisations of these expansion coefficients.

To measure the relative importance of the nonlinear terms induced by the presence of the square root in the action (6.1), it is conventional to define the equivalent of a Lorentz factor for the brane, as in Eq. (3.19), given by

$$\gamma^{-1} \equiv \sqrt{1-f(\phi)\dot{\phi}^2} . \quad (6.3)$$

This is a non-analytical function which has a branch-cut in the negative real axis, which requires γ to be real, and therefore $0 \leq f \dot{\phi}^2 < 1$ [267, 27]. This induces a limiting speed for the motion of the D3-brane moving along the throat; slow-motion corresponds to $\gamma \sim 1$, whereas relativistic motion of the brane gives $\gamma \gg 1$.

In FLRW space-time, the equation of motion for the inflaton is

$$\ddot{\phi} + 3H \frac{\dot{\phi}}{\gamma^2} - \frac{1}{f} \frac{d \ln f}{d\phi} + \frac{3}{2} \frac{d \ln f}{d\phi} \dot{\phi}^2 + \frac{1}{\gamma^3} \left(\frac{1}{f} \frac{d \ln f}{d\phi} + \frac{\partial V}{\partial \phi} \right) = 0 . \quad (6.4)$$

In the non-relativistic limit $\gamma \rightarrow 1$ and for constant f , Eq. (6.4) reduces to the Klein–Gordon equation for a canonically normalised scalar field in a FLRW background.

What is the likely value for γ ? We revisit our discussion of §3.4.1. There, we provided an estimate, valid at next-order in slow-roll, of the bispectrum amplitude in the equilateral mode. For our purposes it is, however, enough to consider its leading-order behaviour $f_{\text{NL}}^{(\text{equilateral})} \simeq -0.32\gamma^2$ [74] [cf. Eq. (3.20)]. Using WMAP 7-year data at 65% confidence level, $f_{\text{NL}}^{(\text{equilateral})} = 26 \pm 140$, we estimate this requires $\gamma \lesssim 9$. In our calculations we assume this upper limit will continue to be eroded especially in anticipation of *Planck*'s results. It might be even possible that the smallness of γ constrains the model to be realised in its non-relativistic limit. This is perhaps the least phenomenologically interesting regime for DBI. Nevertheless, we will show that preheating will display some interesting features. Accordingly, we suppose that inflation is approximately of the slow-roll variety. In this limit, the evolution of ϕ is close to that in a canonical model, where the corrections are controlled by the deviation of γ from unity. We will solve Eq. (6.4) perturbatively in powers of these small deviations.

In this description the brane will slowly drift towards the tip of the throat, where inflation ends. Near the tip of the throat, the warp factor decreases [259, 268]. Silverstein & Tong [27] suggested that the relevant physics of the capped throat could be captured by taking

$$f(\phi) \equiv \frac{\lambda}{(\phi^2 + \mu^2)^2} , \quad (6.5)$$

where λ is the dimensionless 't Hooft coupling and μ is the energy scale associated with the infrared cut-off. For convenience, we choose coordinates so that the final resting place of the brane corresponds to $\phi = 0$. When $\phi \ll \mu$, this becomes independent of the brane position ϕ , and assumes a constant value

$$f \equiv \frac{\lambda}{\mu^4} . \quad (6.6)$$

We suppose $m \gg H$, which is usually true after inflation. This means that during one Hubble time there will occur many oscillations and Hubble friction terms arising in Eq. (6.4) can be ignored. Our analysis assumes the brane will oscillate around this position in warped space with small amplitudes, contained entirely within the cut-off region where f^{-1} is approximately constant. We will justify these statements below.

Making these approximations and assuming the non-relativistic limit in which $\gamma = 1$, coherent oscillations of the brane have constant amplitude, which we shall denote by \mathcal{A} . The respective solution to the equation of motion (6.4) is

$$\phi_0(t) \simeq \mathcal{A} \cos(mt) . \quad (6.7)$$

Our analysis relies on the approximations described above. We list below some important criticisms about the approximations used, and justify our approach.

Perturbative approximation.—What other effects can spoil the dynamics of ϕ given by Eq. (6.7)? After integrating out fluxes and other UV perturbations, we are left with a low-energy theory controlled by an effective potential for the D-brane [264, 265], of the form $V = \sum_i c_i M^{4-\Delta_i} \phi^{\Delta_i}$, where M is some mass scale. In a generic compactification, the interaction coefficients are expected to be $O(1)$. The leading term corresponds to $\Delta = 3/2$. Invoking some symmetry may force this term to be absent. The next $\Delta = 2$ term will typically dominate higher contributions to the potential (which start with $\Delta = 3$) whenever $\phi \ll M$.

On the other hand, the infrared cutoff scale, μ , must satisfy $\mu < m$. Therefore, provided we take $\phi < \mu$, so that we are safely within a region where the warp factor is constant and

given by Eq. (6.6). We can thus expect corrections from both features in the throat geometry and higher-order terms in the D-brane potential to be negligible.

Slowly evolving background.—How good is our approximation that $m \gg H$? In practice, Hubble drag would cause \mathcal{A} to decrease slowly, roughly like $1/mt$ [269], typical of a matter dominated phase. This is because the pressure of the fluid associated with the inflaton should be averaged out over the many oscillations the brane executes around $\phi = 0$. Take H_f and H_i to be two values of the Hubble parameter separated by N oscillations. It follows that

$$\frac{H_i}{H_f} \sim 1 + AN \frac{H_i}{m} , \quad (6.8)$$

where A is some constant of order unity. The corresponding oscillation amplitudes, \mathcal{A}_f and \mathcal{A}_i , are related by

$$\frac{\mathcal{A}_i}{\mathcal{A}_f} \sim 1 + A' N \frac{\mathcal{A}_i}{M_p} , \quad (6.9)$$

in which A' is different from A , but also of order unity. Unless $N \gg 1$, our assumption that $m \gg H$ is sufficient to ensure $H_i \simeq H_f$. In addition, Eq. (6.9) shows that $\mathcal{A}_i \ll M_p$ is sufficient to ensure $\mathcal{A}_i \simeq \mathcal{A}_f$. In view of the requirement $\mathcal{A} \ll m$ to ensure the quadratic potential is an adequate approximation, where m is typically of order the infrared cutoff scale, this is amply satisfied. Therefore, in what follows, we will restrict our attention to a sufficiently large number of oscillations, say $N < 10^2$, and neglect the time-dependence of both H and \mathcal{A} .

Relativistic corrections to the background solution.—According to the approximations listed above, corrections to the non-relativistic motion described by (6.7) will be perturbative provided $|f \dot{\phi}_0^2| \ll 1$. To check that our analysis satisfies this approximation, it is useful to introduce a dimensionless positive quantity, which we shall denote by ζ , satisfying

$$\zeta \equiv f m^2 \mathcal{A}^2 . \quad (6.10)$$

The condition above can then be rewritten as $\zeta \ll 1$. But how small can ζ be? In order for

the small relativistic corrections not to be dominated by others which we have neglected, one needs to impose, for consistency, $\zeta \gtrsim \phi/m$ or μ/m . We should trust our analysis for perhaps $\zeta \sim 10^{-1}$ to 10^{-3} , but certainly not for significantly larger or smaller ζ .

We now evaluate the next-order $O(\zeta)$ corrections to the leading-order solution (6.7). The governing equation can be obtained by dropping Hubble friction terms in Eq. (6.4), in agreement with our approximation, which gives

$$\ddot{\phi} + \left(1 - \frac{3}{2}f\dot{\phi}^2\right) \frac{dV}{d\phi} \simeq 0 . \quad (6.11)$$

One could attempt to solve Eq. (6.11) perturbatively, writing $\phi = \phi_0 + \delta\phi$ with $\delta\phi$ of $O(\zeta)$. However, this procedure does not produce an appropriate, self-consistent solution since Eq. (6.11) also induces corrections to the fundamental oscillation frequency m .

To capture these physical effects, we take another ansatz: we assume a WKB-type solution of the form $\phi = \mathcal{A} \cos \theta(t)$. We now need to solve for the phase $\theta(t)$ to order $O(\zeta)$. To recover Eq. (6.7) in the limit when $\zeta \rightarrow 0$, we require $\theta(t) = mt + \delta\theta(t)$. Replacing in Eq. (6.11), we conclude that $\delta\theta(t)$ must satisfy the following differential equation

$$\delta\ddot{\theta} + 2m \cot(mt) \delta\dot{\theta} + \frac{3m^2\zeta}{2} \sin(mt) \cos(mt) = 0 . \quad (6.12)$$

Dropping an unwanted divergent contribution,² the background solution is

$$\varphi(t) = \mathcal{A} \cos \left[(mt) \left(1 - \frac{3\zeta}{16}\right) + \frac{3\zeta}{32} \sin(2mt) \right] . \quad (6.13)$$

In principle, one can calculate corrections to the amplitude, but we will ignore the time-dependence of \mathcal{A} (we will see in Fig. 6.1 this is indeed a good approximation).

In comparison with the canonical solution, the phase shows a drift proportional to ζmt . Although the calculation remains under perturbative control, this drift generates order unity de-

²This mode is proportional to $\cot mt$, which is divergent at $t = 0$. We choose its coefficient so that this mode is projected out by the boundary conditions, and therefore does not lead to an instability in the solution.

viations from the non-relativistic background after $1/\zeta$ oscillations. There is also a superposed phase oscillation, proportional to $|\zeta \sin 2mt| \ll 1$, which always generates small corrections. To make the comparison with the canonical solution more clear, we write (6.13) as

$$\varphi(t) = \mathcal{A} \left\{ 1 - \frac{3\zeta}{16} \sin^2 \left[(mt) \left(1 - \frac{3\zeta}{16} \right) \right] \right\} \cos \left[(mt) \left(1 - \frac{3\zeta}{16} \right) \right], \quad (6.14)$$

which is equivalent to (6.13) up to $O(\zeta)$. Eq. (6.14) exhibits the first perturbative relativistic corrections to the motion of the brane: first, a frequency shift in the background motion ϕ_0 , corresponding to $m \mapsto m(1 - 3\zeta/16)$; and second, a small periodic fluctuation superposed over the background oscillations.

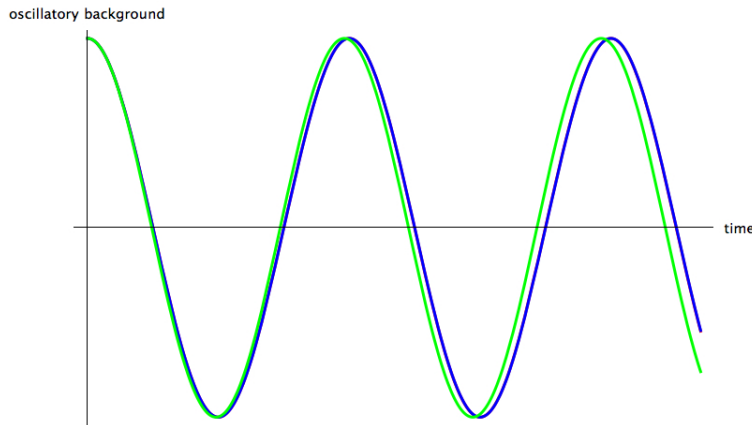


Figure 6.1: Plot of the numerical (red) and approximate (blue) solution of Eq. (6.11), and the cosine function (green).

On the left we plot the numerical solution of Eq. (6.11), which is completely overlaid by the blue curve, given by (6.14). In contrast, the simple trigonometric solution (6.7) stops being a good approximation to the dynamics of the background field $\phi(t)$ soon after one oscillation.

Indeed, the true solution is shown to drift away from the simple cosine—this is the effect of the *phase* drift mentioned above. The amplitude, however, is very lightly modulated over the coherent oscillations, and remains almost constant.

6.2.1 Coupling to matter fields

The reheating phase is designed to populate the universe with Standard Model degrees of freedom, whilst dissipating the energy stored in the inflaton field. Pauli's exclusion principle usually prevents efficient preheating into fermions [270, 271], so we suppose the inflaton ϕ

couples to bosonic degrees of freedom, which are taken to have spin zero for simplicity. The subsequent decay into fermions has also been studied in Refs. [241, 272].

We treat the couplings between the inflaton and the matter modes phenomenologically, denoting the matter field by χ and taking it to be described by the low-energy effective Lagrangian

$$\mathcal{L} \supseteq -\frac{1}{2}(\partial\chi)^2 - \frac{1}{2}m_\chi^2\chi^2 - \frac{1}{2}g^2\phi^2\chi^2, \quad (6.15)$$

where g is a dimensionless coupling and m_χ is a bare mass. Eq. (6.15) should be regarded as a subset of the Lagrangian of the interacting theory. We do not claim that such interactions necessarily arise in string models, although we hope the resulting phenomenology will be representative of those that do. For our purposes, it suffices to consider the subset (6.15) as a possible interaction channel which shall expose the features of the preheating stage in these models. The equation of motion for χ is

$$\ddot{\chi} + 3H\dot{\chi} - \frac{1}{a^2}\nabla^2\chi + (m_\chi^2 + g^2\phi^2)\chi = 0, \quad (6.16)$$

where ∇^2 is the Laplacian operator. Matter production in this model is studied in §6.3.

In §6.3.4 we will study an alternative model, in which the matter field χ is coupled to a symmetry-breaking potential of the form

$$V(\phi, \chi) = \frac{1}{2}m^2(\phi - \sigma)^2 + \frac{1}{2}g^2\phi^2\chi^2. \quad (6.17)$$

This causes the brane to be attracted to a radial position which is not the tip of the throat, but rather $\phi = \sigma$. This can be interpreted as a toy model of compactifications in which the D-branes are brought to rest at a finite point in the warped throat.

6.3 Non-perturbative preheating in DBI inflation

As the brane settles towards $\phi = 0$, its coherent oscillations cause efficient non-perturbative particle production. We briefly review this process.

6.3.1 Brief review of parametric resonance

To perform a quantum field theory treatment of preheating we need to quantize both the inflaton ϕ and the matter field χ . In particular, framing our discussion with respect to χ , we want to write the two linearly independent solutions of

$$\ddot{\chi}_k + 3H\dot{\chi}_k + \left(k^2 + m_\chi^2 + g^2\phi^2\right)\chi_k = 0 \quad , \quad (6.18)$$

where k is the comoving wavenumber. We label these solutions χ_k and χ_k^* . We write the Heisenberg field corresponding to χ in Fourier space as

$$\chi(t, \mathbf{x}) = \int \frac{d^3k}{(2\pi)^3} \left(\chi_k a_k^\dagger + \chi_k^* a_{-k}\right) e^{i\mathbf{k}\cdot\mathbf{x}} \quad ,$$

in which we have assumed that the normalisation of $\{\chi_k, \chi_k^*\}$ has been adjusted so that a_k and a_k^\dagger obey the usual creation-annihilation algebra,

$$[a_k, a_{k'}^\dagger] = (2\pi)^3 \delta(\mathbf{k} - \mathbf{k}') \quad .$$

How many particles are produced with momenta k ? The energy density, ρ_k , associated with χ -quanta of wavenumber k satisfies $2\rho_k = |\dot{\chi}_k|^2 + \omega_k^2 |\chi_k|^2$, where $\omega_k^2 = k^2 + g^2\phi^2$. Subtracting the zero-point energy, the occupancy number is well approximated by

$$n_k \simeq \frac{E_k}{\omega_k} = \frac{\omega_k}{2} \left\{ \frac{|\dot{\chi}_k^{\text{cl}}|^2}{\omega_k^2} + |\chi_k^{\text{cl}}|^2 \right\} - \frac{1}{2} \quad . \quad (6.19)$$

We conclude that whenever $|\chi_k|$ or $|\dot{\chi}_k|$ are large, the occupation numbers will grow. In

particular, if χ_k experiences exponential growth, then Eq. (6.19) shows we can expect n_k to attain macroscopic values very rapidly. Eq. (6.19) therefore describes the phenomenon of preheating, discussed in §6.1, and which we will investigate in detail in §6.3.3.

To determine when χ_k grows, it is often useful to translate the mode equation for χ_k into a version of Mathieu's equation or its generalisations. This is because Mathieu's equation admits solutions which fall under instability bands (in some region of the parameter space), which signal exponentially growing modes when applied to preheating—particle production becomes copious. The standard Mathieu's equation is of the form [273, 274]

$$\frac{d^2\chi_k}{dz^2} + (A_k - 2q \cos 2z)\chi_k = 0 \quad , \quad (6.20)$$

where z is a dimensionless time to be defined below. In the following sections we give explicit model-dependent expressions for A_k and q applicable to both inflaton and matter fluctuations.

For certain combinations of these parameters the solutions exhibit exponential growth. If $q \gtrsim A_k$, the effective mass of the scalar field in question can become temporarily zero, which induces a copious production of χ -quanta. This regime is referred to as *broad resonance*, because there is a width of momenta which are favoured to experience this instability [275].

In the opposite regime, $q \ll A_k$, and the effective mass never vanishes. Instability bands are still present, but the combinations of parameters A_k and q are such that the exponential growth occurs only in narrow bands of momentum space. For this reason this scenario is known as *narrow resonance*. These bands are centred on momenta for which $A_k = \ell^2$, where $\ell \in \mathbb{N}$, corresponding to values of k for which $|A_k - \ell^2| \lesssim q^\ell$ [241]. If $|q| \ll 1$ then at large ℓ these bands become increasingly narrow. We will now study the solutions to Mathieu's equation (6.20) when χ_k are both inflaton and matter field modes.

6.3.2 Inflaton production

First, consider the inflaton mode with momentum k . We set ϕ equal to its background value, which we denote by φ , determined up to first-order relativistic corrections by (6.14). At the onset of oscillations we assume that the matter field, χ , is in its vacuum state, and so $\chi = 0$.

Until the accumulation of χ -quanta causes the background χ field to grow, the inflaton fluctuations $\delta\phi_k$ evolve according to the Klein-Gordon equation. To linear order in ζ , this is

$$\delta\ddot{\phi}_k - 3\frac{fm^2\varphi\dot{\varphi}}{\gamma}\delta\dot{\phi}_k + \left(\frac{m^2}{\gamma^3} + k^2\right)\delta\phi_k = 0 . \quad (6.21)$$

We expand this equation uniformly to leading-order in the perturbative parameter $f\dot{\varphi}^2$ and perform a change of variables so that $\delta\phi_k = \xi y_k$, which can eliminate the friction term in Eq. (6.21). In particular, we choose ξ to satisfy

$$\frac{d\ln\xi}{dt} = \frac{3}{2}fm^2\varphi\dot{\varphi} .$$

The solution to this differential equation is

$$\xi = \xi_0 \exp\left\{\frac{3}{2}fm^2[\varphi^2(t) - \varphi^2(t_0)]\right\} , \quad (6.22)$$

where we have chosen $\xi = \xi_0$ at $t = t_0$. This produces a friction, or “braking” effect, which could be interpreted as a perturbative manifestation of the D-acceleration mechanism [27]. It is a novel effect in the DBI model, with no analogue in canonical scenarios. Accordingly, the braking disappears in the limit $\zeta \rightarrow 0$.

The remaining time-dependence is carried by y_k , which satisfies a Mathieu equation with A_k and q determined, to leading-order in ζ defined by (6.10), by

$$A_k = \left(1 + \frac{k^2}{m^2}\right) \left(1 + \frac{3\zeta}{8}\right) - \frac{3\zeta}{4} \quad \text{and} \quad q = \frac{3\zeta}{8} . \quad (6.23)$$

The dimensionless time z , used to write Eq. (6.20), satisfies $z = mt(1 - 3\zeta/16)$, which corresponds to a rescaled frequency $m \mapsto m(1 - 3\zeta/16)$. Inspection of Eq. (6.23) reveals $q \ll A_k$, giving resonance only in narrow bands. The $\ell = 1$ band is centred at momentum k_1 , given by

$$k_1 = \frac{m}{2} \sqrt{\frac{3\zeta}{2}} . \quad (6.24)$$

Modes with momentum $k = k_1$ will experience exponential growth.

From Floquet's theory it follows that each mode evolves as $\exp(\mu_k z)$. In the $\ell = 1$ band, also called the first band, the Floquet exponent μ_k has positive real solutions which signal exponential growth [273]

$$\mu_k^2 \simeq \left(\frac{q}{2}\right)^2 - (A_k^{1/2} - 1)^2 . \quad (6.25)$$

This exponent is maximal for the central value $k = k_1$ and decreases for larger or smaller k , forming a band of narrow width Δ_1 ,

$$\Delta_1 = \frac{m\sqrt{3\zeta}}{2} \frac{\sqrt{2} - 1}{\sqrt{2}} . \quad (6.26)$$

At the centre of the band, the Floquet exponent takes the value μ_1

$$\mu_1 = \max_{\ell=1 \text{ band}} \mu_k = \frac{3\zeta}{16} . \quad (6.27)$$

So far, our formulae depend on the mass, m , and coupling, g , which appear in the Lagrangian. However, these *bare* quantities only parametrise the theory. To make a meaningful comparison between DBI and the class of canonical models, we must express our answer in terms of a *measurable* mass and coupling, corresponding to *physical* quantities. We denote these by m_* and g_* , to distinguish them from the Lagrangian parameters. In the DBI theory the Lagrangian parameters have no direct physical significance, whereas in the case of canonical kinetic terms they coincide with the measurable mass and coupling at tree-level. The relations $m_*(m)$ and $g_*(g)$ are derived in Appendix C.1.

Collecting Eqs. (6.22) and (6.25), and expressing the answer in terms of the physical m_* and g_* , we find that the inflaton modes grow as

$$\delta\phi_k \sim \exp\left\{\frac{3\zeta}{8} \cos\left[2m_*t\left(1 - \frac{7\zeta}{16}\right)\right] + \frac{3\zeta}{16}m_*t\right\}. \quad (6.28)$$

The undetermined normalisation absorbs ξ_0 in Eq. (6.22). We see that at early times, the DBI friction and the resonant growth have competing effects. After a few oscillations, however, the cosine which represents the friction effect becomes negligible in comparison with the resonant term, and inflaton particle production thrives.

6.3.3 Matter particle production

Ultimately, we are interested in studying the production of matter particles. Consider the interaction potential in the Lagrangian density (6.15). As a result of these interactions the χ -mode receives an effective mass of order $k^2 + g^2\phi^2$. As in §6.3.2 we assume that preheating begins in the vacuum $\chi = 0$, which is a good approximation until the χ -quanta are in such number density that they back-react on the zero mode. In this vacuum, small fluctuations grow governed by a generalised Hill's equation

$$\frac{d^2\delta\chi_k}{dz^2} + (\theta_0 + 2\theta_2 \cos 2z + 2\theta_4 \cos 4z) \delta\chi_k = 0, \quad (6.29)$$

where the parameters θ_0 , θ_2 and θ_4 obey

$$\begin{aligned} \theta_0 &= \frac{k^2}{m^2} \left(1 + \frac{3\zeta}{8}\right) + \frac{g^2 \mathcal{A}^2}{2m^2} \left(1 + \frac{9\zeta}{32}\right), \\ \theta_2 &= \frac{g^2 \mathcal{A}^2}{4m^2} \left(1 + \frac{3\zeta}{8}\right), \text{ and} \\ \theta_4 &= \frac{3}{128} \frac{\mathcal{A}^2}{m^2} \zeta g^2, \end{aligned} \quad (6.30)$$

and $z = mt(1 - 3\zeta/16)$. The solutions of Hill's equation grow and decay with characteristic Floquet exponent μ_k in a way entirely analogous to the solutions of Mathieu's equation. The exponentially growing solutions also organize themselves into bands, defined by integers ℓ .

According to Floquet's theory, one can estimate μ_k for the $\ell = 1$ band

$$\mu_k^2 \simeq \left(\frac{\theta_2}{2}\right)^2 - (\theta_0^{1/2} - 1)^2 \mp \frac{\theta_2}{3} \left(\frac{\theta_4}{2}\right)^2 \mp \frac{\theta_2^3}{2} . \quad (6.31)$$

We believe this expression has not previously appeared in the preheating literature, and we provide the reader with a full derivation in Appendix C.2. In the region where our approximations are valid, $\mathcal{A} \ll m$. Therefore, the terms involving θ_4^2 and θ_2^3 are negligible, and

$$\mu_k^2 \simeq \left(\frac{\theta_2}{2}\right)^2 - (\theta_0^{1/2} - 1)^2 . \quad (6.32)$$

The centre of the $\ell = 1$ band lies at $k = k_1$, where

$$k_1^2 = m^2 \left(1 - \frac{3\zeta}{8}\right) - \frac{g^2 \mathcal{A}^2}{2} \left(1 - \frac{3\zeta}{2}\right) , \quad (6.33)$$

for which $\theta_0(k_1) = 1$. Collecting terms, it follows that the unstable matter modes grow at a rate determined by

$$\delta\chi_k \sim \exp \left\{ \mu_k \Big|_{\max} m_* t \left(1 - \frac{3\zeta}{16}\right) \right\} \sim \exp \left\{ \frac{1}{8} \left(\frac{g_* \mathcal{A}}{m_*}\right)^2 m_* t \left(1 + \frac{3\zeta}{16}\right) \right\} . \quad (6.34)$$

This displays a slight (perturbative) enhancement compared to the equivalent canonical model.

6.3.4 Preheating with a symmetry breaking term

Now consider the symmetry-breaking potential given in Eq. (6.17). In this case, it is more convenient to redefine ϕ so that it describes excitations around the true vacuum at $\phi = \sigma$.

Writing $\phi \rightarrow \phi + \sigma$, the interaction potential can be written

$$V(\phi, \chi) = \frac{1}{2}m^2\phi^2 + \frac{1}{2}g^2\phi^2\chi^2 + g^2\sigma\phi\chi^2 + \frac{1}{2}g^2\sigma^2\chi^2 . \quad (6.35)$$

Around this minimum, ϕ acquires an effective mass $m_{\text{eff}}^2(\chi) = m^2 + g^2\chi^2$.

Making the same assumption as before that preheating begins while $\chi \approx 0$, the inflaton modes will behave as in Eq. (6.28) until the growth of χ_k occupation numbers causes the χ zero-mode to grow. Until that time, χ modes with momentum k obey the equation of motion

$$\delta\ddot{\chi}_k + (k^2 + g^2\phi^2 + 2g^2\sigma\phi + g^2\sigma^2) \delta\chi_k = 0 . \quad (6.36)$$

We will suppose the brane executes oscillations around $\phi = \sigma$ with an amplitude much smaller than the symmetry breaking scale, $\mathcal{A} \ll \sigma$, so that it has reasonably settled at its final position. Assuming that $\sigma \ll m/g$, and again neglecting any bare mass for χ , fluctuations in the matter field will be controlled by Hill's equation,

$$\frac{d^2\delta\chi_k}{dz^2} + (\theta_0 + 2\theta_2 \cos 2z + 2\theta_6 \cos 6z) \delta\chi_k \approx 0 , \quad (6.37)$$

in which $2z = mt(1 - 3\zeta/16)$ and the parameters θ_0 , θ_2 and θ_4 obey

$$\begin{aligned} \theta_0 &= \frac{4}{m^2} (k^2 + g^2\sigma^2) \left(1 + \frac{3\zeta}{8}\right) , \\ \theta_2 &\simeq 4 \frac{g\sigma}{m} \frac{g\mathcal{A}}{m} \left(1 + \frac{21\zeta}{64}\right) , \text{ and} \\ \theta_6 &\simeq \frac{3\zeta}{16} \frac{g\sigma}{m} \frac{g\mathcal{A}}{m} . \end{aligned} \quad (6.38)$$

To determine the growth of each χ -mode we require an estimate of Floquet's exponent associated with Eq. (6.37), which is again derived in Appendix C.2. For the $\ell = 1$ band, it is

given by

$$\mu_k \simeq \sqrt{\left(\frac{\theta_2}{2}\right)^2 \mp \frac{\theta_2 \theta_6^2}{32} \mp \left(\frac{\theta_2}{2}\right)^3 - (\theta_0^{1/2} - 1)^2} . \quad (6.39)$$

As above, the terms involving θ_6^2 and θ_2^3 can be neglected. The result is equivalent to a Mathieu's equation with coefficients A_k and q satisfying

$$A_k = \frac{4}{m^2} (k^2 + g^2 \sigma^2) \left(1 + \frac{3\zeta}{8}\right) \quad \text{and} \quad q = \theta_2 \simeq 4 \frac{g\sigma}{m} \frac{g\mathcal{A}}{m} \left(1 + \frac{21\zeta}{64}\right) \ll A_k . \quad (6.40)$$

Since q is much smaller than A_k , we expect resonance to be of the narrow-type, if it occurs at all. The first instability band occurs when $A_k = 1$ and is centred at momentum $k = k_1$, where

$$k_1 \simeq \frac{m}{2} \left(1 - \frac{3\zeta}{16}\right) , \quad (6.41)$$

which is shifted by $O(\zeta)$ in comparison with the canonical case.

Eqs. (6.33) and (6.41) show that the $\ell = 1$ resonance injects energy into a narrow band of modes with momenta $k \sim m$. Kofman, Linde & Starobinsky interpreted the narrowness of this resonance as a decay process in which a single inflaton particle of mass $\sim m$ decays continuously into two χ -particles with opposite momenta of magnitude $\sim k_1$ [236]. Our results are in agreement with their interpretation.

The width of the resonant band satisfies

$$\Delta k_1 \simeq 2m \frac{g\sigma}{m} \frac{g\mathcal{A}}{m} \left(1 + \frac{9\zeta}{64}\right) . \quad (6.42)$$

Using the appropriate limit of Eq. (6.39) to estimate μ_k , or applying Eq. (6.25), we conclude that there is a perturbative enhancement of preheating efficiency owing to the relativistic DBI correction. Near the centre of the $\ell = 1$ band, the χ -modes grow as

$$\delta \chi_k \sim \exp\{\mu_k|_{\max} z\} \sim \exp\left\{\frac{g_* \sigma}{m_*} \frac{g_* \mathcal{A}}{m_*} m_* t \left(1 + \frac{9\zeta}{64}\right)\right\} , \quad (6.43)$$

in which the growth rate is augmented with respect to the non-relativistic or canonical cases by an $O(\zeta)$ term. This agrees with our expectation that any change in the preheating process would have to be perturbative in ζ , by assumption.

6.3.5 Efficiency of narrow-resonance preheating

How efficient is the preheating mechanism described above? The resonances we have discussed are of narrow-type, and therefore occupation numbers grow only for a very limited range of momenta. This process is much less efficient than broad resonance, where a larger range of momenta experience growing occupation numbers.

Nevertheless, the rate of growth is exponential within the unstable bands, and therefore preheating by narrow resonance may still lead to an acceptably rapid conversion of inflaton modes into matter species. After some oscillations, gravitational redshift will cause modes of fixed comoving wavenumber to drift slowly through each unstable band, from ultraviolet to infrared. It follows that significant particle production will occur only when modes remain within an unstable band for sufficiently long and particle production is not diluted by the universe's expansion [241]. If wavenumbers move through the unstable bands too rapidly, then little stimulated emission occurs, and the resonance is washed out by the expansion of the universe. In this situation preheating is inefficient in repopulating the universe.

The arguments of Floquet's theory show that in each resonant band, the inflaton and matter fluctuations of wavenumber k grow like $\exp(\mu_k z)$. Let us focus on the broadest instability band, which corresponds to $\ell = 1$ and which will generally dominate the particle production. This band has width $\sim q$, so each wavenumber remains within the unstable band for a time of order q/H . The resonance will be stable against Hubble expansion if $(\mu_k z / \Delta t) q/H \gtrsim 1$. It follows that preheating will *efficiently* drain energy from the inflaton provided

$$\sqrt{\frac{2H}{m_*}} \gtrsim \frac{3\sigma}{8} .$$

For the matter field, preheating will operate in the cases $\sigma = 0$ and $\sigma \neq 0$ whenever

$$\sqrt{\frac{2H}{m_*}} \lesssim \frac{1}{4} \left(\frac{g_* \mathcal{A}}{m_*} \right)^2 \left(1 + \frac{13\sigma}{32} \right)$$

or

$$\sqrt{\frac{H}{m_*}} \lesssim 2 \left(\frac{g_* \sigma}{m_*} \right) \left(\frac{g_* \mathcal{A}}{m_*} \right) \left(1 + \frac{23\sigma}{64} \right),$$

apply, respectively. In the absence of knowledge of these parameters, we assume these conditions are verified.

6.4 Perturbative reheating in DBI inflation

The preheating process described and studied above is non-relativistic in nature and generates copious production of particles. While it occurs, it is still possible for perturbative processes to happen, by which the inflaton decays into matter species [276]. Indeed, these processes are necessary to thermalise the post-inflationary universe and bring reheating to an end. Ultimately they should take over the preheating era once this has become inefficient against Hubble expansion.

In the theories we have been considering, such decays are allowed by the symmetry-breaking potential studied in §6.3.4, where there is an effective trilinear interaction $g^2 \sigma \phi \chi^2$ which permits the decay $\phi \rightarrow \chi \chi$. The simple potential (6.15) allows only for two-body scattering. However, in the presence of an oscillating background field we can take the decay rate to be similar to that produced by the $g^2 \sigma \phi \chi$ interaction with $\sigma \sim \mathcal{A}$.

If the inflaton couples directly to the fermionic sector, then perturbative production can proceed via Yukawa interactions described by $h\phi\bar{\psi}\psi$, with ψ denoting the Dirac fermion and $\bar{\psi} = i\psi^\dagger\gamma^0$ its adjoint. In this case it is important to suppose that any interactions in which the inflaton participates are not sufficient to spoil the possibility of successful inflation.

In this section we will continue to assume that the inflaton mass is much larger than the

bare mass of χ , or the mass of any fermionic species where such couplings exist. Under these conditions, the tree-level decay rates for $\phi \rightarrow \chi\chi$ and $\phi \rightarrow \bar{\psi}\psi$ can be calculated straightforwardly. The necessary expressions were given in Kofman, Linde and Starobinsky's review³ [241]

$$\Gamma(\phi \rightarrow \chi\chi) = \frac{g_*^4 \sigma^2}{8\pi m_*} \quad \text{and} \quad \Gamma(\phi \rightarrow \bar{\psi}\psi) = \frac{h_*^2 m}{8\pi} , \quad (6.44)$$

where h_* is the measured Yukawa coupling, determined by matching Eq. (6.44) to observation.

Can perturbative decays compete with preheating? In one oscillation, we can estimate that perturbative decays populate the χ field occupation numbers at a rate Γ/m_* . In the same time interval preheating increases the population at a rate μ_k . We conclude that perturbative decays dominate preheating when

$$\Gamma \gtrsim m_* \mu_k . \quad (6.45)$$

Let us suppose Eq. (6.45) applies. These processes are comparatively slow and it is reasonable to assume that the decay products thermalise. This results in a transition to a radiation dominated universe and we can estimate the *reheating temperature*, T_R , to be [241]

$$T_R \simeq 0.2 \sqrt{\Gamma M_p} , \quad (6.46)$$

where Γ is the rate of the dominant decay channel.

Let us briefly recapitulate the rôle of perturbative processes in canonical inflation. Inflaton decays $\phi \rightarrow \chi\chi$ can become the dominant channel for inflaton decay only in the case of symmetry breaking, for which $\sigma \neq 0$, as illustrated in the interactions (6.17) [241]. These decays begin to dominate when the amplitude of inflaton oscillations has dropped to $\mathcal{A} \sim g_*^2 \sigma / 8\pi$. If we suppose that the curvature perturbation synthesized during the inflationary phase, denoted ζ , was dominated by fluctuations in the inflaton, then we must demand $m \sim 10^{-5} M_p$ enforced by agreement with observations. This, however, need not be the case. For

³Modifications to these rates and cross-sections to incorporate physical quantities in the DBI model are derived in Appendix C.1.

example, if ζ receives a dominant contribution from other sources, a wider range of masses m can be tolerated. Supposing further that the interaction coupling g_* is typically $g_* \sim 10^{-1}$, we find the reheating temperature is of order the symmetry breaking scale

$$T_R \sim \sigma . \quad (6.47)$$

If, on the other hand, the dominant decay is into fermions, then the Yukawa coupling must satisfy

$$h_*^2 \gtrsim 18\pi \left(\frac{g_* \mathcal{A}}{m_*} \right) \left(\frac{g_* \sigma}{m_*} \right) . \quad (6.48)$$

Suitable values for the inflaton mass m_* and couplings $\{g_*, h_*\}$ can be found so that this condition applies, but these choices are fundamentally model-dependent. As an example, if we assume $h_* \sim 10^{-1}$ and $m_* \sim 10^{-5} M_p$, we find the universe reheats at a temperature

$$T_R \simeq 1.3 \times 10^{-5} M_p \simeq 3.12 \times 10^{13} \text{ GeV} . \quad (6.49)$$

6.4.1 Estimates of reheating temperatures

This analysis can be applied to the production mechanisms of §§6.3.2–6.3.4. Let us work with the symmetry-breaking potential, $\sigma \neq 0$. Assuming a typical coupling $g_* \sim 1$, Eq. (6.45) implies that the $\phi \rightarrow \chi\chi$ decay dominates resonant production when the amplitude satisfies

$$\mathcal{A} \lesssim 4 \times 10^{-4} \sigma \left(1 - \frac{25\sigma}{64} \right) . \quad (6.50)$$

The resulting reheating temperature receives relativistic corrections in comparison with the temperature achieved using canonical kinetic terms. In particular, we find

$$T_R \simeq 0.13\sigma \left(1 - \frac{\sigma}{8} \right) . \quad (6.51)$$

Alternatively, decays into fermions will become predominant ($\phi \rightarrow \psi\bar{\psi}$) if the associated Yukawa coupling is sufficiently large. To be more precise the threshold is

$$h_*^2 \gtrsim 8\pi \left(\frac{g_*\sigma}{m_*} \right) \left(\frac{g_*\mathcal{A}}{m_*} \right) \left(1 + \frac{57\sigma}{64} \right) . \quad (6.52)$$

This is compatible with the conditions $g_*\mathcal{A}/m \ll g_*\sigma/m \ll 1$. In this case and for a representative value of the coupling, say $h_* \sim 0.1$, we find that

$$T_R \simeq 3.12 \times 10^{13} \left(1 - \frac{3\sigma}{8} \right) \text{ GeV} . \quad (6.53)$$

The estimates above should not be regarded as rigid predictions following a period of DBI inflation. Rather they are meant to be indicative of the differences with respect to an analogous reheating process after a period of canonical inflation.

6.5 Summary of results

In this short chapter, we have studied mechanisms by which the universe can be repopulated with matter species following an era of D-brane inflation. We work in the limit where the motion of the brane is, at most, perturbatively relativistic. This approximation explores the least phenomenologically interesting regime of DBI inflation, but might be ultimately required by observation if $f_{\text{NL}}^{(\text{equilateral})}$ is small. In our analysis, we assume the amplitude of oscillations of the D-brane as it settles towards the minimum of the potential is significantly smaller than whatever infrared scale caps the throat. The amplitude and phase of these oscillations are slightly modified in comparison with a scenario where inflation is driven by a canonically normalised scalar field.

We encounter some novel, though perturbative effects, which we list below.

- i. In the perturbatively-relativistic limit of DBI inflation, non-linearities arising from the action cause a weak resonance which reaches an $O(1)$ effect only after $\sim 1/\zeta$ oscillations.

This occurs both for inflaton and matter particles. In contrast, in canonical inflation, only matter preheating is possible. Excessive production of inflaton particles is problematic, but since preheating typically concludes after $\lesssim 10$ oscillations this weak resonance is unlikely to be fatal for the DBI model. In the ultra-relativistic limit where $\gamma \gg 1$, the potential becomes unimportant and resonance is dynamically suppressed. This disappointing conclusion has been confirmed in Ref. [277].

- ii. We identify an additional ‘DBI friction’ term in the equation of motion for the inflaton fluctuations, which competes within the first oscillations with the preheating effect.
- iii. We have estimated the final reheating temperature in these models and found these are typically smaller than in the equivalent theory with canonical kinetic terms. This may be beneficial in concrete models, where lower reheating temperatures can allow problems associated with overclosure of the universe by gravitinos to be ameliorated. The most stringent constraint on DBI models comes from observations of the microwave background bispectrum, which presently require $\gamma \lesssim 9$. If our results are representative, and the reheating temperature falls as γ increases, a constraint on γ may also emerge from demanding agreement with the Big Bang nucleosynthesis era, which requires $T_{\text{RH}} \gtrsim \text{MeV}$.

Anyway, I think that numbers are a problem in Astronomy, sizes and numbers. The best thing to do is to relax and enjoy the tininess of us and the enormity of the rest of the universe. Of course, if you are feeling depressed by that, you can always look out the other way and think how big you are compared to the atoms and the parts of atoms, and then you are the enormous universe to those atoms. So you can sort of stand in the middle and enjoy everything both ways.

Richard Feynman [Fun to Imagine, chapter 5 “Big numbers”, 1983]

7

Discussion

In this thesis we have discussed the early inflationary era driven by a single scalar field, and studied the preheating mechanism after a Dirac–Born–Infeld period of inflation. We will recapitulate in §7.1 the questions which motivated the writing up of this thesis, and in §7.2 we will summarise what we have learned in the process. Finally, we present in §7.3 a critical analysis of this work and suggest directions for further research.

7.1 Questions addressed in this thesis

To understand which microphysics describes the early universe is one of the greatest challenges in cosmology. Our only clues have been encoded in the CMBR almost 14 billion of years ago and are at present being mapped with high-sensitivity in sky surveys. This is the oldest exploration in science.

Inflation has become a popular framework which, together with quantum mechanics, explains how small inhomogeneities developed on a perfectly smooth background. A period of inflation during the early universe is a simple idea that ameliorates the problems with the standard cosmological model. In this thesis we have focused on inflation where only one scalar degree of freedom, called the inflaton ϕ , is active. As a result, the comoving perturbation ζ

synthesised during inflation in these models is only due to the quantum fluctuations of ϕ .

During inflation cosmological scales were pushed outside the particle horizon. An important difference between single and multi-field inflation models is that the primordial perturbation ζ does not evolve on super-horizon scales when only adiabatic modes are present. This implies that studying single-field inflation models is comparatively simpler.

The *Planck* satellite will soon be delivering data that it has been collecting since its launch, in 2009. The huge expectations created around *Planck* lie in its ability to make measurements with an unprecedented sensitivity. It might even exhaust the amount of information about the early universe dynamics one is able to extract from CMB observations. On the theory side, there has been a massive effort to understand the statistics of ζ . If the signal is (even slightly) non-gaussian, we might be able to use it to gain access to the microphysical Lagrangian which governed interactions in the early universe.

The eminent arrival of *Planck's* data poses at least two timely questions, which were the main motivation behind the first part of this thesis.

- i. We need to be prepared to use *Planck's* exquisite sensitivity to learn about inflation as much as we possibly can. Do we know what the error associated with the theoretical calculations of our models is?
- ii. A significant effort has been devoted over the last decade to obtain the bispectrum in several classes of single-field inflation models. Do we understand how to efficiently catalogue the single-field features imprinted in the CMBR?

As we have seen, the bispectrum of perturbations in single-field inflation is an incredibly intricate function of the underlying microphysics. By learning more about its structure and characteristics we are increasing our chances to use *Planck's* data more efficiently.

We also turned our attention to single-field models which do not evolve under the slow-roll regime. In particular, we set the task of obtaining the bispectrum signatures corresponding to models where slow-roll was not satisfied, yet allowing for a successful period of inflation and

producing agreement with observation.

In part II we considered the end stage of a Dirac–Born–Infeld inflation model. We wanted to understand how different the preheating mechanism would be compared to an analogous canonical model. The details of the generation of ζ largely decouple from the physics of preheating. Therefore, if a constraint arises from the preheating analysis, it could be used in conjunction with the constraints arising from the primordial density fluctuation.

As a result, one could use constraints arising from different, yet complementary sets of analysis. Ultimately, using constraints from the analysis of the bispectrum and preheating, together with observational data, the parameter space of these theories could become so severely fine-tuned, that it could prove those models highly unlikely.

7.2 Summary of the main results

This thesis is by no means the end of the story for single-field inflation. We hope, however, that it has taken small steps towards decoding the bispectrum in single-field inflation models. We list below a short summary of the main results reported in this thesis.

A universal action for perturbations.—In chapters 2 and 3 we have provided a full derivation of the cubic action for the primordial perturbation in single-field models, which is *exact* in the slow-roll approximation. We have shown it can be written in terms of only five *Horndeski* operators, whose coefficients are model-dependent.

Sizing the theory-error.—We have computed a more precise estimate of the magnitude of the bispectrum in the slow-roll regime which reduces the previous theory-error by several tens of percent. In DBI inflation for example, the uncertainty associated with previous estimates is reduced by more than 90%. This calculation was urgently required by the imminent arrival of *Planck*'s data, which is expected to have a sensitivity far superior to the precision of our previous estimates. In chapter 3 we have reported an analysis of the rescaled magnitude of the bispectrum, f_{NL} , which is valid at *next-order* in the slow-roll approximation.

We have applied our results to several classes of single-field models, and have specified f_{NL} for some common momenta configuration. We have concluded that the previous, leading-order results for f_{NL} , were unexpectedly much more precise than estimated. However, without performing the computation to next-order, it would not have been possible to specify the accuracy of the leading-order results.

The universe of shapes.—We started in chapter 4 by giving a full expression of the scale-dependence of the bispectrum. The remaining of that chapter was devoted to a thorough analysis of the shapes associated with each Horndeski operator at leading and next-order in slow-roll. We have rediscovered an exotic shape which had previously appeared in a class of higher-derivative galileon theories. This shape *did not* correlate with any existing bispectrum templates in CMB analysis. We found that this shape can actually be constructed out of a linear combination of equilateral shapes, provided we are prepared to tolerate some serious fine-tuning. The recurrence of this shape raised two fundamental problems. First, why was this shape appearing in so many distinct microphysics scenarios? Second, if the presence of this shape could not be used as a diagnostic tool, then how could we use the bispectrum shape as a discriminant between models?

These questions motivated a modal decomposition of the bispectrum, which revealed that on a particularly useful basis, the usual templates could be well described by the first few modes. By requiring orthogonality with the templates, one was in fact enhancing the subsequent higher-order modes, which caused the drumlin-like features in the exotic shape. We have learned that from a harmonic decomposition of the bispectrum, one is able to derive consistency relations between the amplitudes of each fundamental mode. Relations which are *observables in terms of observables* are particularly powerful in ruling out models, since they are independent of the parametrisation of the theory. We have specified these relations for DBI and k -inflation scenarios.

Beyond the slow-roll approximation.—In chapter 5 we have abandoned the requirement of slow-roll inflation. We have rather focused on the bispectrum phenomenology of single-field

models which predict an almost scale-invariant spectrum, whilst allowing for some breaking of the slow-roll approximation. The results of this chapter rely on the scale-invariant approximation, which can be regarded as a resummation technique of the slow-roll analysis in the parameter space compatible with a scale-invariant two-point function.

We have found that the resulting bispectrum is strongly scale-dependent, and correctly reproduces the logarithmic dependence obtained in chapter 3 taking the slow-roll limit. We have argued that because of this string scale-dependence, these models are more vulnerable to data constraints arising from different scales (CMB and LSS).

Preheating after DBI inflation.—In the last chapter we have studied the preheating stage after a period of Dirac–Born–Infeld inflation. We have focused on the main differences between the resonances in particle production compared to similar canonical models, and considered the non-relativistic regime of DBI, when preheating can occur. We have found that preheating is perturbatively more efficient in these scenarios, and that it allows for production of inflaton particles. This is a novel feature which does not find an analogue in canonical models where only matter preheating takes place. We have also estimated the reheating temperature in these models, and found it is slightly lower than in their canonical counterparts.

7.3 Outlook

Figure 7.1 is intended to roughly summarise some important advances in theoretical cosmology (it is not to scale). The lower part of the cartogram zooms in some significant developments regarding inflation and the early universe over the last decade. The round rectangular shapes have width which is proportional to the number of scientific papers whose topic is centred on non-gaussianities. In the last two years, the scientific production in this area has been greater than that from 2000 to 2006. This remarkable effort in attempting to understand the microphysics governing the early universe cannot be ignored. It is likely that further investigation will follow the tendency in the last decade, and there is indeed much to be done.

Relevant historical developments in Cosmology at a glance

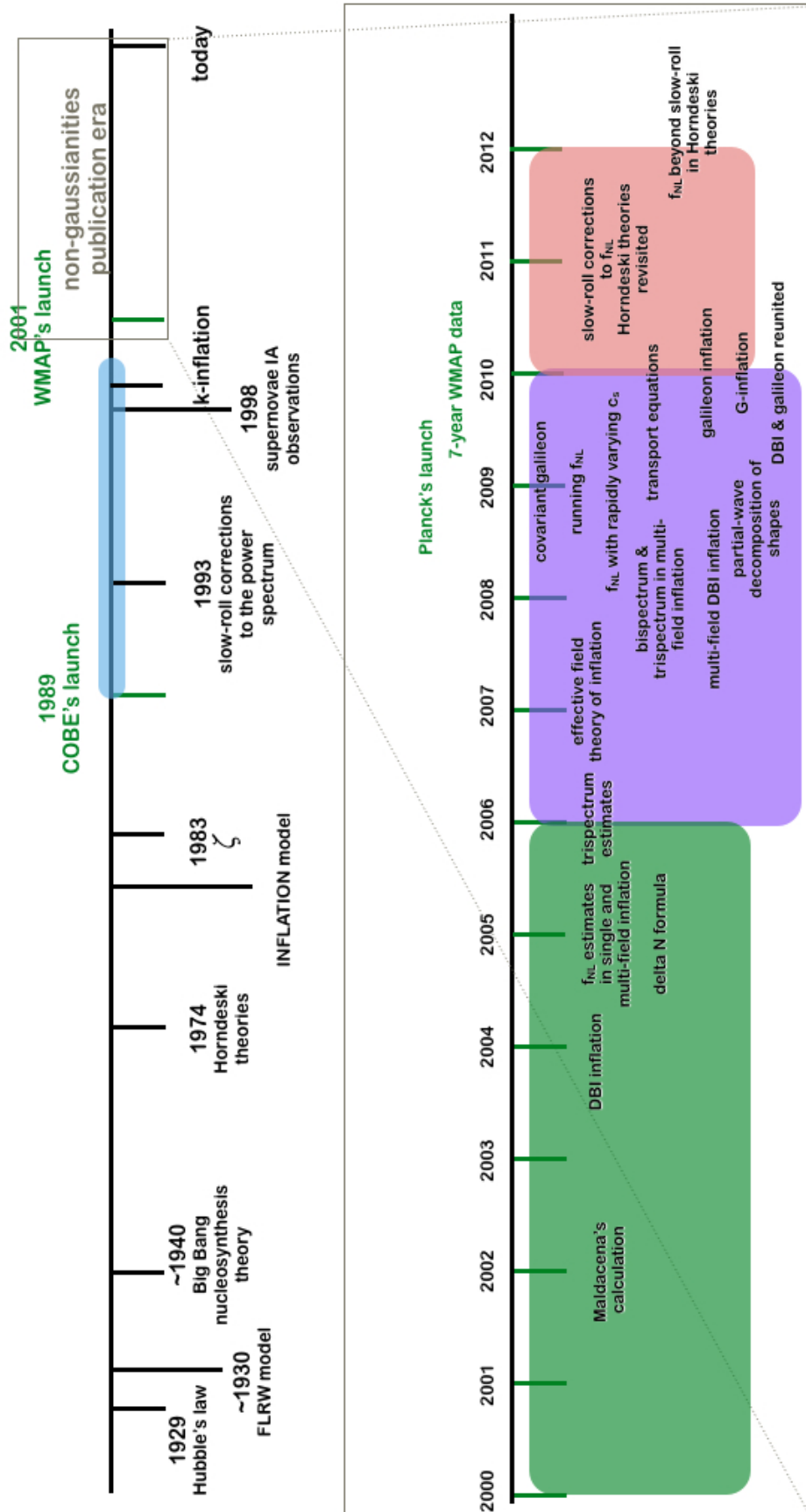


Figure 7.1: Cartogram of significant developments in early universe theoretical cosmology roughly over the last 100 years.

In chapter 4 we have obtained consistency relations between the amplitudes of each bispectrum harmonic, β_n , in two different models. For simplicity, our analysis assumed an almost scale-invariant bispectrum and applied to the primordial bispectrum. For a rigorous comparison to data which is likely to be necessary given the unprecedented sensitivity offered by *Planck*, an improved analysis must be performed. On the one hand, the choice of basis should be suitable for a bispectrum which is not perfectly scale-invariant. In particular the CMB bispectrum shapes should be integrated over some range of cosmologically relevant scales, and this has been neglected in our analysis. In that case, our choice of basis is weak. On the other hand, we inevitably need to evolve the primordial bispectrum we have calculated to become the late-time, CMB bispectrum, which is visible in the data. Conversely, one can use *Planck*'s data and evolve it backwards to obtain the primitive bispectrum, to which our formulae apply.

In chapter 5 we have obtained the bispectrum in single-field inflation theories without invoking the slow-roll approximation. We have observed the bispectrum exhibits a strong scale-dependence, but we have left the study of shapes for future work. It would be extremely interesting to investigate the correlation between the slow-roll approximation and the bispectrum shapes. Are the shapes similar to the ones found before and well approximated by the common templates? What would the modal decomposition reveal?

In this thesis we have largely ignored the progress that has been made on multi-field theories. In these, more than one scalar field is active during inflation, and isocurvature modes are not generally suppressed as a result. Obtaining theoretical predictions in these models is therefore rather challenging. For example, the amplitude of the bispectrum f_{NL} can vary significantly until the modes are frozen upon horizon re-entry (see, for example, Ref. [278]). Numerical tools such as δN [57], transfer matrices [279], and the moment transport equations [138, 139] have been applied to obtain the evolution of the correlation functions in these models. In multi-field models it is helpful to improve our description of the inflationary trajectory in field configuration space, and introduce the concept of *bundle* of trajectories. This concept can help us relate a dramatic change in the magnitude of f_{NL} close to a focusing region

of trajectories. f_{NL} will evolve until all isocurvature modes have decayed and ζ has become constant—we say the *adiabatic limit* has been reached [278].

If *Planck* rules out single-field inflation, this opens up an opportunity to develop models which are not as simple: multiple fields allow for a much richer dynamics and can be in agreement with the observational data. In particular, most of the work on multi-field inflation under the slow-roll approximation so far has focused on models where the fields have canonical kinetic terms (see Refs. [280, 141] for a small sample of these works). It is important to extend these studies to models which contain non-canonical fields and understand the dynamics of inflation [94, 89, 90]. Also relevant is to study the multi-field dynamics when some of the slow-roll parameters become temporarily large, making the slow-roll approximation invalid. Some works have performed an analysis which is higher-order in slow-roll [220]. However, it is likely that more sophisticated techniques are required to describe the evolution of the multi-field system over the course of several e-folds without imposing slow-roll (see, for example, Ref. [99]).

This journey planner can suggest some of the near-future challenges, but it is hard to gauge the precise direction research will take. It will inevitably aim at some of our most elementary questions. Is inflation more than just a good theory? Did it really happen? If so, what is the physical microscopical Lagrangian describing these early times? Understanding inflation may require setting it up in a string theory, but that is a different story. In any case, we can anticipate that with the arrival of *Planck's* data we will be closer to understanding our early universe.

“Abre essa janela! Desvia-me a cortina!
Eu gosto de ver as nuvens...
E o céu azul sobre os horizontes.
Gosto de contemplar os vales e os montes!
E também as fontes de água pura e cristalina!
Gosto de sentir a brisa!
Sentir o pulsar da Natureza e tudo o que se preza!...”

*[“Open that window! Divert me the curtain!
I like to see the clouds ...
And the blue sky on the horizon.
I like to contemplate the valleys and the hills!
And also the fountains of pure crystal water!
I like to feel the breeze!
To feel the pulse of Nature and all that cherishes!...”]*

Joaquim Henriques, unpublished work

Appendices

Algebra is generous: she often gives more than is asked for.

Jean d'Alembert

A

The slow-variation approximation

This appendix contains helpful material related to chapters 2 and 3.

A.1 Propagator corrections

At leading-order, the wavefunctions can be obtained from Eq. (2.23) by setting all slow-variation parameters to zero. Choosing a reference scale k_* , this yields the standard result

$$\zeta_k(\tau) = i \frac{H_*}{2\sqrt{z_*}} \frac{1}{(kc_{s*})^{3/2}} (1 - ikc_{s*}\tau) e^{ikc_{s*}\tau} . \quad (\text{A.1})$$

Next-order corrections to the propagator were discussed by Stewart & Lyth [102], who quoted their result in terms of special functions and expanded uniformly to next-order after taking a late-time limit. The uniform next-order expansion at a generic time was given by Gong & Stewart [104] for canonical models, and by Chen et al. [45] in the non-canonical case. Their result was cast in a more convenient form in Ref. [28] whose argument we briefly review.

The next-order correction is obtained after systematic expansion of each quantity in Eq. (2.23) to linear order in the slow-variation parameters. Contributions arise from each time-dependent factor and from the order of the Hankel function. Collecting the formulae quoted

in Ref. [45], one finds

$$\left. \frac{\partial H_v^{(2)}(x)}{\partial v} \right|_{v=\frac{3}{2}} = -\frac{i}{x^{3/2}} \sqrt{\frac{2}{\pi}} \left\{ e^{ix}(1-ix)\text{Ei}(-2ix) - 2e^{-ix} - i\frac{\pi}{2}e^{-ix}(1+ix) \right\}, \quad (\text{A.2})$$

where $\text{Ei}(x)$ is the exponential integral,

$$\text{Ei}(x) = \int_{-\infty}^x \frac{e^t}{t} dt \quad \text{if } x \in \mathbb{R}. \quad (\text{A.3})$$

This is well-defined for $x < 0$. For $x \geq 0$ it should be understood as a Cauchy principal value. For complex argument—required by (A.2)—one promotes Eq. (A.3) to a contour integral, taken on a path running between $t = x \in \mathbb{C}$ and $|t| \rightarrow \infty$ in the half-plane $\text{Re}(t) < 0$. Using Cauchy's theorem to rotate this contour onto the negative real t -axis, one finds

$$\text{Ei}(2ikc_s\tau) = \lim_{\epsilon \rightarrow 0} \int_{-\infty(1+i\epsilon)}^{\tau} \frac{d\xi}{\xi} e^{2ikc_s\xi}. \quad (\text{A.4})$$

The next-order correction to (A.1), expanded uniformly to $O(\epsilon)$ in slow-variation parameters but including the *exact* time-dependence, is therefore

$$\begin{aligned} \delta\zeta_k(\tau) = & \frac{iH_\star}{2\sqrt{z_\star}(kc_{s\star})^{3/2}} \left\{ -\varpi_\star e^{-ikc_{s\star}\tau} (1 + ikc_{s\star}\tau) \int_{-\infty(1+i\epsilon)}^{\tau} \frac{d\xi}{\xi} e^{2ikc_{s\star}\xi} \right. \\ & \left. + e^{ikc_{s\star}\tau} \left[\mu_{0\star} + i\mu_{1\star}kc_{s\star}\tau + s_\star k^2 c_{s\star}^2 \tau^2 + \Delta N_\star (\varpi_\star - i\varpi_\star kc_{s\star}\tau - s_\star k^2 c_{s\star}^2 \tau^2) \right] \right\}, \end{aligned} \quad (\text{A.5})$$

where

$$\mu_0 \equiv \epsilon + \nu + 2s + i\frac{\pi}{2}\varpi \quad \text{and} \quad \mu_1 \equiv \epsilon + s - i\frac{\pi}{2}\varpi, \quad (\text{A.6})$$

and quantities labelled ' \star ' are evaluated at the horizon-crossing time for the reference scale k_\star . We have used ΔN_\star to denote the number of e-folds which have elapsed since this time, so $\Delta N_\star = \ln|k_\star c_{s\star}\tau|$. The limit $\epsilon \rightarrow 0$ should be understood after the integration has been

performed and merely guarantees convergence as $\xi \rightarrow -\infty$. Eq. (A.5) is *exact* in powers of $k\tau$. Although terms of high-order in $k\tau$ become increasingly irrelevant as $|k\tau| \rightarrow \infty$, all such terms make comparable contributions to a generic n -point function at the time of horizon crossing, when $|k\tau| \sim 1$, and must not be discarded. This reflects interference effects between the growing and decaying modes at horizon exit.

To evaluate the cubic action (3.3) we will require the time-derivative $\delta\zeta'_k$. Using the identity $\mu_0 + \mu_1 - 2\varpi_1 = 0$, it follows that

$$\delta\zeta'_k(\tau) = \frac{iH_*(kc_{s*})^{1/2}}{2\sqrt{z_*}} \tau \left\{ -\varpi_{1*} e^{-ikc_{s*}\tau} \int_{-\infty(1+i\epsilon)}^{\tau} \frac{d\xi}{\xi} e^{2ikc_{s*}\xi} + e^{ikc_{s*}\tau} \left[s_* - \mu_{1*} + is_* kc_{s*} \tau + \Delta N_* (\varpi_{1*} - 2s_* - is_* kc_{s*} \tau) \right] \right\}. \quad (\text{A.7})$$

For the power spectrum to be conserved on super-horizon scales, $\delta\zeta_k \rightarrow \text{constant}$ and $\delta\zeta'_k \rightarrow 0$ as $|k\tau| \rightarrow 0$. The explicitly time-dependent term ΔN_* apparently spoils this behaviour, but is compensated by a logarithmic divergence from the integral in (A.7), and for $\tau \rightarrow 0$ one finds

$$\int_{-\infty(1+i\epsilon)}^{\tau} \frac{d\xi}{\xi} e^{2ikc_{s*}\xi} = \ln |2ikc_{s*}\tau| + O(kc_{s*}\tau). \quad (\text{A.8})$$

This precisely cancels the time-dependence arising from ΔN_* . Note the incomplete cancellation of the logarithm, which leaves a residual of the form $\varpi_* \ln 2$ and is the origin of the $\ln 2$ term in the Stewart–Lyth constant $C = -2 + \ln 2 + \gamma_E$ [102, 106]. This is similar to what happens to the residual $\ln k_i/k_t$ and $\ln k_t/k_*$ terms after cancellation of the $\ln \tau$ logarithms in the three-point function.

A.2 Integrals involving the exponential integral function, $\text{Ei}(z)$

The principal obstruction to evaluation of the next-order corrections using standard methods is the Ei-term in Eq. (A.5). This can not be expressed directly in terms of elementary functions whose integrals can be computed in closed form. It was explained in Appendix A.1 that

although $\text{Ei}(2ik_3c_s\tau)$ contains terms of higher-orders in $k\tau$ which become increasingly irrelevant as $|k\tau| \rightarrow 0$, these cannot usually be neglected when computing n -point functions. The integrals we require are of the form [28]

$$I_m(k_3) = \int_{-\infty}^{\tau} d\zeta \zeta^m e^{i(k_1+k_2-k_3)c_s\zeta} \int_{-\infty}^{\zeta} \frac{d\xi}{\xi} e^{2ik_3c_s\xi} . \quad (\text{A.9})$$

We are again using the convention that, although I_m depends on all three k_i , only the asymmetric momentum is written explicitly. In the following discussion we specialize to I_0 . Results for arbitrary m can be obtained similarly and are given in Ref. [28].

We introduce the dimensionless combinations

$$\vartheta_3 = 1 - \frac{2k_3}{k_t} \quad \text{and} \quad \theta_3 = \frac{k_3}{k_t - 2k_3} = \frac{1 - \vartheta_3}{2\vartheta_3} , \quad (\text{A.10})$$

and perform a contour rotation to express I_0 in terms of ϑ_3 and θ_3 [28]

$$I_0(k_3) = -\frac{i}{\vartheta_3 k_t c_s} \int_0^{\infty} du e^{-u} \int_{\infty}^{\theta_3 u} \frac{dv}{v} e^{-2v} . \quad (\text{A.11})$$

The v -integral has a series representation

$$\int_{\infty}^{\theta_3 u} \frac{dv}{v} e^{-2v} = \gamma_E + \ln(2\theta_3 u) + \sum_{n=1}^{\infty} \frac{(-2\theta_3 u)^n}{n!n} \quad (\text{A.12})$$

where the sum converges uniformly for all complex $\theta_3 u$. The right-hand side has a singularity at $\theta_3 u = 0$, and the logarithm generates a branch cut along the negative real axis. The u -independent term γ_E is the Euler–Mascheroni constant $\gamma_E \equiv \int_{\infty}^0 e^{-x} \ln x dx$ and is obtained by expanding e^{-2v} in series, integrating term-by-term, and matching the undetermined constant of integration with the left-hand side of (A.12) in the limit $u \rightarrow 0$. It follows that [28]

$$I_0(k_3) = -\frac{i}{\vartheta_3 k_t c_s} \left[\ln(2\theta_3) + \sum_{n=1}^{\infty} \frac{(-2\theta_3)^n}{n} \right] . \quad (\text{A.13})$$

This is singular when $\vartheta_3 \rightarrow 0$, which is the squeezed limit where either k_1 or $k_2 \rightarrow 0$. There is nothing unphysical about this arrangement of momenta, for which $\theta_3 \rightarrow \infty$, but $I_0(k_3)$ will be power-law divergent unless the bracket $[\dots]$ vanishes sufficiently rapidly in the same limit.

The sum above is absolutely convergent if $-1/2 < \text{Re}(\theta_3) < 1/2$, corresponding to the narrow physical region $0 < k_3 < k_t/4$ where k_3 is being squeezed. For θ_3 satisfying this condition the summation can be performed explicitly, yielding $\ln(1 + 2\theta_3)^{-1} = \ln \vartheta_3$. It can be verified that $I_0(k_3)$ is analytic in the half-plane $\text{Re}(\theta_3) > 0$. Therefore it is possible to analytically continue to $\theta_3 \geq 1/2$, allowing the behaviour as $\theta_3 \rightarrow \infty$ and $\vartheta_3 \rightarrow 0$ to be studied. We find

$$I_0(k_3) = -\frac{i}{\vartheta_3 k_t c_s} \ln(1 - \vartheta_3) \equiv -\frac{i}{k_t c_s} J_0(k_3) . \quad (\text{A.14})$$

It is more convenient to express our final bispectra in terms of J_0 rather than I_0 . In the limit $\vartheta_3 \rightarrow 0$, Eq. (A.14) is finite with $J_0 \rightarrow -1$. The $\theta_3 \rightarrow \infty$ behaviour of the sum has subtracted both the power-law divergence of the prefactor and the logarithmic divergence of $\ln(2\theta_3)$. Had we truncated the $k_3 c_s \zeta$ -dependence of Eq. (A.9), or equivalently the $\theta_3 u$ -dependence of Eq. (A.12), and we would have encountered a spurious divergence in the squeezed limit and a misleading prediction of a strong signal in the local mode. Several of our predictions, including recovery of Maldacena's limit described by Eq. (3.15), depend on the precise numerical value of J_0 as $\theta_3 \rightarrow \infty$ and therefore constitute tests of this procedure.

We can now evaluate $I_m(k_3)$ for arbitrary m , although only the cases $m \leq 2$ are required for the calculation presented in the main text. The necessary expressions are

$$I_1(k_3) = \frac{1}{(\vartheta_3 k_t c_s)^2} [\vartheta_3 + \ln(1 - \vartheta_3)] \equiv \frac{1}{(k_t c_s)^2} J_1(k_3) \quad (\text{A.15a})$$

$$I_2(k_3) = \frac{i}{(\vartheta_3 k_t c_s)^3} [\vartheta_3(2 + \vartheta_3) + 2 \ln(1 - \vartheta_3)] \equiv \frac{i}{(k_t c_s)^3} J_2(k_3) . \quad (\text{A.15b})$$

In the squeezed limit when $\vartheta_3 \rightarrow 0$ one can verify that $J_1 \rightarrow -1/2$ and $J_2 \rightarrow -2/3$.

A.3 Useful integrals

To simplify evaluation of the integrals arising in the calculation of the bispectrum, we introduce a master integral, \mathcal{J}_* , for which the integrals of interest are special cases [28]. We define

$$\mathcal{J}_* = i \int_{-\infty}^{\tau} d\xi e^{ik_t c_{s^*} \xi} \left\{ \gamma_0 + i\gamma_1 c_{s^*} \xi + \gamma_2 c_{s^*}^2 \xi^2 + i\gamma_3 c_{s^*}^3 \xi^3 + \gamma_4 c_{s^*}^4 \xi^4 \right. \\ \left. + N_* \left(\delta_0 + i\delta_1 c_{s^*} \xi + \delta_2 c_{s^*}^2 \xi^2 + i\delta_3 c_{s^*}^3 \xi^3 + \delta_4 c_{s^*}^4 \xi^4 \right) \right\}, \quad (\text{A.16})$$

where $N_* = \ln |k_* c_{s^*} \xi|$. Eq. (A.16) is an oscillatory integral, for which asymptotic techniques are well-developed, and which can be evaluated using repeated integration by parts. To evaluate the N_* -dependent terms one requires the standard integral

$$\lim_{\tau \rightarrow 0} \int_{-\infty}^{\tau} d\xi N_* e^{ik_t c_{s^*} \xi} = \frac{i}{k_t c_{s^*}} \left(\gamma_E + i\frac{\pi}{2} \right). \quad (\text{A.17})$$

We conclude

$$\mathcal{J}_* = \frac{1}{k_t c_{s^*}} \left\{ \gamma_0 - \frac{\gamma_1 + \delta_1}{k_t} - \frac{2\gamma_2 + 3\delta_2}{k_t^2} + \frac{6\gamma_3 + 11\delta_3}{k_t^3} + \frac{24\gamma_4 + 50\delta_4}{k_t^4} \right. \\ \left. - \left(\gamma_E + \ln \frac{k_t}{k_*} + i\frac{\pi}{2} \right) \left(\delta_0 - \frac{\delta_1}{k_t} - 2\frac{\delta_2}{k_t^2} + 6\frac{\delta_3}{k_t^3} + 24\frac{\delta_4}{k_t^4} \right) \right\}. \quad (\text{A.18})$$

We use this result repeatedly in §3.2 to evaluate integrals in closed form.

B

Steps beyond exact scale-invariance

In this appendix we include some details of the calculation described in chapter 5. Some of the material is similar to that discussed in appendix A. Nevertheless we include it here for completeness, since the choice of time coordinates is different.

B.1 Dynamics in y —why?

In this appendix we motivate the use of the time-coordinate y instead of the conformal time variable, τ . Why is this choice of space-time foliation, which defines a hypersurface at each $y = \text{constant}$, preferred compared to the more traditional conformal time? Were we to solve for the perturbations starting from Eq. (5.2) in τ coordinates, we would obtain a formula for the propagator for scalar perturbations, G_k , which corresponds to the two-point correlator:

$$\langle \zeta(\mathbf{x}, \tau) \zeta(\mathbf{y}, \tilde{\tau}) \rangle = G(\mathbf{x}, \tau; \mathbf{y}, \tilde{\tau}) \quad (\text{B.1})$$

We would proceed to solve the Green's function equation for the propagator, in Fourier

space, which reads

$$\left\{ \frac{d^2}{d\tau^2} + \left(\frac{1}{z} \frac{dz}{d\tau} + \frac{2}{a} \frac{da}{d\tau} \right) \frac{d}{d\tau} + k^2 c_s^2 \right\} G_k(\tau; \tilde{\tau}) = -\frac{i}{2a^2 z} \delta(\tau - \tilde{\tau}) , \quad (\text{B.2})$$

where k is the comoving wavenumber and the Dirac delta enforces evaluation at $\tau = \tilde{\tau}$. Because scalar fluctuations will propagate at a phase velocity c_s generically different from that of the light, one usually performs a change of variables, $z = -kc_s\tau$, so that the propagator is a function of the sound horizon. To get the equation for the evolution of G_k in z would demand inverting $dz/d\tau$, which without the premiss of working with perturbative s becomes algebraically challenging when plugging into the equations of motion since a Taylor expansion could not be truncated. In particular, it would be very hard to show that the propagator is explicitly symmetric under the interchange $\tau \leftrightarrow \tilde{\tau}$.

It turns out that expressing the y -evolution of background quantities allows to naturally accommodate a rapidly changing c_s , and therefore large s , avoiding the difficulty just described. In other words, the y variable allows to sum all the powers in s .

Moreover, writing the quadratic action for the fluctuations in the form (5.3) makes the reproduction of Bessel's equation more transparent, without any need for perturbative expansions. For these reasons, our dynamical analysis is presented in y -time, and follows the analysis of Khoury & Piazza [174].

B.2 The spectral index beyond exact scale-invariance

In chapter 5 we use $n_s - 1$ as a perturbative parameter, but never its explicit formula, since it is not necessary throughout the calculation. We have surpassed the need to know this because of the special properties of the two-point correlator of single-field models, in particular that it should be time-independent on super-horizon scales. Here we present the formula for $n_s - 1$ for completeness. In the action (5.3) the variable $q = a\sqrt{zc_s}$ obeys the following differential

equation

$$\frac{d \ln q}{d \ln y} = -\frac{1}{1-\varepsilon-s} \left[1 + \frac{w}{2} + \frac{s}{2} \right] \left[1 + \frac{\varepsilon\eta + ts}{(1-\varepsilon-s)^2} \right],$$

which implies

$$\frac{q''}{q} = \frac{1}{2y^2} \frac{\rho}{1-\varepsilon-s} + \frac{1}{2y^2} \frac{1}{(1-\varepsilon-s)^2} \left[\frac{\rho^2}{2} + wx + ts + \frac{\varepsilon\eta + ts}{(1-\varepsilon-s)^2} \rho(4-2\varepsilon-s+w) \right], \quad (\text{B.3})$$

where $\rho \equiv 2 + w + s$ and $x \equiv d \ln w / dN$ (which contributes at next-order only in the scale-invariant approximation). We conclude that the spectral index in these theories satisfies

$$n_s - 1 = 3 - \sqrt{1 + \frac{2\rho}{1-\varepsilon-s} + \frac{2}{(1-\varepsilon-s)^2} \left[\frac{\rho^2}{2} + wx + ts + \frac{\rho(\varepsilon\eta + ts)}{(1-\varepsilon-s)^2} (4-2\varepsilon-s+w) \right]}. \quad (\text{B.4})$$

To leading-order in the scale-invariant approximation, we find

$$n_s - 1 = \frac{-2\varepsilon - 3s - w}{1-\varepsilon-s}, \quad (\text{B.5})$$

in agreement with the result from table 2.1. If we instead assume that ε and s are strictly constant and consider only $P(X, \phi)$ models, we recover the formula deduced in Ref. [174] that

$$n_s - 1 = -\frac{2\varepsilon + s}{1-\varepsilon-s}, \quad (\text{B.6})$$

which reproduces the exact scale-invariance relation $s = -2\varepsilon$. In the slow-roll approximation this reduces to

$$n_s - 1 \simeq -2\varepsilon - s \quad (\text{B.7})$$

at leading-order, which again agrees with the results from table 2.1.

In the scale-invariant approximation scheme, δ is a next-order quantity defined by $\delta = s + 2\varepsilon$, in $P(X, \phi)$ models. The general formula for δ in a generic Horndeski model will

depend on the form of w , and therefore x . Using (B.4) we conclude that

$$n_s - 1 = -\frac{\eta + \delta}{1 + \varepsilon} - \frac{2}{3(1 + \varepsilon)^2} \left\{ 2\varepsilon x + 4(\varepsilon\eta + ts) - \varepsilon t \right\}. \quad (\text{B.8})$$

This formula agrees with our expectation that δ is indeed a parameter contributing at next-order only.

B.3 Next-order corrections—useful formulae

When applying the Schwinger-Keldysh formalism we will summon formulae for the corrections of the elementary wavefunctions for ζ at next-order in scale-invariance. This is because one should perform a uniform expansion in the slow-variation parameters which include the interaction vertices, but also the propagator for scalar perturbations. In this appendix we collect some of the necessary formulae for this expansion.

Background evolution.—As explained in the main text, we wish to study the evolution of the background quantities in the time coordinate y . To do so, we make a Taylor expansion around the time y of horizon crossing of some reference scale k_* and make a uniform expansion for small η_* and t_* . Such expansion is well defined provided we restrict our analysis to a few e-folds after horizon crossing. This ensures that ε and s have not varied significantly up to that point, such that we can treat η and t as perturbative parameters in the dynamics. As justified in the main text, this is indeed a good approximation.

To get the y -evolution of the speed of sound, c_s , we start by evaluating

$$\frac{d \ln c_s}{d \ln(-k_* y)} = -\frac{s_*}{1 - \varepsilon_* - s_*} \left\{ 1 + \frac{\varepsilon_* \eta_* + t_* s_*}{(1 - \varepsilon_* - s_*)^2} - \left[\frac{t_*}{1 - \varepsilon_* - s_*} + \frac{\varepsilon_* \eta_* + t_* s_*}{(1 - \varepsilon_* - s_*)^2} \right] \ln(-k_* y) \right\}. \quad (\text{B.9})$$

To avoid cluttering the notation, we introduce the following parameters which contribute at

next-order only in scale-invariance:

$$\alpha = \frac{t}{1 - \varepsilon - s} + \frac{\varepsilon\eta + ts}{(1 - \varepsilon - s)^2} \quad (\text{B.10a})$$

$$\beta = \frac{\varepsilon\eta + ts}{(1 - \varepsilon - s)^2} . \quad (\text{B.10b})$$

Upon integration, we find

$$c_s = c_{s_*} (-k_* y)^{-\frac{s_*}{1 - \varepsilon_* - s_*}} \left\{ 1 - \frac{s_*}{1 - \varepsilon_* - s_*} \left[\beta_* \ln(-k_* y) - \frac{\alpha_*}{2} (\ln(-k_* y))^2 \right] \right\} . \quad (\text{B.11})$$

This simplifies if we write $s_* = -2\varepsilon_* + \delta_*$ and work perturbatively in δ_* [that is, assuming $O(\delta_*) = O(\eta_*) = O(t_*)$], as follows

$$c_s = c_{s_*} (-k_* y)^{\frac{2\varepsilon_*}{1 + \varepsilon_*}} \left\{ 1 + \frac{2\varepsilon_*}{1 + \varepsilon_*} \left[\beta_* + \frac{\delta_*(\varepsilon_* - 1)}{2\varepsilon_*(1 + \varepsilon_*)} \right] \ln(-k_* y) - \frac{\alpha_*\varepsilon_*}{1 + \varepsilon_*} (\ln(-k_* y))^2 \right\} . \quad (\text{B.12})$$

In the limit when ε and s are both strictly constant, $\alpha_* = 0 = \beta_*$, and we reproduce the results of Ref. [174]:

$$c_s \sim (-k_* y)^{-\frac{s_*}{1 - \varepsilon_* - s_*}} ,$$

where we have temporarily restored the dependence in s through δ . The additional contributions appearing in Eq. (B.12) are precisely the corrections to this purely power-law behaviour and are relevant whenever ε and s are slowly-varying.

Proceeding similarly to get the dynamical evolution of the Hubble parameter, we obtain

$$H = H_* (-k_* y)^{\frac{\varepsilon_*}{1 - \varepsilon_* - s_*}} \left\{ 1 + \frac{\varepsilon_*}{1 - \varepsilon_* - s_*} \left[\beta_* \ln(-k_* y) - \frac{\alpha_*}{2} (\ln(-k_* y))^2 \right] \right\} , \quad (\text{B.13})$$

which in the limit of constant ε and s reduces to simply

$$H \sim (-k_* y)^{\frac{\varepsilon_*}{1 - \varepsilon_* - s_*}} .$$

Again, recasting this result in terms of only one non-perturbative parameter, we find

$$H = H_*(-k_*y)^{\frac{\varepsilon_*}{1+\varepsilon_*}} \left\{ 1 + \frac{\varepsilon_*}{1+\varepsilon_*} \left[\left(\beta_* + \frac{\delta_*}{1+\varepsilon_*} \right) \ln(-k_*y) - \frac{\alpha_*}{2} (\ln(-k_*y))^2 \right] \right\}. \quad (\text{B.14})$$

The explicit formulae in Eqs. (B.12) and (B.14) are relevant when replacing in Eq. (5.7) for the scale factor, $a(y)$.

Derivatives of the elementary wavefunctions.—When calculating the bispectra of Horndeski operators which are at least once y -differentiated, we will require the derivatives of the elementary wavefunctions. We find

$$\frac{d}{dy} \zeta_k^{(\text{background})} = \frac{iH_*(1+\varepsilon_*)}{2\sqrt{z_*}(kc_{s*})^{3/2}} k^2 y e^{iky}, \quad (\text{B.15})$$

whereas the wavefunction corrections to the internal lines of the Feynman diagram obey

$$\begin{aligned} \frac{d}{dy} \delta \zeta_k^{(\text{internal})} = \frac{iH_*(1+\varepsilon_*)}{2\sqrt{z_*}(kc_{s*})^{3/2}} k^2 (-y) & \left\{ -\frac{n_s-1}{2} e^{-iky} \int_{-\infty}^y \frac{e^{2ik\xi}}{\xi} d\xi \right. \\ & \left. + e^{iky} \left[\frac{\delta_*}{1+\varepsilon_*} - \frac{\varepsilon_* \eta_*}{(1+\varepsilon_*)^2} + i\frac{\pi}{4}(n_s-1) + \frac{n_s-1}{2} \ln(-k_*y) \right] \right\}. \end{aligned} \quad (\text{B.16})$$

To obtain these we have explicitly eliminated the non-perturbative dependence in the variation of the speed of sound, parametrised by s , in favour of the perturbative parameter, δ .

The time variation of the wavefunctions is relevant in correctly reproducing the time-independence of the correlation functions for ζ .

B.4 Useful integrals

In this appendix we list the integrals which occur when computing the three-point correlators. They fall in essentially two different varieties: integrals involving the exponential integral function (which first appeared in Eq. (5.18)) and those which involve power-laws and loga-

rithmic integrand functions. We will identify master integrals for each of these families and analyse them separately. This section generalises the results obtained in §A.2.

B.4.1 Integrals involving the exponential integral function, $\text{Ei}(\xi)$

These integrals appear in the form

$$I_\gamma(k_3) \equiv \int_{-\infty}^0 dy \left\{ (-y)^\gamma e^{i(k_1+k_2-k_3)y} \int_{-\infty}^y \frac{d\xi}{\xi} e^{2ik_3\xi} \right\} \quad (\text{B.17})$$

where we have explicitly written I as a function of the asymmetric momentum (in this case k_3), even though it is a function of the three momenta through k_t (perimeter in momentum space, $k_t = k_1 + k_2 + k_3$). The constant γ need not be an integer, and this is where the algebra differs from that presented in Refs. [28, 1] and in appendix A.

In what follows we consider positive, arbitrary γ . To simplify this integral, one follows the algorithm developed in these references: we apply a transformation of variables to convert this integral into its dimensionless version [defining $x = i(k_t - 2k_3)y$]. We then make a rotation in the complex plane [using $w = -ik_3\xi$]. Applying Cauchy's integral theorem we arrive at

$$I_\gamma(k_3) = \left(\frac{1}{i\vartheta_3 k_t} \right) \int_0^\infty dx \left\{ x^\gamma e^{-x} \int_\infty^{\theta_3 x} \frac{dw}{w} e^{-2w} \right\} \quad (\text{B.18})$$

where

$$\theta_3 \equiv \frac{k_3}{k_t - 2k_3} \quad \text{and} \quad \vartheta_3 \equiv \frac{1}{k_t} (k_t - 2k_3) .$$

Focusing on the inner integral in (B.18), upon integrating by parts and using the expansion series of the exponential function, we find it has a convergent series representation

$$\int_\infty^{\theta_3 x} \frac{dw}{w} e^{-2w} = \gamma_E + \ln(2\theta_3 x) + \sum_{n=1}^{+\infty} \frac{(-1)^n (2\theta_3 x)^n}{n! n} . \quad (\text{B.19})$$

Plugging this result into Eq. (B.17) gives

$$I_\gamma(k_3) = \left(\frac{1}{i\vartheta_3 k_t} \right)^{\gamma+1} \left\{ \Gamma(1+\gamma) \left[\gamma_E + \ln(2\theta_3) + \psi^{(0)}(1+\gamma) \right] + \sum_{n=1}^{\infty} \frac{(-2\theta_3)^n (n+\gamma)!}{n n!} \right\}, \quad (\text{B.20})$$

in which $\psi^{(0)}(z)$ denotes the polygamma function of order zero and argument z .¹ In obtaining this result we assumed $\text{Re}(\gamma) > -1$ for the first two contributions, whereas $\text{Re}(\gamma) > -2$ for the last term. This is true for all the integrals since γ is strictly non-negative. Finally, we can perform the last sum in Eq. (B.20) by observing that it converges for $-1/2 < \text{Re}(\theta_3) < 1/2$ [. We conclude that the integral (B.17) has a closed-form representation, given by

$$I_\gamma(k_3) = \left(\frac{1}{i\vartheta_3 k_t} \right)^{\gamma+1} \left\{ \Gamma(1+\gamma) \left[\gamma_E + \ln(2\theta_3) + \psi^{(0)}(1+\gamma) \right] - 2\theta_3 \Gamma(2+\gamma) {}_3F_2 \left(\{1, 1, 2+\gamma\}, \{2, 2\}, -2\theta_3 \right) \right\}, \quad (\text{B.21})$$

where F is a (convergent) generalised hypergeometric function, HypergeometricPFQ [281]. In chapter 5 we will use the following abbreviated notation

$$I_\gamma(k_3) = \left(\frac{1}{i\vartheta_3 k_t} \right)^{\gamma+1} \tilde{I}_\gamma(k_3), \quad (\text{B.22})$$

which, given that \tilde{I}_γ is a real-valued function, makes the identification of the real part of the result of the integral more transparent. Explicit results for positive integers $\gamma = 0, 1, 2$ are listed in Eqs. (A.14) and (A.15).

Eq. (B.21) generalises Eqs. (A.14) and (A.15) for non-negative, but otherwise arbitrary γ . In particular, Eq. (B.21) is valid for non-integer values of γ , which did not arise in chapter 3. This generalisation arises from the deviation of the slow-roll approximation.

¹The polygamma function of order m , $\psi^{(m)}(z)$, is the $(m+1)$ th-derivative of the logarithm of the gamma function, Γ . We will only require polygamma functions of order zero and one in our formulae.

B.4.2 Other integrals

The other family of integrals which arises in the calculation of the bispectrum is of the form

$$J_\gamma \equiv \int_{-\infty}^0 dy e^{ik_t y} (-y)^\gamma \left\{ A_* + B_* \ln(-k_* y) + C_* (\ln(-k_* y))^2 \right\}, \quad (\text{B.23})$$

where the constant coefficients A_* , B_* and C_* contain, in general, leading and next-order contributions in the scale-invariant approximation. This integral is a generalisation of Eq. (A.16) in §A.3. Provided $\text{Re}(\gamma) > -1$, which is indeed the case for all the integrals which arise in chapter 5, this integral converges and gives

$$\begin{aligned} J_\gamma = \left(\frac{1}{ik_t} \right)^{1+\gamma} \Gamma(1+\gamma) \left\{ A_* + \left[\ln(k_*/k_t) - i\frac{\pi}{2} \right] \left[B_* + C_* \left(\ln(k_*/k_t) - i\frac{\pi}{2} \right) \right] + \right. \\ \left. + \psi^{(0)}(1+\gamma) \left[B_* + 2C_* \left(\ln(k_*/k_t) - i\frac{\pi}{2} \right) + C_* \psi^{(0)}(1+\gamma) \right] + \right. \\ \left. + C_* \psi^{(1)}(1+\gamma) \right\}. \end{aligned} \quad (\text{B.24})$$

Again, to simplify the notation we will refer to this integral in the form

$$J_\gamma \equiv \left(\frac{1}{ik_t} \right)^{1+\gamma} \tilde{J}_\gamma. \quad (\text{B.25})$$

We note that \tilde{J}_γ is a complex-valued function, but given we only require the real part of J_γ we need to use Euler's function to write

$$\left(\frac{1}{ik_t} \right)^{1+\gamma} = \left(\frac{1}{k_t} \right)^{1+\gamma} \left\{ \cos \left[\frac{\pi}{2}(1+\gamma) \right] - i \sin \left[\frac{\pi}{2}(1+\gamma) \right] \right\}.$$

This explains the presence of trigonometric functions in tables 5.3 and 5.5.

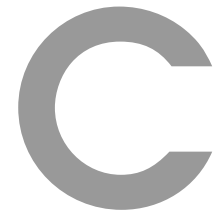
These integrals are the generalisation of the integrals discussed in appendix A.

B.5 Listing variables

In the main tables of chapter 5, to simplify the formulae, we have introduced a compact notation for combinations of momenta and slow-variation parameters. This is summarised in the following table.

variable	mathematical expression
\tilde{k}	$-k_t + \frac{\kappa^2}{k_t} + \frac{k_1 k_2 k_3}{k_t^2}$
κ^2	$k_1 k_2 + k_1 k_3 + k_2 k_3$
$\Omega_{1\star}$	$1 + 3\tilde{E}_\star + \frac{n_s - 1}{2} \ln \left(\frac{k_1 k_2 k_3}{k_\star^3} \right) + \frac{2\delta_\star}{1 + \varepsilon_\star} - \frac{2\varepsilon_\star \eta_\star}{(1 + \varepsilon_\star)^2}$
$\Omega_{2\star}$	$-\frac{\delta_\star + h_{3\star}}{1 + \varepsilon_\star} + \frac{2\varepsilon_\star \eta_\star}{(1 + \varepsilon_\star)^2}$
$\Omega_{3\star}$	$\Omega_{1\star} - \frac{\delta_\star}{1 + \varepsilon_\star} + \frac{\varepsilon_\star \eta_\star}{(1 + \varepsilon_\star)^2}$
$f(k_1, k_2, k_3)$	$(n_s - 1) \left[-k_t \ln \frac{8k_1 k_2 k_3}{k_t^3} + 2(k_1 \ln 2k_1/k_t + k_2 \ln 2k_2/k_t + k_3 \ln 2k_3/k_t) \right. \\ \left. + 3\tilde{k}(\gamma_E - \ln k_\star/k_t) - 3\frac{k_1 k_2 k_3}{k_t^2} + 4k_t - 2\kappa^2/k_t \right] \\ - 3\tilde{k} \left(\frac{\delta_\star}{1 + \varepsilon_\star} - \frac{\varepsilon_\star \eta_\star}{(1 + \varepsilon_\star)^2} \right)$
Ξ	$\Gamma \left(1 + \frac{4\varepsilon_\star}{1 + \varepsilon_\star} \right) \cos \left[\frac{2\pi\varepsilon_\star}{1 + \varepsilon_\star} \right]$

Table B.1: Collection of the abbreviated variables used in the tables included in chapter 5.



Details of the preheating stage

This appendix serves two purposes. First, in §C.1 we present the dictionary between physical and bare quantities in a DBI theory. The discussion is presented in the language of an arbitrary non-canonical field theory for generality. Second, in §C.2 we give details of our derivation of the Floquet exponent in Hill's equation. This generalises what is known for Mathieu's equation. This appendix is companion of chapter 6.

C.1 Canonically normalised theory

We start by considering a general higher-derivative Lagrangian of the form $P(\phi, X)$, given by Eq. (6.1) in chapter 6. We let $\delta\phi$ denote small excitations around the background field ϕ_0 . Assuming derivatives of ϕ_0 are negligible then we can write $\delta X = \delta\dot{\phi}^2 - (\partial\delta\phi)^2$. To quadratic order in $\delta\phi$ but including all orders in other fields, the field propagates in a locally Minkowski region according to the action

$$S = \int d^4x \left\{ P_0 + \frac{\partial P}{\partial\phi} \delta\phi + \frac{\partial P}{\partial X} [\delta\dot{\phi}^2 - (\partial\delta\phi)^2] + \frac{1}{2} \frac{\partial^2 P}{\partial\phi^2} \delta\phi^2 + \dots \right\}, \quad (\text{C.1})$$

where $P_0 = P(X=0, \phi_0)$ and '...' denotes higher-order terms in $\delta\phi$ and its derivatives.

Eq. (C.1) will give a reliable description of scattering and decay processes involving inflaton particles provided derivatives of the background field are negligible over the relevant time and distance scales our analysis applies. In this limit we can neglect the curvature of space-time and work in a locally flat region, which should be chosen to be somewhat larger than the interaction region. Eq. (C.1) therefore applies within this patch. Local scattering probabilities can be described by taking the associated S -matrix elements. On the other hand, if the background field ϕ varies significantly over the timescale of the scattering event then the definition of asymptotic *in*- and *out*-states becomes more complicated, and the concept of well-defined particles with an associated S -matrix may be invalidated.¹

Canonical normalisation.—If the vacuum is locally stable on timescales comparable with decay processes, then $\langle \partial P / \partial \phi \rangle$ must be negligible when evaluated there. We must nevertheless retain perturbative excitations contained in this term, whenever fermion Yukawa couplings are present. After canonical normalisation of $\delta\phi$, the interaction terms in the Lagrangian arise from

$$\mathcal{L}_{\text{int}} \supseteq \frac{P_{,\phi}}{\sqrt{2P_{,X}}} \delta\phi + \frac{1}{4} \frac{P_{,\phi\phi}}{P_{,X}} \delta\phi^2, \quad (\text{C.2})$$

where a comma denotes a partial derivative evaluated in the background. In a cut-off throat, the models we have been considering correspond to $P = -f^{-1}(1 - fX)^{1/2} + f^{-1} - V(\phi)$ with f constant and $V(\phi)$ chosen to be Eq. (6.15) or (6.17). Consider the symmetry-breaking potential (6.17). We only wish to canonically normalize $\delta\phi$, which represents fluctuations around the mean field visible to local observers as particles. Therefore, one should shift to canonical normalisation only after expanding in powers of fluctuations around the background field. Applying this procedure implies that we should make the transformations

$$m^2 \rightarrow m_*^2 = \frac{m^2}{2P_{,X}} \quad \text{and} \quad g^2 \rightarrow g_*^2 = \frac{g^2}{\sqrt{2P_{,X}}}. \quad (\text{C.3})$$

¹For example, this may happen in models where ϕ_0 evolves at a constant rate, such as the ghost inflation proposal of Arkani-Hamed et al. [72, 73]. We do not consider these models here.

Measurable masses and couplings.—Whatever model we consider, the predictions of the preheating theory should refer to the *same* particles. Therefore our results should be written in terms of the masses and couplings which are measured, for example, by a local observer who can record the outcome of scattering events. We therefore need to abandon the comfort of bare quantities, and rewrite our final formulae in terms of physical quantities.

For non-canonical kinetic terms, it is possible that the evolution of the background field causes the masses and couplings to change in time. In this case, it is the masses and couplings measured by a local observer at the time of reheating which are the relevant quantities.

At tree-level, the coupling g_* of the canonically normalized field is the coupling which is measured by experiment, and the mass m_* of the canonically normalized field determines the position of the pole in its propagator. These are unambiguous, physical definitions of the interaction coefficient and the mass of a particle. It is therefore the quantities m_* and g_* which should be compared with the mass and coupling in a theory with canonical kinetic terms.

If a Yukawa coupling is present then we should similarly rescale its coupling constant:

$$h \rightarrow h_* = \frac{h}{\sqrt{2P_X}}. \quad (\text{C.4})$$

C.2 Floquet exponents from Hill's equation

In this appendix we derive the Floquet exponent associated with Hill's equation.²

C.2.1 $\theta_0, \theta_2, \theta_4 \neq 0$

We start with the case when $\theta_2, \theta_4 \neq 0$, and $\theta_{2n} = 0$, for $n > 2$ and by noting that in the edges of the resonance bands $\mu_k = 0$; it turns out that for the most important instability band and for $\theta_2, \theta_4 < 1$

$$\theta_0 \simeq 1 \pm \theta_2 \left[1 \mp \frac{(\theta_4)^2}{6\theta_2} \right].$$

²I thank Joel Weller for sharing his preheating notes, which have helped me to arrive at this result.

For $\theta_4^2/\theta_2 \ll 1$, this essentially reduces to

$$\theta_0 \simeq 1 \pm \theta_2 \quad . \quad (\text{C.5})$$

This implies that, at lowest-order, $\theta_0^{1/2} \simeq 1 \pm \theta_2/2$.

Now, the instability parameter is given by [273]

$$\sin^2 \left[i\mu_k \frac{\pi}{2} \right] = \Delta(0) \sin^2 \left[\theta_0^{1/2} \frac{\pi}{2} \right] \quad , \quad (\text{C.6})$$

where $\Delta(0)$ is exclusively determined by θ_0 , θ_2 and θ_4 and is approximately given by

$$\Delta(0) \simeq 1 + \frac{\pi}{4\theta_0^{1/2}} \cot \left[\theta_0^{1/2} \frac{\pi}{2} \right] \left\{ \frac{\theta_2^2}{1-\theta_0} + \frac{\theta_4^2}{4-\theta_0} \right\} \quad .$$

We can show that this yields

$$\Delta(0) \simeq 1 \mp \left(\frac{\pi}{2} \right)^2 \left[\mp \left(\frac{\theta_2}{2} \right)^2 + \frac{\theta_2}{3} \left(\frac{\theta_4}{2} \right)^2 + \frac{(\theta_2)^3}{2} \right] \quad . \quad (\text{C.7})$$

We thus arrive at an approximate expression for the Floquet exponent

$$\mu_k \simeq \sqrt{\left(\frac{\theta_2}{2} \right)^2 - (\theta_0^{1/2} - 1)^2 \mp \frac{\theta_2}{3} \left(\frac{\theta_4}{2} \right)^2 \mp \frac{(\theta_2)^3}{2}} \quad . \quad (\text{C.8})$$

This expression for μ_k is valid for $\theta_2, \theta_4 \ll 1$.

C.2.2 $\theta_0, \theta_2, \theta_6 \neq 0$

If we now proceed and consider the case with non-vanishing θ_0 , θ_2 and θ_6 , we observe that the instability parameter may be computed using again (C.6), where now

$$\Delta(0) \simeq 1 + \frac{\pi \cot \left[\frac{\pi}{2} \theta_0^{1/2} \right]}{4\theta_0^{1/2}} \left(\frac{\theta_2^2}{1-\theta} + \frac{\theta_6^2}{9-\theta_0} \right) \quad . \quad (\text{C.9})$$

By considering the first instability band, we take $\theta_0 \simeq 1 \pm \theta_2$, so that

$$\theta_0^{1/2} \simeq 1 \pm \frac{\theta_2}{2}, \quad \frac{\theta_2^2}{1-\theta_0} = \mp \theta_2, \quad \frac{\theta_6^2}{9-\theta_0} \simeq \mp \frac{\theta_6^2}{8} \left(1 \pm \frac{\theta_2}{8}\right), \quad \text{and} \quad \cot \left[\frac{\pi}{2} \theta_0^{1/2} \right] \simeq \mp \frac{\pi}{4} \theta_2. \quad (\text{C.10})$$

Plugging these into (C.9), we find that, up to lowest-order

$$\Delta(0) \simeq 1 \mp \left(\frac{\pi}{4}\right)^2 \left(\mp \theta_2^2 + \frac{\theta_2 \theta_6^2}{8} + \frac{\theta_2^3}{2} \right).$$

Moreover,

$$\sin \left[\frac{\pi}{2} \theta_0^{1/2} \right] \simeq 1 - \frac{1}{2} \left(\frac{\pi}{2}\right)^2 (\theta_0^{1/2} - 1)^2.$$

Finally, by substituting into (C.6), we obtain

$$\mu_k \simeq \sqrt{\left(\frac{\theta_2}{2}\right)^2 \mp \frac{\theta_2 \theta_6^2}{32} \mp \left(\frac{\theta_2}{2}\right)^3 - (\theta_0^{1/2} - 1)^2}. \quad (\text{C.11})$$

This generalises Eq. (6.25) suitable to compute the Floquet exponent in Mathieu's equation.

Bibliography

- [1] C. Burrage, R. H. Ribeiro, and D. Seery, *Large slow-roll corrections to the bispectrum of noncanonical inflation*, *JCAP* **1107** (2011) 032, [[arXiv:1103.4126](#)], [[doi:10.1088/1475-7516/2011/07/032](#)].
- [2] R. H. Ribeiro and D. Seery, *Decoding the bispectrum of single-field inflation*, *JCAP* **1110** (2011) 027, [[arXiv:1108.3839](#)], [[doi:10.1088/1475-7516/2011/10/027](#)].
- [3] R. H. Ribeiro, *Inflationary signatures of single-field models beyond slow-roll*, *JCAP* **1205** (2012) 037, [[arXiv:1202.4453](#)], [[doi:10.1088/1475-7516/2012/05/037](#)].
- [4] N. Bouatta, A.-C. Davis, R. H. Ribeiro, and D. Seery, *Preheating in Dirac–Born–Infeld inflation*, *JCAP* **1009** (2010) 011, [[arXiv:1005.2425](#)], [[doi:10.1088/1475-7516/2010/09/011](#)].
- [5] S. Perlmutter, *Supernovae, dark energy, and the accelerating universe*, *Physics Today* **April** (2003) 53–60.
- [6] **WMAP** Collaboration, E. Komatsu *et al.*, *Seven-year Wilkinson Microwave Anisotropy Probe (WMAP) observations: cosmological interpretation*, *Astrophys. J. Suppl.* **192** (2011) 18, [[arXiv:1001.4538](#)], [[doi:10.1088/0067-0049/192/2/18](#)].
- [7] D. Larson, J. Dunkley, G. Hinshaw, E. Komatsu, M. Nolta, *et al.*, *Seven-year Wilkinson Microwave Anisotropy Probe (WMAP) observations: power spectra and WMAP-derived parameters*, *Astrophys. J. Suppl.* **192** (2011) 16, [[arXiv:1001.4635](#)], [[doi:10.1088/0067-0049/192/2/16](#)].
- [8] S. Weinberg, *Quantum contributions to cosmological correlations*, *Phys. Rev. D* **72** (2005) 043514, [[arXiv:hep-th/0506236](#)], [[doi:10.1103/PhysRevD.72.043514](#)].
- [9] J. R. Fergusson and E. P. S. Shellard, *The shape of primordial non-gaussianity and the CMB bispectrum*, *Phys. Rev. D* **80** (2009) 043510, [[arXiv:0812.3413](#)], [[doi:10.1103/PhysRevD.80.043510](#)].
- [10] D. Babich, P. Creminelli, and M. Zaldarriaga, *The shape of non-gaussianities*, *JCAP* **0408** (2004) 009, [[arXiv:astro-ph/0405356](#)], [[doi:10.1088/1475-7516/2004/08/009](#)].
- [11] P. Creminelli, G. D’Amico, M. Musso, J. Noreña, and E. Trincherini, *Galilean symmetry in the effective theory of inflation: new shapes of non-gaussianity*, *JCAP* **1102** (2011) 006, [[arXiv:1011.3004](#)], [[doi:10.1088/1475-7516/2011/02/006](#)].

- [12] E. J. Copeland, *Inflation after the COsmic Background Explorer (COBE)*, *Contemp. Phys.* **34** (1993) 303–316, [[doi:10.1080/00107519308213825](https://doi.org/10.1080/00107519308213825)].
- [13] **Supernova Cosmology Project** Collaboration, S. Perlmutter *et al.*, *Discovery of a supernova explosion at half the age of the Universe and its cosmological implications*, *Nature* **391** (1998) 51–54, [[arXiv:astro-ph/9712212](https://arxiv.org/abs/astro-ph/9712212)], [[doi:10.1038/34124](https://doi.org/10.1038/34124)].
- [14] **Supernova Search Team** Collaboration, A. G. Riess *et al.*, *Observational evidence from supernovae for an accelerating universe and a cosmological constant*, *Astron. J.* **116** (1998) 1009–1038, [[arXiv:astro-ph/9805201](https://arxiv.org/abs/astro-ph/9805201)], [[doi:10.1086/300499](https://doi.org/10.1086/300499)].
- [15] **Supernova Search Team** Collaboration, J. L. Tonry *et al.*, *Cosmological results from high- z supernovae*, *Astrophys. J.* **594** (2003) 1–24, [[arXiv:astro-ph/0305008](https://arxiv.org/abs/astro-ph/0305008)], [[doi:10.1086/376865](https://doi.org/10.1086/376865)].
- [16] D. H. Lyth and A. R. Liddle, *The primordial density perturbation: Cosmology, inflation and the origin of structure*. Cambridge University Press, Cambridge, UK, 2009.
- [17] A. H. Guth, *The inflationary universe: a possible solution to the horizon and flatness problems*, *Phys. Rev. D* **23** (1981) 347–356, [[doi:10.1103/PhysRevD.23.347](https://doi.org/10.1103/PhysRevD.23.347)].
- [18] M. Sasaki and T. Tanaka, *Superhorizon scale dynamics of multiscalar inflation*, *Prog. Theor. Phys.* **99** (1998) 763–782, [[arXiv:gr-qc/9801017](https://arxiv.org/abs/gr-qc/9801017)], [[doi:10.1143/PTP.99.763](https://doi.org/10.1143/PTP.99.763)].
- [19] T. Hirai and K.-i. Maeda, *Gauge invariant cosmological perturbations in generalized Einstein theories*, *Astrophys. J.* **431** (1994) 6–19, [[arXiv:astro-ph/9404023](https://arxiv.org/abs/astro-ph/9404023)], [[doi:10.1086/174463](https://doi.org/10.1086/174463)].
- [20] R. M. Wald, *General relativity*. The University of Chicago Press, Chicago, USA, 1984.
- [21] P. Brax, C. van de Bruck, A.-C. Davis, and D. J. Shaw, *$f(R)$ gravity and chameleon theories*, *Phys. Rev. D* **78** (2008) 104021, [[arXiv:0806.3415](https://arxiv.org/abs/0806.3415)], [[doi:10.1103/PhysRevD.78.104021](https://doi.org/10.1103/PhysRevD.78.104021)].
- [22] C. Brans and R. Dicke, *Mach's principle and a relativistic theory of gravitation*, *Phys. Rev.* **124** (1961) 925–935, [[doi:10.1103/PhysRev.124.925](https://doi.org/10.1103/PhysRev.124.925)].
- [23] S. Nojiri and S. D. Odintsov, *Introduction to modified gravity and gravitational alternative for dark energy*, *eConf C0602061* (2006) 06, [[arXiv:hep-th/0601213](https://arxiv.org/abs/hep-th/0601213)], [[doi:10.1142/S0219887807001928](https://doi.org/10.1142/S0219887807001928)], [[10.1142/S0219887807001928](https://doi.org/10.1142/S0219887807001928)].
- [24] P. Brax, C. van de Bruck, and A.-C. Davis, *Brane world cosmology*, *Rept. Prog. Phys.* **67** (2004) 2183–2232, [[arXiv:hep-th/0404011](https://arxiv.org/abs/hep-th/0404011)], [[doi:10.1088/0034-4885/67/12/R02](https://doi.org/10.1088/0034-4885/67/12/R02)].
- [25] T. Clifton, P. G. Ferreira, A. Padilla, and C. Skordis, *Modified gravity and cosmology*, *Phys. Rept.* **513** (2012) 1–189, [[arXiv:1106.2476](https://arxiv.org/abs/1106.2476)], [[doi:10.1016/j.physrep.2012.01.001](https://doi.org/10.1016/j.physrep.2012.01.001)].
- [26] C. Armendáriz-Picón, T. Damour, and V. F. Mukhanov, *k -inflation*, *Phys. Lett. B* **458** (1999) 209–218, [[arXiv:hep-th/9904075](https://arxiv.org/abs/hep-th/9904075)], [[doi:10.1016/S0370-2693\(99\)00603-6](https://doi.org/10.1016/S0370-2693(99)00603-6)].

- [27] E. Silverstein and D. Tong, *Scalar speed limits and Cosmology: acceleration from D-cceleration*, *Phys. Rev. D* **70** (2004) 103505, [[arXiv:hep-th/0310221](#)], [[doi:10.1103/PhysRevD.70.103505](#)].
- [28] C. Burrage, C. de Rham, D. Seery, and A. J. Tolley, *Galileon inflation*, *JCAP* **1101** (2011) 014, [[arXiv:1009.2497](#)], [[doi:10.1088/1475-7516/2011/01/014](#)].
- [29] S. Céspedes, V. Atal, and G. A. Palma, *On the importance of heavy fields during inflation*, *JCAP* **1205** (2012) 008, [[arXiv:1201.4848](#)], [[doi:10.1088/1475-7516/2012/05/008](#)].
- [30] A. Achúcarro, J.-O. Gong, S. Hardeman, G. A. Palma, and S. P. Patil, *Effective theories of single field inflation when heavy fields matter*, *JHEP* **1205** (2012) 066, [[arXiv:1201.6342](#)], [[doi:10.1007/JHEP05\(2012\)066](#)].
- [31] A. Avgoustidis, S. Cremonini, A.-C. Davis, R. H. Ribeiro, K. Turzyński, and S. Watson, *Decoupling survives inflation: a critical look at effective field theory violations during inflation*, *JCAP* **1206** (2012) 025, [[arXiv:1203.0016](#)], [[doi:10.1088/1475-7516/2012/06/025](#)].
- [32] P. Binétruy, G. Dvali, R. Kallosh, and A. Van Proeyen, *Fayet-Iliopoulos terms in supergravity and cosmology*, *Class. Quant. Grav.* **21** (2004) 3137–3170, [[arXiv:hep-th/0402046](#)], [[doi:10.1088/0264-9381/21/13/005](#)].
- [33] K. Choi, A. Falkowski, H. P. Nilles, M. Olechowski, and S. Pokorski, *Stability of flux compactifications and the pattern of supersymmetry breaking*, *JHEP* **11** (2004) 076, [[arXiv:hep-th/0411066](#)], [[doi:10.1088/1126-6708/2004/11/076](#)].
- [34] A. D. Linde, *Generation of isothermal density perturbations in the inflationary universe*, *JETP Lett.* **40** (1984) 1333–1336.
- [35] L. Kofman and A. D. Linde, *Generation of density perturbations in the inflationary cosmology*, *Nucl. Phys. B* **282** (1987) 555, [[doi:10.1016/0550-3213\(87\)90698-5](#)].
- [36] J. Silk and M. S. Turner, *Double inflation*, *Phys. Rev. D* **35** (1987) 419, [[doi:10.1103/PhysRevD.35.419](#)].
- [37] C. de Rham and G. Gabadadze, *Generalization of the Fierz-Pauli action*, *Phys. Rev. D* **82** (2010) 044020, [[arXiv:1007.0443](#)], [[doi:10.1103/PhysRevD.82.044020](#)].
- [38] C. de Rham, G. Gabadadze, and A. J. Tolley, *Resummation of massive gravity*, *Phys. Rev. Lett.* **106** (2011) 231101, [[arXiv:1011.1232](#)], [[doi:10.1103/PhysRevLett.106.231101](#)].
- [39] S. Hassan and R. A. Rosen, *Resolving the ghost problem in non-linear massive gravity*, *Phys. Rev. Lett.* **108** (2012) 041101, [[arXiv:1106.3344](#)], [[doi:10.1103/PhysRevLett.108.041101](#)].
- [40] A. H. Guth and S. Pi, *Fluctuations in the new inflationary universe*, *Phys. Rev. Lett.* **49** (1982) 1110–1113, [[doi:10.1103/PhysRevLett.49.1110](#)].

- [41] S. Hawking, *The development of irregularities in a single bubble inflationary universe*, *Phys. Lett. B* **115** (1982) 295, [[doi:10.1016/0370-2693\(82\)90373-2](https://doi.org/10.1016/0370-2693(82)90373-2)].
- [42] J. M. Bardeen, P. J. Steinhardt, and M. S. Turner, *Spontaneous creation of almost scale-free density perturbations in an inflationary universe*, *Phys. Rev. D* **28** (1983) 679, [[doi:10.1103/PhysRevD.28.679](https://doi.org/10.1103/PhysRevD.28.679)].
- [43] **Boomerang** Collaboration, A. Melchiorri *et al.*, *A measurement of omega from the North American test flight of BOOMERANG*, *Astrophys. J.* **536** (2000) L63–L66, [[arXiv:astro-ph/9911445](https://arxiv.org/abs/astro-ph/9911445)], [[doi:10.1086/312744](https://doi.org/10.1086/312744)].
- [44] **Boomerang** Collaboration, P. de Bernardis *et al.*, *A flat universe from high resolution maps of the cosmic microwave background radiation*, *Nature* **404** (2000) 955–959, [[arXiv:astro-ph/0004404](https://arxiv.org/abs/astro-ph/0004404)], [[doi:10.1038/35010035](https://doi.org/10.1038/35010035)].
- [45] X. Chen, M.-x. Huang, S. Kachru, and G. Shiu, *Observational signatures and non-Gaussianities of general single field inflation*, *JCAP* **0701** (2007) 002, [[arXiv:hep-th/0605045](https://arxiv.org/abs/hep-th/0605045)], [[doi:10.1088/1475-7516/2007/01/002](https://doi.org/10.1088/1475-7516/2007/01/002)].
- [46] G. Altarelli, R. Barbieri, and F. Caravaglios, *Electroweak precision tests: a concise review*, *Int. J. Mod. Phys. A* **13** (1998) 1031–1058, [[arXiv:hep-ph/9712368](https://arxiv.org/abs/hep-ph/9712368)], [[doi:10.1142/S0217751X98000469](https://doi.org/10.1142/S0217751X98000469)].
- [47] E. Komatsu, N. Afshordi, N. Bartolo, D. Baumann, J. Bond, *et al.*, *Non-gaussianity as a probe of the physics of the primordial universe and the astrophysics of the low redshift universe*, [arXiv:0902.4759](https://arxiv.org/abs/0902.4759).
- [48] D. Wands, K. A. Malik, D. H. Lyth, and A. R. Liddle, *A new approach to the evolution of cosmological perturbations on large scales*, *Phys. Rev. D* **62** (2000) 043527, [[arXiv:astro-ph/0003278](https://arxiv.org/abs/astro-ph/0003278)], [[doi:10.1103/PhysRevD.62.043527](https://doi.org/10.1103/PhysRevD.62.043527)].
- [49] N. Jarosik, C. Bennett, J. Dunkley, B. Gold, M. Greason, *et al.*, *Seven-year Wilkinson Microwave Anisotropy Probe (WMAP) observations: sky maps, systematic errors, and basic results*, *Astrophys. J. Suppl.* **192** (2011) 14, [[arXiv:1001.4744](https://arxiv.org/abs/1001.4744)], [[doi:10.1088/0067-0049/192/2/14](https://doi.org/10.1088/0067-0049/192/2/14)].
- [50] L. Verde, L.-M. Wang, A. Heavens, and M. Kamionkowski, *Large scale structure, the cosmic microwave background, and primordial non-gaussianity*, *Mon. Not. Roy. Astron. Soc.* **313** (2000) L141–L147, [[arXiv:astro-ph/9906301](https://arxiv.org/abs/astro-ph/9906301)].
- [51] E. Komatsu and D. N. Spergel, *Acoustic signatures in the primary microwave background bispectrum*, *Phys. Rev. D* **63** (2001) 063002, [[arXiv:astro-ph/0005036](https://arxiv.org/abs/astro-ph/0005036)], [[doi:10.1103/PhysRevD.63.063002](https://doi.org/10.1103/PhysRevD.63.063002)].
- [52] F. Bernardeau, S. Colombi, E. Gaztañaga, and R. Scoccimarro, *Large scale structure of the universe and cosmological perturbation theory*, *Phys. Rept.* **367** (2002) 1–248, [[arXiv:astro-ph/0112551](https://arxiv.org/abs/astro-ph/0112551)], [[doi:10.1016/S0370-1573\(02\)00135-7](https://doi.org/10.1016/S0370-1573(02)00135-7)].

- [53] J. Smidt, A. Amblard, C. T. Byrnes, A. Cooray, A. Heavens, *et al.*, *CMB constraints on primordial non-gaussianity from the bispectrum (f_{NL}) and trispectrum (g_{NL} and τ_{NL}) and a new consistency test of single-field inflation*, *Phys. Rev. D* **81** (2010) 123007, [[arXiv:1004.1409](#)], [[doi:10.1103/PhysRevD.81.123007](#)].
- [54] J. Fergusson, D. Regan, and E. Shellard, *Optimal trispectrum estimators and WMAP constraints*, [arXiv:1012.6039](#).
- [55] A. A. Starobinsky, *Multicomponent de Sitter (inflationary) stages and the generation of perturbations*, *JETP Lett.* **42** (1985) 152–155.
- [56] M. Sasaki and E. D. Stewart, *A general analytic formula for the spectral index of the density perturbations produced during inflation*, *Prog. Theor. Phys.* **95** (1996) 71–78, [[arXiv:astro-ph/9507001](#)], [[doi:10.1143/PTP.95.71](#)].
- [57] D. H. Lyth and Y. Rodríguez, *The inflationary prediction for primordial non-gaussianity*, *Phys. Rev. Lett.* **95** (2005) 121302, [[arXiv:astro-ph/0504045](#)], [[doi:10.1103/PhysRevLett.95.121302](#)].
- [58] S. W. Hawking and I. G. Moss, *Fluctuations in the inflationary universe*, *Nucl. Phys. B* **224** (1983) 180, [[doi:10.1016/0550-3213\(83\)90319-X](#)].
- [59] D. Lyth, *Large scale energy density perturbations and inflation*, *Phys. Rev. D* **31** (1985) 1792–1798, [[doi:10.1103/PhysRevD.31.1792](#)].
- [60] V. F. Mukhanov, *Gravitational instability of the universe filled with a scalar field*, *JETP Lett.* **41** (1985) 493–496.
- [61] M. Sasaki, *Large scale quantum fluctuations in the inflationary universe*, *Prog. Theor. Phys.* **76** (1986) 1036, [[doi:10.1143/PTP.76.1036](#)].
- [62] T. Allen, B. Grinstein, and M. B. Wise, *Nongaussian density perturbations in inflationary cosmologies*, *Phys. Lett. B* **197** (1987) 66, [[doi:10.1016/0370-2693\(87\)90343-1](#)].
- [63] T. Falk, R. Rangarajan, and M. Srednicki, *The angular dependence of the three point correlation function of the cosmic microwave background radiation as predicted by inflationary cosmologies*, *Astrophys. J.* **403** (1993) L1, [[arXiv:astro-ph/9208001](#)].
- [64] A. Gangui, F. Lucchin, S. Matarrese, and S. Mollerach, *The three point correlation function of the cosmic microwave background in inflationary models*, *Astrophys. J.* **430** (1994) 447–457, [[arXiv:astro-ph/9312033](#)], [[doi:10.1086/174421](#)].
- [65] L.-M. Wang and M. Kamionkowski, *The Cosmic microwave background bispectrum and inflation*, *Phys. Rev. D* **61** (2000) 063504, [[arXiv:astro-ph/9907431](#)], [[doi:10.1103/PhysRevD.61.063504](#)].
- [66] J. M. Maldacena, *Non-gaussian features of primordial fluctuations in single field inflationary models*, *JHEP* **0305** (2003) 013, [[arXiv:astro-ph/0210603](#)], [[doi:10.1088/1126-6708/2003/05/013](#)].

- [67] D. Seery and J. E. Lidsey, *Primordial non-gaussianities from multiple-field inflation*, *JCAP* **0509** (2005) 011, [[arXiv:astro-ph/0506056](#)], [[doi:10.1088/1475-7516/2005/09/011](#)].
- [68] D. Seery, J. E. Lidsey, and M. S. Sloth, *The inflationary trispectrum*, *JCAP* **0701** (2007) 027, [[arXiv:astro-ph/0610210](#)], [[doi:10.1088/1475-7516/2007/01/027](#)].
- [69] D. Seery, M. S. Sloth, and F. Vernizzi, *Inflationary trispectrum from graviton exchange*, *JCAP* **0903** (2009) 018, [[arXiv:0811.3934](#)], [[doi:10.1088/1475-7516/2009/03/018](#)].
- [70] N. Kaloper, M. Kleban, A. E. Lawrence, and S. Shenker, *Signatures of short distance physics in the cosmic microwave background*, *Phys. Rev. D* **66** (2002) 123510, [[arXiv:hep-th/0201158](#)], [[doi:10.1103/PhysRevD.66.123510](#)].
- [71] P. Creminelli, *On non-gaussianities in single-field inflation*, *JCAP* **0310** (2003) 003, [[arXiv:astro-ph/0306122](#)], [[doi:10.1088/1475-7516/2003/10/003](#)].
- [72] N. Arkani-Hamed, H.-C. Cheng, M. A. Luty, and S. Mukohyama, *Ghost condensation and a consistent infrared modification of gravity*, *JHEP* **0405** (2004) 074, [[arXiv:hep-th/0312099](#)], [[doi:10.1088/1126-6708/2004/05/074](#)].
- [73] N. Arkani-Hamed, P. Creminelli, S. Mukohyama, and M. Zaldarriaga, *Ghost inflation*, *JCAP* **0404** (2004) 001, [[arXiv:hep-th/0312100](#)], [[doi:10.1088/1475-7516/2004/04/001](#)].
- [74] M. Alishahiha, E. Silverstein, and D. Tong, *DBI in the sky*, *Phys. Rev. D* **70** (2004) 123505, [[arXiv:hep-th/0404084](#)], [[doi:10.1103/PhysRevD.70.123505](#)].
- [75] T. Kobayashi, M. Yamaguchi, and J. Yokoyama, *G-inflation: inflation driven by the galileon field*, *Phys. Rev. Lett.* **105** (2010) 231302, [[arXiv:1008.0603](#)], [[doi:10.1103/PhysRevLett.105.231302](#)].
- [76] S. Mizuno and K. Koyama, *Primordial non-gaussianity from the DBI galileons*, *Phys. Rev. D* **82** (2010) 103518, [[arXiv:1009.0677](#)], [[doi:10.1103/PhysRevD.82.103518](#)].
- [77] S. E. Vázquez, *Constraining modified gravity with large non-gaussianities*, *Phys. Rev. D* **79** (2009) 043520, [[arXiv:0806.0603](#)], [[doi:10.1103/PhysRevD.79.043520](#)].
- [78] X. Gao, *Testing gravity with non-gaussianity*, *Phys. Lett. B* **702** (2011) 197–200, [[arXiv:1008.2123](#)], [[doi:10.1016/j.physletb.2011.07.022](#)].
- [79] G. Dvali, G. Gabadadze, and M. Porrati, *4-D gravity on a brane in 5-D Minkowski space*, *Phys. Lett. B* **485** (2000) 208–214, [[arXiv:hep-th/0005016](#)], [[doi:10.1016/S0370-2693\(00\)00669-9](#)].
- [80] C. Deffayet, G. Dvali, and G. Gabadadze, *Accelerated universe from gravity leaking to extra dimensions*, *Phys. Rev. D* **65** (2002) 044023, [[arXiv:astro-ph/0105068](#)], [[doi:10.1103/PhysRevD.65.044023](#)].

- [81] C. Deffayet, O. Pujolàs, I. Sawicki, and A. Vikman, *Imperfect dark energy from kinetic gravity braiding*, *JCAP* **1010** (2010) 026, [[arXiv:1008.0048](#)], [[doi:10.1088/1475-7516/2010/10/026](#)].
- [82] T. Kobayashi, M. Yamaguchi, and J. Yokoyama, *Generalized G-inflation: inflation with the most general second-order field equations*, *Prog. Theor. Phys.* **126** (2011) 511–529, [[arXiv:1105.5723](#)], [[doi:10.1143/PTP.126.511](#)].
- [83] T. Kobayashi, M. Yamaguchi, and J. Yokoyama, *Primordial non-gaussianity from G-inflation*, *Phys. Rev. D* **83** (2011) 103524, [[arXiv:1103.1740](#)], [[doi:10.1103/PhysRevD.83.103524](#)].
- [84] X. Gao and D. A. Steer, *Inflation and primordial non-gaussianities of ‘generalized galileons’*, *JCAP* **1112** (2011) 019, [[arXiv:1107.2642](#)], [[doi:10.1088/1475-7516/2011/12/019](#)].
- [85] C. Deffayet, G. Esposito-Farèse, and A. Vikman, *Covariant Galileon*, *Phys. Rev. D* **79** (2009) 084003, [[arXiv:0901.1314](#)], [[doi:10.1103/PhysRevD.79.084003](#)].
- [86] J. Garriga and V. F. Mukhanov, *Perturbations in k-inflation*, *Phys. Lett. B* **458** (1999) 219–225, [[arXiv:hep-th/9904176](#)], [[doi:10.1016/S0370-2693\(99\)00602-4](#)].
- [87] A. Gruzinov, *Consistency relation for single scalar inflation*, *Phys. Rev. D* **71** (2005) 027301, [[arXiv:astro-ph/0406129](#)], [[doi:10.1103/PhysRevD.71.027301](#)].
- [88] D. Seery and J. E. Lidsey, *Primordial non-gaussianities in single field inflation*, *JCAP* **0506** (2005) 003, [[arXiv:astro-ph/0503692](#)], [[doi:10.1088/1475-7516/2005/06/003](#)].
- [89] D. Langlois and S. Renaux-Petel, *Perturbations in generalized multi-field inflation*, *JCAP* **0804** (2008) 017, [[arXiv:0801.1085](#)], [[doi:10.1088/1475-7516/2008/04/017](#)].
- [90] D. Langlois, S. Renaux-Petel, D. A. Steer, and T. Tanaka, *Primordial perturbations and non-gaussianities in DBI and general multi-field inflation*, *Phys. Rev. D* **78** (2008) 063523, [[arXiv:0806.0336](#)], [[doi:10.1103/PhysRevD.78.063523](#)].
- [91] F. Arroja, S. Mizuno, and K. Koyama, *Non-gaussianity from the bispectrum in general multiple field inflation*, *JCAP* **0808** (2008) 015, [[arXiv:0806.0619](#)], [[doi:10.1088/1475-7516/2008/08/015](#)].
- [92] X. Chen, M.-x. Huang, and G. Shiu, *The inflationary trispectrum for models with large non-gaussianities*, *Phys. Rev. D* **74** (2006) 121301, [[arXiv:hep-th/0610235](#)], [[doi:10.1103/PhysRevD.74.121301](#)].
- [93] F. Arroja and K. Koyama, *Non-gaussianity from the trispectrum in general single field inflation*, *Phys. Rev. D* **77** (2008) 083517, [[arXiv:0802.1167](#)], [[doi:10.1103/PhysRevD.77.083517](#)].

- [94] D. Langlois, S. Renaux-Petel, D. A. Steer, and T. Tanaka, *Primordial fluctuations and non-gaussianities in multi-field DBI inflation*, *Phys. Rev. Lett.* **101** (2008) 061301, [[arXiv:0804.3139](#)], [[doi:10.1103/PhysRevLett.101.061301](#)].
- [95] F. Arroja, S. Mizuno, K. Koyama, and T. Tanaka, *On the full trispectrum in single field DBI-inflation*, *Phys. Rev. D* **80** (2009) 043527, [[arXiv:0905.3641](#)], [[doi:10.1103/PhysRevD.80.043527](#)].
- [96] S. Mizuno, F. Arroja, and K. Koyama, *On the full trispectrum in multi-field DBI inflation*, *Phys. Rev. D* **80** (2009) 083517, [[arXiv:0907.2439](#)], [[doi:10.1103/PhysRevD.80.083517](#)].
- [97] X. Gao and C. Lin, *On the primordial trispectrum from exchanging scalar modes in general multiple field inflationary models*, *JCAP* **1011** (2010) 035, [[arXiv:1009.1311](#)], [[doi:10.1088/1475-7516/2010/11/035](#)].
- [98] N. Agarwal, R. Bean, L. McAllister, and G. Xu, *Universality in D-brane inflation*, *JCAP* **1109** (2011) 002, [[arXiv:1103.2775](#)], [[doi:10.1088/1475-7516/2011/09/002](#)].
- [99] M. Dias, J. Frazer, and A. R. Liddle, *Multifield consequences for D-brane inflation*, [arXiv:1203.3792](#).
- [100] **CMBPol Study Team** Collaboration, D. Baumann *et al.*, *CMBPol mission concept study: probing inflation with CMB polarization*, *AIP Conf. Proc.* **1141** (2009) 10–120, [[arXiv:0811.3919](#)], [[doi:10.1063/1.3160885](#)].
- [101] T. C. Collaboration, *COrE (Cosmic Origins Explorer) a white paper*, [arXiv:1102.2181](#).
- [102] E. D. Stewart and D. H. Lyth, *A more accurate analytic calculation of the spectrum of cosmological perturbations produced during inflation*, *Phys. Lett. B* **302** (1993) 171–175, [[arXiv:gr-qc/9302019](#)], [[doi:10.1016/0370-2693\(93\)90379-V](#)].
- [103] I. J. Grivell and A. R. Liddle, *Accurate determination of inflationary perturbations*, *Phys. Rev. D* **54** (1996) 7191–7198, [[arXiv:astro-ph/9607096](#)], [[doi:10.1103/PhysRevD.54.7191](#)].
- [104] J.-O. Gong and E. D. Stewart, *The density perturbation power spectrum to second-order corrections in the slow-roll expansion*, *Phys. Lett. B* **510** (2001) 1–9, [[arXiv:astro-ph/0101225](#)], [[doi:10.1016/S0370-2693\(01\)00616-5](#)].
- [105] J.-O. Gong and E. D. Stewart, *The power spectrum for a multicomponent inflaton to second order corrections in the slow roll expansion*, *Phys. Lett.* **538** (2002) 213–222, [[arXiv:astro-ph/0202098](#)], [[doi:10.1016/S0370-2693\(02\)02004-X](#)].
- [106] J. E. Lidsey, A. R. Liddle, E. W. Kolb, E. J. Copeland, T. Barreiro, *et al.*, *Reconstructing the inflation potential : an overview*, *Rev. Mod. Phys.* **69** (1997) 373–410, [[arXiv:astro-ph/9508078](#)], [[doi:10.1103/RevModPhys.69.373](#)].

- [107] H. Wei, R.-G. Cai, and A. Wang, *Second-order corrections to the power spectrum in the slow-roll expansion with a time-dependent sound speed*, *Phys. Lett. B* **603** (2004) 95–106, [[arXiv:hep-th/0409130](#)], [[doi:10.1016/j.physletb.2004.10.034](#)].
- [108] D. H. Lyth, *What would we learn by detecting a gravitational wave signal in the cosmic microwave background anisotropy?*, *Phys. Rev. Lett.* **78** (1997) 1861–1863, [[arXiv:hep-ph/9606387](#)], [[doi:10.1103/PhysRevLett.78.1861](#)].
- [109] D. Baumann and L. McAllister, *A microscopic limit on gravitational waves from D-brane inflation*, *Phys. Rev. D* **75** (2007) 123508, [[arXiv:hep-th/0610285](#)], [[doi:10.1103/PhysRevD.75.123508](#)].
- [110] J. E. Lidsey and I. Huston, *Gravitational wave constraints on Dirac–Born–Infeld inflation*, *JCAP* **0707** (2007) 002, [[arXiv:0705.0240](#)], [[doi:10.1088/1475-7516/2007/07/002](#)].
- [111] J. E. Lidsey and D. Seery, *Primordial non-gaussianity and gravitational waves: observational tests of brane inflation in string theory*, *Phys. Rev. D* **75** (2007) 043505, [[arXiv:astro-ph/0610398](#)], [[doi:10.1103/PhysRevD.75.043505](#)].
- [112] R. Bean, X. Chen, H. Peiris, and J. Xu, *Comparing infrared Dirac–Born–Infeld brane inflation to observations*, *Phys. Rev. D* **77** (2008) 023527, [[arXiv:0710.1812](#)], [[doi:10.1103/PhysRevD.77.023527](#)].
- [113] A. J. Christopherson and K. A. Malik, *The non-adiabatic pressure in general scalar field systems*, *Phys. Lett. B* **675** (2009) 159–163, [[arXiv:0809.3518](#)], [[doi:10.1016/j.physletb.2009.04.003](#)].
- [114] H. Kodama and M. Sasaki, *Cosmological perturbation theory*, *Prog. Theor. Phys. Suppl.* **78** (1984) 1–166, [[doi:10.1143/PTPS.78.1](#)].
- [115] K. A. Malik and D. Wands, *Cosmological perturbations*, *Phys. Rept.* **475** (2009) 1–51, [[arXiv:0809.4944](#)], [[doi:10.1016/j.physrep.2009.03.001](#)].
- [116] R. L. Arnowitt, S. Deser, and C. W. Misner, *The dynamics of general relativity*, [arXiv:gr-qc/0405109](#).
- [117] P. D’Eath, *Supersymmetric quantum Cosmology*. Cambridge Monographs on Mathematical Physics, Cambridge University Press, Cambridge, UK, 1996.
- [118] S. Weinberg, *A tree theorem for inflation*, *Phys. Rev. D* **78** (2008) 063534, [[arXiv:0805.3781](#)], [[doi:10.1103/PhysRevD.78.063534](#)].
- [119] S. Weinberg, *Quantum contributions to cosmological correlations. II. Can these corrections become large?*, *Phys. Rev. D* **74** (2006) 023508, [[arXiv:hep-th/0605244](#)], [[doi:10.1103/PhysRevD.74.023508](#)].
- [120] M. van der Meulen and J. Smit, *Classical approximation to quantum cosmological correlations*, *JCAP* **0711** (2007) 023, [[arXiv:0707.0842](#)], [[doi:10.1088/1475-7516/2007/11/023](#)].

- [121] T. Prokopec and G. Rigopoulos, *Path integral for inflationary perturbations*, *Phys. Rev. D* **82** (2010) 023529, [[arXiv:1004.0882](#)], [[doi:10.1103/PhysRevD.82.023529](#)].
- [122] V. F. Mukhanov, H. Feldman, and R. H. Brandenberger, *Theory of cosmological perturbations. Part 1. Classical perturbations. Part 2. Quantum theory of perturbations. Part 3. Extensions*, *Phys. Rept.* **215** (1992) 203–333, [[doi:10.1016/0370-1573\(92\)90044-Z](#)].
- [123] D. H. Lyth, K. A. Malik, and M. Sasaki, *A general proof of the conservation of the curvature perturbation*, *JCAP* **0505** (2005) 004, [[arXiv:astro-ph/0411220](#)], [[doi:10.1088/1475-7516/2005/05/004](#)].
- [124] D. S. Salopek and J. R. Bond, *Nonlinear evolution of long wavelength metric fluctuations in inflationary models*, *Phys. Rev. D* **42** (1990) 3936–3962, [[doi:10.1103/PhysRevD.42.3936](#)].
- [125] C. Cheung, P. Creminelli, A. Fitzpatrick, J. Kaplan, and L. Senatore, *The effective field theory of inflation*, *JHEP* **0803** (2008) 014, [[arXiv:0709.0293](#)], [[doi:10.1088/1126-6708/2008/03/014](#)].
- [126] D. Baumann and D. Green, *Equilateral non-gaussianity and new physics on the horizon*, *JCAP* **1109** (2011) 014, [[arXiv:1102.5343](#)], [[doi:10.1088/1475-7516/2011/09/014](#)].
- [127] A. R. Liddle and D. H. Lyth, *The cold dark matter density perturbation*, *Phys. Rept.* **231** (1993) 1–105, [[arXiv:9303019](#)], [[doi:10.1016/0370-1573\(93\)90114-S](#)].
- [128] D. H. Lyth and A. Riotto, *Particle physics models of inflation and the cosmological density perturbation*, *Phys. Rept.* **314** (1999) 1–146, [[arXiv:hep-ph/9807278](#)], [[doi:10.1016/S0370-1573\(98\)00128-8](#)].
- [129] J. Choe, J.-O. Gong, and E. D. Stewart, *Second order general slow-roll power spectrum*, *JCAP* **0407** (2004) 012, [[arXiv:hep-ph/0405155](#)], [[doi:10.1088/1475-7516/2004/07/012](#)].
- [130] X. Chen, R. Easther, and E. A. Lim, *Large non-gaussianities in single field inflation*, *JCAP* **0706** (2007) 023, [[arXiv:astro-ph/0611645](#)], [[doi:10.1088/1475-7516/2007/06/023](#)].
- [131] X. Chen, R. Easther, and E. A. Lim, *Generation and characterization of large non-gaussianities in single field inflation*, *JCAP* **0804** (2008) 010, [[arXiv:0801.3295](#)], [[doi:10.1088/1475-7516/2008/04/010](#)].
- [132] X. Chen, *Folded resonant non-gaussianity in general single field inflation*, *JCAP* **1012** (2010) 003, [[arXiv:1008.2485](#)], [[doi:10.1088/1475-7516/2010/12/003](#)].
- [133] L. Leblond and E. Pajer, *Resonant trispectrum and a dozen more primordial N-point functions*, *JCAP* **1101** (2011) 035, [[arXiv:1010.4565](#)], [[doi:10.1088/1475-7516/2011/01/035](#)].

- [134] P. Adshead, W. Hu, C. Dvorkin, and H. V. Peiris, *Fast computation of bispectrum features with generalized slow roll*, *Phys. Rev. D* **84** (2011) 043519, [[arXiv:1102.3435](#)], [[doi:10.1103/PhysRevD.84.043519](#)].
- [135] D. Seery, *One-loop corrections to the curvature perturbation from inflation*, *JCAP* **0802** (2008) 006, [[arXiv:0707.3378](#)], [[doi:10.1088/1475-7516/2008/02/006](#)].
- [136] C. Burgess, L. Leblond, R. Holman, and S. Shandera, *Super-hubble de Sitter fluctuations and the dynamical RG*, *JCAP* **1003** (2010) 033, [[arXiv:0912.1608](#)], [[doi:10.1088/1475-7516/2010/03/033](#)].
- [137] D. Seery, *Infrared effects in inflationary correlation functions*, *Class. Quant. Grav.* **27** (2010) 124005, [[arXiv:1005.1649](#)], [[doi:10.1088/0264-9381/27/12/124005](#)].
- [138] D. J. Mulryne, D. Seery, and D. Wesley, *Moment transport equations for non-gaussianity*, *JCAP* **1001** (2010) 024, [[arXiv:0909.2256](#)], [[doi:10.1088/1475-7516/2010/01/024](#)].
- [139] D. J. Mulryne, D. Seery, and D. Wesley, *Moment transport equations for the primordial curvature perturbation*, *JCAP* **1104** (2011) 030, [[arXiv:1008.3159](#)], [[doi:10.1088/1475-7516/2011/04/030](#)].
- [140] C. M. Peterson and M. Tegmark, *Non-gaussianity in two-field inflation*, *Phys. Rev. D* **84** (2011) 023520, [[arXiv:1011.6675](#)], [[doi:10.1103/PhysRevD.84.023520](#)].
- [141] D. Seery, D. J. Mulryne, J. Frazer, and R. H. Ribeiro, *Inflationary perturbation theory is geometrical optics in phase space*, [arXiv:1203.2635](#).
- [142] G. Rigopoulos and E. Shellard, *The separate universe approach and the evolution of nonlinear superhorizon cosmological perturbations*, *Phys. Rev. D* **68** (2003) 123518, [[arXiv:astro-ph/0306620](#)], [[doi:10.1103/PhysRevD.68.123518](#)].
- [143] A. Naruko and M. Sasaki, *Conservation of the nonlinear curvature perturbation in generic single-field inflation*, *Class. Quant. Grav.* **28** (2011) 072001, [[arXiv:1101.3180](#)], [[doi:10.1088/0264-9381/28/7/072001](#)].
- [144] T. S. Bunch and P. C. W. Davies, *Quantum field theory in de Sitter space: renormalization by point splitting*, *Proc. Roy. Soc. Lond.* **A360** (1978) 117–134.
- [145] M. Dias and D. Seery, *Transport equations for the inflationary spectral index*, *Phys. Rev. D* **85** (2012) 043519, [[arXiv:1111.6544](#)], [[doi:10.1103/PhysRevD.85.043519](#)].
- [146] D. Seery and J. E. Lidsey, *Non-gaussian inflationary perturbations from the dS/CFT correspondence*, *JCAP* **0606** (2006) 001, [[arXiv:astro-ph/0604209](#)], [[doi:10.1088/1475-7516/2006/06/001](#)].
- [147] J. S. Schwinger, *Brownian motion of a quantum oscillator*, *J. Math. Phys.* **2** (1961) 407–432.
- [148] L. Keldysh, *Diagram technique for nonequilibrium processes*, *Zh. Eksp. Teor. Fiz.* **47** (1964) 1515–1527.

- [149] R. D. Jordan, *Effective field equations for expectation values*, *Phys. Rev. D* **33** (1986) 444–454, [[doi:10.1103/PhysRevD.33.444](https://doi.org/10.1103/PhysRevD.33.444)].
- [150] E. Calzetta and B. Hu, *Closed time path functional formalism in curved space-time: application to cosmological back reaction problems*, *Phys. Rev. D* **35** (1987) 495, [[doi:10.1103/PhysRevD.35.495](https://doi.org/10.1103/PhysRevD.35.495)].
- [151] X. Chen, *Primordial non-gaussianities from inflation models*, *Adv. Astron.* **2010** (2010) 638979, [[arXiv:1002.1416](https://arxiv.org/abs/1002.1416)], [[doi:10.1155/2010/638979](https://doi.org/10.1155/2010/638979)].
- [152] K. Koyama, *Non-gaussianity of quantum fields during inflation*, *Class. Quant. Grav.* **27** (2010) 124001, [[arXiv:1002.0600](https://arxiv.org/abs/1002.0600)], [[doi:10.1088/0264-9381/27/12/124001](https://doi.org/10.1088/0264-9381/27/12/124001)].
- [153] F. Arroja and T. Tanaka, *A note on the role of the boundary terms for the non-gaussianity in general k -inflation*, *JCAP* **1105** (2011) 005, [[arXiv:1103.1102](https://arxiv.org/abs/1103.1102)], [[doi:10.1088/1475-7516/2011/05/005](https://doi.org/10.1088/1475-7516/2011/05/005)].
- [154] A. De Felice and S. Tsujikawa, *Inflationary non-gaussianities in the most general second-order scalar-tensor theories*, *Phys. Rev. D* **84** (2011) 083504, [[arXiv:1107.3917](https://arxiv.org/abs/1107.3917)], [[doi:10.1103/PhysRevD.84.083504](https://doi.org/10.1103/PhysRevD.84.083504)].
- [155] S. Renaux-Petel, *On the redundancy of operators and the bispectrum in the most general second-order scalar-tensor theory*, *JCAP* **1202** (2012) 020, [[arXiv:1107.5020](https://arxiv.org/abs/1107.5020)], [[doi:10.1088/1475-7516/2012/02/020](https://doi.org/10.1088/1475-7516/2012/02/020)].
- [156] C. Deffayet, X. Gao, D. Steer, and G. Zahariade, *From k -essence to generalised galileons*, *Phys. Rev. D* **84** (2011) 064039, [[arXiv:1103.3260](https://arxiv.org/abs/1103.3260)], [[doi:10.1103/PhysRevD.84.064039](https://doi.org/10.1103/PhysRevD.84.064039)].
- [157] G. W. Horndeski, *Second-order scalar-tensor field equations in a four-dimensional space*, *Int. J. Theor. Phys.* **10** (1974) 363.
- [158] A. Nicolis, R. Rattazzi, and E. Trincherini, *The galileon as a local modification of gravity*, *Phys. Rev. D* **79** (2009) 064036, [[arXiv:0811.2197](https://arxiv.org/abs/0811.2197)], [[doi:10.1103/PhysRevD.79.064036](https://doi.org/10.1103/PhysRevD.79.064036)].
- [159] C. Deffayet, S. Deser, and G. Esposito-Farèse, *Generalized galileons: all scalar models whose curved background extensions maintain second-order field equations and stress-tensors*, *Phys. Rev. D* **80** (2009) 064015, [[arXiv:0906.1967](https://arxiv.org/abs/0906.1967)], [[doi:10.1103/PhysRevD.80.064015](https://doi.org/10.1103/PhysRevD.80.064015)].
- [160] C. de Rham and A. J. Tolley, *DBI and the galileon reunited*, *JCAP* **1005** (2010) 015, [[arXiv:1003.5917](https://arxiv.org/abs/1003.5917)], [[doi:10.1088/1475-7516/2010/05/015](https://doi.org/10.1088/1475-7516/2010/05/015)].
- [161] C. Charmousis, E. J. Copeland, A. Padilla, and P. M. Saffin, *General second order scalar-tensor theory, self tuning, and the Fab Four*, *Phys. Rev. Lett.* **108** (2012) 051101, [[arXiv:1106.2000](https://arxiv.org/abs/1106.2000)], [[doi:10.1103/PhysRevLett.108.051101](https://doi.org/10.1103/PhysRevLett.108.051101)].

- [162] L. Senatore, K. M. Smith, and M. Zaldarriaga, *Non-gaussianities in single field inflation and their optimal limits from the WMAP 5-year data*, *JCAP* **1001** (2010) 028, [[arXiv:0905.3746](#)], [[doi:10.1088/1475-7516/2010/01/028](#)].
- [163] M. Gell-Mann and F. Low, *Quantum electrodynamics at small distances*, *Phys. Rev.* **95** (1954) 1300–1312, [[doi:10.1103/PhysRev.95.1300](#)].
- [164] J. Collins, *Foundations of perturbative QCD*. Cambridge Monographs on Particle Physics, Nuclear Physics and Cosmology (No. 32), Cambridge University Press, Cambridge, UK, 2005.
- [165] D. Seery, *A parton picture of de Sitter space during slow-roll inflation*, *JCAP* **0905** (2009) 021, [[arXiv:0903.2788](#)], [[doi:10.1088/1475-7516/2009/05/021](#)].
- [166] J. C. Collins, D. E. Soper, and G. F. Sterman, *Factorization of hard processes in QCD*, *Adv. Ser. Direct. High Energy Phys.* **5** (1988) 1–91, [[arXiv:hep-ph/0409313](#)].
- [167] P. Creminelli and M. Zaldarriaga, *Single field consistency relation for the 3-point function*, *JCAP* **0410** (2004) 006, [[arXiv:astro-ph/0407059](#)], [[doi:10.1088/1475-7516/2004/10/006](#)].
- [168] J. Ganc and E. Komatsu, *A new method for calculating the primordial bispectrum in the squeezed limit*, *JCAP* **1012** (2010) 009, [[arXiv:1006.5457](#)], [[doi:10.1088/1475-7516/2010/12/009](#)].
- [169] S. Renaux-Petel, *On the squeezed limit of the bispectrum in general single field inflation*, *JCAP* **1010** (2010) 020, [[arXiv:1008.0260](#)], [[doi:10.1088/1475-7516/2010/10/020](#)].
- [170] P. Creminelli, A. Nicolis, L. Senatore, M. Tegmark, and M. Zaldarriaga, *Limits on non-gaussianities from WMAP data*, *JCAP* **0605** (2006) 004, [[arXiv:astro-ph/0509029](#)], [[doi:10.1088/1475-7516/2006/05/004](#)].
- [171] P. Creminelli, L. Senatore, M. Zaldarriaga, and M. Tegmark, *Limits on f_{NL} parameters from WMAP 3yr data*, *JCAP* **0703** (2007) 005, [[arXiv:astro-ph/0610600](#)], [[doi:10.1088/1475-7516/2007/03/005](#)].
- [172] F. Lucchin and S. Matarrese, *Power law inflation*, *Phys.Rev.* **D32** (1985) 1316, [[doi:10.1103/PhysRevD.32.1316](#)].
- [173] F. Lucchin and S. Matarrese, *Kinematical properties of generalized inflation*, *Phys. Lett. B* **164** (1985) 282, [[doi:10.1016/0370-2693\(85\)90327-2](#)].
- [174] J. Khoury and F. Piazza, *Rapidly-varying speed of sound, scale invariance and non-gaussian signatures*, *JCAP* **0907** (2009) 026, [[arXiv:0811.3633](#)], [[doi:10.1088/1475-7516/2009/07/026](#)].
- [175] L. Leblond and S. Shandera, *Simple bounds from the perturbative regime of inflation*, *JCAP* **0808** (2008) 007, [[arXiv:0802.2290](#)], [[doi:10.1088/1475-7516/2008/08/007](#)].

- [176] M. Shmakova, *One loop corrections to the D3-brane action*, *Phys. Rev. D* **62** (2000) 104009, [[arXiv:hep-th/9906239](#)], [[doi:10.1103/PhysRevD.62.104009](#)].
- [177] A. De Giovanni, A. Santambrogio, and D. Zanon, $(\alpha')^4$ corrections to the $N=2$ supersymmetric Born–Infeld action, *Phys. Lett. B* **472** (2000) 94–100, [[arXiv:hep-th/9907214](#)], [[doi:10.1016/S0370-2693\(99\)01319-2](#)], [[10.1016/S0370-2693\(99\)01319-2](#)].
- [178] A. A. Tseytlin, *Born–Infeld action, supersymmetry and string theory*, [arXiv:hep-th/9908105](#).
- [179] D. A. Easson and R. Gregory, *Circumventing the eta problem*, *Phys. Rev. D* **80** (2009) 083518, [[arXiv:0902.1798](#)], [[doi:10.1103/PhysRevD.80.083518](#)].
- [180] P. Franche, R. Gwyn, B. Underwood, and A. Wissanji, *Attractive lagrangians for non-canonical inflation*, *Phys. Rev. D* **81** (2010) 123526, [[arXiv:0912.1857](#)], [[doi:10.1103/PhysRevD.81.123526](#)].
- [181] X. Chen, *Multi-throat brane inflation*, *Phys. Rev. D* **71** (2005) 063506, [[arXiv:hep-th/0408084](#)], [[doi:10.1103/PhysRevD.71.063506](#)].
- [182] X. Chen, *Inflation from warped space*, *JHEP* **0508** (2005) 045, [[arXiv:hep-th/0501184](#)], [[doi:10.1088/1126-6708/2005/08/045](#)].
- [183] X. Chen, *Running non-gaussianities in DBI inflation*, *Phys. Rev. D* **72** (2005) 123518, [[arXiv:astro-ph/0507053](#)], [[doi:10.1103/PhysRevD.72.123518](#)].
- [184] R. Bean, S. E. Shandera, S. H. Henry Tye, and J. Xu, *Comparing brane inflation to WMAP*, *JCAP* **0705** (2007) 004, [[arXiv:hep-th/0702107](#)], [[doi:10.1088/1475-7516/2007/05/004](#)].
- [185] H. V. Peiris, D. Baumann, B. Friedman, and A. Cooray, *Phenomenology of D-brane inflation with general speed of sound*, *Phys. Rev. D* **76** (2007) 103517, [[arXiv:0706.1240](#)], [[doi:10.1103/PhysRevD.76.103517](#)].
- [186] L. Alabidi and J. E. Lidsey, *Single-field inflation after WMAP5*, *Phys. Rev. D* **78** (2008) 103519, [[arXiv:0807.2181](#)], [[doi:10.1103/PhysRevD.78.103519](#)].
- [187] J. Noller and J. Magueijo, *Non-gaussianity in single field models without slow-roll*, *Phys. Rev. D* **83** (2011) 103511, [[arXiv:1102.0275](#)], [[doi:10.1103/PhysRevD.83.103511](#)].
- [188] **CMBPol Study Team** Collaboration, D. Baumann *et al.*, *CMBPol mission concept study: a mission to map our origins*, *AIP Conf. Proc.* **1141** (2009) 3–9, [[arXiv:0811.3911](#)], [[doi:10.1063/1.3160890](#)].
- [189] E. J. Copeland, E. W. Kolb, A. R. Liddle, and J. E. Lidsey, *Reconstructing the inflation potential, in principle and in practice*, *Phys. Rev. D* **48** (1993) 2529–2547, [[arXiv:hep-ph/9303288](#)], [[doi:10.1103/PhysRevD.48.2529](#)].

- [190] E. J. Copeland, E. W. Kolb, A. R. Liddle, and J. E. Lidsey, *Reconstructing the inflaton potential: perturbative reconstruction to second order*, *Phys. Rev. D* **49** (1994) 1840–1844, [[arXiv:astro-ph/9308044](#)], [[doi:10.1103/PhysRevD.49.1840](#)].
- [191] L. Grishchuk, *Amplification of gravitational waves in an isotropic universe*, *Sov. Phys. JETP* **40** (1975) 409–415.
- [192] L. Colombo, E. Pierpaoli, and J. Pritchard, *Cosmological parameters after WMAP5: forecasts for Planck and future galaxy surveys*, *Mon. Not. Roy. Astron. Soc.* **398** (2009) 1621, [[arXiv:0811.2622](#)], [[doi:10.1111/j.1365-2966.2009.14802.x](#)].
- [193] P. Adshead, C. Dvorkin, W. Hu, and E. A. Lim, *Non-gaussianity from step features in the inflationary potential*, *Phys. Rev. D* **85** (2012) 023531, [[arXiv:1110.3050](#)], [[doi:10.1103/PhysRevD.85.023531](#)].
- [194] M. Cortês, A. R. Liddle, and P. Mukherjee, *On what scale should inflationary observables be constrained?*, *Phys. Rev. D* **75** (2007) 083520, [[arXiv:astro-ph/0702170](#)], [[doi:10.1103/PhysRevD.75.083520](#)].
- [195] A. Kosowsky and M. S. Turner, *CBR anisotropy and the running of the scalar spectral index*, *Phys. Rev. D* **52** (1995) 1739–1743, [[arXiv:astro-ph/9504071](#)], [[doi:10.1103/PhysRevD.52.R1739](#)].
- [196] M. Cortês and A. R. Liddle, *The consistency equation hierarchy in single-field inflation models*, *Phys. Rev. D* **73** (2006) 083523, [[arXiv:astro-ph/0603016](#)], [[doi:10.1103/PhysRevD.73.083523](#)].
- [197] M. LoVerde, A. Miller, S. Shandera, and L. Verde, *Effects of scale-dependent non-gaussianity on cosmological structures*, *JCAP* **0804** (2008) 014, [[arXiv:0711.4126](#)], [[doi:10.1088/1475-7516/2008/04/014](#)].
- [198] E. Sefusatti, M. Liguori, A. P. Yadav, M. G. Jackson, and E. Pajer, *Constraining running non-gaussianity*, *JCAP* **0912** (2009) 022, [[arXiv:0906.0232](#)], [[doi:10.1088/1475-7516/2009/12/022](#)].
- [199] C. T. Byrnes, S. Nurmi, G. Tasinato, and D. Wands, *Scale dependence of local f_{NL}* , *JCAP* **1002** (2010) 034, [[arXiv:0911.2780](#)], [[doi:10.1088/1475-7516/2010/02/034](#)].
- [200] C. T. Byrnes, M. Gerstenlauer, S. Nurmi, G. Tasinato, and D. Wands, *Scale-dependent non-gaussianity probes inflationary physics*, *JCAP* **1010** (2010) 004, [[arXiv:1007.4277](#)], [[doi:10.1088/1475-7516/2010/10/004](#)].
- [201] J. Fergusson, M. Liguori, and E. Shellard, *General CMB and primordial bispectrum estimation I: mode expansion, map-making and measures of f_{NL}* , *Phys. Rev. D* **82** (2010) 023502, [[arXiv:0912.5516](#)], [[doi:10.1103/PhysRevD.82.023502](#)].
- [202] P. D. Meerburg, J. P. van der Schaar, and P. S. Corasaniti, *Signatures of initial state modifications on bispectrum statistics*, *JCAP* **0905** (2009) 018, [[arXiv:0901.4044](#)], [[doi:10.1088/1475-7516/2009/05/018](#)].

- [203] X. Chen, *Primordial non-gaussianities from inflation models*, *Adv. Astron.* **2010** (2010) 638979, [[arXiv:1002.1416](#)], [[doi:10.1155/2010/638979](#)].
- [204] P. Meerburg, *Oscillations in the Primordial Bispectrum I: Mode Expansion*, *Phys. Rev. D* **82** (2010) 063517, [[arXiv:1006.2771](#)], [[doi:10.1103/PhysRevD.82.063517](#)].
- [205] M. Sasaki, J. Valiviita, and D. Wands, *Non-gaussianity of the primordial perturbation in the curvaton model*, *Phys. Rev. D* **74** (2006) 103003, [[arXiv:astro-ph/0607627](#)], [[doi:10.1103/PhysRevD.74.103003](#)].
- [206] C. T. Byrnes, M. Sasaki, and D. Wands, *The primordial trispectrum from inflation*, *Phys. Rev. D* **74** (2006) 123519, [[arXiv:astro-ph/0611075](#)], [[doi:10.1103/PhysRevD.74.123519](#)].
- [207] D. Seery and J. E. Lidsey, *Non-gaussianity from the inflationary trispectrum*, *JCAP* **0701** (2007) 008, [[arXiv:astro-ph/0611034](#)], [[doi:10.1088/1475-7516/2007/01/008](#)].
- [208] T. Suyama and M. Yamaguchi, *Non-gaussianity in the modulated reheating scenario*, *Phys. Rev. D* **77** (2008) 023505, [[arXiv:0709.2545](#)], [[doi:10.1103/PhysRevD.77.023505](#)].
- [209] K. M. Smith, M. LoVerde, and M. Zaldarriaga, *A universal bound on N-point correlations from inflation*, *Phys. Rev. Lett.* **107** (2011) 191301, [[arXiv:1108.1805](#)], [[doi:10.1103/PhysRevLett.107.191301](#)].
- [210] J.-L. Lehners, *Ekpyrotic and cyclic Cosmology*, *Phys. Rept.* **465** (2008) 223–263, [[arXiv:0806.1245](#)], [[doi:10.1016/j.physrep.2008.06.001](#)].
- [211] J. Khoury and G. E. Miller, *Towards a cosmological dual to inflation*, *Phys. Rev. D* **84** (2011) 023511, [[arXiv:1012.0846](#)], [[doi:10.1103/PhysRevD.84.023511](#)].
- [212] D. Baumann, L. Senatore, and M. Zaldarriaga, *Scale-invariance and the strong coupling problem*, *JCAP* **1105** (2011) 004, [[arXiv:1101.3320](#)], [[doi:10.1088/1475-7516/2011/05/004](#)].
- [213] N. Bartolo, M. Fasiello, S. Matarrese, and A. Riotto, *Tilt and running of cosmological observables in generalized single-field inflation*, *JCAP* **1012** (2010) 026, [[arXiv:1010.3993](#)], [[doi:10.1088/1475-7516/2010/12/026](#)].
- [214] S. Weinberg, *Effective field theory for inflation*, *Phys. Rev. D* **77** (2008) 123541, [[arXiv:0804.4291](#)], [[doi:10.1103/PhysRevD.77.123541](#)].
- [215] E. Nalson, A. J. Christopherson, I. Huston, and K. A. Malik, *Quantifying the behaviour of curvature perturbations during inflation*, [arXiv:1111.6940](#).
- [216] D. Wands, N. Bartolo, S. Matarrese, and A. Riotto, *An observational test of two-field inflation*, *Phys. Rev. D* **66** (2002) 043520, [[arXiv:astro-ph/0205253](#)], [[doi:10.1103/PhysRevD.66.043520](#)].

- [217] S. Groot Nibbelink and B. van Tent, *Scalar perturbations during multiple field slow-roll inflation*, *Class. Quant. Grav.* **19** (2002) 613–640, [[arXiv:hep-ph/0107272](#)], [[doi:10.1088/0264-9381/19/4/302](#)].
- [218] Z. Lalak, D. Langlois, S. Pokorski, and K. Turzyński, *Curvature and isocurvature perturbations in two-field inflation*, *JCAP* **0707** (2007) 014, [[arXiv:0704.0212](#)], [[doi:10.1088/1475-7516/2007/07/014](#)].
- [219] C. M. Peterson and M. Tegmark, *Testing two-field inflation*, *Phys. Rev. D* **83** (2011) 023522, [[arXiv:1005.4056](#)], [[doi:10.1103/PhysRevD.83.023522](#)].
- [220] A. Avgoustidis, S. Cremonini, A.-C. Davis, R. H. Ribeiro, K. Turzyński, and S. Watson, *The importance of slow-roll corrections during multi-field inflation*, *JCAP* **1202** (2012) 024, [[arXiv:1110.4081](#)], [[doi:10.1088/1475-7516/2012/02/038](#)].
- [221] C. M. Peterson and M. Tegmark, *Testing multi-field inflation: a geometric approach*, [arXiv:1111.0927](#).
- [222] D. H. Lyth and D. Seery, *Classicality of the primordial perturbations*, *Phys. Lett. B* **662** (2008) 309–313, [[arXiv:astro-ph/0607647](#)], [[doi:10.1016/j.physletb.2008.03.010](#)].
- [223] S. Matarrese, L. Verde, and R. Jimenez, *The abundance of high-redshift objects as a probe of non-gaussian initial conditions*, *Astrophys. J.* **541** (2000) 10, [[arXiv:astro-ph/0001366](#)], [[doi:10.1086/309412](#)].
- [224] E. Sefusatti and E. Komatsu, *The bispectrum of galaxies from high-redshift galaxy surveys: primordial non-gaussianity and non-linear galaxy bias*, *Phys. Rev. D* **76** (2007) 083004, [[arXiv:0705.0343](#)], [[doi:10.1103/PhysRevD.76.083004](#)].
- [225] N. Afshordi and A. J. Tolley, *Primordial non-gaussianity, statistics of collapsed objects, and the integrated Sachs-Wolfe effect*, *Phys. Rev. D* **78** (2008) 123507, [[arXiv:0806.1046](#)], [[doi:10.1103/PhysRevD.78.123507](#)].
- [226] L. Verde, *Non-gaussianity from large-scale structure surveys*, [arXiv:1001.5217](#).
- [227] V. Desjacques and U. Seljak, *Primordial non-gaussianity from the large scale structure*, *Class. Quant. Grav.* **27** (2010) 124011, [[arXiv:1003.5020](#)], [[doi:10.1088/0264-9381/27/12/124011](#)].
- [228] C. T. Byrnes, K. Enqvist, and T. Takahashi, *Scale-dependence of non-gaussianity in the curvaton model*, *JCAP* **1009** (2010) 026, [[arXiv:1007.5148](#)], [[doi:10.1088/1475-7516/2010/09/026](#)].
- [229] C. V. Johnson, *D-branes*, Cambridge University Press (2003).
- [230] L. McAllister and E. Silverstein, *String Cosmology: a review*, *Gen. Rel. Grav.* **40** (2008) 565–605, [[arXiv:0710.2951](#)], [[doi:10.1007/s10714-007-0556-6](#)].

- [231] J. M. Cline, H. Firouzjahi, and P. Martineau, *Reheating from tachyon condensation*, *JHEP* **11** (2002) 041, [[arXiv:hep-th/0207156](#)], [[doi:10.1088/1126-6708/2002/11/041](#)].
- [232] J. H. Brodie and D. A. Easson, *Brane inflation and reheating*, *JCAP* **0312** (2003) 004, [[arXiv:hep-th/0301138](#)], [[doi:10.1088/1475-7516/2003/12/004](#)].
- [233] G. Dvali, A. Gruzinov, and M. Zaldarriaga, *Cosmological perturbations from inhomogeneous reheating, freezeout, and mass domination*, *Phys. Rev. D* **69** (2004) 083505, [[arXiv:astro-ph/0305548](#)], [[doi:10.1103/PhysRevD.69.083505](#)].
- [234] A. R. Frey, A. Mazumdar, and R. C. Myers, *Stringy effects during inflation and reheating*, *Phys. Rev. D* **73** (2006) 026003, [[arXiv:hep-th/0508139](#)], [[doi:10.1103/PhysRevD.73.026003](#)].
- [235] D. Chialva, G. Shiu, and B. Underwood, *Warped reheating in multi-throat brane inflation*, *JHEP* **01** (2006) 014, [[arXiv:hep-th/0508229](#)], [[doi:10.1088/1126-6708/2006/01/014](#)].
- [236] L. A. Kofman, *The origin of matter in the universe: reheating after inflation*, [arXiv:astro-ph/9605155](#).
- [237] D. I. Kaiser, *Post inflation reheating in an expanding universe*, *Phys. Rev. D* **53** (1996) 1776–1783, [[arXiv:astro-ph/9507108](#)], [[doi:10.1103/PhysRevD.53.1776](#)].
- [238] J. H. Traschen and R. H. Brandenberger, *Particle production during out-of-equilibrium phase transitions*, *Phys. Rev. D* **42** (1990) 2491–2504, [[doi:10.1103/PhysRevD.42.2491](#)].
- [239] L. Kofman, A. D. Linde, and A. A. Starobinsky, *Reheating after inflation*, *Phys. Rev. Lett.* **73** (1994) 3195–3198, [[arXiv:hep-th/9405187](#)], [[doi:10.1103/PhysRevLett.73.3195](#)].
- [240] Y. Shtanov, J. H. Traschen, and R. H. Brandenberger, *Universe reheating after inflation*, *Phys. Rev.* **51** (1995) 5438–5455, [[arXiv:hep-ph/9407247](#)], [[doi:10.1103/PhysRevD.51.5438](#)].
- [241] L. Kofman, A. D. Linde, and A. A. Starobinsky, *Towards the theory of reheating after inflation*, *Phys. Rev. D* **56** (1997) 3258–3295, [[arXiv:hep-ph/9704452](#)], [[doi:10.1103/PhysRevD.56.3258](#)].
- [242] B. A. Bassett, S. Tsujikawa, and D. Wands, *Inflation dynamics and reheating*, *Rev. Mod. Phys.* **78** (2006) 537–589, [[arXiv:astro-ph/0507632](#)], [[doi:10.1103/RevModPhys.78.537](#)].
- [243] K. Kohri, D. H. Lyth, and C. A. Valenzuela-Toledo, *On the generation of a non-gaussian curvature perturbation during preheating*, *JCAP* **1002** (2010) 023, [[arXiv:0904.0793](#)], [[doi:10.1088/1475-7516/2010/02/023](#)].
- [244] L. Kofman, *Preheating after inflation*, *Lect. Notes Phys.* **738** (2008) 55–79.

- [245] G. N. Felder, J. García-Bellido, P. B. Greene, L. Kofman, A. D. Linde, and I. Tkachev, *Dynamics of symmetry breaking and tachyonic preheating*, *Phys. Rev. Lett.* **87** (2001) 011601, [[arXiv:hep-ph/0012142](#)], [[doi:10.1103/PhysRevLett.87.011601](#)].
- [246] G. N. Felder, L. Kofman, and A. D. Linde, *Tachyonic instability and dynamics of spontaneous symmetry breaking*, *Phys. Rev. D* **64** (2001) 123517, [[arXiv:hep-th/0106179](#)], [[doi:10.1103/PhysRevD.64.123517](#)].
- [247] E. J. Copeland, S. Pascoli, and A. Rajantie, *Dynamics of tachyonic preheating after hybrid inflation*, *Phys. Rev. D* **65** (2002) 103517, [[arXiv:hep-ph/0202031](#)], [[doi:10.1103/PhysRevD.65.103517](#)].
- [248] J. F. Dufaux, G. N. Felder, L. Kofman, M. Peloso, and D. Podolsky, *Preheating with trilinear interactions: tachyonic resonance*, *JCAP* **0607** (2006) 006, [[arXiv:hep-ph/0602144](#)], [[doi:10.1088/1475-7516/2006/07/006](#)].
- [249] A. D. Linde, *Hybrid inflation*, *Phys. Rev. D* **49** (1994) 748–754, [[arXiv:astro-ph/9307002](#)], [[doi:10.1103/PhysRevD.49.748](#)].
- [250] D. H. Lyth, *Issues concerning the waterfall of hybrid inflation*, *Prog. Theor. Phys. Suppl.* **190** (2011) 107–119, [[arXiv:1005.2461](#)], [[doi:10.1143/PTPS.190.107](#)].
- [251] D. H. Lyth, *Contribution of the hybrid inflation waterfall to the primordial curvature perturbation*, *JCAP* **1107** (2011) 035, [[arXiv:1012.4617](#)], [[doi:10.1088/1475-7516/2011/07/035](#)].
- [252] S. Kachru, R. Kallosh, A. D. Linde, J. M. Maldacena, L. P. McAllister, *et al.*, *Towards inflation in string theory*, *JCAP* **0310** (2003) 013, [[arXiv:hep-th/0308055](#)], [[doi:10.1088/1475-7516/2003/10/013](#)].
- [253] N. Barnaby, C. P. Burgess, and J. M. Cline, *Warped reheating in brane-antibrane inflation*, *JCAP* **0504** (2005) 007, [[arXiv:hep-th/0412040](#)], [[doi:10.1088/1475-7516/2005/04/007](#)].
- [254] A. Sen, *Tachyon dynamics in open string theory*, *Int. J. Mod. Phys. A* **20** (2005) 5513–5656, [[arXiv:hep-th/0410103](#)], [[doi:10.1142/S0217751X0502519X](#)].
- [255] J. Lachapelle and R. H. Brandenberger, *Preheating with non-standard kinetic term*, *JCAP* **0904** (2009) 020, [[arXiv:0808.0936](#)], [[doi:10.1088/1475-7516/2009/04/020](#)].
- [256] G. Gibbons, *Born-Infeld particles and Dirichlet p-branes*, *Nucl. Phys. B* **514** (1998) 603–639, [[arXiv:hep-th/9709027](#)], [[doi:10.1016/S0550-3213\(97\)00795-5](#)].
- [257] S. R. Das and S. P. Trivedi, *Three-brane action and the correspondence between $N=4$ Yang-Mills theory and anti-De Sitter space*, *Phys. Lett. B* **445** (1998) 142–149, [[arXiv:hep-th/9804149](#)], [[doi:10.1016/S0370-2693\(98\)01450-6](#)].
- [258] O. Aharony, S. S. Gubser, J. M. Maldacena, H. Ooguri, and Y. Oz, *Large N field theories, string theory and gravity*, *Phys. Rept.* **323** (2000) 183–386, [[arXiv:hep-th/9905111](#)], [[doi:10.1016/S0370-1573\(99\)00083-6](#)].

- [259] I. R. Klebanov and M. J. Strassler, *Supergravity and a confining gauge theory: Duality cascades and χ SB resolution of naked singularities*, *JHEP* **0008** (2000) 052, [[arXiv:hep-th/0007191](#)], [[doi:10.1088/1126-6708/2000/08/052](#)].
- [260] D. Baumann *et al.*, *On D3-brane potentials in compactifications with fluxes and wrapped D-branes*, *JHEP* **11** (2006) 031, [[arXiv:hep-th/0607050](#)], [[doi:10.1088/1126-6708/2006/11/031](#)].
- [261] D. Baumann, A. Dymarsky, I. R. Klebanov, L. McAllister, and P. J. Steinhardt, *A delicate universe*, *Phys. Rev. Lett.* **99** (2007) 141601, [[arXiv:0705.3837](#)], [[doi:10.1103/PhysRevLett.99.141601](#)].
- [262] D. Baumann, A. Dymarsky, I. R. Klebanov, and L. McAllister, *Towards an explicit model of D-brane inflation*, *JCAP* **0801** (2008) 024, [[arXiv:0706.0360](#)], [[doi:10.1088/1475-7516/2008/01/024](#)].
- [263] A. Krause and E. Pajer, *Chasing brane inflation in string-theory*, *JCAP* **0807** (2008) 023, [[arXiv:0705.4682](#)], [[doi:10.1088/1475-7516/2008/07/023](#)].
- [264] D. Baumann, A. Dymarsky, S. Kachru, I. R. Klebanov, and L. McAllister, *Compactification effects in D-brane inflation*, *Phys. Rev. Lett.* **104** (2010) 251602, [[arXiv:0912.4268](#)], [[doi:10.1103/PhysRevLett.104.251602](#)].
- [265] D. Baumann, A. Dymarsky, S. Kachru, I. R. Klebanov, and L. McAllister, *D3-brane potentials from fluxes in AdS/CFT*, *JHEP* **1006** (2010) 072, [[arXiv:1001.5028](#)], [[doi:10.1007/JHEP06\(2010\)072](#)].
- [266] S. Shandera, *The structure of correlation functions in single field inflation*, *Phys. Rev. D* **79** (2009) 123518, [[arXiv:0812.0818](#)], [[doi:10.1103/PhysRevD.79.123518](#)].
- [267] D. N. Kabat and G. Lifschytz, *Gauge theory origins of supergravity causal structure*, *JHEP* **05** (1999) 005, [[arXiv:hep-th/9902073](#)], [[doi:10.1088/1126-6708/1999/05/005](#)].
- [268] S. Kecskeneti, J. Maiden, G. Shiu, and B. Underwood, *DBI inflation in the tip region of a warped throat*, *JHEP* **09** (2006) 076, [[arXiv:hep-th/0605189](#)], [[doi:10.1088/1126-6708/2006/09/076](#)].
- [269] C. Armendáriz-Picón, M. Trodden, and E. J. West, *Preheating in derivatively-coupled inflation models*, *JCAP* **0804** (2008) 036, [[arXiv:0707.2177](#)], [[doi:10.1088/1475-7516/2008/04/036](#)].
- [270] P. B. Greene and L. Kofman, *Preheating of fermions*, *Phys. Lett. B* **448** (1999) 6–12, [[arXiv:hep-ph/9807339](#)], [[doi:10.1016/S0370-2693\(99\)00020-9](#)].
- [271] P. B. Greene and L. Kofman, *On the theory of fermionic preheating*, *Phys. Rev. D* **62** (2000) 123516, [[arXiv:hep-ph/0003018](#)], [[doi:10.1103/PhysRevD.62.123516](#)].
- [272] L. Abbott, E. Farhi, and M. B. Wise, *Particle production in the new inflationary Cosmology*, *Phys. Lett. B* **117** (1982) 29, [[doi:10.1016/0370-2693\(82\)90867-X](#)].

- [273] N. W. McLachlan, *Theory and application of Mathieu functions*. Clarendon Press, Oxford, UK, 1947.
- [274] F. M. Arscott, *Periodic differential equations – an introduction to Lamé and allied functions*. Pergamon Press, Oxford, UK, 1964.
- [275] V. Mukhanov, *Physical foundations of Cosmology*. Cambridge University Press, Cambridge, UK, 2005.
- [276] A. J. Albrecht, P. J. Steinhardt, M. S. Turner, and F. Wilczek, *Reheating an inflationary universe*, *Phys. Rev. Lett.* **48** (1982) 1437, [[doi:10.1103/PhysRevLett.48.1437](https://doi.org/10.1103/PhysRevLett.48.1437)].
- [277] J. Karouby, B. Underwood, and A. C. Vincent, *Preheating with the brakes on: the effects of a speed limit*, *Phys. Rev. D* **84** (2011) 043528, [[arXiv:1105.3982](https://arxiv.org/abs/1105.3982)], [[doi:10.1103/PhysRevD.84.043528](https://doi.org/10.1103/PhysRevD.84.043528)].
- [278] J. Elliston, D. J. Mulryne, D. Seery, and R. Tavakol, *Evolution of f_{NL} to the adiabatic limit*, *JCAP* **1111** (2011) 005, [[arXiv:1106.2153](https://arxiv.org/abs/1106.2153)], [[doi:10.1088/1475-7516/2011/11/005](https://doi.org/10.1088/1475-7516/2011/11/005)].
- [279] L. Amendola, C. Gordon, D. Wands, and M. Sasaki, *Correlated perturbations from inflation and the cosmic microwave background*, *Phys. Rev. Lett.* **88** (2002) 211302, [[arXiv:astro-ph/0107089](https://arxiv.org/abs/astro-ph/0107089)], [[doi:10.1103/PhysRevLett.88.211302](https://doi.org/10.1103/PhysRevLett.88.211302)].
- [280] F. Vernizzi and D. Wands, *Non-gaussianities in two-field inflation*, *JCAP* **0605** (2006) 019, [[arXiv:astro-ph/0603799](https://arxiv.org/abs/astro-ph/0603799)], [[doi:10.1088/1475-7516/2006/05/019](https://doi.org/10.1088/1475-7516/2006/05/019)].
- [281] M. Abramowitz and I. A. Stegun, *Handbook of mathematical functions*. Dover, New York, 1970.